result, the domain walls that were pinned during ageing can become active again. This de-ageing can increase the dielectric responses, as clearly observed in the 0.6PIN–0.4PT composition in both the parallel and the perpendicular stress cases. As stated earlier, the rather immobile domains in the 0.5PIN–0.5PT composition explain a near constant of the dielectric constant and loss under applied stress. It should also be noted that the competing influence between the domain clamping and de-ageing mechanisms can be a cause of a slight difference in the dielectric loss response to the applied stress. These results clearly demonstrate that the contribution of each mechanism to the dielectric responses of the PIN–PT ceramics depends on the compositions and the stress level and direction.

4. Conclusions

In this study, the dielectric properties of PIN–PT ceramics with a formula $(1-x)Pb(In_{1/2}Nb_{1/2})O_3$–$xPbTiO_3$ (for $x = 0.1$–0.5) prepared by the two stage mixed-oxide method are measured under the compressive stress applied both parallel and perpendicular to the electric field direction. The results clearly show that the superimposed compression stress has pronounced effects on the dielectric properties of the PIN–PT ceramics. In general, with increasing compressive stress the dielectric constant of the ceramics increases and decreases when the stress is applied parallel and perpendicular, respectively, to the electric field direction. The dielectric loss tangent, however, decreases in both stress cases. The observations are mainly interpreted in terms of competing influences of the intrinsic contribution, and the extrinsic contribution from domain switching through non-180° domain walls, clamping of domain walls, de-ageing and the stress-induced decrease in the switchable part of spontaneous polarization.

Acknowledgments

This work was jointly supported by the Thailand Research Fund (TRF), Commission on Higher Education (CHE), Royal Golden Jubilee PhD program, Faculty of Science and Graduate School of Chiang Mai University.

References

[1] Alberta E F and Bhalla A S 1998 *J. Korean Phys. Soc.* **32** 1265
[2] Halliyal A, Kumar U, Newnham R E and Cross L E 1987 *Am. Ceram. Soc. Bull.* **66** 671
[3] Belsick J R, Halliyal A, Kumar U and Newnham R E 1987 *Am. Ceram. Soc. Bull.* **66** 664
[4] Kuwata J, Uchino K and Nomura S 1982 *Japan. J. Appl. Phys.* **21** 1298
[5] Park S and Shrout T R 1997 *J. Appl. Phys.* **82** 1804
[6] Viehland D and Powers J 2001 *Appl. Phys. Lett.* **78** 3112
[7] Cross L E 1987 *Ferroelectric* **76** 241
[8] Uchino K 1997 *Piezoelectric Actuators and Ultrasonic Motors* (Boston, MA: Kluwer)
[9] Stansfield D 1991 *Underwater Electroacoustic Transducers* (Bath, UK: Bath University Press)
[10] Lynch C S 1996 *Acta. Mater.* **44** 4137
[11] Zhou D, Wang Z and Kamlah M 2005 *J. Appl. Phys.* **97** 084105
[12] Hilczer A, Szafranski M and Kosec M 2007 *Ferroelectric Lett.* **34** 29
[13] Yimnirun R, Ananta S and Chamunglap S 2007 *Mater. Chem. Phys.* **102** 165
[14] Yimnirun R, Ananta S, Ngamjarurojana A and Wongsaenmai S 2006 *Curr. Appl. Phys.* **6** 520
[15] Yang G, Liu S F, Ren W and Mukherjee B K 2000 *Proc. SPIE Symp. Smart Struct. Mater.* **3992** 103
[16] Yimnirun R, Unruan M, Laosiritaworn Y and Ananta S 2006 *J. Phys. D: Appl. Phys.* **39** 3097
[17] Yimnirun R 2006 *Int. J. Mod. Phys.* B **20** 3409
[18] Zhou D, Kamlah M and Munz D 2005 *J. Eur. Ceram. Soc.* **25** 425
[19] Wongsaenmai S, Ananta S, Meechoowas E and Yimnirun R 2003 *J. Phys. D: Appl. Phys.* **36** 1615
[20] Krueger H 1967 *J. Acoust. Soc. Am.* **42** 636
[21] Zhang Q M, Zhao J, Uchino K and Zheng J 1997 *J. Mater. Res.* **12** 226
[22] Steiner O, Tagantsev A K, Colla E L and Setter N 1999 *J. Eur. Ceram. Soc.* **19** 1243
[23] Nomura K, Shingai T, Ishino S, Terauchi H, Yasuda N and Ohwa H 1999 *J. Phys. Soc. Japan* **68** 39
[24] Yasuda N and Fujie M 1992 *Japan. J. Appl. Phys.* **31** 3128
[25] Wongsaenmai S, Khamman O, Ananta S and Yimnirun R 2008 *J. Electroceram.* at press, doi: 10.1007/s10832-007-9311-3
[26] Yimnirun R, Ananta S, Ngamjarurojana A and Wongsaenmai S 2005 *Appl. Phys. A: Mater. Sci. Proc.* **81** 1227
[27] Yimnirun R, Laosiritaworn Y and Wongsaenmai S 2006 *J. Phys. D: Appl. Phys.* **39** 759
[28] Wongsaenmai S, Bhalla A, Tan X, Ananta S and Yimnirun R 2007 *Ferroelectric Lett.* **34** 36
[29] Wongsaenmai S, Tan X, Ananta S and Yimnirun R 2008 *J. Alloys Compounds* at press, doi: 10.1016/j.jallcom.2006.12.053
[30] Zhao J, Glazounov A E and Zhang Q M 1999 *Appl. Phys. Lett.* **74** 436
[31] Yang G, Liu S F, Ren W and Mukherjee B K 2001 *Ferroelectrics* **262** 207
[32] Triamnak N, Wongsaenmai S, Ananta S and Yimnirun R 2007 *Ceram. Int.* submitted
[33] Augier C, Pham-Thi M, Dammak H and Gaucher P 2005 *J. Eur. Ceram. Soc.* **25** 2429
[34] Krueger H 1967 *J. Acoust. Soc. Am.* **43** 583

Provided for non-commercial research and education use.
Not for reproduction, distribution or commercial use.

This article appeared in a journal published by Elsevier. The attached copy is furnished to the author for internal non-commercial research and education use, including for instruction at the authors institution and sharing with colleagues.

Other uses, including reproduction and distribution, or selling or licensing copies, or posting to personal, institutional or third party websites are prohibited.

In most cases authors are permitted to post their version of the article (e.g. in Word or Tex form) to their personal website or institutional repository. Authors requiring further information regarding Elsevier's archiving and manuscript policies are encouraged to visit:

http://www.elsevier.com/copyright

Author's personal copy

ELSEVIER

Journal of Alloys and Compounds 454 (2008) 331–339

Journal of ALLOYS AND COMPOUNDS

www.elsevier.com/locate/jallcom

Dielectric and ferroelectric properties of fine grains $Pb(In_{1/2}Nb_{1/2})O_3$–$PbTiO_3$ ceramics

Supattra Wongsaenmai [a], Xiaoli Tan [b], Supon Ananta [a], Rattikorn Yimnirun [a,*]

[a] *Department of Physics, Faculty of Science, Chiang Mai University, Chiang Mai 50200, Thailand*
[b] *Department of Materials Science and Engineering, Iowa State University, Ames, IA 50011, USA*

Received 3 October 2006; accepted 10 December 2006
Available online 20 December 2006

Abstract

The dielectric and ferroelectric properties of $(1-x)Pb(In_{1/2}Nb_{1/2})O_3$–$xPbTiO_3$ (when $x = 0.1$, 0.2, 0.3, 0.4, and 0.5) ceramics prepared by an oxide-mixing method via a vibro-milling technique were investigated. Fine grains ceramics were achieved with average grain size of 1–2 μm, indicating advantage of the vibro-milling technique used. While PIN ceramic exhibited relaxor behavior, the dielectric properties of PIN–PT ceramics showed a mixed relaxor and normal ferroelectric behavior, with more normal ferroelectric behavior observed with increasing PT content. In addition, the ferroelectric properties of the ceramics in PIN–PT system changed from the relaxor ferroelectric behavior in PIN ceramic to the normal ferroelectric behavior in PIN–PT ceramics. These results clearly show the significance of the added PT in reducing the relaxor ferroelectric behavior in PIN ceramic. Finally, the existence of the MPB composition between $x = 0.3$ and 0.4 has been confirmed from the XRD analysis, and dielectric and ferroelectric properties measurements.
© 2006 Elsevier B.V. All rights reserved.

Keywords: Dielectric properties; Ferroelectric properties; Mixed-oxide; PIN–PT

1. Introduction

Lead-based perovskite-type solid solutions consisting of the ferroelectric and relaxor materials have attracted a growing fundamental and practical interest because of their excellent dielectric, piezoelectric and electrostrictive properties which are useful in actuating and sensing applications [1–3]. Among the lead-based complex perovskites, lead magnesium niobate–lead titanate ($(1-x)Pb(Mg_{1/3}Nb_{2/3})O_3$–$xPbTiO_3$ or PMN-PT) and lead zinc niobate–lead titanate ($(1-x)Pb(Zn_{1/3}Nb_{2/3})O_3$–$xPbTiO_3$ or PZN-PT) have attracted much attention due to their superior electrical properties [4–7]. However, the major disadvantage of the two ceramic systems is relatively low Curie temperatures (T_C) of the morphotropic phase boundary (MPB) compositions, i.e. lower than 200 °C for the two systems [5–8]. This low T_C comes with the expenses of more temperature dependent properties and less polarization stability, which in turn restrict the operating temperature range to less than 100 °C [7,8]. Interestingly, the MPB composition of the lead indium niobate–lead titanate ($(1-x)Pb(In_{1/2}Nb_{1/2})O_3$–$xPbTiO_3$ or PIN–PT) solid solution system has been reported to possess T_C higher than 250 °C [8–13], and therefore potential for high temperature applications. Many previous studies have focused on the processing and properties of PIN–PT single crystals, particularly the MPB composition [9,12,14,15], while the information on PIN–PT ceramics is still limited [8,10,13]. In addition, most of the PIN–PT ceramics studied were prepared by the mixed-oxide method with a conventional ball-milling technique, which resulted in coarse grains ceramics [11,13], even though it is well known that fine grains ceramics usually show superior electrical properties [16,17]. Recently, a vibro-milling technique has been employed to produce nano-sized powders which can be used to fabricate ceramics with fine grain microstructure [18–20]. Therefore, as an extension to the research on the PIN–PT ceramics, the overall purpose of this study was to systematically determine the dielectric and ferroelectric properties of ceramics in the $(1-x)Pb(In_{1/2}Nb_{1/2})O_3$–$xPbTiO_3$ (when $x = 0.0$, 0.1, 0.2, 0.3, 0.4, and 0.5) system prepared by the mixed-oxide method via the vibro-milling technique. The vibro-milling technique

* Corresponding author. Tel.: +66 53 943 367; fax: +66 53 943 445.
E-mail addresses: rattikor@chiangmai.ac.th, rattikornyimnirun@yahoo.com (R. Yimnirun).

0925-8388/$ – see front matter © 2006 Elsevier B.V. All rights reserved.
doi:10.1016/j.jallcom.2006.12.053

Author's personal copy

was employed to explore the potential in obtaining fine grains ceramics, which would in turn lead to superior electrical properties.

2. Experimental

The $Pb(In_{1/2}Nb_{1/2})O_3$–$PbTiO_3$ ceramics used in this study were prepared from $Pb(In_{1/2}Nb_{1/2})O_3$ and $PbTiO_3$ starting powders obtained via the vibro-milling technique. In this technique, a vibratory laboratory mill (McCrone Micronizing Mill) was employed. A total of 48 polycrystalline corundum milling media with a powder weight of 20 g was kept constant in each batch. The milling operation was carried out in isopropanal inert to the polypropylene jar [18–20]. Initially, pure-phase PIN powders were obtained via a well-known wolframite method [21,22], while PT powders were prepared by a mixed-oxide method [23]. With the wolframite method, the single-phase indium niobate ($InNbO_4$) powders were first prepared by mixing starting indium oxide (In_2O_3) and niobium oxide (Nb_2O_5) (Aldrich, 99.9% purity) powders by employing the vibro-milling technique for 0.5 h and then calcining the mixed powders at 900 °C for 4 h with heating/cooling rates of 30 °C/min [24]. This yielded a so-called wolframite ($InNbO_4$) powder. The wolframite precursor powders were subsequently vibro-milled with lead oxide (PbO) (Fluka, 99% purity) for 0.5 h. The mixed powders were calcined at 1100 °C for 2 h with heating/cooling rates of 10 °C/min to form a single-phase PIN [25]. It should, however, be noted that to obtain the pure-phase PIN powders 2 mol% excess of In_2O_3 and PbO had to be added to compensate the loss during calcination [25]. With a more conventional oxide-mixing route, PT powders were prepared from PbO and titanium oxide (TiO_2) (Riedel-de Haën, 99% purity) starting powders. These powders were vibro-milled for 0.5 h and later calcined at 600 °C for 2 h with heating/cooling rates of 5 °C/min [23]. The $(1-x)Pb(In_{1/2}Nb_{1/2})O_3$–$xPbTiO_3$ (when $x = 0.0, 0.1, 0.2, 0.3, 0.4$, and 0.5) ceramics were then prepared from the PIN and PT powders by the same mixed-oxide method. The PIN and PT powders were weighed in the required stoichiometric ratio and vibro-milled for 0.5. The thoroughly mixed powders were then pressed hydraulically to form disc-shaped pellets 10 mm in diameter and 2 mm thick, with 3 wt.% polyvinyl alcohol as a binder. The pellets were placed on the alumina powder-bed inside alumina crucible and surrounded with atmosphere powders of the same composition. Finally, the pellets were sintered at 1175 °C (1050 °C for PIN) for 2 h with heating/cooling rates of 10 °C/min.

The densities of the sintered ceramics were measured by Archimedes method. The phase formations of the sintered specimens were studied by an X-ray diffractometer (XRD; Siemen-D500 diffractometer). The microstructure analyses were undertaken by a scanning electron microscopy (SEM: JEOL Model JSM 840A). Grain size was determined from SEM micrographs by a linear intercept method. The dielectric properties were evaluated with a computer-controlled dielectric measurement system consisted of a precision LCR-meter (Hewlett Packard, model 4284A), a temperature chamber (Delta Design, model 9023), and a sample holder (Norwegian Electroceramics) capable of high temperature measurement. The room temperature ferroelectric polarization versus electric field (*P–E*) measurements was made using a standardized ferroelectric test system (RT-66A, Radiant Technologies) with an applied field of 30–60 kV/cm.

3. Results and discussion

The XRD patterns of $(1-x)$PIN–xPT ceramics with various x values are shown in Fig. 1(a). It can be seen that a complete crystalline solution of perovskite structure is formed throughout the composition range without the presence of pyrochlore or unwanted phases. From the patterns, PIN ceramic is identified as a single-phase material with a perovskite structure having cubic symmetry which could be matched with JCPDS file no. 87-0304. The XRD patterns of the PIN–PT compositions show a combination between PIN and PT patterns, showing a perovskite structure having the symmetry varying between pseudo-cubic and tetragonal types. For better comparison, the

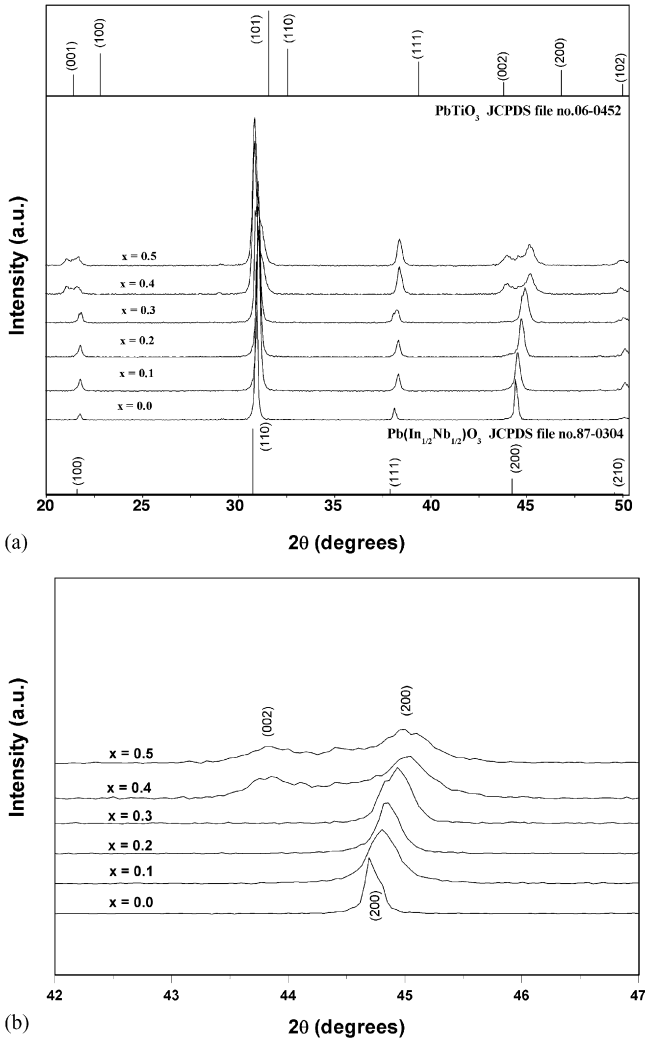

Fig. 1. (a) XRD patterns of $(1-x)$PIN–xPT ceramics and (b) selected region of the diffraction patterns.

JCPDS file no. 06-0452 for PT with a tetragonal structural symmetry is also displayed in Fig. 1(a). More interestingly, the composition with $x = 0.3$ began to exhibit broadening of peaks at $2\theta \approx 21.5°$, 30.5°, and 44.5° for (1 0 0)/(0 0 1), (1 1 0)/(1 0 1), and (2 0 0)/(0 0 2), respectively. Fig. 1(b) shows the broadened peaks at $2\theta \sim 44.5$–45°, indicating the structural transformation from the pseudo-cubic phase to the tetragonal phase, characterized by (2 0 0)/(0 0 2) peaks. This observation is obviously associated with the composition with coexistence of two symmetries, which in this case are tetragonal and pseudo-cubic phases. To a first approximation, it could be said that the composition between $x = 0.3$ and 0.4 is close to the morphotropic phase boundary (MPB) of the $Pb(In_{1/2}Nb_{1/2})O_3$–$PbTiO_3$ system, where the structure of the PIN–PT compositions is gradually changing from pseudo-cubic to tetragonal. Earlier studies have reported the MPB composition for PIN–PT system at $x \sim 0.37$ [9–12]. Electrical data described later further support this observation.

SEM micrographs in Fig. 2 reveal fine grains microstructure in all PIN–PT ceramics with little variation of the average grain

Author's personal copy

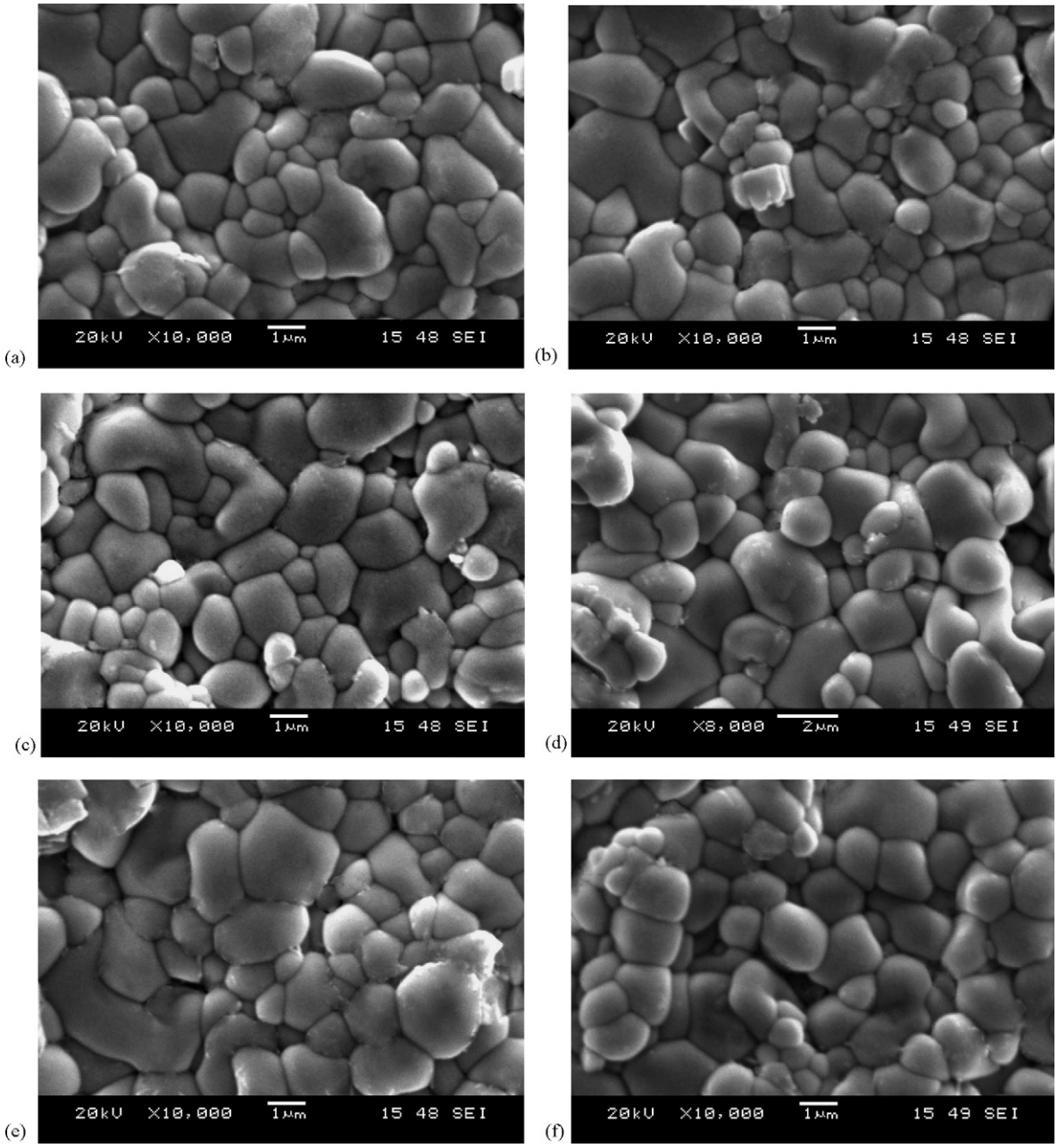

Fig. 2. SEM micrographs of $(1-x)$PIN–xPT with various compositions: (a) $x=0.0$, (b) $x=0.1$, (c) $x=0.2$, (d) $x=0.3$, (e) $x=0.4$, and (f) $x=0.5$.

size between 1 and 2 μm. The average grain size, as well as the density, does not vary significantly with the ceramic compositions, as listed in Table 1. However, it should be noticed that the microstructure of all the compositions also represents two distinct grain sizes, i.e. large grains (∼2 μm) and submicron grains. Earlier study on PIN–PT ceramics prepared with the conventional ball-milling method has also reported bimodal grain sizes but with large grains over 10 μm and fine grains about 1–2 μm [10]. Clearly, this shows the advantage of the vibro-milling technique in producing fine grains PIN–PT ceramics.

The dielectric properties, e.g. dielectric constant (ε_r) and $\tan\delta$, are measured as functions of both temperature and frequency, as shown in Fig. 3(a)–(f). As listed in Table 1 and plotted separately in Fig. 4, the maximum dielectric constant increases steadily with increasing PT content up to 30 mol% (ε_r increases from 4310 in PIN to 16028 in 0.7PIN–0.3PT). Then a drop in the dielectric constant is observed with further increase in PT content to 40 mol%. This supports the XRD observation that the MPB composition should lie between compositions $x=0.3$ and 0.4. It should also be noted that a rise in the dielectric constant with more PT content (50 mol%) is possibly caused by large thermal conduction at high temperature [26]. Furthermore, as listed in Table 1, since the transition temperature of PT is very high (490 °C) [27], it is expected to observe that the transition temperature increases with increasing amount of PT in the PIN–PT system. This is clearly evident in Fig. 4. Again, it should also be noted here that, as shown in Fig. 3, the dielectric properties of most compositions increase significantly at high temperature

Author's personal copy

Table 1
Physical features and dielectric properties of $(1-x)$PIN–xPT ceramics (measured at 1 kHz)

x	Density (g/cm^3)	Grain size (μm)	T_{max} (°C)	ε_r at		$\Delta T = T_{m,100\,kHz} - T_{m,100\,Hz}$ (°C)	Diffusivity (γ)
				T_{max}	25 °C		
0.0	7.83	1.22 ± 0.08	71	4310	3345	26.2	1.89
0.1	7.51	1.29 ± 0.10	175	7120	2336	8.0	1.83
0.2	7.95	1.41 ± 0.12	210	10,733	1659	5.4	1.75
0.3	8.09	1.84 ± 0.16	267	16,028	1056	1.6	1.70
0.4	7.98	1.51 ± 0.16	327	11,867	1291	1.0	1.65
0.5	7.95	1.33 ± 0.10	375	15,038	573	0.4	1.62

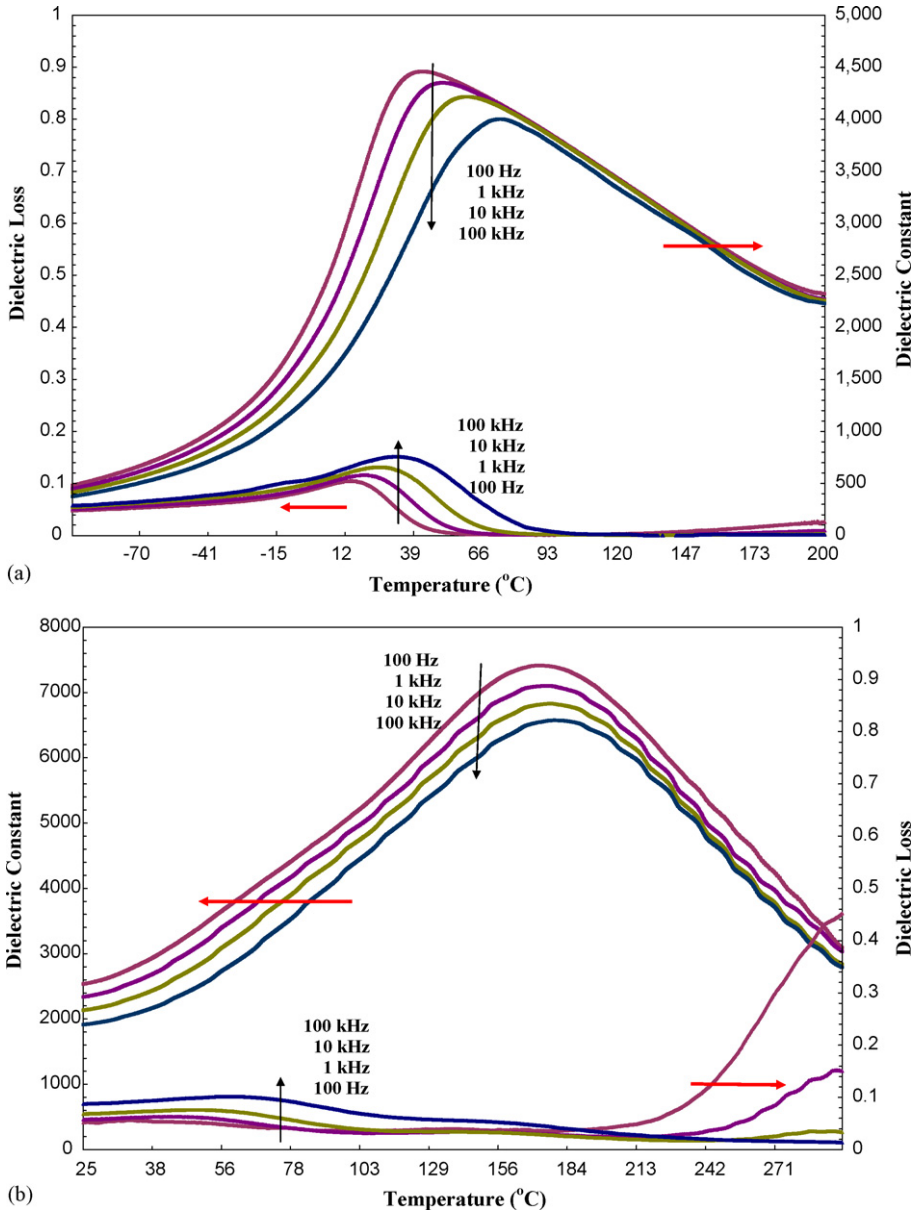

Fig. 3. (a) Temperature and frequency dependences of dielectric properties of PIN ceramic. (b) Temperature and frequency dependences of dielectric properties of 0.9PIN–0.1PT ceramic. (c) Temperature and frequency dependences of dielectric properties of 0.8PIN–0.2PT ceramic. (d) Temperature and frequency dependences of dielectric properties of 0.7PIN–0.3PT ceramic. (e) Temperature and frequency dependences of dielectric properties of 0.6PIN–0.4PT ceramic. (f) Temperature and frequency dependences of dielectric properties of 0.5PIN–0.5PT ceramic.

Author's personal copy

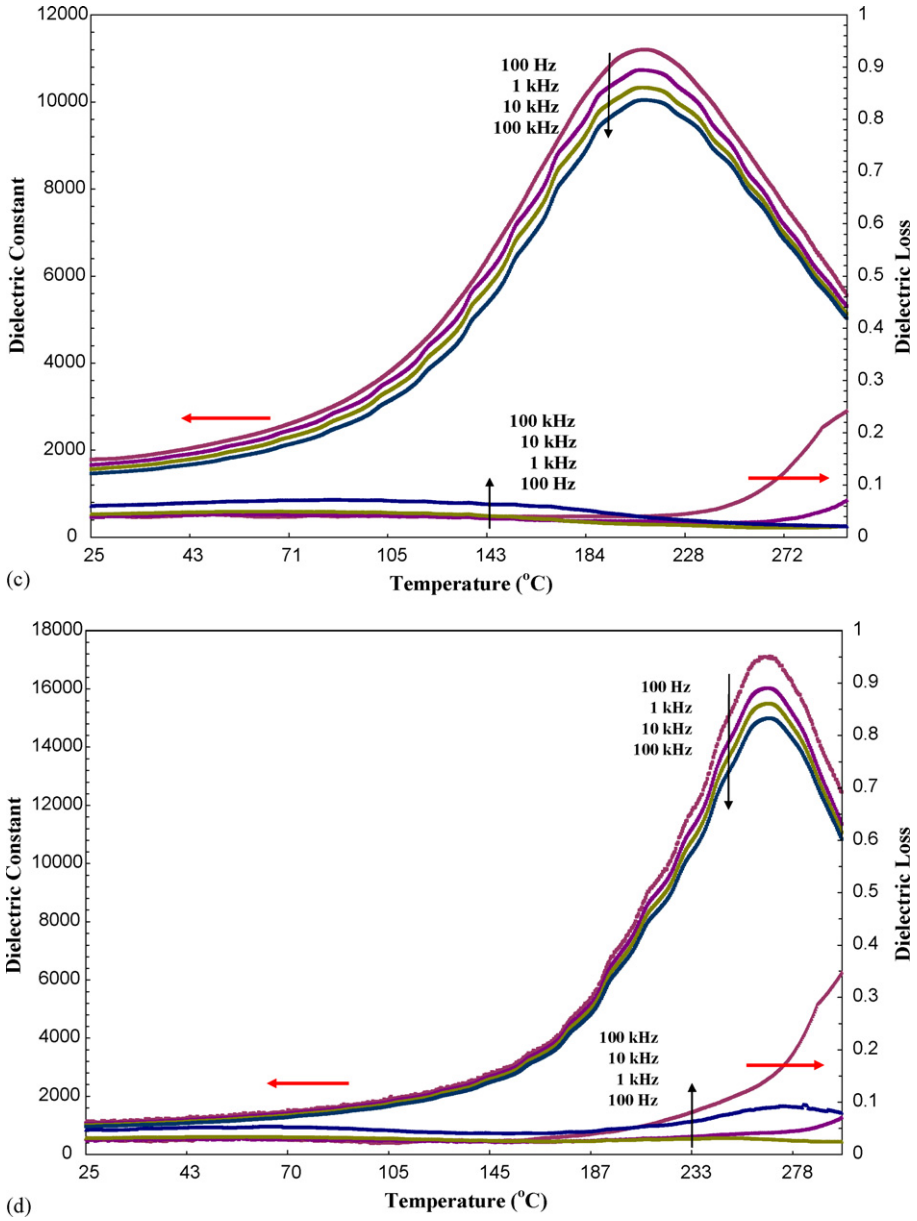

Fig. 3. (*Continued*)

as a result of thermally activated space charge conduction [26].

The dielectric properties of PIN ceramic, as plotted in Fig. 3(a), change significantly with temperature and frequency. Both dielectric constant (ε_r) and dielectric loss tangent ($\tan\delta$) exhibit strong temperature-frequency dependence below the transition temperature, indication of a typical relaxor ferroelectric behavior. In this case, the temperatures of maximum dielectric constant and dielectric loss tangent are shifted to higher temperature with increasing frequency. The maximum value of the dielectric constant decreases with increasing frequency, while that of the dielectric loss tangent increases. The dielectric properties then become frequency independence above the transition temperature [2,26]. While PIN exhibits a relaxor ferroelectric behavior, PT is a normal ferroelectric with nearly frequency-independent dielectric properties [27]. When PT is added to form the binary system with PIN, the dielectric behavior of PIN–PT should shift towards that of normal ferroelectric materials. As seen in Fig. 3(b)–(f), the dielectric properties exhibit a mixture of both normal and relaxor characteristics, in which the transition temperature is not shifted with frequency as much as for the PIN ceramic and the dielectric properties exhibit weaker temperature-frequency dependence below the transition temperature. This frequency dispersion in the dielectric properties can be quantified with $\Delta T = T_{m,100\,kHz} - T_{m,100\,Hz}$, which can be used as a rough estimate for more relaxor behavior with higher ΔT. As listed in Table 1, an addition of PT results in smaller ΔT. These results indicate the decreasing of relaxor behavior with increasing PT content [28]. Consequently, the dielectric peaks have become sharper with increasing PT content. Similar tendency has also been observed in several prior investigations [4–7,9,11].

Author's personal copy

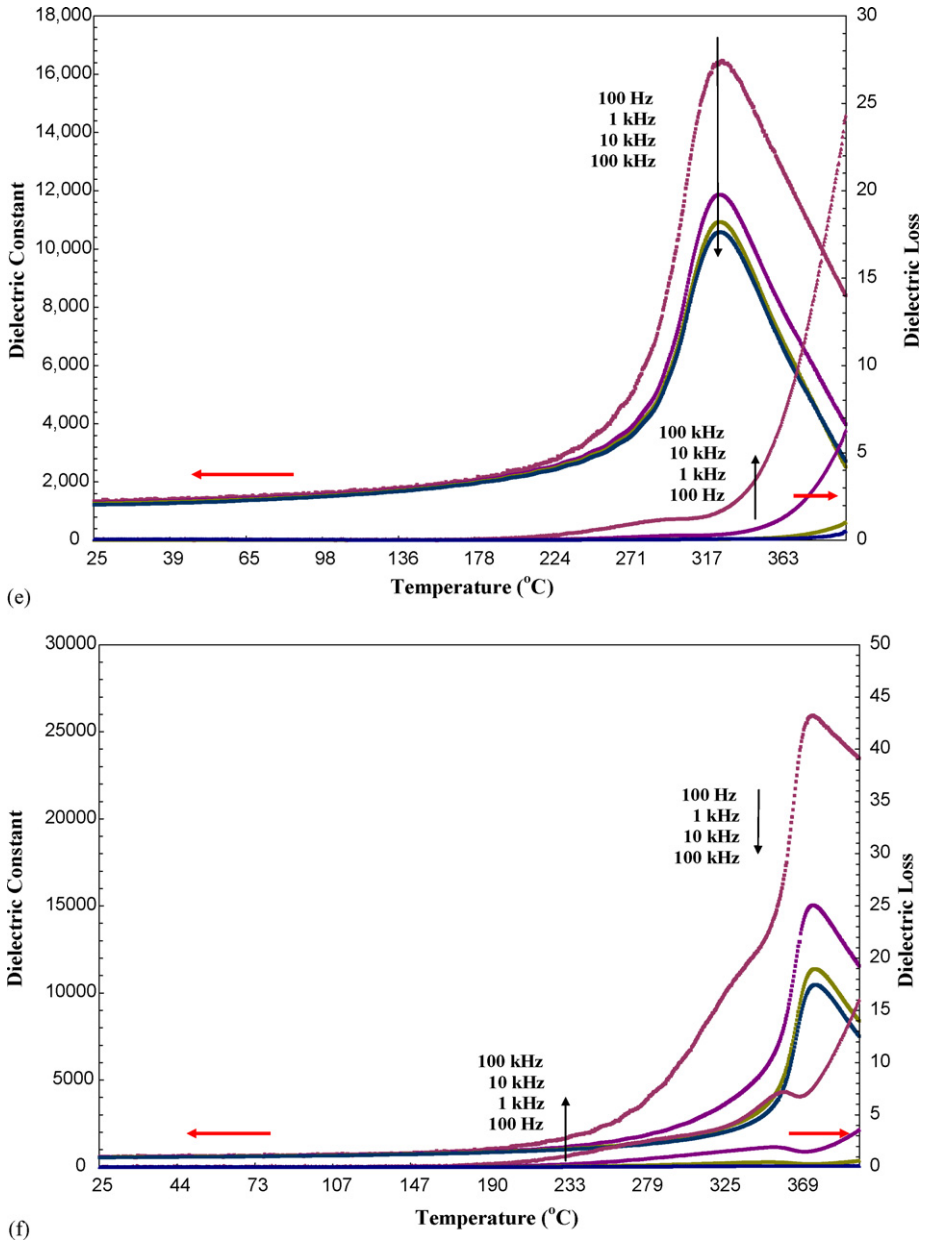

Fig. 3. (*Continued*).

The degree of broadening or diffuseness in the observed dielectric variation could also be estimated with the diffusivity (γ) using the expression $\ln(1/\varepsilon_r - 1/\varepsilon_{max})$ versus $(T - T_{max})^{\gamma}$. The value of γ can vary from 1, for normal ferroelectrics with a normal Curie–Weiss behavior, to 2, for completely disordered relaxor ferroelectrics [6,26]. The values of γ listed in Table 1 vary between 1.89 and 1.62, which confirms that diffuse phase transitions (DPT) occur in PIN–PT ceramics with a high degree of disorder. This observation clearly quantifies the decreasing of relaxor behavior with increasing PT content, as discussed earlier. Decreasing trend of γ value with increasing of PT content observed in PIN–PT system agrees with the previous study [29].

The dependence of temperature of maximum dielectric constant (T_m) on frequency of PIN–PT system can be explained with Vogel–Fulcher equation:

$$\varpi = f_0 \exp\left[\frac{-E_a}{k(T_m - T_f)}\right] \quad (1)$$

where f_0, E_a and T_f are the Debye frequency, the activation energy and the static freezing temperature, respectively [30]. The Debye frequency, the activation energy and the static freezing temperature obtained by fitting the experimental data with Eq. (1) are listed in Table 2. From Eq. (1), it is known that the activation energy is an internal energy of the cluster, which concerns with an anisotropy energy, K_{anis} and the cluster volume, V [31]. The fitting results show that the activation energy increases with increasing PT content for PIN–PT system, indicating that PT induces the increasing of the anisotropy energy and the cluster

Author's personal copy

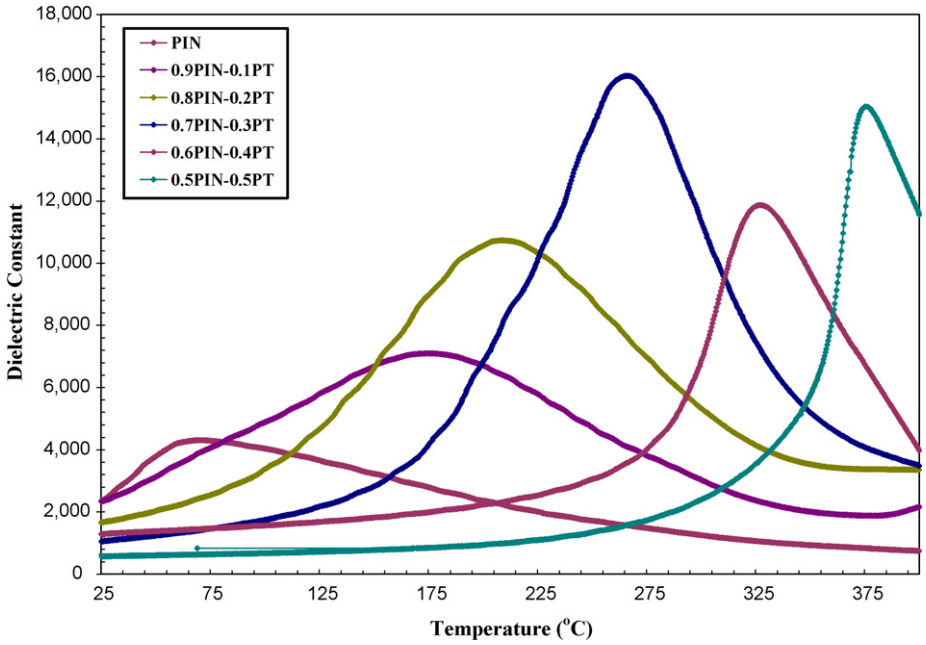

Fig. 4. Temperature dependence of dielectric constant of $(1-x)$PIN–xPT ceramics (measured at 1 kHz).

volume. It can be implied that size of isolated cluster or ordering increase with increasing PT contents [30,31]. For relaxor ferroelectrics, the value of Debye frequency concerns with size of polar nano-region and interaction between polar nano-regions [30]. In general, the stronger interaction and larger size show the smaller of the Debye frequency value [31]. Therefore, it can be implied that the increasing PT content shows marked effect in decreasing relaxor behavior by increasing size of and interaction between polar nano-regions, in good agreement with the observations discussed earlier. Similar observation has also been reported in other relaxor-based systems [32].

Fig. 5 illustrates a series of polarization (P–E) hysteresis loops for the PIN–PT ceramics. It is clearly evident that the shape of P–E loops varies greatly with the ceramic compositions. The hysteresis curve of PIN ceramic is of a "slim" loop type, a characteristic of the suppressed ferroelectric interaction [2,26]. This is typically found in the relaxor ferroelectrics with polar nano-regions. The hysteresis loops of PIN–PT ceramics become more developed showing large remnant polarization (P_r: remaining polarization when electric field is decreased to zero) and large saturated polarization (P_s) with increasing PT content up to 30 mol%. The hysteresis loops are of a typical "square" form as a result of domain switching in an applied field. This is a typical characteristic of a phase that contains long-range interaction between dipoles in the ferroelectric micro-domain state [26]. From the loops, the polarizations (P_r and P_s) and the coercive field E_C (indicating an electric field required to zero the polarization) are determined and listed in Table 3. In addition, the ferroelectric characteristic of the ceramics can be assessed with the hysteresis loop squareness (R_{sq}) which is typically understood to be the ratio of P_r/P_s where P_r is the remnant polarization at zero electric field and P_s is the saturated polarization obtained at some finite field strength below the dielectric breakdown. Jin et al. [33] used the loop squareness to measure not only the deviation in the polarization axis but also that in the electric field axis with the empirical expression $R_{sq} = (P_r/P_s) + (P_{1.1E_c}/P_r)$, where $P_{1.1E_c}$ is the polarization at the field equal to $1.1E_c$. For the ideal square loop, R_{sq} is equal to 2.00. As listed in Table 3, the value of R_{sq} increases with increasing PT content up to 30 mol%.

These results clearly indicate that an addition of PT induces the normal ferroelectric behaviors of PT into the PIN–PT ceramic system. More interestingly, it should also be noticed that a conclusion drawn from the XRD analysis and dielectric properties measurements discussed earlier that the MPB composition should exist between $x = 0.3$ and 0.4 is supported further

Table 2
The parameters obtained from fitting Vogel–Fulcher equation for $(1-x)$PIN–xPT ceramics

x	T_f (K)	f_0 (Hz)	E_a (eV)
0.0	310	3.9×10^{10}	0.042
0.1	434	3.0×10^{10}	0.015
0.2	471	2.8×10^{10}	0.010
0.3	535	2.6×10^{10}	0.004
0.4	599	2.3×10^{10}	0.002
0.5	649	1.4×10^{10}	0.001

Table 3
Ferroelectric properties of $(1-x)$PIN–xPT ceramics

x	Ferroelectric properties (at 25 °C)			Loop squareness (R_{sq})
	P_r (μC/cm^2)	P_s (μC/cm^2)	E_C (kV/cm)	
0.0	–	–	–	–
0.1	6.46	14.25	6.57	0.73
0.2	15.52	19.63	9.47	1.31
0.3	20.43	27.05	8.58	0.97
0.4	5.65	11.99	11.68	0.59
0.5	1.28	3.75	8.70	0.46

Author's personal copy

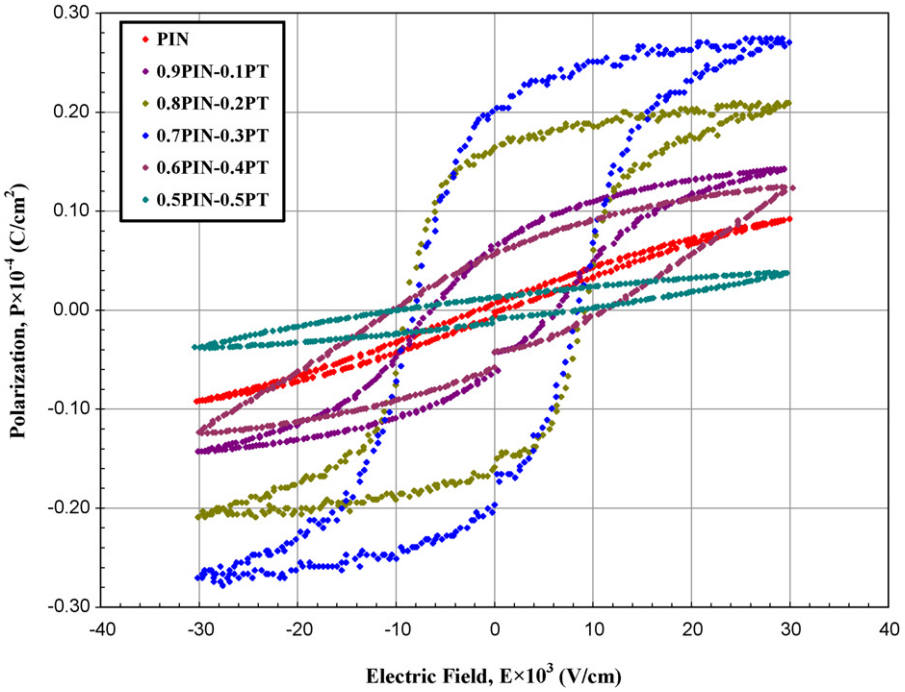

Fig. 5. *P–E* hysteresis loops of $(1-x)$PIN–xPT ceramics.

by the ferroelectric properties, as seen from a strong enhancement of polarization values with increasing PT content up to $x=0.3$, then a sudden drop of the polarization values with further increase in PT content. Finally, it is worthy noting that the fine grains PIN–PT ceramics obtained via the vibro-milling technique used in this study yield slightly better dielectric properties than the coarse grains PIN–PT ceramics in previous investigations [10–13]. However, as only very few investigations have been performed on PIN–PT ceramics, further investigations are still needed for more thoroughly and better comparison.

4. Conclusion

The $(1-x)Pb(In_{1/2}Nb_{1/2})O_3$–$xPbTiO_3$ (when $x=0.1$, 0.2, 0.3, 0.4, and 0.5) ceramics were prepared by an oxide-mixing method via a vibro-milling technique. The dielectric properties of the ceramics were determined as functions of both temperature and frequency with an automated dielectric measurement system, while the room temperature ferroelectric properties were measured by means of a standardized ferroelectric test system. The dielectric measurement took place over the temperature range of 25 and 400 °C with measuring frequency between 100 Hz and 100 kHz. Fine grains ceramics were achieved with average grain size of 1–2 μm, indicating advantage of the vibro-milling technique used. The results indicated that the dielectric properties of PIN ceramic were of relaxor ferroelectric behavior. The dielectric properties of PIN–PT ceramics showed a mixed relaxor and normal ferroelectric behavior, with more normal ferroelectric behavior observed with increasing PT content. The *P–E* hysteresis loop measurements demonstrated that the ferroelectric properties of the ceramics in PIN–PT system changed from the relaxor ferroelectric behavior in PIN ceramic to the normal ferroelectric behavior in PIN–PT ceramics. These results clearly show the significance of the added PT in reducing the relaxor ferroelectric behavior in PIN ceramic. More interestingly, XRD analysis, and dielectric and ferroelectric properties measurements also indicated the existence of the MPB composition between $x=0.3$ and 0.4. Finally, the fine grains PIN–PT ceramics showed slightly better dielectric properties than the coarse grains ceramics in previous investigations.

Acknowledgments

The authors would like to express their gratitude for financial supports from the Thailand Research Fund (TRF), Commission on Higher Education (CHE), Graduate School and Faculty of Science of Chiang Mai University, and Ministry of University Affairs in Thailand.

References

[1] K. Uchino, Ferroelectric Devices, Marcel Dekker, New York, 2000.
[2] G.H. Haertling, J. Am. Ceram. Soc. 82 (1999) 797–818.
[3] L.E. Cross, Mater. Chem. Phys. 43 (1996) 108–115.
[4] S.E. Park, T.R. Shrout, J. Appl. Phys. 82 (1997) 1804–1811.
[5] J. Kuwata, K. Uchino, S. Nomura, Jpn. J. Appl. Phys. 21 (1982) 1298–1302.
[6] R. Yimnirun, Int. J. Mod. Phys. B, in press.
[7] G. Xu, H. Luo, Y. Guo, Y. Gao, H. Xu, Z. Qi, W. Zhong, Z. Yin, Solid State Commun. 120 (2001) 321–324.
[8] N. Yasuda, H. Ohwa, M. Kume, Y. Yamashita, Jpn. J. Appl. Phys. 39 (2000) 5586–5588.
[9] N. Yasuda, H. Ohwa, D. Hasegawa, H. Hosono, Y. Yamashita, M. Iwata, Y. Ishibashi, Ferroelectrics 270 (2002) 247–252.
[10] M. Pham-Thi, C. Augier, H. Dammak, P. Gaucher, Ultrasonics 44 (2006) e627–e631.
[11] C. Augier, M. Pham-Thi, H. Dammak, P. Gaucher, J. Eur. Ceram. Soc. 25 (2005) 2429–2432.

Author's personal copy

[12] Y. Guo, H. Luo, T. He, Z. Yin, Solid State Commun. 123 (2002) 417–420.
[13] E.F. Alberta, A.S. Bhalla, J. Phys. Korea 32 (1998) s1265–s1269.
[14] N. Yasuda, M. Sakaguchi, Y. Itoh, H. Ohwa, Y. Yamashita, M. Iwata, Y. Ishibashi, Jpn. J. Appl. Phys. 42 (2003) 6205–6208.
[15] N. Yasuda, H. Ohwa, M. Kume, K. Hayashi, Y. Hosono, Y. Yamashita, J. Cryst. Growth 229 (2001) 299–304.
[16] B. Jaffe, W.R. Cook, H. Jaffe, Piezoelectric Ceramics, Academic Press, New York, 1971.
[17] Y.H. Xu, Ferroelectric Materials and their Applications, North Holland, Los Angeles, 1991.
[18] R. Wongmaneerung, R. Yimnirun, S. Ananta, Mater. Lett. 60 (2006) 2666–2671.
[19] R. Wongmaneerung, T. Sarnkonsri, R. Yimnirun, S. Ananta, Mater. Sci. Eng. B 130 (2006) 246–253.
[20] A. Ngamjarurojana, O. Khamman, R. Yimnirun, S. Ananta, Mater. Lett. 60 (2006) 2867–2872.
[21] S. Wongsaenmai, R. Yimnirun, S. Ananta, Mater. Lett., in press.
[22] E.F. Alberta, A.S. Bhalla, Mater. Lett. 29 (1996) 127–129.
[23] R. Wongmaneerung, R. Yimnirun, S. Ananta, Mater. Lett. 60 (2006) 1447–1452.
[24] S. Wongsaenmai, R. Yimnirun, S. Ananta, J. Mater. Sci., in press.
[25] S. Wongsaenmai, O. Khamman, S. Ananta, R. Yimnirun, J. Electroceram., in press.
[26] L.E. Cross, Ferroelectrics 76 (1987) 241–267.
[27] R. Wongmaneerung, R. Yimnirun, S. Ananta, Appl. Phys. A 86 (2007) 249–255.
[28] C. Lei, K. Chen, X. Zhang, J. Wang, Solid State Commun. 123 (2002) 445–450.
[29] M. Kuwabara, S. Takahashi, K. Goda, K. Oshima, K. Watanabe, Jpn. J. Appl. Phys. 31 (1992) 3241–3244.
[30] D. Viehland, S.-J. Jang, L.E. Cross, J. Appl. Phys. 68 (1990) 2916–2921.
[31] D. Viehland, S.-J. Jang, L.E. Cross, M. Wutting, Phys. Rev. B 46 (1992) 8003–8006.
[32] G. Singh, V.S. Triwari, V.K. Waghawan, Solid State Commun. 129 (2004) 665–670.
[33] B.M. Jin, J. Kim, S.C. Kim, Appl. Phys. A 65 (1997) 53–56.

Phys. Scr. **77** (2008) 045702 (4pp) doi:10.1088/0031-8949/77/04/045702

Dielectric properties of PZT–PCN ceramics under compressive stress

Muangjai Unruan, Anurak Prasatkhetragarn, Yongyut Laosiritaworn, Supon Ananta and Rattikorn Yimnirun

Department of Physics, Faculty of Science, Chiang Mai University, Chiang Mai, 50200, Thailand

E-mail: rattikornyimnirun@yahoo.com

Received 16 November 2007
Accepted for publication 12 March 2008
Published 3 April 2008
Online at stacks.iop.org/PhysScr/77/045702

Abstract

In this study, ceramics in PZT–PCN systems with a formula $(1-x)Pb(Zr_{1/2}Ti_{1/2})O_3$–$(x)Pb(Co_{1/3}Nb_{2/3})O_3$ ($x = 0.1$–0.5) were prepared by a solid-state mixed-oxide technique. The phase formation and microstructure were studied using x-ray diffraction (XRD) and scanning electron microscopy (SEM), respectively. Effects of compressive stress on the dielectric properties of PZT–PCN ceramics were investigated at stress up to 230 MPa using a compressometer. The results clearly showed that the dielectric constant of the PZT–PCN ceramics increased significantly with increasing applied stress, while the dielectric loss tangent showed an opposing trend. The experimental observations have been attributed to a combination of the domain switching and the deaging mechanisms from the application of the compressive stress.

PACS numbers: 77.80.−e, 77.80.Fm, 77.84.−s

(Some figures in this article are in colour only in the electronic version.)

1. Introduction

A family of ferroelectric materials which are of great interest due to their high polarizability is lead-based relaxor ferroelectrics. Much attention for this type of material has been focused on lead magnesium niobate ($Pb(Mg_{1/3}Nb_{2/3})O_3$ or PMN), which is widely accepted as a prototype for relaxor material. However, there is a series of relaxor materials based on $Pb(B_{1/3}Nb_{2/3})O_3$ system that also possesses interesting properties. This current study is focused on lead cobalt niobate ($Pb(Co_{1/3}Nb_{2/3})O_3$ or PCN). However, the temperature related to the maximum dielectric constant (T_{max}) of PCN in relaxor phase is very low ($T_{max} = -70\,^{\circ}C$). Thus, in order to increase T_{max} of PCN, lead zirconate titanate ($PbZr_{0.5}Ti_{0.5}O_3$ or PZT) was added to PCN to form a solid solution of PZT–PCN ceramics. The solid solutions between PZT and PCN are expected to synergistically combine the properties of both normal ferroelectric PZT and relaxor ferroelectric PCN, which could exhibit better piezoelectric and dielectric properties than those of the single-phase PZT and PCN [1, 2]. Our recent investigations have already revealed very interesting electrical properties of PZT–PCN ceramic systems [3, 4]. More importantly, when used this type of material is often subjected to self-induced or external stress. Information on the material properties under stress is critical for designing and selecting material for specific applications. Earlier studies on the influence of stress on electrical properties of other systems, i.e. PMN–PT, PMN–PZT, etc [5–7] indicate the importance of this subject matter. However, there has been no study on the effects of stress on electrical properties of PZT–PCN ceramics. It is, therefore, of interest to investigate the influence of compressive stress on properties of the PZT–PCN ceramics.

2. Experimental procedure

The reagent-grade oxides of PbO, CoO, Nb_2O_5, ZrO_2 and TiO_2 (anatase-structure) were used as raw materials. The columbite $CoNb_2O_6$ and wolframite $ZrTiO_4$ precursors were used as starting materials for PZT–PCN ceramics. The $CoNb_2O_6$ and $ZrTiO_4$ powders were prepared at calcination temperatures at 1100 and 1450 °C for 2 h, respectively. In the present work, the $(1-x)Pb(Zr_{1/2}Ti_{1/2})O_3$–$(x)Pb(Co_{1/3}Nb_{2/3})O_3$ with ($x = 0.1$–0.5) compositions were prepared from $ZrTiO_4$, $CoNb_2O_6$ and PbO powders. The

 © 2008 The Royal Swedish Academy of Sciences Printed in the UK

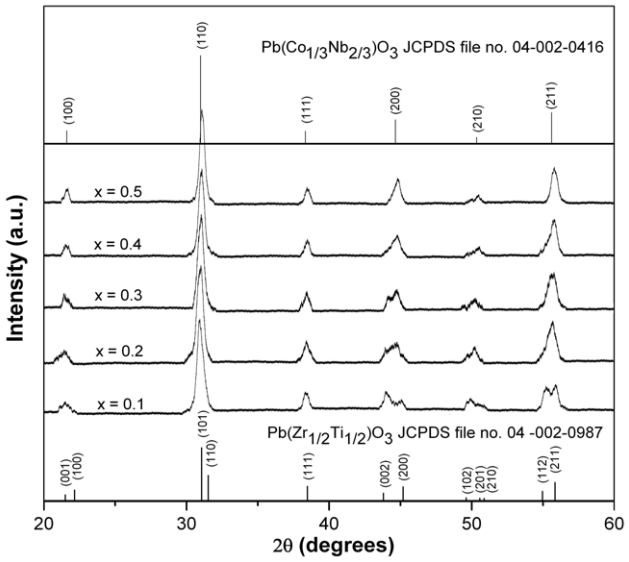

Figure 1. The XRD patterns of $(1-x)$PZT–(x)PCN ceramics.

PZT–PCN powders were synthesized by the solid-state reaction of these raw materials and mixed by the vibro-milling technique in ethanol for 1 h. A constant PbO excess of 2.0 mol.% was added to compensate for lead losses during calcination and sintering [8]. After drying, the product was calcined in alumina crucibles at temperatures between 900 and 950 °C. The calcined powders were pressed hydraulically to form disc-shape pellets 10 mm in diameter and 1 mm thick, with 1 wt.% polyvinyl alcohol (PVA) added as a binder. The pellets were sintered at 1200 °C for 2 h with heating/cooling rates 5 °C min^{-1}. The phase structure of the powders was analyzed by x-ray diffraction (XRD; Siemens-D500 diffractometer) using the CuK_α radiation. The microstructures of the sintered samples were examined using scanning electron microscopy (SEM; JEOL JSM-840A).

For dielectric property characterizations under compressive stress, the sintered samples were lapped to obtain parallely faced disc-shaped specimens, and the faces were then coated with silver paint as electrodes. To study the effects of the compressive stress on the dielectric properties, a compressometer was employed [7, 9]. Measurements were performed as a function of mechanical stress applied discretely between 0 and 230 MPa. The measurements were carried out on the samples for loading and unloading conditions. During the measurements, a desired stress was first applied to the sample and the dielectric properties were then recorded. The dielectric properties were measured through the LCR-meter (Instrek LCR-821). The room temperature (25 °C) capacitance and the dielectric loss tangent were obtained at a frequency of 1 kHz under compressive stress up to 230 MPa. The dielectric constant was then calculated from a parallel-plate capacitor equation, e.g. $\varepsilon_r = \text{Cd}/\varepsilon_0\text{A}$, where C is the capacitance of the specimens, d and A are, respectively, the thickness and the area of the electrode, and ε_0 is the dielectric permittivity of vacuum (8.854×10^{-12} F m^{-1}).

3. Results and discussion

The XRD patterns of $(1-x)$PZT–(x)PCN ceramics with various x values are shown in figure 1. It can be seen that a complete crystalline solution of perovskite structure is formed throughout the whole composition range without the presence of pyrochlore or unwanted phases. From the patterns, $\text{Pb}(\text{Zr}_{1/2}\text{Ti}_{1/2})\text{O}_3$ ceramic is identified as a single-phase material with a perovskite structure having tetragonal symmetry which could be matched with ICDD file no. 04-002-0987. The XRD patterns of the PZT–PCN compositions show a combination between PZT and PCN patterns, showing a perovskite structure having symmetry varying between tetragonal and pseudo-cubic types [3, 4]. For better comparison, the ICDD file no. 04-002-0416 for $\text{Pb}(\text{Co}_{1/3}\text{Nb}_{2/3})\text{O}_3$ with a pseudo-cubic structural symmetry is also displayed in figure 1. More interestingly, the composition with $x = 0.3$ exhibited broadening of peaks at $2\theta \sim 44$–$45°$, indicating the structural transformation from the tetragonal phase, characterized by (002)/(200) peaks, to the pseudo-cubic phase. This observation is obviously associated with the composition with coexistence of two symmetries, which in this case are tetragonal and pseudo-cubic phases. To a first approximation, it could be said that the composition with $x = 0.3$ is close to the morphotropic phase boundary (MPB) of he $(1-x)$ $\text{Pb}(\text{Zr}_{1/2}\text{Ti}_{1/2})\text{O}_3$–$(x)\text{Pb}(\text{Co}_{1/3}\text{Nb}_{2/3})\text{O}_3$ system, where the structure of the PZT–PCN compositions is gradually changing from tetragonal to pseudo-cubic phases [3, 4].

SEM micrographs in figure 2 reveal that the PCN-modification increases degrees of grain close-packing behavior of PZT ceramics. Some grains are observed to have irregular shapes with both open and closed pores as a result of a high rate of evaporation of PbO during the sintering process [8].

The micrographs also show that the grain size of the ceramics varies considerably from <0.47 to 19.6 μm. Furthermore, the average grain size decreases significantly with increasing PCN in the ceramic compositions. It can also be noticed that the maximum density is obtained in 0.7PZT–0.3PCN ceramics, while the minimum density is observed in 0.5PZT–0.5PCN ceramics. Interestingly, the density results can be correlated to the microstructure as high-density 0.7PZT–0.3PCN ceramics show high degrees of grain close packing, whereas low-density 0.5PZT–0.5PCN ceramics contain many pores.

The experimental results of the compressive stress dependence of the dielectric properties of the ceramics in the PZT–PCN system are shown in figures 3 and 4. There is a significant change of both the dielectric constant and the dielectric loss tangent of the ceramics when the applied stress increases from 0 to 230 MPa. The changes of the dielectric constant with the applied stress can be divided into three different groups. For PZT-rich compositions (0.9PZT–0.1PCN and 0.8PZT–0.2PCN), the dielectric constant increases with applied stress. It can be seen that the dielectric constant is enhanced by approximately 10% at 230 MPa applied stress. For the compositions near MPB of the $(1-x)\text{Pb}(\text{Zr}_{1/2}\text{Ti}_{1/2})\text{O}_3$–$(x)\text{Pb}(\text{Co}_{1/3}\text{Nb}_{2/3})\text{O}_3$ system, the dielectric constant increases more than other compositions with the increasing applied stress. The changes in the dielectric constant 30% at 230 MPa applied stress are obviously higher than that observed in PZT-rich compositions. For PCN-rich composition (0.5PZT–0.5PCN), the dielectric

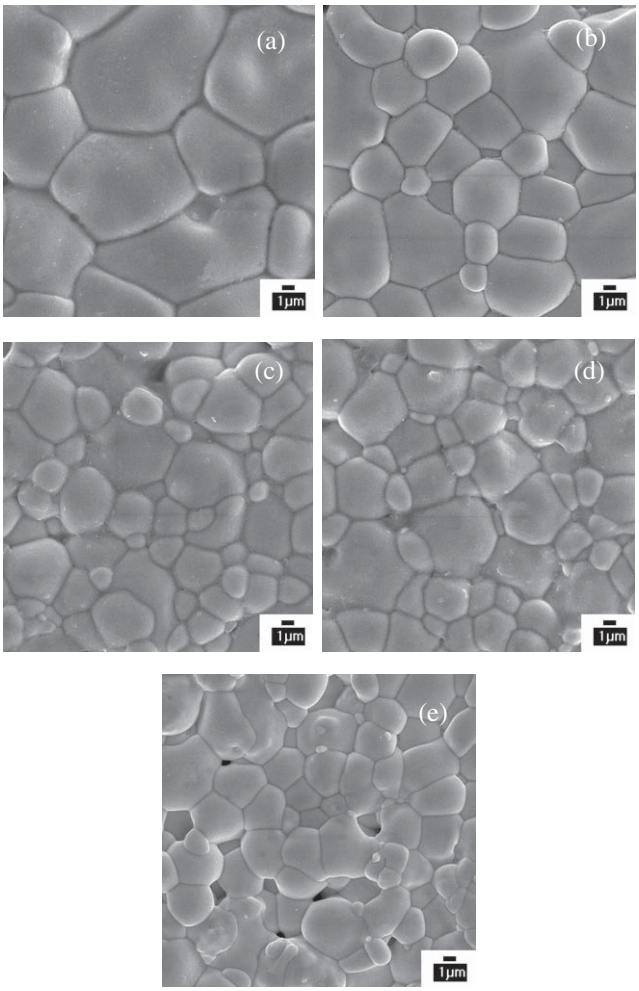

Figure 2. SEM micrographs of $(1-x)$PZT–(x)PCN with various compositions: (a) $x = 0.1$, (b) $x = 0.2$, (c) $x = 0.3$, (d) $x = 0.4$ and (e) $x = 0.5$.

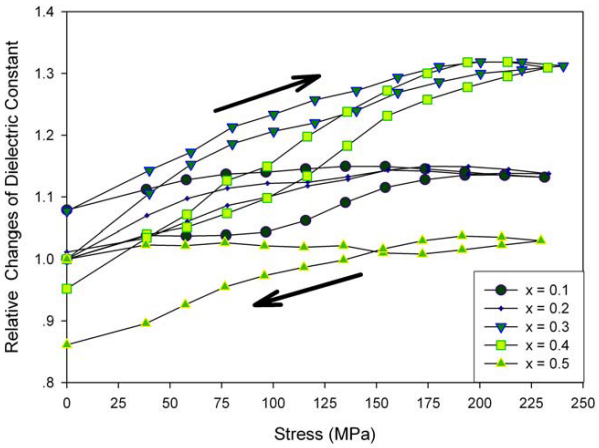

Figure 3. Relative changes of the dielectric constant as a function of compressive stress for $(1-x)$PZT–(x)PCN ceramics.

constant rises only slightly (<3%) when the applied stress increases to the maximum amplitude. The dielectric loss tangent for all compositions is found to decrease significantly and linearly when the applied stress is raised from 0 to 230 MPa. The largest changes occur in PZT-rich compositions (0.9PZT–0.1PCN and 0.8PZT–0.2PCN) with

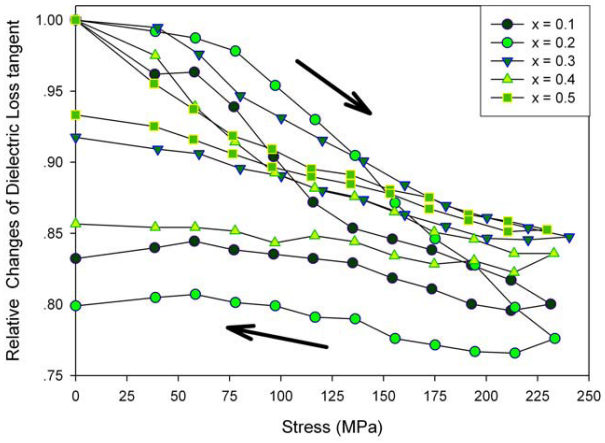

Figure 4. Relative changes of the dielectric loss tangent as a function of compressive stress for $(1-x)$PZT–(x)PCN ceramics.

the dielectric loss tangent decreasing nearly by 20%. For other compositions, the dielectric loss tangent decreased nearly 15% at 230 MPa applied stress.

To understand these experimental results, various effects have to be considered. Normally, the properties of ferroelectric materials are derived from both the intrinsic contribution, which is the response from a single domain, and extrinsic contributions, which are from domain wall motions [10–12]. When a mechanical stress is applied to a ferroelectric material, the domain structure in the material will change to maintain the domain energy at a minimum; during this process some of the domains engulf other domains or change shape irreversibly. Under a stress, the domain structure of ferroelectric ceramics may undergo domain switching, clamping of domain walls, de-aging and de-poling [13, 14]. In this study, the results on the compressive stress dependence of the dielectric properties can easily be explained with the above statements. When the compressive stress is applied in the direction parallel to the polar axis direction, the stress will move some of the polarization away from the polar axis direction resulting in a change in domain structures [10–13]. This change increases the non-180° domain wall density. Hence the increase of the dielectric constant with the applied stress is observed. The de-aging mechanism is also expected to play a role here [10, 12]. Therefore, a combination of the domain switching and the de-aging mechanisms is believed to be a reason for the increase of the dielectric constant with increasing applied stress in the PZT–PCN system, as shown in figure 3. The stress dependence of the dielectric loss tangent, as depicted in figure 4 is caused by the stress-induced de-aging mechanism. The de-aging in the materials normally causes the decrease of the dielectric loss tangent observed in some compositions [11]. This is an irreversible effect with the dielectric constant and dielectric loss tangents not returning to their original values after a stress cycle, as seen in figures 3 and 4.

4. Conclusions

In this study, ceramics in the $(1-x)$Pb$(Zr_{1/2}Ti_{1/2})O_3$–(x)Pb$(Co_{1/3}Nb_{2/3})O_3$ system (when $x = 0.1$–0.5) were successfully prepared by a solid-state mixed-oxide technique (the columbite–wolframite precursor method). PZT ceramic

was identified by XRD as a single-phase material with a perovskite structure having tetragonal symmetry, while the mixed compositions showed a gradual change from tetragonal to pseudo-cubic symmetry, with a possible MPB between the two phases near the 0.7PZT–0.3PCN composition. The dielectric properties under the compressive stress of the PZT–PCN ceramics are observed at stress levels up to 230 MPa using a compressometer. The results clearly show that the dielectric constant of the PZT–PCN ceramics increase significantly with increasing applied stress. Larger changes in the dielectric properties with the applied stress are observed in the compositions near MPB of the $(1-x)Pb(Zr_{1/2}Ti_{1/2})O_3-(x)Pb(Co_{1/3}Nb_{2/3})O_3$ system. However, the dielectric loss tangent of all compositions decreases with increasing applied stress. This study shows that the applied stress has significant influences on the dielectric properties of the PZT–PCN ceramics.

Acknowledgments

This work was supported by the Commission on Higher Education (CHE), Thailand Research Fund (TRF), Royal Golden Jubilee PhD. Program, the Faculty of Science and the Graduate School of Chiang Mai University.

References

[1] Kudo T, Yazaki T, Naito F and Sugaya S 1970 *J. Am. Ceram. Soc.* **53** 326
[2] Hachiga T, Fujimoto S and Yasuda N 1987 *J. Phys. D: Appl. Phys.* **20** 1291
[3] Vittayakorn N, Wirunchit S, Traisak S, Yimnirun R and Rujijanagul G 2008 *Curr. Appl. Phys.* **8** 128
[4] Prasartkhetragarn A, Vittayakorn N, Ananta S, Yimnirun R and Cann D P 2008 *Japan J. Appl. Phys.* **47** 998
[5] Yimnirun R, Unruan M, Laosiritaworn Y and Ananta S 2006 *J. Phys. D: Appl. Phys.* **39** 3097
[6] Triamnak N, Unruan M, Ananta S and Yimnirun R 2007 *J. Electroceram.* at press
[7] Yimnirun R, Ananta S, Meechoowas E and Wongsaenmai S 2003 *J. Phys. D: Appl. Phys.* **36** 1615
[8] Vittayakorn N, Rujijanagul G, Tunkasiri T, Tan X and Cann D P 2004 *Mater. Sci. Eng.* B **108** 258
[9] Yimnirun R, Ananta S, Ngnamjarurojana A and Wongsaenmai S 2006 *Appl. Phys.* A **6** 520
[10] Yang G, Ren W, Liu S F, Masys A J and Mukherjee B K 2000 *Proc. IEEE Ultrason. Symp.* **2** 1005
[11] Audigier D, Richard C, Descamps C, Troccaz M and Eyraud L 1994 *Ferroelectrics* **154** 219
[12] Fritz I J 1978 *J. Appl. Phys.* **49** 4922
[13] Yang G, Liu S F, Ren W and Mukherjee B K 2000 *Proc. SPIE Symp. Smart Struct. Mater.* **3992** 103
[14] Steiner O, Tagantsev A K, Colla E L and Setter N 1999 *J. Euro. Ceram. Soc.* **19** 1243

Stress-dependent scaling behavior of subcoercive field dynamic ferroelectric hysteresis in $Pb(Zn_{1/3}Nb_{2/3})O_3$-modified $Pb(Zr_{1/2}Ti_{1/2})O_3$ ceramic

R. Yimnirun,[a] N. Wongdamnern, N. Triamnak, M. Unruan, A. Ngamjarurojana, S. Ananta, and Y. Laosiritaworn
Department of Physics, Faculty of Science, Chiang Mai University, Chiang Mai 50200, Thailand

(Received 6 February 2008; accepted 19 February 2008; published online 23 April 2008)

Scaling behavior of subcoercive field dynamic ferroelectric hysteresis under influence of stress was investigated in $Pb(Zn_{1/3}Nb_{2/3})O_3$-modified $Pb(Zr_{1/2}Ti_{1/2})O_3$ (PZT) bulk ceramic. The scaling relation of hysteresis area $\langle A \rangle$ against frequency f, field amplitude E_0, and stress σ for the minor loops takes a form of $\langle A - A_{\sigma=0} \rangle \propto f^{-0.42} E_0^{3.65} \sigma^{0.24}$, which is very similar to that of soft and hard PZT ceramics. However, slightly faster responses to f and E_0 indicate the ease of polarization orientation in this simpler domain structure ceramic as compared to commercial PZT ceramics.
© *2008 American Institute of Physics*. [DOI: 10.1063/1.2907755]

The dynamic hysteresis characteristics have become important consideration since hysteresis area $\langle A \rangle$ as a function of the field amplitude E_0 and frequency f presents lots of information critical for many ferroelectric applications.[1,2] Theoretical studies have been carried out to understand the dynamic response of hysteresis curves in spin and polarization systems.[3–7] In particular, attention is focused on scaling law

$$\langle A \rangle \propto f^m E_0^n, \tag{1}$$

where m and n are exponents that depend on the dimensionality and symmetry of the system. Based on three-dimensional models, it has been suggested that $m=1/3$ and $n=2/3$ as $f \to 0$, whereas $m=-1$ and $n=2$ as $f \to \infty$.[3,5,8] Experimental investigations on a few thin-film systems have also been reported with variation in the scaling relations obtained.[9–12] On the contrary, there are only few reports on the scaling behavior studies of ferroelectric hysteresis loops of bulk ferroelectric ceramics.[13–16] More importantly, in many applications the ceramic specimens are often subjected to mechanical loading, either from the design of the device itself or from operating conditions which induce stresses.[1,17] Therefore, a prior knowledge of how the material properties change under different load conditions in materials is inevitably crucial for proper design of a device and for suitable selection of materials for a specific application.[18–22]

Previous works on $Pb(Zn_{1/3}Nb_{2/3})O_3$ (PZN)-modified PZT (or PZN-PZT) have reported excellent electrical properties suitable for various applications.[23–25] Interestingly, transmission electron microscopy study has revealed a clear regular lamellar 90° domain configuration in 0.9PZT-0.1PZN ceramic with tetragonal symmetry.[26] Therefore, the 0.9PZT-0.1PZN ceramic was chosen for this study. Practically, ferroelectric ceramics are used under subcoercive field condition in most applications; it is therefore of interest to obtain scaling relations for such condition. This present work is aimed at obtaining the stress-dependent scaling behavior of subcoercive field dynamic ferroelectric hysteresis in 0.9PZT-0.1PZN ceramic.

The disk-shaped samples of tetragonal-structure 0.9PZT-0.1PZN ceramic with diameter of 10 mm and thickness of 1 mm were used in this study. The dynamic hysteresis (P-E) loops were characterized at room temperature (25 °C) by using a modified Sawyer–Tower circuit with f covering from 2 to 100 Hz and E_0 from 0 to 18 kV/cm. The electric field was applied to a sample by a high voltage ac amplifier (Trek 610D) with the input sinusoidal signal from a function generator (HP 3310A). The P-E loops were recorded by a digital oscilloscope (HP 54645A, 100 MHz). The detailed descriptions of this system were explained elsewhere.[21] The compressive stress, applying parallel to the electric field direction, was supplied by the servohydraulic load frame and monitored with the pressure gauge. The P-E loops were recorded as a function of mechanical stress discretely applied between 0 and 173 MPa for each applied field and frequency. At each constant stress, the loop was obtained after 20 sampling cycles to average out the noise deformation.

The hysteresis profiles for various frequencies f, field amplitude E_0, and stress σ are obtained and shown in Figs. 1(a)–1(c). For a particular applied stress, as expected, the dependence of the loop pattern and area $\langle A \rangle$ on f and E is remarkable. At fixed E_0, the loop area $\langle A \rangle$ and remnant polarization (P_r) decrease with an increase of frequency, as shown in Fig. 1(a). The dependence of the hysteresis loop on E_0 is depicted in Fig. 1(b). Similar observations have also been reported in soft and hard PZT ceramics.[27–29] In addition, the P-E loop area $\langle A \rangle$ is found to steadily decrease with increasing the stress. Several previous investigations also reported similar stress-dependent behavior.[20–22]

To obtain the suitable scaling relation for the bulk ceramic, one can first follow the suggested scaling law given in Eq. (1) to directly determine exponents m and n from the experimental data. By plotting $\langle A \rangle$ against f at fixed E_0, one obtains the exponent m. On the other hand, the exponent n can be obtained from plotting $\langle A \rangle$ against E_0 at fixed f. As plotted in Fig. 2, it is revealed that the experimental data can

[a]Author to whom correspondence should be addressed. Electronic mail: rattikornyimnirun@yahoo.com.

 © 2008 American Institute of Physics

Downloaded 27 Apr 2008 to 202.28.244.211. Redistribution subject to AIP license or copyright; see http://jap.aip.org/jap/copyright.jsp

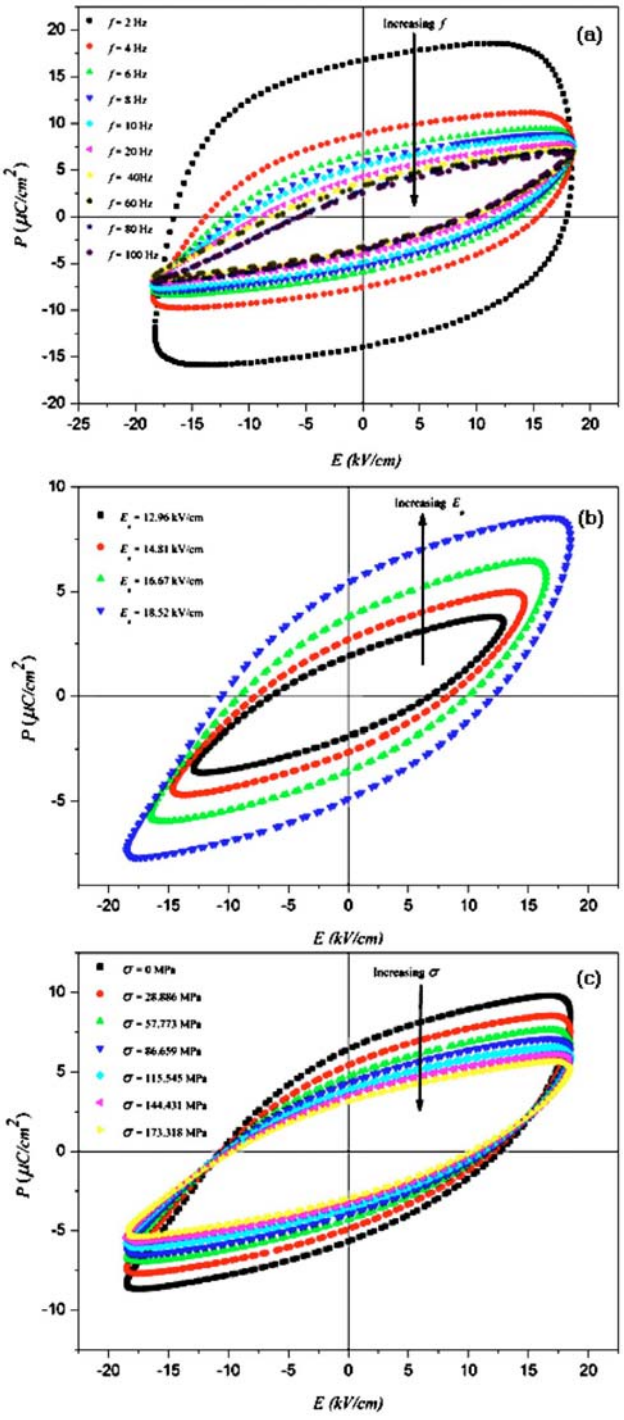

FIG. 1. (Color online) Hysteresis loops under subcoercive field condition for 0.9PZT-0.1PZN ceramic (a) at various f (E_0=18.5 kV/cm and σ =27 MPa), (b) at various E_0 (f=10 Hz and σ=27 MPa), and (c) at various σ (f=10 Hz and E_0=18.5 kV/cm).

be fitted (with R^2=0.99), within the measured uncertainty, by

$$\langle A\rangle \propto f^{-0.42}E_0^{3.65}. \tag{2}$$

Here, the first interesting observation is that the minor-loop scaling in PZN-modified PZT bulk ceramics is generally similar to that of PZT thin film,[5,9] as well as that of minor loop of PZT bulk ceramics.[13,15] As explained in our previous investigation,[13] this was attributed to the fact that

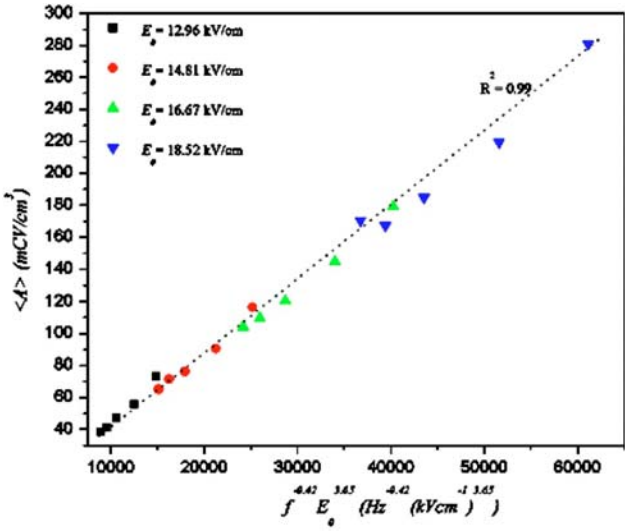

FIG. 2. (Color online) Scaling of hysteresis area $\langle A\rangle$ against $f^{-0.42}E_0^{3.65}$ for 0.9PZT-0.1PZN ceramic under subcoercive field condition.

main polarization orientation mechanism in thin films and in subcoercive field condition for bulk ceramics likely is from the 180° domain reversal. This explains why the scaling behavior of PZT bulk ceramics at low E fields is similar to that of thin films. More importantly, the scaling relation obtained in Eq. (2) indicates that $\langle A\rangle$ more quickly decays with f and more quickly grows with E_0 than the minor-loop scaling relations obtained earlier for commercial soft PZT bulk ceramic with $\langle A\rangle \propto f^{-0.33}E_0^3$.[13] This clearly indicates the ease of the polarization orientation process in tetragonal 0.9PZT-0.1PZN ceramics with a clear regular lamellar 90° domain configuration[26] that leads to faster polarization orientation kinetics, as compared to complex domain structures of commercial PZT bulk ceramics which require higher energy barrier for the polarization orientation process.

To investigate the scaling behavior under the effect of applied stresses, instead of including only the field amplitude E_0 and the frequency term f, the scaling relation should also include the stress (σ) term, i.e.,

$$\langle A\rangle \propto f^m E_0^n \sigma^p. \tag{3}$$

However, due to increasing number of exponents, to simplify the problem, the validity of the scaling law $\langle A\rangle(\sigma) \propto f^{-0.42}E_0^{3.65}$ is assumed for all applied stresses. Consequently, the area $\langle A\rangle$ for each stress is plotted against $f^{-0.42}E_0^{3.65}$, as shown in Fig. 3(a), and it can be seen from the least-square linear fits that reasonably good linear relations can be found. As a result, the condition of universality having m=−0.42 and n=3.65 in 0.9PZT-0.1PZN bulk ceramic is confirmed. Consequently, $\langle A\rangle \propto (a+b\sigma^c)f^{-0.42}E_0^{3.65}$ may be written and by substituting the fitted parameters, it is found that

$$\langle A\rangle - \langle A_{\sigma=0}\rangle = \langle A - A_{\sigma=0}\rangle \propto f^{-0.42}E_0^{3.65}\sigma^{0.24}, \tag{4}$$

where $\langle A_{\sigma=0}\rangle$ refers to stress-free hysteresis area which will be a dominant term for zero stress. The data collapsing of the scaling area from all f, E_0, and σ was found to confirm Eq. (4), as evident in Fig. 3(b). Note that from the appearance of

Downloaded 27 Apr 2008 to 202.28.244.211. Redistribution subject to AIP license or copyright; see http://jap.aip.org/jap/copyright.jsp

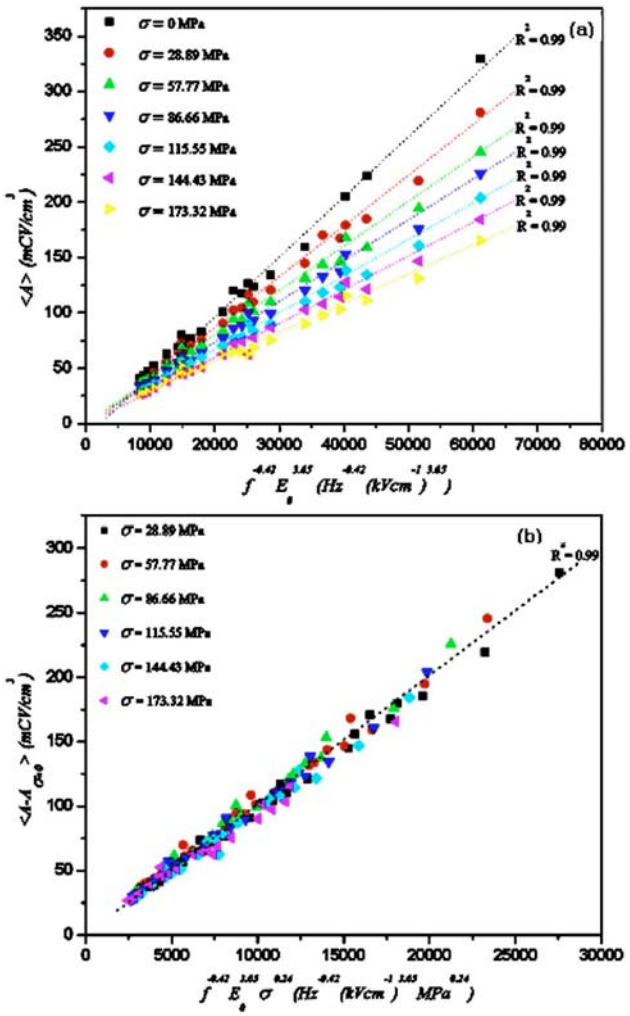

FIG. 3. (Color online) (a) Scaling of hysteresis area $\langle A \rangle$ against $f^{-0.42}E_0^{3.65}$ at various σ, (b) the collapse of the scaling area $\langle A - A_{\sigma=0} \rangle$ against $f^{-0.42}E_0^{3.65}\sigma^{0.24}$ on a same linear line (with small fluctuation) for 0.9PZT-0.1PZN ceramic under subcoercive field condition.

stress σ, $\langle A - A_{\sigma=0} \rangle$, referring to the difference in energy dissipation between understress and stress-free conditions, increases with increasing stress suggesting a decay of $\langle A \rangle$ with σ at a rate of $\sigma^{0.24}$, as observed in experiments. As a result, it can be concluded that the difference of the hysteresis area between understress and stress-free condition scales with frequency, field amplitude, and stress via exponents $m=-0.42$, $n=3.65$, and $p=0.24$. However, at a particular fixed stress, Eq. (4) gives $f^{-0.42}E_0^{3.65}$ which is the original form for how the area scales with the frequency and the field amplitude.

In summary, the scaling behavior of the subcoercive field dynamic ferroelectric hysteresis of PZN-modified PZT bulk ceramics under the effect of mechanical stress has been investigated. The scaling relation for the minor loops takes the form of $\langle A - A_{\sigma=0} \rangle \propto f^{-0.42}E_0^{3.65}\sigma^{0.24}$, which is very similar to that of soft and hard PZT ceramics. However, slightly faster responses to f and E_0 indicate the ease of polarization orientation in this simpler domain structure ceramic as compared to commercial PZT ceramics. As a result, this study suggests that the domain structures play partial role in controlling dynamic hysteresis behavior of ferroelectric materials.

Financial supports from the Thailand Research Fund (TRF), Commission on Higher Education (CHE), Royal Golden Jubilee Ph.D. Program, Faculty of Science, and Graduate School of Chiang Mai University are gratefully acknowledged.

[1] K. Uchino, *Ferroelectric Devices* (Dekker, New York, 2000).
[2] O. Auciello, J. F. Scott, and R. Ramesh, Phys. Today **51**, 22 (1998).
[3] M. Rao, H. R. Krishnamurthy, and R. Pandit, Phys. Rev. B **42**, 856 (1990).
[4] M. Acharyya and B. K. Chakrabarti, Phys. Rev. B **52**, 6560 (1995).
[5] J.-M. Liu, H. L. W. Chan, C. L. Choy, Y. Y. Zhu, S. N. Zhu, Z. G. Liu, and N. B. Ming, Appl. Phys. Lett. **79**, 236 (2001).
[6] H. B. Zuo, M. F. Zhang, J. C. Han, and J. M. Liu, Mater. Lett. **61**, 2697 (2007).
[7] M. Sarjala, E. T. Seppälä, and M. J. Alava, Physica B **403**, 418 (2008).
[8] M. Rao and R. Pandit, Phys. Rev. B **43**, 3373 (1991).
[9] J.-M. Liu, H. L. W. Chan, C. L. Choy, and C. K. Ong, Phys. Rev. B **65**, 014416 (2001).
[10] B. Pan, H. Yu, D. Wu, X. H. Zhou, and J.-M. Liu, Appl. Phys. Lett. **83**, 1406 (2003).
[11] Y.-H. Kim and J.-J. Kim, Phys. Rev. B **55**, R11933 (1997).
[12] J.-H. Park, C.-S. Kim, B.-C. Choi, B. K. Moon, J. H. Jeong, and I. W. Kim, Appl. Phys. Lett. **83**, 536 (2003).
[13] R. Yimnirun, Y. Laosiritaworn, S. Wongsaenmai, and S. Ananta, Appl. Phys. Lett. **89**, 162901 (2006).
[14] R. Yimnirun, S. Wongsaenmai, S. Ananta, and Y. Laosiritaworn, Appl. Phys. Lett. **89**, 242901 (2006).
[15] R. Yimnirun, R. Wongmaneerung, S. Wongsaenmai, A. Ngamjarurojana, S. Ananta, and Y. Laosiritaworn, Appl. Phys. Lett. **90**, 112908 (2007).
[16] R. Yimnirun, R. Wongmaneerung, S. Wongsaenmai, A. Ngamjarurojana, S. Ananta, and Y. Laosiritaworn, Appl. Phys. Lett. **90**, 112906 (2007).
[17] K. Uchino, *Piezoelectric Actuators and Ultrasonic Motors* (Kluwer Academic, Boston, 1997).
[18] J. Zhao, A. E. Glazounov, and Q. M. Zhang, Appl. Phys. Lett. **74**, 436 (1999).
[19] D. Viehland and J. Powers, J. Appl. Phys. **89**, 1820 (2001).
[20] D. Zhou, M. Kamlah, and D. Munz, J. Eur. Ceram. Soc. **25**, 425 (2005).
[21] R. Yimnirun, Y. Laosiritaworn, and S. Wongsaenmai, J. Phys. D **39**, 759 (2006).
[22] R. Yimnirun, S. Ananta, A. Ngamjarurojana, and S. Wongsaenmai, Appl. Phys. A: Mater. Sci. Process. **81**, 1227 (2005).
[23] X. P. Jiang, J. W. Fang, H. R. Zeng, B. J. Chu, G. R. Li, D. R. Chen, and Q. R. Yin, Mater. Lett. **44**, 219 (2000).
[24] H. Fan and H. E. Kim, J. Appl. Phys. **91**, 317 (2002).
[25] N. Vittayakorn, G. Rujijanagul, T. Tunkasiri, X. Tan, and D. P. Cann, J. Mater. Res. **18**, 2881 (2003).
[26] N. Vittayakorn, G. Rujijanagul, X. Tan, and D. P. Cann, J. Electroceram. **16**, 141 (2006).
[27] D. A. Hall and P. J. Stevenson, Ferroelectrics **228**, 139 (1999).
[28] J. E. Garcia, R. Perez, and A. Albareda, J. Phys. D **34**, 3279 (2001).
[29] M. Morozov, D. Damjanovic, and N. Setter, J. Eur. Ceram. Soc. **25**, 2483 (2005).

Downloaded 27 Apr 2008 to 202.28.244.211. Redistribution subject to AIP license or copyright; see http://jap.aip.org/jap/copyright.jsp

ELSEVIER

Materials Science and Engineering B 150 (2008) 12–17

MATERIALS SCIENCE & ENGINEERING B

www.elsevier.com/locate/mseb

Effect of vibro-milling time on phase formation and particle size of nickel niobate nanopowders

O. Khamman, R. Yimnirun, S. Ananta *

Department of Physics, Faculty of Science, Chiang Mai University, Chiang Mai 50200, Thailand

Received 3 December 2007; received in revised form 8 January 2008; accepted 12 January 2008

Abstract

A columbite-type phase of nickel niobate, $NiNb_2O_6$, nanopowder was synthesized by a solid-state reaction via a rapid vibro-milling technique. The effect of milling time on the phase formation and particle size of $NiNb_2O_6$ powder was investigated. Powder samples were characterized using DTA, XRD, SEM and laser diffraction techniques. It was found that the smallest particle size of 32 nm was achieved at 25 h of vibro-milling after which a higher degree of particle agglomeration was observed on continuation of milling to 35 h. In addition, by employing an appropriate choice of the milling time, a narrow particle size distribution curve was also observed.
© 2008 Elsevier B.V. All rights reserved.

Keywords: Nickel niobate; Milling; Nanopowders; Phase formation; Particle size

1. Introduction

Earlier works concerning the columbite-type nickel niobate ($NiNb_2O_6$) have been directed towards determining microwave dielectric, magnetic and optical properties [1,2]. Recently, this compound is also a potential material for the development of wireless communication and lithium batteries [3,4]. Moreover, it is well established as a key precursor for the successful preparation of single-phase ferroelectric perovskite $Pb(Ni_{1/3}Nb_{2/3})O_3$ (PNN)-based ceramics, which is becoming increasingly important for multilayer ceramic capacitor, electrostrictor, ultrasonic transducer and actuator applications [5,6].

There has been a great deal of interest in the preparation of single-phase PNN powders as well as in the sintering and electrical properties of PNN-based ceramics [7–9]. In general, the constituents NiO and Nb_2O_5 are first mixed and reacted together to form $NiNb_2O_6$, prior to mixing and reacting with PbO in the second step of calcination at elevated temperature. Interestingly, this mixed oxide route has been employed with minor modifications in the synthesis of $NiNb_2O_6$ itself [8,9]. However, powders prepared by a mixed oxide route have spatial fluctuations in their compositions. The extent of the fluctuation depends on the characteristics of the starting powders as well as on the processing schedule.

Recently, the studies of nanoparticles are also a very attractive field [10,11]. The evolution of a method to produce nanopowders of precise stoichiometry and desired properties is complex, depending on a number of variables such as starting materials, processing history, temperature, etc. The advantage of using mechanical milling for preparation of nanosized powders lies in its ability to produce mass quantities of powders in the solid-state using simple equipment and low-cost starting precursors [11]. Although some research has been done in the preparation of $NiNb_2O_6$ powders via a vibro-milling technique [8,12], to our knowledge a systematic study regarding the influence of milling time on the preparation of $NiNb_2O_6$ powders has not yet been reported. Thus, in the present study, the effect of milling time on phase formation and particle size of nickel niobate powders was investigated in this connection. The potential of the vibro-milling technique as a simple method to obtain usable quantities of single-phase nickel niobate powders at low temperature and with nanosized particles was also examined.

2. Experimental

The starting materials were commercially available nickel oxide, NiO (JCPDS file number 73-1519) and niobium oxide, Nb_2O_5 (JCPDS file number 30-873) (Aldrich, 99.9% purity).

* Corresponding author. Tel.: +66 53 943 376; fax: +66 53 943 445.
E-mail address: suponananta@yahoo.com (S. Ananta).

0921-5107/$ – see front matter © 2008 Elsevier B.V. All rights reserved.
doi:10.1016/j.mseb.2008.01.006

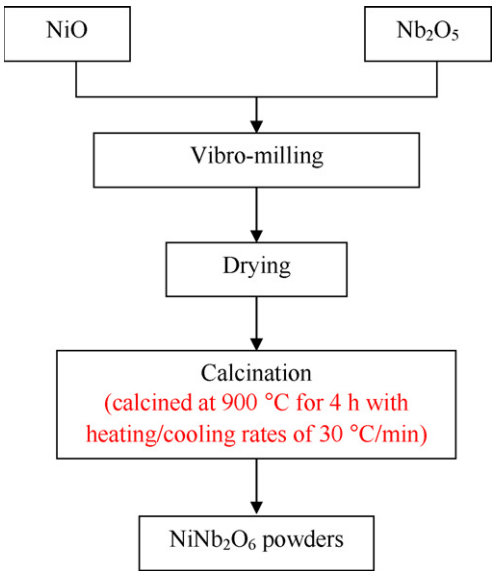

Fig. 1. Preparation route for $NiNb_2O_6$ powders.

The two oxide powders exhibited an average particle size in the range of 3.0–5.0 μm. $NiNb_2O_6$ powders were synthesized by the solid-state reaction of these raw materials. Powder-processing (Fig. 1) was carried out in a manner similar to that employed in our previous works [11–13]. A vibratory laboratory mill (McCrone Micronizing Mill) powered by a 1/30 HP motor was employed for preparing the stoichiometric $NiNb_2O_6$ powders. The grinding vessel consists of a 125 ml capacity polypropylene jar fitted with a screw-capped, gasketless, polythene closure. The jar is packed with an ordered array of identical, cylindrical, grinding media of polycrystalline corundum (instead of employing zirconia media under alcohol [8,9]). A total of 48 milling media cylinder with a powder weight of 20 g was kept constant in each batch. The milling operation was carried out in isopropanal inert to the polypropylene jar. Various milling times ranging from 0.5 to 35 h were selected in order to investigate the phase formation characteristic of nickel niobate and the smallest particle size. After drying at 120 °C for 2 h, the reaction of the uncalcined powders taking place during heat treatment was investigated by differential thermal analysis technique (DTA, Shimadzu) at a heating rate of 10 °C/min in air from room temperature up to 900 °C. Based on the DTA result and literature [8,12], the mixture was calcined at 900 °C (in closed alumina crucible) for 4 h with heating/cooling rates of 30 °C/min.

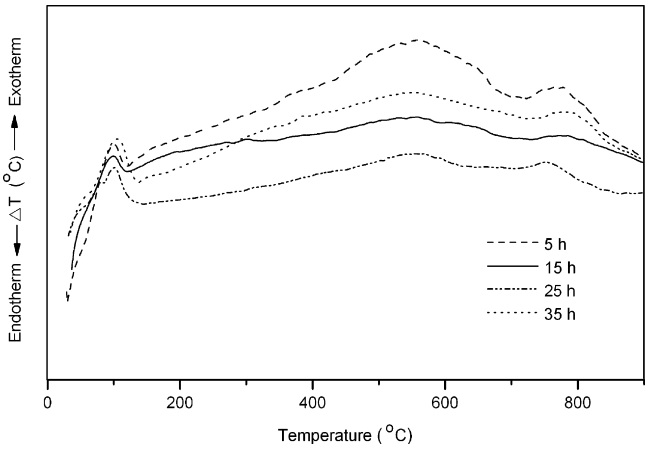

Fig. 2. DTA analysis for the mixture of NiO and Nb_2O_5 powders milled at different times.

All powders were subsequently examined by room temperature X-ray diffraction (XRD; Siemens-D500 diffractometer), using Ni-filtered Cu Kα radiation to identify the phases formed and optimum milling time for the production of $NiNb_2O_6$ powders having the smallest particle size. The relative amount of columbite and secondary phases was determined from XRD patterns of the samples by measuring the major characteristic peak intensities for the columbite (3 1 1) or I_P and secondary (+) phases or I_S. The following qualitative equation was used [14].

$$\text{Columbite phase (wt\%)} = \frac{I_P}{I_P + I_S} \times 100 \quad (1)$$

The crystalline lattice constants and average particle size were also estimated from XRD patterns [15]. The particle size distributions of the powders were determined by laser diffraction technique (DIAS 1640 laser diffraction spectrometer) with the particle sizes and morphologies of the powders observed by scanning electron microscopy (JEOL JSM-840A SEM). The particle sizes of $NiNb_2O_6$ powders milled at different times obtained from different measuring techniques are provided in Table 1.

3. Results and discussion

The DTA results for the powders milled at different times are compared and displayed in Fig. 2. In general, similar thermal characteristics are observed in all cases, consistent with

Table 1
Effect of milling time on the phase formation and particle size of $NiNb_2O_6$ powders measured by different techniques

Milling time (h)	Columbite phase (wt%)	XRD				SEM		Laser scattering	
		A (nm)	*a* (Å)	*b* (Å)	*c* (Å)	*D* (nm)	*P* (nm)	*D* (nm)	*P* (nm)
0.5	87	173.40	15.72	4.96	4.98	900	560–1400	3200	400–5000
1	92	93.69	15.50	5.00	5.02	820	500–1300	2500	320–5000
5	100	73.12	15.01	5.24	5.02	708	467–1160	1500	250–3000
15	100	59.44	14.71	5.32	5.00	545	167–949	450	250–750
25	100	34.54	15.64	4.99	4.99	120	32–164	240	40–750
35	100	20.57	15.52	5.05	5.00	250	63–570	690	45–6000

A: crystallite size; *a*, *b*, and *c*: lattice parameters; *D*: average particle size; *P*: particle size range or distribution.

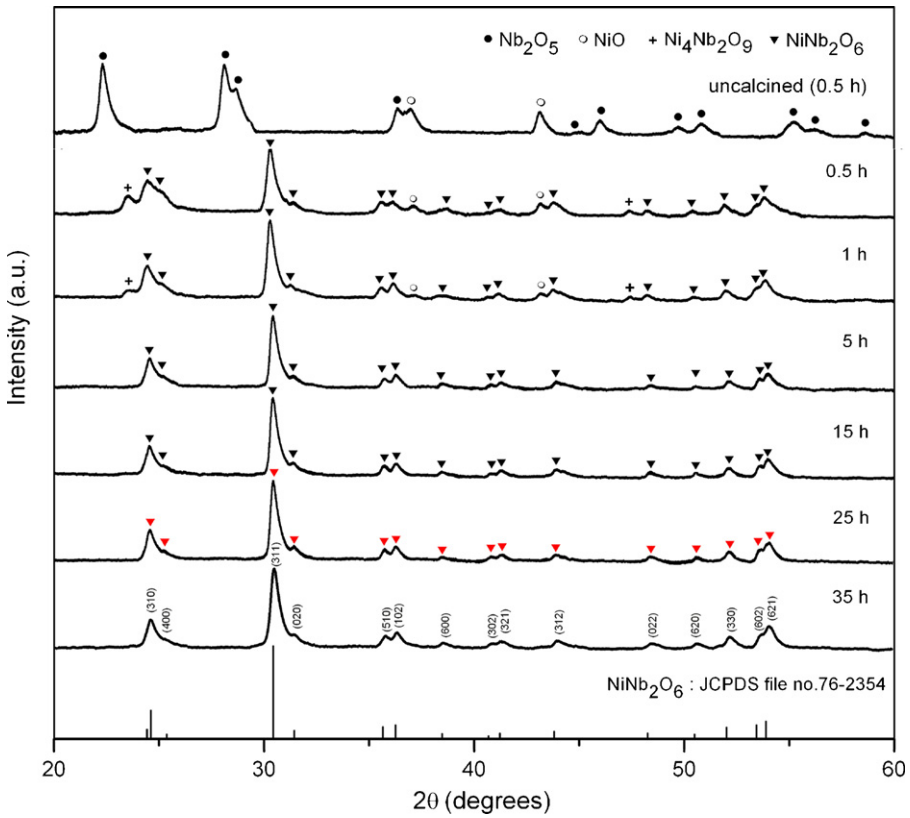

Fig. 3. XRD patterns of $NiNb_2O_6$ powders milled at different times (calcined at 900 °C for 4 h with heating/cooling rates of 30 °C/min).

our previous work [12]. In the temperature range from room temperature to ~150 °C, all samples show both exothermic and endothermic peaks in the DTA curves. These observations can be attributed to the decomposition of the organic species originating from the milling process [11–13]. Increasing the temperature up to ~900 °C, the solid-state reaction occurred between NiO and Nb_2O_5 [12,16]. The broad exotherm with several peaks in the DTA curves represents that reaction, which has a maximum at ~550 and 750 °C. The slightly different temperature, intensities and shapes of the thermal peaks for the powders are probably related to the different sizes of the powders subjected to different milling times [9,11].

To further study the effect of milling time on phase formation, each of the powders milled for different times was calcined at 900 °C for 4 h in air, followed by phase analysis using XRD. For the purpose of estimating the concentrations of the phase present, Eq. (1) has been applied to the powder XRD patterns obtained, as given in Table 1. As shown in Fig. 3, for the uncalcined powder subjected to 0.5 h of vibro-milling, only X-ray peaks of precursors NiO (◯) and Nb_2O_5 (●) are present, indicating that no reaction had been initiated during the milling process. However, after calcination, it is seen that the columbite-type $NiNb_2O_6$ becomes the predominant phase in the powder milled for 0.5 h, indicating that the reaction has occurred to a considerable extent. It is seen that traces of unreacted NiO and Nb_2O_5 precursors and corundum-type $Ni_4Nb_2O_9$ earlier reported by the authors [16] have been found along with the $NiNb_2O_6$ parent phase at a milling time of 1 h or less. This observation could be attributed mainly to the poor mixing capability under short milling time, similar with other work [11–13]. With milling time of 5 h or more, it is apparent that a single-phase columbite $NiNb_2O_6$ (yield of 100% within the limitations of the XRD technique) was found to be possible after the same calcination process was applied.

In general, the strongest reflections found in the majority of these XRD patterns indicate the formation of the $NiNb_2O_6$. These can be matched with JCPDS file number 76-2354 for the orthorhombic phase, in space group *Pbcn* (no. 60) with cell parameters $a = 1403$ pm, $b = 568.7$ pm and $c = 503.3$ pm [17], consistent with other works [12,18]. It should be noted that no

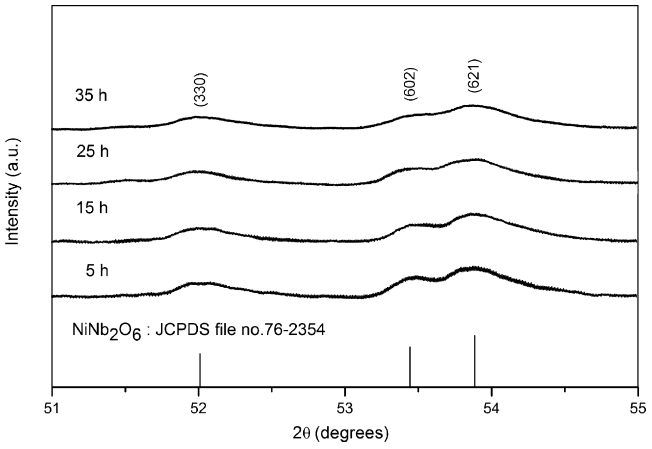

Fig. 4. Enlarged zone of XRD patterns showing (6 0 2) and (6 2 1) peaks broadening as a function of milling times.

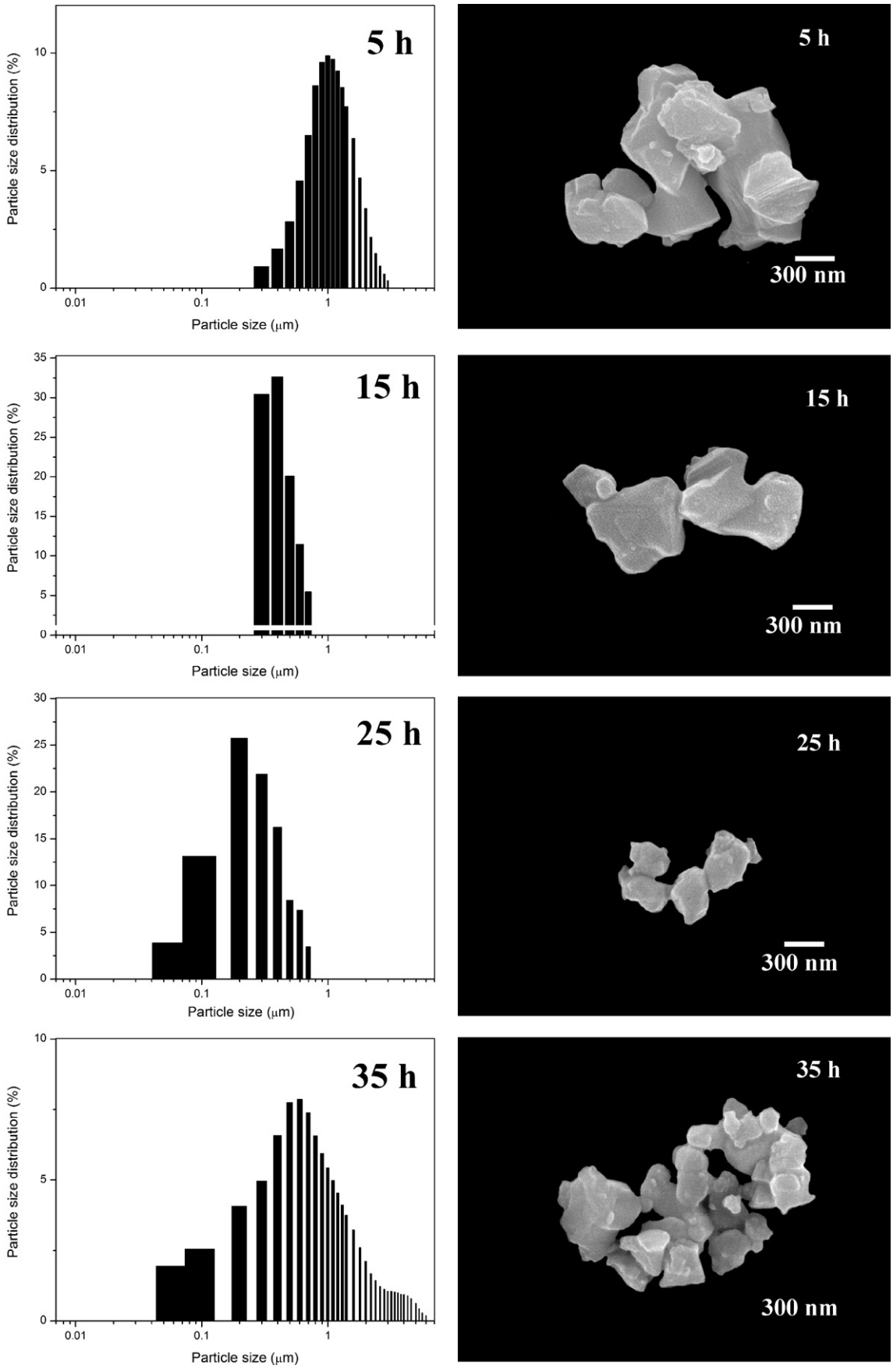

Fig. 5. SEM micrographs and particle size distribution of $NiNb_2O_6$ powders milled at different times.

evidence for the introduction of impurity due to wear debris from the milling process was observed in any of the calcined powders (within the milling periods of 0.5–35 h), demonstrating the effectiveness of the vibro-milling technique for the production of high purity $NiNb_2O_6$ nanopowders, without any introduction of excess NiO [9]. Moreover, it has been observed that with increasing milling time, all diffraction lines broaden, e.g. (6 0 2) and (6 2 1) peaks at $2\theta \sim 53$–54° (Fig. 4), an indication of a continuous decrease in particle size and of the introduction of lattice strain. These observations indicate that the prolonged milling treatment affects the particle size and evolution of crystallinity of the phase formed (Table 1), in good agreement with other similar system [14,19]. For $NiNb_2O_6$ powders, the longer the milling time, the finer is the particle size, down to a certain level. The results suggest that the steady state of the vibro-milling is attained at ~25 h of milling. Moreover, it is worthy to note that, in this condition, the mean crystalline size is close to ~35 nm. Also, the relative intensities of the Bragg peaks for the powders tend to decrease with the increase of milling time. However, it is well documented that, as Scherer's analysis provides only a measurement of the extension of the coherently diffracting domains, the particle sizes estimated by this method can be significantly under estimated [11,20]. In addition to strain, factors such as dislocations, stacking faults, heterogeneities in composition and instrumental broadening can contribute to peak broadening, making it almost impossible to extract a reliable particle size solely from XRD [15,21].

In this connection, scanning electron microscopy was also employed for particle size measurement (Table 1). The morphological evolution of the powders and their corresponding particle size distributions as a function of milling time were also revealed, as illustrated in Fig. 5. At first sight, the morphological characteristic of $NiNb_2O_6$ powders with various milling times is similar for all cases. In general, the particles are agglomerated and basically irregular in shape, with a substantial variation in particle sizes. The powders consist of primary particles nanometers in size. Increasing the milling time over the range 5–35 h, the average size of the $NiNb_2O_6$ particles decreases significantly, until at 25 h, the smallest particle size (estimated from SEM micrographs to be ~32 nm) is obtained. However, it is also of interest to point out that larger particle size was obtained for a milling time longer than 25 h. This may be attributed to the occurrence of hard agglomeration with strong inter-particle bonds within each aggregate resulting from dissipated heat energy of prolong milling [11,22]. Fig. 5 also illustrates that vibro-milling has slightly changed the shape of the particles which become more rounded at long milling times. At the same time, the particle size is reduced. Fracture is considered to be the major mechanism at long milling times. As shown in Fig. 5, after milling times of 5, 15 and 25 h, the powders exhibit a single peak covering the size ranging from 40 to 3000 nm. With milling time of 25 h, a uniform particle size distribution with a much lower degree of particle agglomeration (<1 μm) is found. However, upon further increase of milling time up to 35 h, a bimodal distribution curve with peak broadening between 45 and 6000 nm is observed. First is a monomodal distribution corresponding to the primary size of the $NiNb_2O_6$ particles. The second group (peak) is believed to arise mainly from particle agglomeration. The results obtained for $NiNb_2O_6$ powders milled for different times via different techniques are also compared in Table 1. Variations in these data may be attributed mainly to the formation of hard and large agglomerations, as observed in the SEM results.

In this work, it is seen that the optimum milling time for the production of the smallest nanosized high purity $NiNb_2O_6$ powder was found to be at 25 h. The finding of this investigation indicates a strong relationship between the vibro-milling process and the yield of $NiNb_2O_6$ nanopowders. However, in case of the vibro-milling technique, other factors such as the milling speed, milling scale and type of milling media also need to be taken into account.

4. Conclusions

The results infer that the milling time influences not only the development of the solid-state reaction of nickel niobate phase but also the particle size and morphology. The resulting $NiNb_2O_6$ powders have a range of particle size, depending on vibro-milling times. Production of a single-phase nickel niobate nanopowder can be successfully achieved by employing a combination of 25 h milling time and calcination condition of 900 °C for 4 h, with heating/cooling rates of 30 °C/min.

Acknowledgements

This work was supported by the Thailand Research Fund (TRF), the Commission on Higher Education (CHE), the National Nanotechnology Center (NANOTEC) through its program of Center of Excellence Network and the Faculty of Science, Chiang Mai University.

References

[1] R.C. Pullar, J.D. Breeze, N.M. Alford, J. Am. Ceram. Soc. 88 (2005) 2466.
[2] C. Heid, H. Weitzel, F. Bourdarot, R. Calemczuk, T. Vogt, H. Fuess, J. Phys. Condens. Mater. 8 (1996) 10609.
[3] D. Prabhakaran, F.R. Wondre, A.T. Boothroyd, J. Cryst. Growth 250 (2003) 72.
[4] A.M. Cruz, N.L. Alcaraz, A.F. Fuentes, L.M. Torres-Martinez, J. Power Sources 81/82 (1999) 255.
[5] A.J. Moulson, J.M. Herbert, Electroceramics, 2nd ed., Wiley, Chichester, 2003.
[6] Y. Xu, Ferroelectric Materials and their Applications, North-Holland, New York, 1991.
[7] T. Zhong, Y.D. Hou, M.K. Zhu, B.C. Xu, J.L. Tang, J.B. Liu, H. Wang, H. Yan, Mater. Lett. 59 (2005) 1169.
[8] E.F. Alberta, A.S. Bhalla, Mater. Lett. 54 (2002) 47.
[9] C.H. Lu, H.J. Hwang, Ceram. Int. 22 (1996) 373.
[10] N. Setter, R. Waser, Acta Mater. 48 (2000) 151.
[11] R. Wongmaneerung, R. Yimnirun, S. Ananta, Mater. Lett. 60 (2006) 1447.
[12] O. Khamman, R. Yimnirun, S. Ananta, Mater. Lett. 61 (2007) 639.
[13] A. Udomporn, S. Ananta, Mater. Lett. 58 (2004) 1154.
[14] S. Ananta, Mater. Lett. 58 (2004) 2781.
[15] H. Klug, L. Alexander, X-Ray Diffraction Procedures for Polycrystalline and Amorphous Materials, 2nd ed., Wiley, New York, 1974.
[16] O. Khamman, R. Yimnirun, S. Ananta, Mater. Lett. 61 (2007) 2565–2570.

[17] Powder Diffraction File no. 76-2354. International Centre for Diffraction Data, Newtown Square, PA, 2000.
[18] J. Ye, Z. Zou, A. Matsushita, Int. J. Hydrogen Energy 28 (2003) 651.
[19] A. Ngamjarurojana, O. Khamman, R. Yimnirun, S. Ananta, Mater. Lett. 60 (2006) 2867.
[20] C. Suryanarayana, Prog. Mater. Sci. 46 (2001) 1.
[21] A. Revesz, T. Ungar, A. Borbely, J. Lendvai, Nanostruct. Mater. 7 (1996) 779.
[22] P.C. Kang, Z.D. Yin, O. Celestine, Mater. Sci. Eng. A-Struct. 395 (2005) 167.

Giant dielectric properties of $CaCu_3Ti_4O_{12}$/(Li,Ti)-doped NiO composites subjected to postsintering annealing and compressive stress

Prasit Thongbai,[1] Santi Maensiri,[1,a)] Teerapon Yamwong,[2] and Rattikorn Yimnirun[3]
[1]*Department of Physics, Faculty of Science, Khon Kaen University, Khon Kaen 40002, Thailand*
[2]*National Metals and Materials Technology Center (MTEC), Thailand Science Park, Pathumthani 12120, Thailand*
[3]*Department of Physics, Faculty of Science, Chiang Mai University, Chiang Mai 50200, Thailand*

(Received 22 August 2007; accepted 29 March 2008; published online 9 June 2008)

We report the effects of postsintering annealing in argon and compressive prestress on the giant dielectric properties of $CaCu_3Ti_4O_{12}$–$Li_{0.3}Ti_{0.02}Ni_{0.68}O$ composites in the frequency range from 100 Hz to 1 MHz. After postsintering annealing, all compounds investigated still display a Debye-like relaxation, which can be interpreted based on the Maxwell–Wagner model. The dielectric behavior and the effect of compressive prestress of $CaCu_3Ti_4O_{12}$ and $CaCu_3Ti_4O_{12}$–$Li_{0.3}Ti_{0.02}Ni_{0.68}O$ after annealing are closely related to the oxygen vacancies in the grain boundaries. © *2008 American Institute of Physics*. [DOI: 10.1063/1.2937238]

I. INTRODUCTION

Giant dielectric ceramics with good thermal stability and Ba/Pb-free have recently attracted much attention due to their potential applications in microelectronics such as capacitors and memory devices. Giant-permittivity dielectric response with weakly temperature-dependent permittivity has been observed in $CaCu_3Ti_4O_{12}$ (CCTO) ($\varepsilon' \sim 10^4$ for polycrystalline ceramics and $\varepsilon' \sim 10^5$ for single crystals),[1–3] NiO-based ceramic ($\varepsilon' \sim 10^4$–10^5),[4–8] $Ba_4YMn_3O_{11.5}$ ($\varepsilon' \sim 10^4$),[9] and CuO ($\varepsilon' \sim 10^4$).[10] Most recently, our group[11] reported the giant values of $\varepsilon' \sim 10^5$ observed in polycrystalline $CaCu_3Ti_4O_{12}$ ceramics reinforced with 10 mol % of 39 nm $Li_{0.3}Ti_{0.02}Ni_{0.68}O$ (LTNO) nanoparticles. The dielectric behavior of these composites exhibits Debye-like relaxation, which can be explained based on the Maxwell–Wagner model, and the dielectric dispersions of the composites arise from the internal barrier layer capacitor (IBLC) effect.[12,13]

Interestingly, the colossal dielectric constant of $\sim 10^6$ at room temperature can also be obtained in $CaCu_3Ti_4O_{12}$ after annealing in argon at 1000 °C for 6 h, and this enhancement was attributed to the increase in concentration of oxygen vacancies and hence charge carriers.[14] The influence of postsintering annealing on dielectric properties of $CaCu_3Ti_4O_{12}$ was further investigated by Wang and Zhang.[15,16] They showed that the annealing treatment on $CaCu_3Ti_4O_{12}$ in reducing (nitrogen) and oxidizing (oxygen) atmospheres has strong effects on dielectric properties of the $CaCu_3Ti_4O_{12}$. These results support the results reported in Ref. 14 and strongly suggest that the concentration of oxygen plays an important role in the dielectric properties of $CaCu_3Ti_4O_{12}$. In addition to its interesting dielectric property, $CaCu_3Ti_4O_{12}$ has remarkably strong nonlinear current-voltage characteristics without the addition of dopants.[13] These excellent properties render this material particularly attractive for a wide range of applications. However, in some practical applications, dielectric ceramics may be subjected to mechanical or thermal stresses causing changes on their properties. A prior knowledge of how the material properties change under different load conditions is therefore crucial for proper design of a device and for suitable selection of materials for a specific application. Despite that fact, material constants used in many design calculations are often obtained from a stress-free measuring condition, which in turn may lead to incorrect or inappropriate device designs.

Most recently, we observed that postsintering annealing in argon for 5 h leads to a significant increase in ε' for $CaCu_3Ti_4O_{12}$ ceramic, which is closely related to the oxygen vacancies.[17] The dielectric properties of the argon-annealed samples were also found to change significantly with the applied compressive stress (the absolute change can reach 25% at a maximum stress of 130 MPa), which could be explained by the stress-induced aging mechanism.[17] The stress dependence of the permittivity in $CaCu_3Ti_4O_{12}$-based ceramics has not been thoroughly studied. Herein, we investigate the influences of the postsintering annealing in argon and compressive prestress on the giant dielectric properties of the $(1-x)CaCu_3Ti_4O_{12}\cdot xLi_{0.3}Ti_{0.02}Ni_{0.68}O$ (CCTO-LTNO) composites sintered in air at 1100 °C for 16 h.

II. EXPERIMENT

The sample preparations of $(1-x)CaCu_3Ti_4O_{12}\cdot xLi_{0.3}Ti_{0.02}Ni_{0.68}O$ ($x=0$, 0.1, 0.25, and 0.5) composites are given in our previous publication.[11] The dimensions of the samples were ~12 mm in diameter and ~3 mm in height. Here, we assign symbols of CCTO, 10%LTNO, 25%LTNO, and 50%LTNO, for the sintered samples of $(1-x)CaCu_3Ti_4O_{12}\cdot xLi_{0.3}Ti_{0.02}Ni_{0.68}O$, with $x=0$, 0.1, 0.25, and 0.5, respectively. A postsintering annealing process was carried out in flowing argon (99.999% purity) at 1000 °C for 5 h, and we assign symbols of CCTO-Ar, 10%LTNO-Ar, 25%LTNO-Ar, and 50%LTNO-Ar, for the sintered samples of CCTO, 10%LTNO, 25%LTNO, and 50%LTNO, after argon annealing. The sintered ceramics were characterized by x-ray diffraction (XRD) (Philips PW3710, The Netherlands)

a)Electronic address: santimaensiri@gmail.com and sanmae@kku.ac.th.

 © 2008 American Institute of Physics

Author complimentary copy. Redistribution subject to AIP license or copyright, see http://jap.aip.org/jap/copyright.jsp

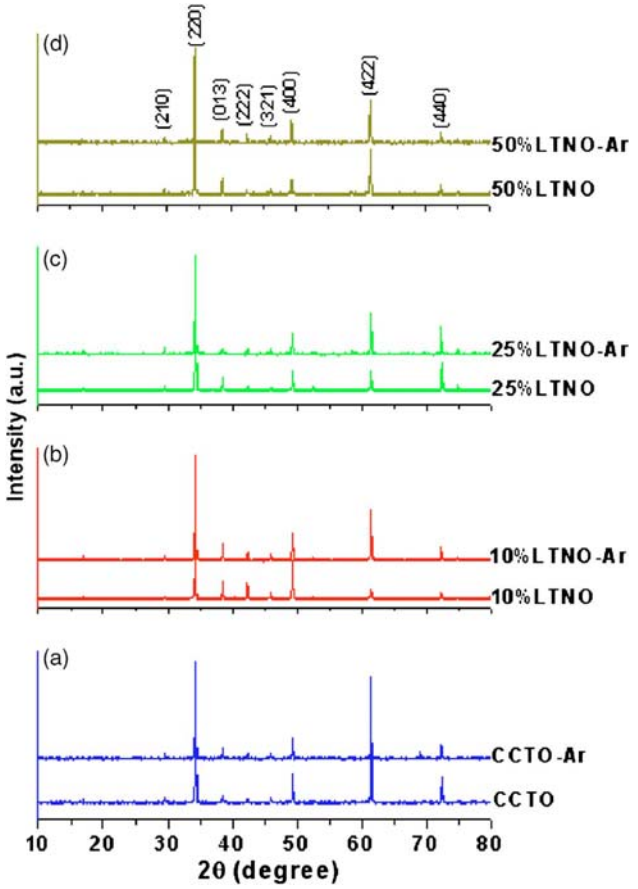

FIG. 1. (Color online) XRD patterns of the sintered materials of CCTO and CCTO-LTNO before and after annealing at 1000 °C for 5 h under flowing argon. (a) CCTO, (b) 10%LTNO, (c) 25%LTNO, and (d) 50%LTNO.

and scanning electron microscopy (SEM) (LEO 1450VP, UK). The frequency and temperature dependences of dielectric properties for the as-sintered samples were measured using a Hewlett Packard 4194A impedance gain phase analyzer. Silver paste was used as the electrode, and it was coated on both surfaces of the sample and dried overnight. The dielectric properties of the samples after postsintering annealing were measured under the influence of the compressive stress through spring-loaded pins connected to an inductance capacitance impedance (LCZ) meter (Hewlett Packard 4276A) at the frequency of 100 kHz at room temperature (25 °C). The details of the system are described elsewhere.[18]

III. RESULTS AND DISCUSSION

Figure 1 shows XRD patterns of the sintered ceramics before and after postsintering annealing, confirming only a main phase of $CaCu_3Ti_4O_{12}$ in all the samples with no diffraction peaks of LTNO and other possible impurities such as TiO_2, CuO, $CaTiO_3$, and $NiTiO_3$. The values of lattice parameter a calculated from XRD spectra are shown in Table I; these values are close to 0.7391 nm of that reported in literature.[1] Higher concentrations of LTNO did not result in any noticeable shift in lattice parameter, suggesting that the added LTNO is most likely present in the microstructure either in the grain boundaries or as a second phase. Moreover,

TABLE I. Lattice parameter a and activation energies (E_a) for CCTO-LTNO ceramics before and after postannealing sintering.

	Lattice parameter (nm)		Activation energy (eV)	
Materials	Before	After	Before	After
CCTO	0.7385	0.7391	0.112	0.112
10%LTNO	0.7385	0.7391	0.112	0.112
25%LTNO	0.7388	0.7389	0.116	0.112
50%LTNO	0.7387	0.7392	0.116	0.112

the values of lattice parameter of the CCTO-LTNO composites after postsintering annealing also did not result in any noticeable shift in lattice parameter. Their values show little change, which is comparable to the values of samples before postsintering. These results indicate that the postannealing sintering treatments did not change the crystal structure—the structure of all samples remains cubic and centric.

Microstructures of the sintered composites ceramics were revealed by SEM. The samples were fractured in order to observe their composite morphologies. Figures 2(a)–2(d) show SEM micrographs of the sintered samples revealing polycrystalline grains with estimated grain sizes of 9.0 ± 1.9, 8.8 ± 1.7, 12.4 ± 2.8, and 13.4 ± 2.7 μm for CCTO, 10%LTNO, 25%LTNO, and 50%LTNO, respectively. No change in grain size of the samples before and after annealing was observed. It is important to note that the thickness of grain boundary cannot be accurately measured by SEM technique. However, the thickness of grain boundary was estimated to about 50–200 nm for CCTO ceramic. It is seen from the backscattered electron images of the fracture surfaces of the samples [Figs. 2(e)–2(h)] that a large portion of porosity increases with increasing amount of LTNO, as can be clearly observed in the microstructures of 25%LTNO and 50%LTNO. The LTNO nanoparticles distribute inhomogeneously and form clusters or agglomerates and locate between grain boundaries of CCTO matrix (indicated by arrows). It is noted that no diffraction peaks of LTNO and the other possible layer is impurities were detected by XRD, but the inhomogeneous distribution of LTNO was observed by the backscattered SEM images of the fracture surfaces of the CCTO-LTNO composites. This indicates that the outmost layer of the composites is LTNO and other possible impurity deficient. Similar observation was reported for $CaCu_3Ti_4O_{12}$/Ag composites having the Ag deficient in the outmost layer and Ag rich in the inner part of the composites.[19]

Figure 3 shows the real (ε') and imaginary (ε'') parts of dielectric dispersion for the Ar-annealed samples, measured at −50 °C over the frequency range of 100 Hz–1 MHz. It is clearly seen from Fig. 3(a) that all of the samples exhibit the giant dielectric constant ($\varepsilon' \sim 1 \times 10^4 - 3.5 \times 10^4$) below the relaxation frequency ($f < 100$ kHz). The drastic decrease in the real parts of dielectric spectra of all samples is seen in the frequency range above 20 kHz, accompanied by the appearance of corresponding peaks in the imaginary parts of dielectric spectra, as shown in Fig. 3(b). Moreover, the relaxation peak in all samples shifts to higher frequency at a higher temperature (not shown). The dielectric behavior of all

Author complimentary copy. Redistribution subject to AIP license or copyright, see http://jap.aip.org/jap/copyright.jsp

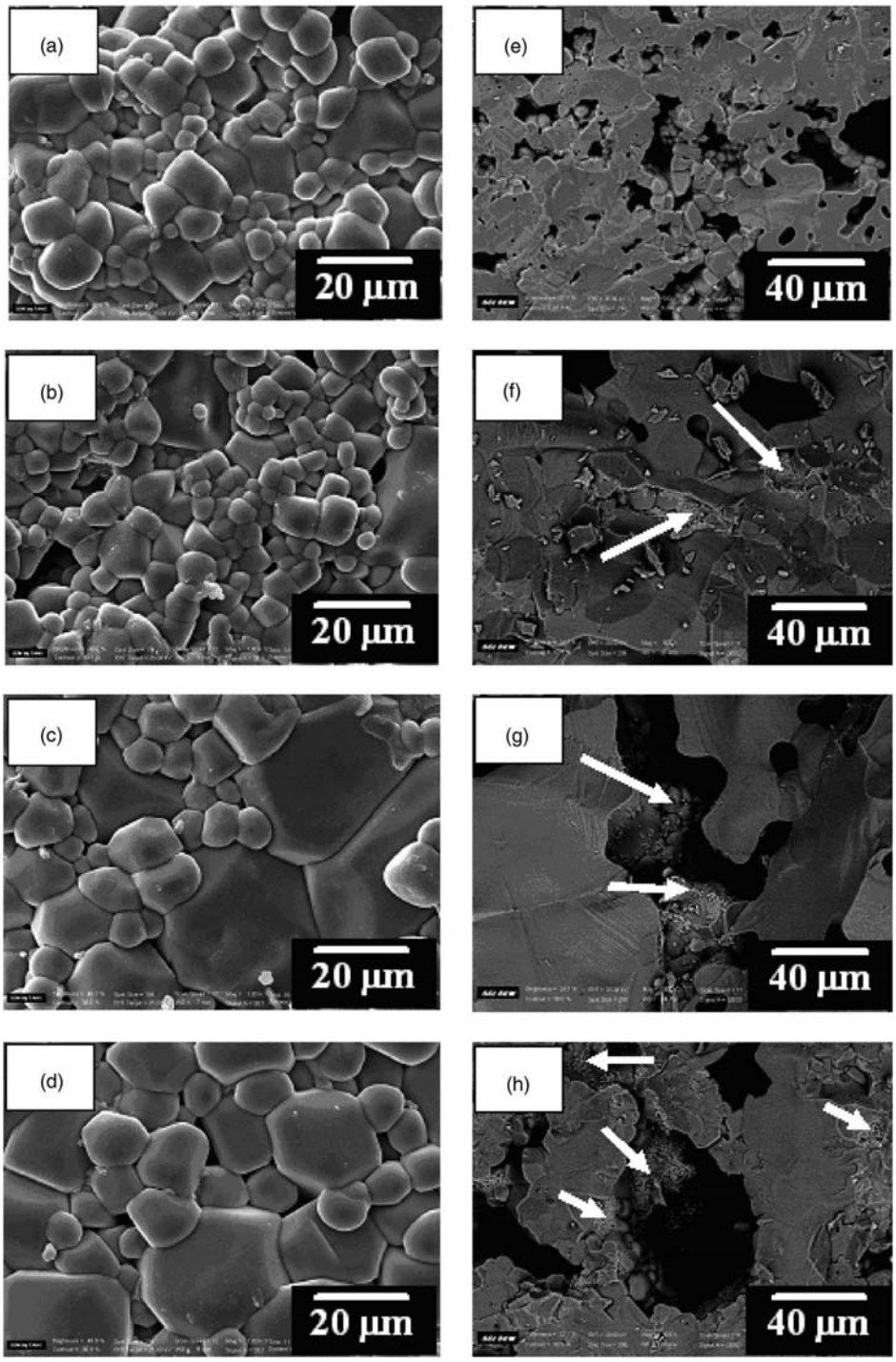

FIG. 2. SEM micrographs of the ceramic samples sintered in air at 1100 °C for 16 h: (a) CCTO, (b) 10%LTNO, (c) 25%LTNO, and (d) 50%LTNO; (e)-(d) show the backscattered SEM micrograph of fracture surface of CCTO, 10%LTNO, 25%LTNO, and 50%LTNO, respectively.

samples after postsintering annealing still exhibits a Debye-like relaxation similar to that of the as-sintered samples. The dielectric behavior of the nonannealed and annealed samples can be interpreted based on the Maxwell–Wagner model and their dielectric dispersions arise from the IBLC effect.[11,17] This behavior is also similar to that observed in $CaCu_3T_{i4}O_{12}$ ceramics reported in literatures.[2,17,20–22]

The E_a values of the low-temperature relaxation determined from the slopes of Arrhenius plot of log τ vs $1/T$ [the inset of Fig. 3(b)] were obtained to be ~0.112 eV for all of the Ar-annealed samples. Annealing in argon results in a slight decrease in E_a values of the 25%LTNO-Ar and 50%LTNO-Ar, whereas the E_a values of CCTO-Ar and 10%LTNO-Ar do not change with annealing treatment and show the same value of 0.112 eV. This value is comparable to the reported values of 0.067,[23] 0.08,[12,24] 0.093,[25] 0.059–0.076,[26] and 0.084–0.132 eV (Refs. 20 and 22) for the grains of $CaCu_3T_4O_{12}$. The E_a values are also tabulated in Table I. Based on the Maxwell–Wagner model, it is seen that the E_a of the dielectric process is approximately equal to that of the grain conduction process.[17,21] Thus, the postsintering annealing does not change the electrical properties of the part of grains in CCTO matrix.

Figure 4 shows the dielectric constant (ε') and loss tan-

Author complimentary copy. Redistribution subject to AIP license or copyright, see http://jap.aip.org/jap/copyright.jsp

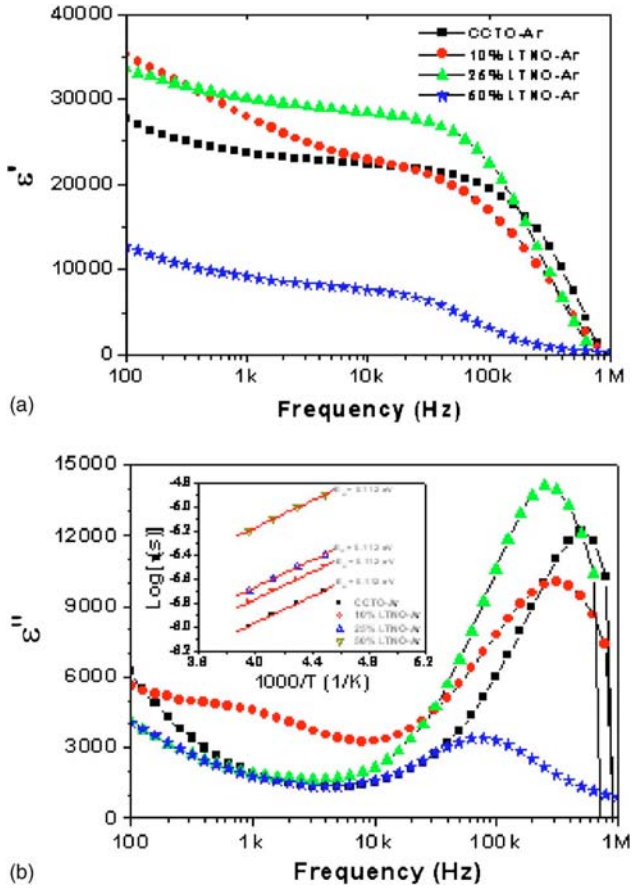

FIG. 3. (Color online) The frequency dependence of dielectric dispersions of CCTO ceramic and CCTO-LTNO composites after postsintering annealing in argon at 1000 °C measured at −50 °C. (a) the real part ε' and (b) the imaginary part ε''. The inset displays the Arrhenius plot of log $\log(\tau)$ vs $1000/T$.

gent (tan δ) of CCTO and CCTO-Ar, 25%LTNO, and 25%LTNO-Ar. Figure 4(a) shows a significant increase in ε' at low frequency for the CCTO after postsintering annealing (CCTO-Ar), accompanied by the increase in tan δ at the same frequency range. At high frequency, the ε' value of CCTO-Ar gradually decreases to the ε' value of CCTO. For the 25%LTNO and 25%LTNO-Ar [Fig. 4(b)], the ε' values of these composite samples show a little change after annealing. The dramatic increase in ε' for CCTO-Ar is closely related to the oxygen vacancies, as previously reported.[17] Annealing the $CaCu_3Ti_4O_{12}$ sample in argon atmosphere at high temperature would increase the concentration of the oxygen vacancies and thus increase ε' values, as obtained in the nitrogen-annealed $CaCu_3Ti_4O_{12}$ reported by Wang and Zhang.[16]

At present, the extrinsic effect of IBLC is widely accepted as the origin of the giant dielectric response in both (Li, Ti)-doped NiO (Refs. 4 and 5) and $CaCu_3Ti_4O_{12}$.[12,13,15–17,20–27] However, many aspects for the origin of semiconducting grains and insulating grain boundary regions for CCTO ceramics remain unclear. Li *et al.*[28] proposed that the grain and grain boundary regions in CCTO ceramics may consist of the same phase but with slightly different compositions. Sinclair *et al.*[12] reported that heat treatment of CCTO pellets in N_2 at 1000 °C caused a significant change in electrical properties at room temperature, in which the resistance of grain boundary (R_{gb}) decreased by two orders of magnitude but the resistance of grain remained unchanged. They proposed a plausible explanation that the semiconductivity of the grains arises from a small but significant loss of oxygen during ceramic processing in air at high temperatures, whereas furnace cooling allows reoxidation to occur along the grain boundary regions, which converts these regions into insulators. From this proposal, it implied that the grain boundary region (the shell of grain) of CCTO ceramic is the nonoxygen vacancy region. Interestingly, the low-R_{gb} value of the sample after heat treatment in N_2 can be reverted to the high-R_{gb} value of the as sample by annealing in oxygen.[29] From these results, it is strongly believed that the electrical properties of grain boundary have a close relation to the stoichiometry of oxygen at this region. Therefore, the difference in dielectric properties for our CCTO and CCTO-Ar is greatly affected by the oxygen vacancies at the grain boundary. These indicate that an oxygen at the grain boundary for our CCTO ceramic has been oxidized during annealing treatment in argon, and the reoxidation process during furnace cooling has been limited by annealing in this reducing atmosphere. Hence, the thickness of grain boundary layers for the CCTO-Ar has reduced to a thinner layer compared to CCTO.

In our previous work,[17] the dielectric behavior of CCTO has been interpreted based on the Maxwell–Wagner model. From this model, Liu *et al.*[21] estimated the dielectric constant of bulk CCTO, i.e., $\varepsilon'_s \approx \varepsilon_{gb}(d_g+d_{gb})/d_{gb}$, where ε_{gb} is the dielectric constant of grain boundary layer, and d_g and d_{gb} are the thicknesses of grain and grain boundary layers, respectively. Therefore, the increase in the dielectric constant of CCTO-Ar is possibly due to the decrease in its d_{gb}. Bueno *et al.*[30] used dielectric spectroscopy to examine CCTO to demonstrate that at low frequency, the contribution of the grain boundary can be separated from the total dielectric response. At present, we propose that the increment of ε' for CCTO-Ar at low frequency is contributed by grain boundaries, which arise from the loss of oxygen and limited reoxidation during furnace cooling. This suggests that the annealing treatment modifies the defect equilibrium at this region. At high frequency, the ε' of CCTO-Ar slightly changes, as compared to the ε' of CCTO. This corresponds to the unchanged value of E_a for the grains of the samples before and after postsintering annealing. In contrast, the values of ε' and tan δ for the 25%LTNO-Ar are unchanged with Ar annealing over the measured frequencies. We think that annealing in argon does not cause a significant change in the total polarization at the grain boundary of the 25%LTNO-Ar because there are LTNO nanoparticles located between grain boundaries of the CCTO matrix.[11] This suggests that the LTNO has more contribution on polarization at this region than the grain boundary of CCTO matrix.

Figures 5(a) and 5(b) show the stress dependent dielectric properties of CCTO-Ar and 25%LTNO-Ar, respectively. It is clearly observed that the dielectric properties of both samples change significantly with applied compressive stress. The absolute change of ε' can reach 16% and 7% at

Author complimentary copy. Redistribution subject to AIP license or copyright, see http://jap.aip.org/jap/copyright.jsp

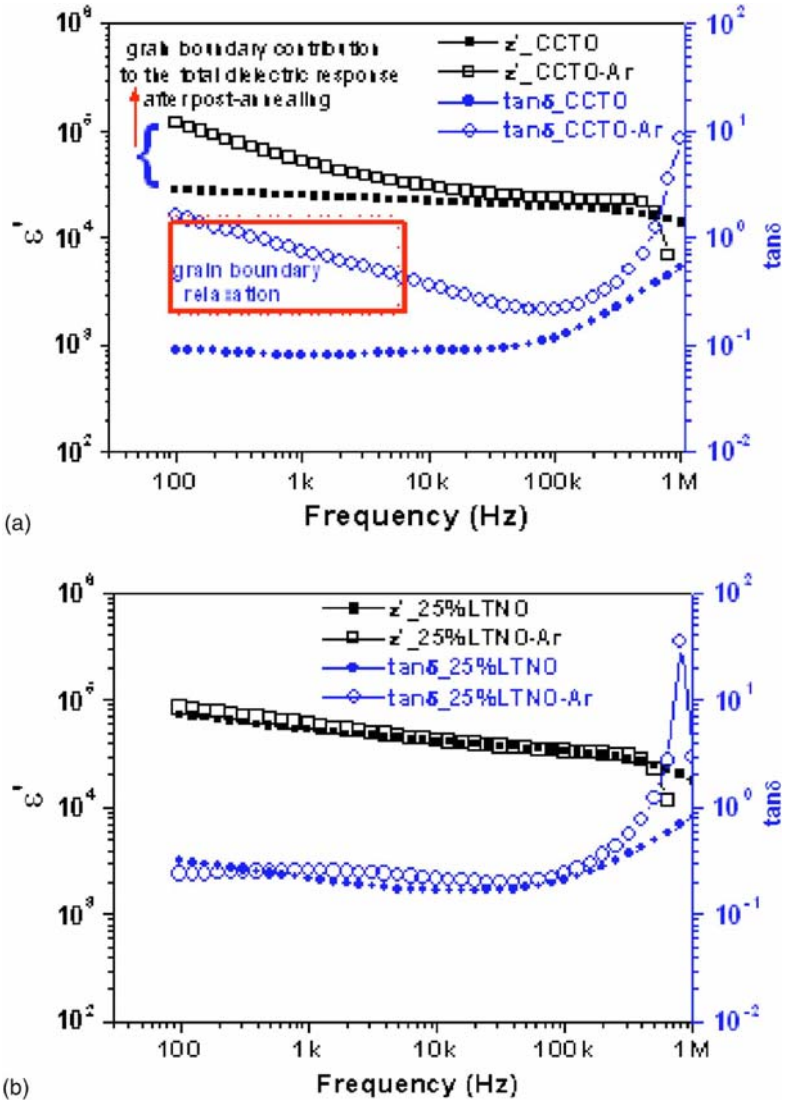

FIG. 4. (Color online) Room temperature ε' and tan δ of (a) CCTO and (b) 25%LTNO, before and after postsintering annealing.

the maximum stress of 130 MPa for CCTO-Ar and 25%LTNO-Ar, respectively. However, the changes in dielectric properties with the stress in the CCTO-Ar and 25%LTNO-Ar follow opposing trends. For the CCTO-Ar, both ε' and tan δ increase with increasing stress and interestingly continue to decrease upon the reduction of the applied stress [Fig. 5(a)]. On the other hand, the dielectric properties of the 25%LTNO-Ar sample decrease when the stress is increased in the range of 0–40 MPa, and beyond this range, ε' and tan δ are almost unchanged with compressive stress [Fig. 5(b)]. As previously discussed,[17] the CCTO-Ar possesses very much higher concentration of the oxygen vacancies in the grain boundaries, as compared to the 25%LTNO-Ar. With lower concentration of oxygen vacancies, 25%LTNO-Ar should contain more mobile dipoles that can easily be activated by the applied stress. Hence, this leads to a stress-induced aging mechanism,[17,31] which results in the decrease in ε' and tan δ at the low stress level. In the case of the CCTO-Ar, with very high concentration of the oxygen vacancies, there are competing mechanisms between the stress-induced aging and the elastic deformation. Initially, with the stress-induced aging mechanism still dominating, most of the oxygen vacancies come to rest at the grain boundaries and stabilize the stress influence, as it is observed that the dielectric properties are rather stable at a lower stress level.[17,31] A further increase in the compressive stress may result in a slight decrease in the grain boundary thickness. The effective dielectric properties of this ceramic, which can be regarded as the IBLC,[12] therefore increase, and the decrease in the effective dielectric properties follows with the reduction of the stress, as observed in Fig. 5(a). Here, we attribute that the differenes in the absolute change of ε' under compressive stress are closely related to the concentration of oxygen vacancies in the grain boundary.

IV. CONCLUSION

In conclusion, the giant dielectric behaviors of polycrystalline $CaCu_3Ti_4O_{12}$ and $CaCu_3Ti_4O_{12}$–$Li_{0.3}Ti_{0.02}Ni_{0.68}O$ composites subjected to postsintering annealing and compressive stress were investigated. The dielectric behavior of all samples after postsintering annealing still exhibits a Debye-like relaxation. A significant increase in ε' was observed for CCTO-Ar at low frequency, whereas an unchange

Author complimentary copy. Redistribution subject to AIP license or copyright, see http://jap.aip.org/jap/copyright.jsp

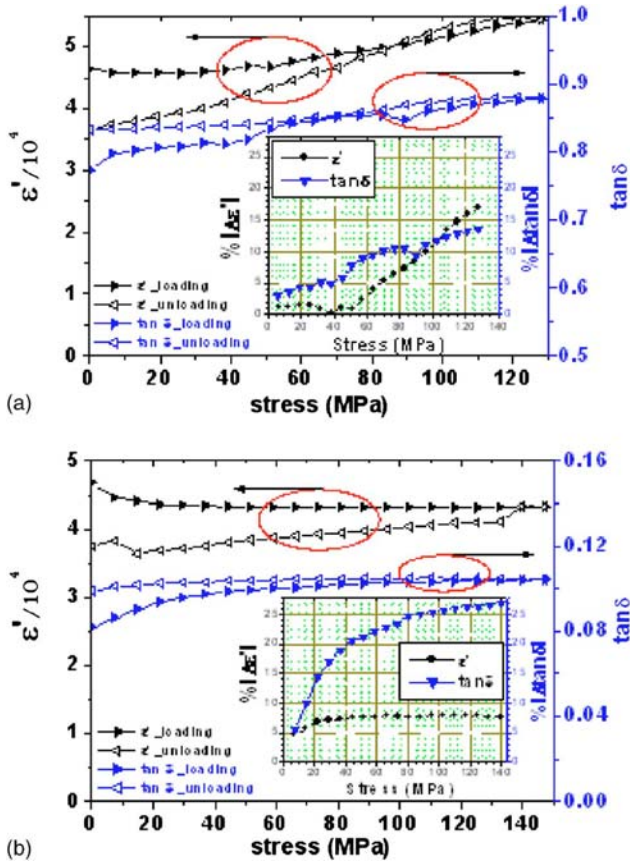

FIG. 5. (Color online) Compressive stress dependence of ε' and tan δ at a frequency of 100 kHz for the samples of (a) CCTO-Ar and (b) 25% after annealing at 1000 °C for 5 h under flowing argon. The insets of Figs. 5(a) and 5(b) show the absolute change (%) of ε' and tan δ. Here, $\%|\Delta\varepsilon'|$ and $\%|\Delta \tan \delta|$ are defined as $|(\varepsilon'_\sigma - \varepsilon'_0)/\varepsilon'_0| \times 100(\%)$ and $|(\tan \delta_\sigma - \tan \delta_0)/\tan \delta_0| \times 100(\%)$, respectively, where $(\varepsilon'_\sigma, \varepsilon'_0)$, and $(\tan \delta_\sigma, \tan \delta_0)$, are the dielectric constants and dissipation factors with the applied compressive stress and without the applied compressive stress, respectively.

in ε' was observed for 25%LTNO-Ar. The dielectric properties of both CCTO-Ar and 25%LTNO-Ar samples change significantly with the applied compressive stress, and this can be explained by the stress-induced aging mechanism. The different bases in dielectric behaviors of the two ceramics can be explained by the level of concentration of oxygen vacancies in the grain boundaries after postsintering annealing.

ACKNOWLEDGMENTS

This work is financially supported by The Thailand Research Fund (TRF), and The Commission on Higher Education (CHE), The Ministry of Education, Thailand. P.T. would like to thank the Thailand Graduate Institute of Science and Technology (TGIST) for his PhD scholarship.

[1] M. A. Subramanian, D. Li, N. Duan, B. A. Reisner, and A. W. Sleight, J. Solid State Chem. **151**, 323 (2000).
[2] A. P. Ramirez, M. A. Subramanian, M. Gardela, G. Blumberg, D. Li, T. Vogt, and S. M. Shapiro, Solid State Commun. **115**, 217 (2000).
[3] C. C. Homes, T. Vogt, S. M. Shapiro, S. Wakimoto, and A. P. Ramirez, Science **293**, 673 (2001).
[4] J. Wu, C. W. Nan, Y. Lin, and Y. Deng, Phys. Rev. Lett. **89**, 217601 (2002).
[5] S. Maensiri, P. Thongbai, and T. Yamwong, Acta Mater. **55**, 2851 (2007).
[6] Y. Lin, J. Wang, L. Jiang, Y. Chen, and C. W. Nan, Appl. Phys. Lett. **85**, 5664 (2004).
[7] P. K. Jana, S. Sarkar, and B. K. Chaudhuri, Appl. Phys. Lett. **88**, 182901 (2006).
[8] Y. Lin, L. Jiang, R. Zhao, and C. W. Nan, Phys. Rev. B **72**, 014103 (2005).
[9] X. Kuang, C. Bridges, M. Allix, J. B. Claridge, H. Hughes, and M. J. Rosseinsky, Chem. Mater. **18**, 5130 (2006).
[10] S. Sarkar, P. K. Jana, B. K. Chaudhuri, and H. Sakata, Appl. Phys. Lett. **89**, 212905 (2006).
[11] S. Maensiri, P. Thongbai, and T. Yamwong, Appl. Phys. Lett. **90**, 202908 (2007).
[12] D. C. Sinclair, T. B. Adams, F. D. Morrison, and A. R. West, Appl. Phys. Lett. **80**, 2153 (2002).
[13] S. Y. Chung, I. L. D. Kim, and S. J. L. Kang, Nat. Mater. **3**, 774 (2004).
[14] B. A. Bender and M. J. Pan, Mater. Sci. Eng., B **117**, 339 (2005).
[15] C. C. Wang and L. W. Zhang, Appl. Phys. Lett. **88**, 042906 (2006).
[16] C. C. Wang and L. W. Zhang, Phys. Rev. B **74**, 024106 (2006).
[17] P. Thongbai, C. Masingboon1, S. Maensiri, T. Yamwong, S. Wongsaenmai, and R. Yimnirun, J. Phys.: Condens. Matter **19**, 236208 (2007).
[18] R. Yimnirun, P. J. Moses, R. J. Mayer, and R. E. Newnham, Rev. Sci. Instrum. **74**, 3429 (2003).
[19] C. C. Wang, Y. J. Yan, L. W. Zhang, M. Y. Cui, G. L. Xie, and B. S. Cao, Scr. Mater. **54**, 1501 (2006).
[20] S. F. Shao, J. L. Zhang, P. Zheng, W. L. Zhong, and C. L. Wang, J. Appl. Phys. **99**, 084106 (2006).
[21] J. Liu, Y. Sui, C. G. Duan, W. N. Mei, R. W. Smith, and J. R. Hardy, Chem. Mater. **18**, 3878 (2006).
[22] J. L. Zhang, P. Zheng, C. L. Wang, M. L. Zhao, J. C. Li, and J. F. Wang, Appl. Phys. Lett. **87**, 142901 (2005).
[23] L. Zhang and Z. J. Tang, Phys. Rev. B **70**, 174306 (2004).
[24] A. R. West, T. B. Adams, F. D. Morrison, and D. C. Sinclair, J. Eur. Ceram. Soc. **24**, 1439 (2004).
[25] G. Chiodelli, V. Massarotti, D. Capsoni, M. Bini, C. B. Azzoni, M. C. Mozzati, and P. Lupotto, Solid State Commun. **132**, 241 (2004).
[26] D. Capsoni, M. Bini, V. Massarotti, G. Chiodelli, M. C. Mozzatic, and C. B. Azzoni, J. Solid State Chem. **177**, 4494 (2004).
[27] C. Masingboon, S. Maensiri, T. Yamwong, P. Anderson, and S. Seraphin, Appl. Phys. A: Mater. Sci. Process. **91**, 87 (2008).
[28] M. Li, A. Feteira, D. C. Sinclair, and A. R. West, Appl. Phys. Lett. **88**, 232903 (2006).
[29] T. B. Adams, D. C. Sinclair, and A. R. West, J. Am. Ceram. Soc. **89**, 10 (2006).
[30] P. R. Bueno, M. A. Ramírez, J. A. Varela, and E. Longo, Appl. Phys. Lett. **89**, 191117 (2006).
[31] R. Yimnirun, M. Unruan, Y. Laosiritaworn, and S. Ananta, J. Phys. D: Appl. Phys. **39**, 3097 (2006).

Author complimentary copy. Redistribution subject to AIP license or copyright, see http://jap.aip.org/jap/copyright.jsp

ELSEVIER

Journal of Alloys and Compounds 461 (2008) 565–569

Journal of ALLOYS AND COMPOUNDS

www.elsevier.com/locate/jallcom

Thermal expansion properties of PMN–PT ceramics

Rewadee Wongmaneerung [a,b,*], Ruyan Guo [b], Amar Bhalla [b], Rattikorn Yimnirun [a], Supon Ananta [a]

[a] *Department of Physics, Faculty of Science, Chiang Mai University, Chiang Mai 50200, Thailand*
[b] *Pennsylvania State University, Materials Research Laboratory, PA, USA*

Received 5 June 2007; received in revised form 10 July 2007; accepted 14 July 2007
Available online 27 July 2007

Abstract

Thermal expansion properties of $(1-x)$PMN–xPT ceramics were determined in the temperature range of approximately −150 to +550 °C by dilatometer thermal expansion measurement. We reported the temperature-dependent measurements of the strain, thermal expansion coefficient and the magnitude of polarization (P_d). The anomaly behaviors were observed at Burns temperature (T_d). From the experimental data, it appeared that far above the ferroelectric phase transition temperature, up to T_d, these materials possessed a local randomly oriented polarization P_d. Various aspects of understanding the polarization behavior and other effects in this ferroelectric system were also examined and discussed.
© 2007 Elsevier B.V. All rights reserved.

Keywords: Thermal expansion; Polarization; Relaxors; Perovskites

1. Introduction

Relaxor ferroelectrics, such as lead magnesium niobate (PMN), lead zinc niobate (PZN) and strontium barium niobate (SBN) attract considerable interest owing to rich diversity of their physical properties and possible applications in various technological schemes. These relaxors possess very large dielectric constants; attractive for capacitors, exceptionally large electrostrictive coefficients; important for actuators and micropositioners and large electro-optic constants [1,2].

The main features of the relaxors are connected with their structural inhomogeneity or disorder and with the presence of polar nanodomains in non-polar matrix. The structural investigations and physical properties studies reveal three peculiar temperatures: T_d, T_c and T_m. T_d, so-called the Burn temperature, is the temperature where randomly oriented polar nanoregions become detectable within the otherwise non-polar paraelectric phase of several ferroelectrics. Originally observed in $BaTiO_3$ due to the characteristic anomaly of the refractive index [3], polar precursor clusters were later on detected in $PbTiO_3$ [4], $KNbO_3$ [5] and in the relaxor ferroelectrics PLZT [6], PMN, PZN [7] and SBN [8]. The polar regions are formed in the course of cooling at a temperature $T_d \approx 350\,^{\circ}C$, which is considerably higher than the temperature T_m ($T_m \approx -10\,^{\circ}C$ for PMN). At temperature below T_d, the temperature dependences of the birefringence and the elongation per unit length $\Delta l/l$ for PMN deviate from linear behavior (characteristic of higher temperatures), which is associated with the formation of polar nanoregions and increase in their total volume with a decrease in the temperature [9–11]. T_c, Curie temperature, is the temperature where the sample will undergo a cooperative ferroelectric phase transition. T_m is the temperature of the dielectric permittivity maximum, leading to an isotropic relaxor state with random orientation of polar domains [2].

A variety of experimental techniques, including refractive index measurements [3], Raman scattering [12], second-harmonic-generation (SHG) measurement [13], neutron powder diffraction [14], neutron elastic scattering [15], dynamic light scattering [16] and dielectric measurements [17–19] has been employed to confirm the existence (and value) of T_d. It was pointed out by Bhalla et al. [8] that due to electrostrictive coupling between the lattice strain and the polar nanoregions, T_d should also be detectable from thermal expansion measurements. Indeed, deviations from the linear temperature dependence of the thermal strain had been observed at tempera-

* Corresponding author at: Department of Physics, Faculty of Science, Chiang Mai University, Chiang Mai 50200, Thailand. Tel.: +6681 8854973.
E-mail address: re_nok@yahoo.com (R. Wongmaneerung).

0925-8388/$ – see front matter © 2007 Elsevier B.V. All rights reserved.
doi:10.1016/j.jallcom.2007.07.086

ture $T \geq T_m$ in PLZT [20] and SBN [8], and had been attributed to the condensation of randomly oriented local polarization at T_d [3].

In this work, we studied thermal expansion of $(1-x)$PMN–xPT ceramics with end member compositions and compositions close to a morphotropic phase boundary (MPB), i.e., $x = 0$, 0.2, 0.3, 0.35 and 1.0. Thermal expansion and thermal expansion coefficient data were then reported. Moreover, it is always a challenge to measure the temperature dependence of the polarization of these relaxor ferroelectrics over the entire temperature range. In this study, we also reported polarization values from the ferroelectric hysteresis (P–E) and thermal expansion measurements. From the phenomenological approach [8], it is known that the P_d values can be extracted by using the relation;

$$x_{ij} = \frac{\Delta l}{l} = Q_{ijkk} P_k^2 \quad (1)$$

where x_{ij} is the strain, $\Delta l/l$ is the thermal expansion, Q_{ijkk} is the electrostrictive coefficient and P_k is the polarization. Electrostrictive coefficients (Q) are determined in paraelectric phase and considered constant.

2. Experimental

The compositions of the ceramics in this investigation are $(1-x)Pb(Mg_{1/3}Nb_{2/3})O_{3-x}PbTiO_3$, $x = 0$, 0.20, 0.30, 0.35 and 1.0, and these samples were prepared from B-site precursor mixed oxide synthetic route, as reported earlier [21,22]. Pure $PbTiO_3$ powders were synthesized by a simple mixed oxide method [23]. Starting precursors were PbO, MgO, Nb_2O_5 and TiO_2. Ceramic fabrication was achieved by adding 3 wt% polyvinyl alcohol binder, prior to pressing as pellets in a pseudo-uniaxial die press at 100 MPa. Each pellet was placed in an alumina crucible together with an atmosphere powder of identical chemical composition. Sintering was carried out with a dwell time of 2 h, with constant heating/cooling rates of 20 °C/min and then heated to a sintering temperature of 1100–1250 °C. For PT ceramics, in order to achieve sinterable product, the samples were sintered using two-stage sintering [24], three sets of the first sintering temperature were assigned for the two-stage sintering case: 700, 800 and 900 °C. The second sintering temperature was set at 1200 °C. Sintering was carried out with a dwell time of 2 h at each step, with constant heating/cooling rates of 1 °C/min.

For thermal expansion measurement, all samples were cut in bar shape (5 mm long and 1 mm thick), placed inside a fused silica holder, heated at a rate of 2 °C/min from −100 to 450 °C and the thermal expansion was measured as a function of temperature using a linear voltage-differential transformer (LVDT) dilatometer. The LVDT has an advantage over the other transformers as it gives a linear output for every unit displacement. The polarization hysteresis measurement was carried out with a standardized ferroelectric test system (RT-66A, Radiant technologies).

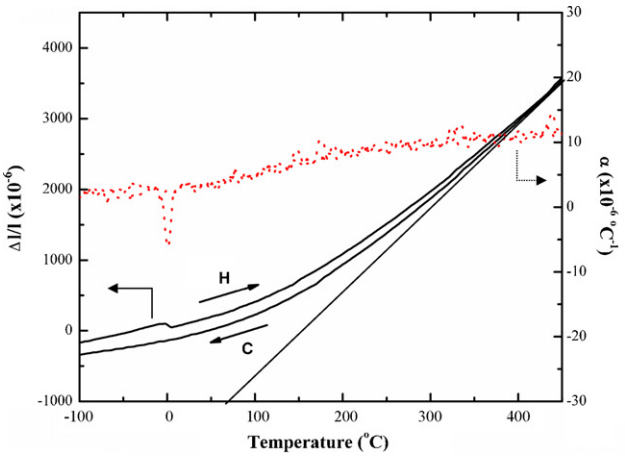

Fig. 1. Thermal expansion ($\Delta l/l$) and thermal expansion coefficient (α) as a function of temperature for pure PMN ceramics (H = heating cycle and C = cooling cycle).

3. Results and discussion

The results of dilatometric measurements of $(1-x)$PMN–xPT ceramics are presented in Figs. 1–3 (solid line is thermal expansion and dot line is thermal expansion coefficient). The dependence of $\Delta l/l$ for pure PMN ceramic in the course of heating and cooling is shown in Fig. 1. The thermal expansion is very low with low thermal expansion coefficient near room temperature or near the Curie point. The temperature of the dielectric permittivity maximum, T_m of this ceramic occurs at around −10 °C, in good agreement with the previously published values [1,20]. Table 1 lists the thermal expansion and transition temperature of PMN–PT compositions, derived from the thermal strain versus temperature measurements. Fig. 2(a–c) indicate that the respective paraelectric–ferroelectric phase transition occurs at ∼100, 120 and 175 °C, for samples with $x = 0.2$, 0.3 and 0.35, respectively. The phase transition temperatures are consistent with literatures [21,22]. Most of these compositions exhibit low thermal expansion coefficient near the Curie temperature. The values of thermal expansion coefficient in the temperature range of −100 to 100 °C, as determined from heating cycle for 0.8PMN–0.2PT, 0.7PMN–0.3PT and 0.65PMN–0.35PT are

Table 1
Various important features of the thermal expansion measurements in the selected PMN–PT ceramics

Sample	T_c (°C)	Thermal expansion coefficient ($\times 10^{-6}$ °C^{-1})[a]	Calculates P_s at room temperature (μC/cm^2)[b]
PMN	−10	1.6	72.97
0.8PMN–0.2PT	100	2.0	94.58
0.7PMN–0.3PT	120	2.4	56.33
0.65PMN–0.35PT	175	3.2	54.76
PT (700/1200 °C)	489	−64	74.99
PT (800/1200 °C)	481	−70	75.49
PT (900/1200 °C)	478	−83	76.85

[a] The estimate precision of these values is approximately ±0.01%.
[b] The estimate precision of these values is approximately ±0.1%.

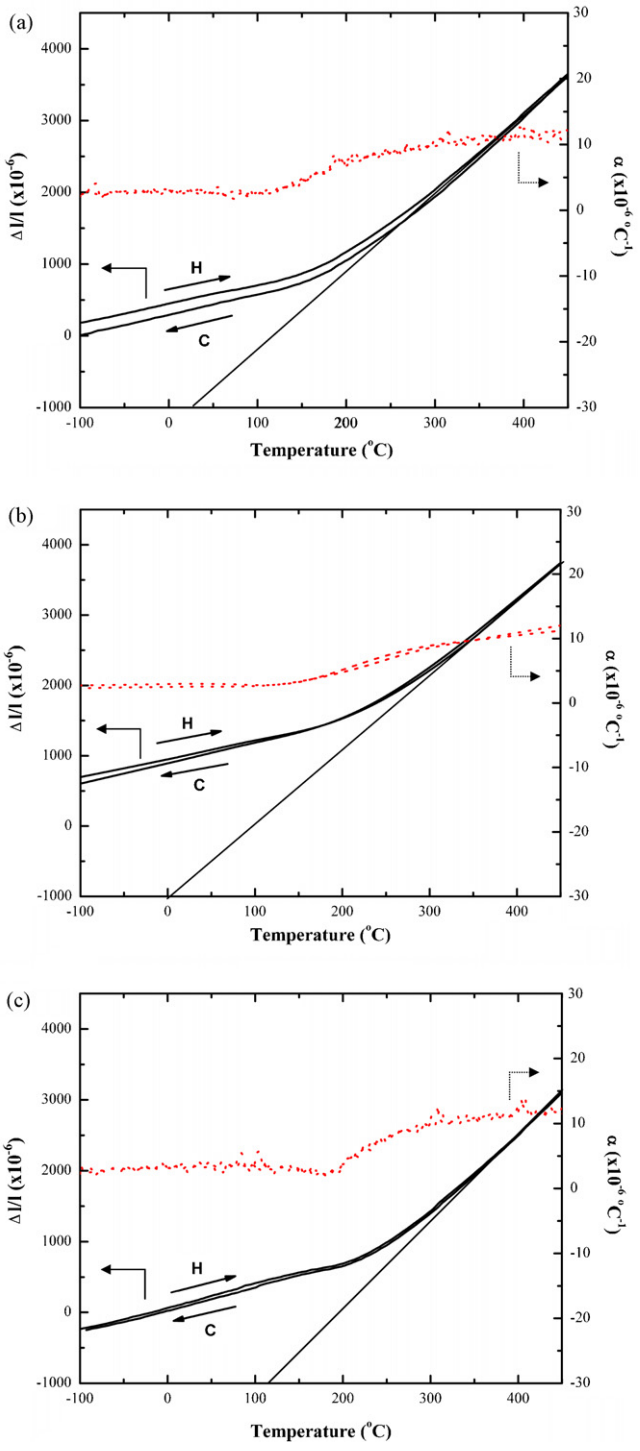

Fig. 2. Thermal expansion ($\Delta l/l$) and thermal expansion coefficient (α) as a function of temperature for $(1-x)$PMN–xPT ceramics: (a) $x=0.20$, (b) $x=0.30$ and (c) $x=0.35$.

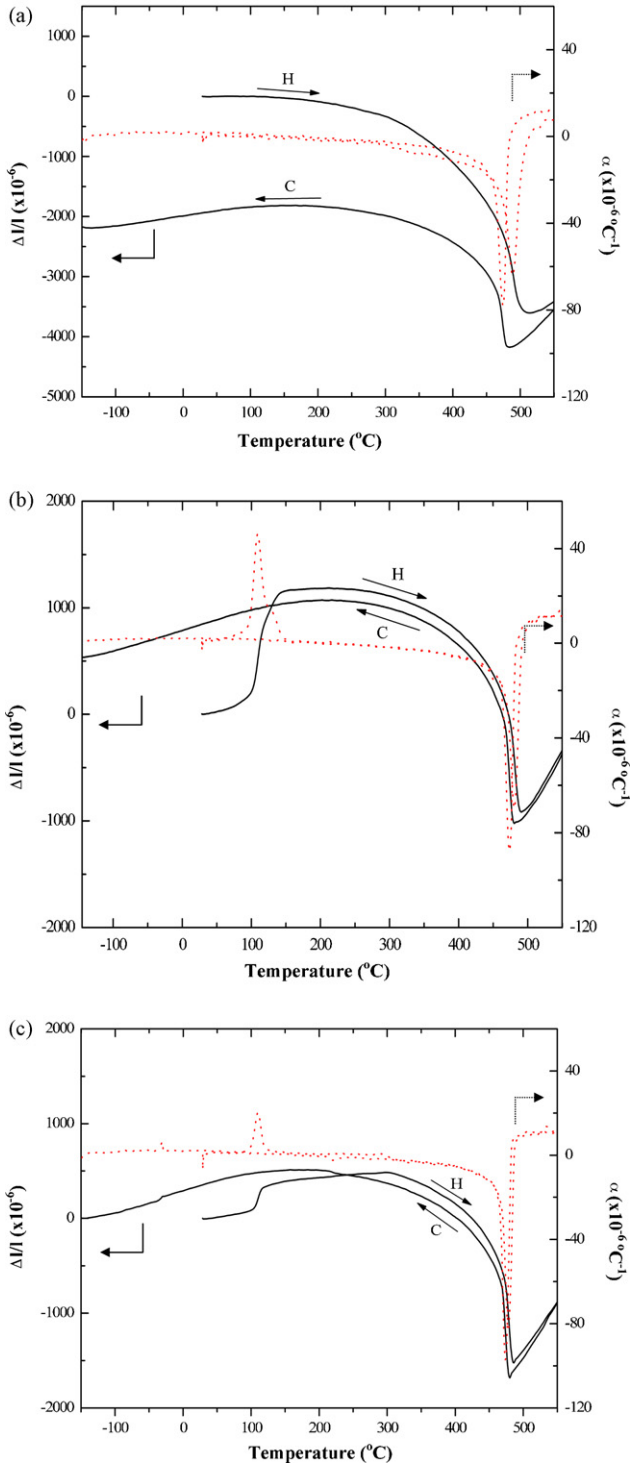

Fig. 3. Thermal expansion ($\Delta l/l$) and thermal expansion coefficient (α) as a function of temperature for PT ceramics doubly sintered at (a) 700/1200, (b) 800/1200 and (c) 900/1200 °C.

2×10^{-6}, 2.4×10^{-6} and $3.2\times10^{-6}\,^{\circ}C^{-1}$, respectively. Furthermore, the highest temperature data, far above T_c, can be approximated by a straight line, as can be seen in the figures. The deviation from this linear high-temperature behavior occurs at 325 °C for $x=0.2$, at 350 °C for $x=0.3$ and at 360 °C for $x=0.35$.

The results of the thermal expansion for double sintered PT ceramics, shown in Fig. 3(a–c), indicate that the respective paraelectric–ferroelectric phase transition occur at around 489 °C for 700/1200 °C PT, at 481 °C for 800/1200 °C PT and at 478 °C for 900/1200 °C PT samples. It should be noted that the thermal expansion behavior of PT differs significantly from

that of pure PMN and PMN–PT. This can be explained by the fact that PT is a normal ferroelectric, whereas pure PMN and PMN–PT ceramics are relaxor ferroelectric. Moreover, the other reason is possible; their structures are different (structure of PT is tetragonal, pure PMN and PMN–PT is cubic). The thermal expansion coefficients change sharply at the T_c, as determined from heating of three unpoled samples and the values are -64×10^{-6}, -70×10^{-6} and $-83 \times 10^{-6}\,^{\circ}C^{-1}$, respectively. The phase transition temperature values are slightly different in the three samples. However, they are in good agreement with literatures [25,26]. Furthermore, the thermal expansion (or strain) curve in these samples is linear at temperatures above $T_c \approx 490\,^{\circ}C$. At temperatures below Curie temperature, these linear thermal expansions are superimposed by a ceramic's spontaneous polarization. Following a thermal cycle, an unpoled ceramic will obviously return very much to the state of distortion it had before the cycle except for 700/1200 °C PT ceramic. The thermal expansion could not be highly reproducible that may be related to the average grain sizes which are smaller than that observed in the other two samples (not show in this paper). It should also be noticed in Fig. 3(b and c) that the anomaly occurs between 100 and 150 °C during heating cycle. This is believed to be due to space charges, as well as moisture, accumulated on the sample surfaces, which then disappeared during cooling cycle.

On analyzing the deviation of the strain from the high-temperature linear behavior and by using Eq. (1), P_d values can be obtained at various temperatures. Using the values of $Q_{11} = 0.123 \times 10^{-2}\ m^4/C^2$ and $Q_{12} = -0.049 \times 10^{-2}\ m^4/C^2$ [27] for $x = 0$, 0.20, 0.30 and 0.35, P_d values can be calculated, as plotted in Fig. 4. When calculating the spontaneous strains of the rhombohedral at a particular temperature, the cubic cell constant should be extrapolated to that temperature accounting for the thermal expansion. A linear extrapolation from above the transition temperature can be made over a narrow range with fairly good accuracy. In Fig. 4, we calculated the P_d, really $((P_d^2)^{1/2})$, values obtained from $\Delta l/l$. Also plotted is the normal reversible polarization data, P_r, determined from the *P–E* measurements. It is evident that the polarization calculated from the strain is larger than P_r and extends several hundred degrees above T_c due to quadratic electrostrictive effects. Moreover, for temperatures well below T_c, although not equal, P_d and P_r are comparable; they are obtained by totally independent techniques. It has been known that the ferroelectric–paraelectric

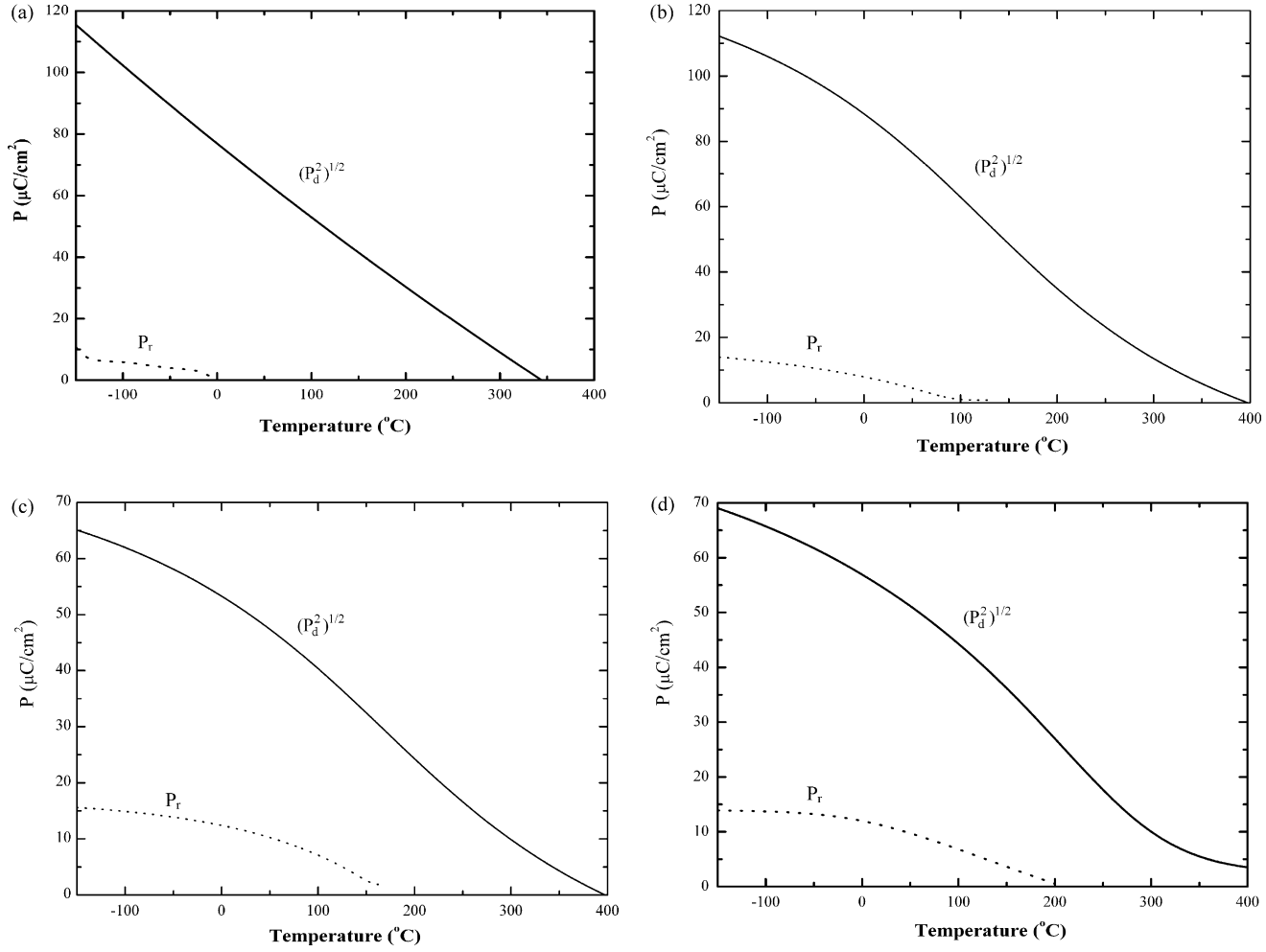

Fig. 4. $(P_d^2)^{1/2}$ as a function of temperature for $(1-x)$PMN–xPT ceramics from Eq. (1) and the reversible ferroelectric polarizations P_r (dot lines): (a) $x = 0$, (b) $x = 0.20$, (c) $x = 0.30$ and (d) $x = 0.35$.

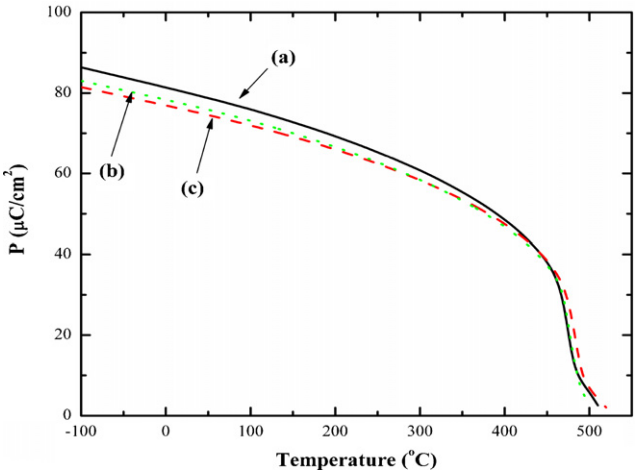

Fig. 5. $(P_d^2)^{1/2}$ as a function of temperature for PT ceramics from Eq. (1): (a) 700/1200, (b) 800/1200 and (c) 900/1200 °C.

phase transition becomes more diffuse when the PT content decreases, indication of a more pronounced relaxor behavior. Ceramic with $x = 0.20$ shows more pronounced relaxor behavior, for which the P_d decays slowly with temperature compared to the other compositions ($x = 0.30$ and 0.35). Nevertheless, all $x = 0.20$, 0.30 and 0.35 show similar T_d value, even though there are differences in their compositions. These T_d values are several hundred degrees above the ferroelectric T_c (≈100 °C for $x = 0.2$, 120 °C for $x = 0.3$ and 175 °C for $x = 0.35$) indicating glassy polarization behavior over the range [6,7]. It seems that at ≈T_d small local regions of the sample begin to show a polarization due to a favorable arrangement of the atoms. The strain measurements can detect this effect because P_d^2 rather than P_d contributes to these terms. Once local regions of polarization occur, the cooperative effect that occurs at T_c can be understood.

For PT sample, using the values of $Q_{11} = 8.9 \times 10^{-2}$ m^4/C^2 and $Q_{12} = -2.6 \times 10^{-2}$ m^4/C^2 [28]. The result is plotted in Fig. 5. When calculating the spontaneous strains of the tetragonal at a particular temperature, the cubic cell constant should be extrapolated to that temperature accounting for the thermal expansion. In Fig. 5, the P_d values calculated from the thermal expansion data are shown. The agreement in the P_s values is excellent. The values are also in good agreement not only in magnitude but also in the T_c values with the earlier reported results [29,30]. All samples sintered under different conditions, the polarization behaviors are slightly different. However, for the 800/1200 and 900/1200 °C ceramics, the magnitude of P_d and trend of polarization behavior are similar to those of 700/1200 °C PT ceramic. The sharpness of the transition increases and the hyteresis space gradually decreases for the samples sintered at higher temperature in first step of the two-stage sintering process. It should be noted that the polarization behavior at high temperature of PMN–PT samples differs from PT samples because the PMN–PT samples have diffuse phase transition whereas PT has the first-order phase transition [25,26].

4. Conclusion

In this work, an anolmaly behavior of thermal expansion in $(1-x)$PMN–xPT ceramics was observed. High temperature anomaly is connected with symmetry change and polar nanodomains arising at the Burns temperature T_d. The obtained results are in good agreement with the reported values and also suggesting that thermal strain data can be used for reliable estimating the polarization.

Acknowledgements

We thank the Thailand Research Fund (TRF) and the Commission on Higher Education (CHE), the Thailand Toray Science Foundation (TTSF), the Graduate School of Chiang Mai University and NSF Relaxor program, Materials Research Laboratory and MRI of Penn State University for all the support.

References

[1] L.E. Cross, Ferroelectrics 76 (1987) 241–267.
[2] G.A. Samara, J. Phys. Condens. Matter 15 (2003) R367–R411.
[3] G. Burns, F.H. Dacol, Solid State Commun. 42 (1982) 9–12.
[4] W. Kleemann, F.J. Schäfer, D. Rytz, Phys. Rev. B 34 (1986) 7873–7879.
[5] W. Kleemann, F.J. Schäfer, M.D. Fontana, Phys. Rev. B 30 (1984) 1148.
[6] G. Burns, F.H. Dacol, Phys. Rev. B 28 (1983) 2527–2530.
[7] G. Burns, F.H. Dacol, Solid State Commun. 48 (1983) 853–856.
[8] A.S. Bhalla, R. Guo, L.E. Cross, G. Burns, F.H. Dacol, R.R. Neurgaonkar, Phys. Rev. B 36 (1987) 2030–2035.
[9] N.N. Krainik, L.A. Markova, V.V. Zhdanova, Ferroelectrics 90 (1989) 119–124.
[10] P. Bonneau, P. Garnier, C. Calvarin, J. Solid State Chem. 91 (1991) 350–361.
[11] M. Damdekalne, K. Bormanis, L. Chakare, A. Sternberg, Ferroelectrics 186 (1996) 293–296.
[12] G. Burns, F.H. Dacol, Solid State Commun. 58 (1986) 567–571.
[13] T. Heinz, G. Burns, N. Halas, Bull. Am. Phys. Soc. 31 (1986) 603.
[14] J. Zhao, A.E. Glazounov, Q.M. Zhang, B. Toby, Appl. Phys. Lett. 72 (1998) 1048–1050.
[15] D. La-Orauttapong, J. Toulouse, Z.-G. Ye, W. Chen, R. Erwin, J.L. Robertson, Phys. Rev. B 67 (2003) 134110–134120.
[16] W. Kleemann, P. Licinio, T. Woike, R. Pankrath, Phys. Rev. Lett. 86 (2001) 6014–6017.
[17] D. Viehland, S.J. Jang, L.E. Cross, M. Wutting, Phys. Rev. B 46 (1992) 8003–8006.
[18] V. Bovtun, J. Petzelt, V. Porokhonskyy, S. Kamba, Y. Yakimenko, J. Eur. Ceram. Soc. 21 (2001) 1307–1311.
[19] J. Dec, W. Kleemann, V. Bobnar, Z. Kutnjak, A. Levstik, R. Pirc, R. Pankrath, Europhys. Lett. 55 (2001) 781–787.
[20] S.L. Swartz, T.R. Shrout, W.A. Schulze, L.E. Cross, J. Am. Ceram. Soc. 67 (1984) 311–315.
[21] H. Arndt, G. Schmidt, Ferroelectrics 79 (1988) 149–152.
[22] S. Ananta, N.W. Thomas, J. Eur. Ceram. Soc. 19 (1999) 155–163.
[23] R. Wongmaneerung, R. Yimnirun, S. Ananta, Mater. Lett. 60 (2006) 2666–2671.
[24] S. Ananta, N.W. Thomas, J. Eur. Ceram. Soc. 19 (1999) 2917–2930.
[25] G. Shirane, S. Hoshino, J. Phys. Soc. Jpn. 6 (1951) 265–270.
[26] G. Shirane, R. Pepinsky, B.C. Frazer, Acta Crystallogr. 9 (1956) 131–140.
[27] G. Robert, M.D. Maeder, D. Damjanovic, N. Setter, J. Am. Ceram. Soc. 84 (2001) 2869–2872.
[28] M.J. Huan, E. Furman, S.J. Jang, H.A. McKinstry, L.E. Cross, J. Appl. Phys. 62 (1987) 3331–3338.
[29] V.G. Gavrilyachenko, R.I. Spinko, M.A. Martynenko, E.G. Fesenko, Fiz. Tverd. Tela 12 (1970) 1532–1534.
[30] F. Jona, G. Shirane, Ferroelectric Crystal, Pergamon Press, Oxford, 1962.

Influences of perpendicular compressive stress on the dielectric and ferroelectric properties of electrostrictive and piezoelectric $Pb(Mg_{1/3}Nb_{2/3})O_3$-$PbTiO_3$ ceramics

Muangjai Unruan, Athipong Ngamjarurojana, Yongyut Laosiritaworn, Supon Ananta, and Rattikorn Yimnirun[a)]
Department of Physics, Faculty of Science, Chiang Mai University, Chiang Mai 50200, Thailand

(Received 26 February 2008; accepted 26 May 2008; published online 1 August 2008)

The dielectric and ferroelectric properties of $(1-x)Pb(Mg_{1/3}Nb_{2/3})O_3$-$(x)PbTiO_3$ or $(1-x)$PMN-(x)PT $(x=0.1-0.4)$ ceramics were measured under compressive stress applied perpendicular to the electric field. For the dielectric properties, the experimental results revealed that the superimposed perpendicular compression stress reduced the dielectric constant but increased the dielectric loss tangent of all the compositions. On the other hand, for the ferroelectric properties the applied stress noticeably enhanced the dissipation energy, the polarizations, and the coercive field of all the compositions. These results were interpreted through the non-180° ferroelastic domain switching processes, the stress clamping of domain walls, the deaging mechanism, and the stress induced enhancement in the switchable part of spontaneous polarization. More importantly, the influences of the stress applied in the perpendicular direction to the electric field were generally opposite to those of the parallel stress. © *2008 American Institute of Physics*.
[DOI: 10.1063/1.2960518]

I. INTRODUCTION

Perovskite relaxor ferroelectric lead magnesium niobate, $Pb(Mg_{1/3}Nb_{2/3})O_3$ (PMN), and its solid solution with normal ferroelectric lead titanate, $PbTiO_3$ (PT), the so-called PMN-PT, are of great interest due to their high polarizabilities and excellent combined electrical properties suitable for various electronic device applications. These compounds have dielectric constants in excess of 20 000, making them potential candidates for capacitive applications. In addition, they also exhibit large electrostrictive coefficients at temperatures above their phase transition temperatures. This behavior extends their use to transducer and actuator applications.[1–5] In general, the $(1-x)Pb(Mg_{1/3}Nb_{2/3})O_3$-$(x)PbTiO_3$ or $(1-x)$PMN-(x)PT ceramic compositions with $x<0.2$ have been studied for electrostrictive applications,[4–7] while those with $x>0.2$ can be utilized as piezoelectric materials.[4,6,8,9] The differences between the electrostrictive and piezoelectric compositions of PMN-PT are due to differences in the degree of long-range polar order.[4,7,10] In the compositions with lower PT content, relaxor ferroelectric characteristics with polar clusters or nanodomains are observed.[4,11,12] On the other hand, long-range polar order with normal micron-sized ferroelectric domains exists in the compositions with higher PT content.[4,9,10]

Practically, when used in specific applications PMN-PT ceramics are often subjected to mechanical loading, either deliberately in the design of the device itself or because the device is used to change shapes as in many smart structure applications or the device is used under environmental stresses.[8,13–17] A prior knowledge of how the material properties change under different load conditions is crucial for proper design of a device and for suitable selection of materials for a specific application. Despite this fact, material constants used in any design calculations are often obtained from a stress-free measuring condition, which in turn may lead to incorrect or inappropriate actuator and transducer designs. It is therefore important to determine the properties of these materials as a function of applied stress. Previous investigations on the stress dependence of the electrical properties of many ceramic systems have clearly emphasized the importance of the matter.[7,15,18–23] Recently, the stress dependence of dielectric and ferroelectric properties has been investigated in several perovskite-based materials such as $BaTiO_3$ (BT), $Pb(Zr_{0.52}Ti_{0.48})O_3$ (PZT), PMN, PZT-BT, PMN-PZT, and $Pb(Zn_{1/3}Nb_{2/3})O_3$ (PZN)-PZT.[19–22,24–26] Since PMN-PT ceramics are practically employed in many electromechanical devices, there have been previous reports on the electromechanical properties of electrostrictive 0.9PMN-0.1PT and piezoelectric 0.7PMN-0.3PT ceramics under various mechanical and electrical loading conditions.[7,15,23,27] In addition, our previous investigation on the influence of the applied stress on the dielectric properties of PMN-PT ceramic systems also revealed that the superimposed compression stress significantly reduced both the dielectric constant and the dielectric loss tangent of 0.9PMN-0.1PT ceramics, while the changes were not as significant in the other PMN-PT ceramic compositions.[24] The results clearly showed that the effects of stress on the dielectric properties depended significantly on the ceramic chemical compositions and stress levels. In addition, significant changes in the ferroelectric properties of PMN-PT ceramics under the compressive stress applied parallel to the electric field were observed in our recent investihgation.[28] Previously, many investigations also reported the electrical properties of ferroelectric ceramics under the influences of the

[a)]Electronic mail: rattikornyimnikirun@yahoo.com.

 © 2008 American Institute of Physics

Downloaded 14 Apr 2009 to 202.28.246.2. Redistribution subject to AIP license or copyright; see http://jap.aip.org/jap/copyright.jsp

TABLE I. Characteristics of PMN-PT ceramics with optimized processing conditions (Refs. 24, 28, and 32).

Ceramic	Density[a] (g/cm^3)	Grain size range (μm)	Average grain size[b] (μm)	T_m or T_C (1 kHz) (°C)	Stress-free dielectric properties[c] ε_r	tan δ	Stress-free ferroelectric properties[d] $\langle A \rangle$ (kJ/m^3)	P_{sat} ($\mu C/cm^2$)	P_r ($\mu C/cm^2$)	E_c (kV/cm)	Stress-free differential permittivity
0.9PMN-0.1PT	7.98	0.42–3.66	2.07	45	5321	0.082	57	12.3	1.7	1.5	13 062
0.8PMN-0.2PT	7.94	0.44–3.02	2.02	100	2674	0.045	121	14.1	6.6	2.8	15 439
0.7PMN-0.3PT	7.86	0.41–2.80	1.72	150	2019	0.050	184	12.9	7.5	4.5	9126
0.6PMN-0.4PT	7.83	0.41–3.45	1.93	210	1223	0.024	235	9.7	6.1	8.2	5013

[a]The estimated precision of the density is ±1%.
[b]The estimated precision of the average grain size is ±1%.
[c]Measured at 1 V/mm (25 °C and 1 kHz).
[d]Measured at 25 °C and 50 Hz.

compressive stress applied perpendicular to the electric field.[20,22,27,29–31] Therefore, as an extension of our previous investigations on PMN-PT ceramics,[24,28] it is the aim of this study to examine the dielectric and ferroelectric properties of the electrostrictive and piezoelectric PMN-PT ceramic compositions under compressive stress applied perpendicular to the electric field.

II. EXPERIMENTAL METHOD

As described in our previous investigations,[24,28] dense perovskite-phase electrostrictive 0.9PMN-0.1PT and 0.8PMN-0.2PT ceramics and piezoelectric 0.7PMN-0.3PT and 0.6PMN-0.4PT ceramics with uniform microstructure and similar density values used in this study were prepared from PMN and PT powders by the mixed-oxide columbite precursor method. Details of the ceramic processing and characterizations were already provided elsewhere.[32] Table I summarizes the physical characteristics of the PMN-PT ceramics used in this study. More importantly, since the physical and microstructure features of all the ceramic compositions are not significantly different, these parameters should not play an important role in the composition-dependent ferroelectric properties under compressive stress.

Before studying the dielectric and ferroelectric properties under compressive stress, the sintered specimens were cut as rectangular bars (approximate dimensions of $6 \times 2 \times 2$ mm^3) and lapped to obtain parallel faces. After coating with silver paint as electrode at the faces, the specimens were heated at 750 °C for 12 min with heating/cooling rates of 10 °C/min to ensure the contact between the electrode and surface of ceramics. The electrodes were applied on the other two opposite faces with silver wire attached to the electrodes for electrical measurement. To study the effects of the compressive stress on the dielectric and ferroelectric properties, the uniaxial compressometer was constructed for simultaneous applications of the mechanical stress and the electric field.[33–35] Figure 1 shows a schematic of the experimental setup with stress and electric field applied perpendicularly. The compressometer cell consisting of a cylindrical brass cell with a heavy brass base, a brass ram, and a precisely guided loading platform provided true uniaxial stress during mechanical loading. The compressive stress was supplied by the servohydraulic load frame and the applied stress level was monitored with the pressure gauge of the load frame. Measurements were performed as a function of mechanical stress applied discretely between 0 and 170 MPa depending on the samples. The low-field dielectric properties were measured by an *LCR* meter (Instrek LCR-821) with an applied voltage of 1 V. The room temperature (25 °C) capacitance and the dielectric loss tangent were determined at a frequency of 1 kHz. The dielectric constant was then calculated from a parallel-plate capacitor equation, e.g., $\varepsilon_r = Cd/\varepsilon_0 A$, where C is the capacitance of the specimens, d and A are, respectively, the thickness and the area of the electrode, and ε_0 is the dielectric permittivity of vacuum (8.854×10^{-12} F/m). The room temperature (25 °C) ferroelectric hysteresis (P-E) loops were characterized by using a computer controlled modified Sawyer–Tower circuit. The electric field of 15–20 kV/cm was applied to a sample by a high voltage ac amplifier (Trek, model 610D) with input sinusoidal signal with a frequency of 50 Hz from a signal generator (Goodwill, model GAG-809). The parameters obtained from the loops were the saturation polarization (P_{sat}), the remanent polarization (P_r), and the coercive field (E_c), which were defined as the points where the loops reach the maximum polarization, cross the zero field, and cross the zero polarization, respectively. The measurements reported were for the samples during their first mechanical stress cycle. It should also be noted that the reported ferroelectric

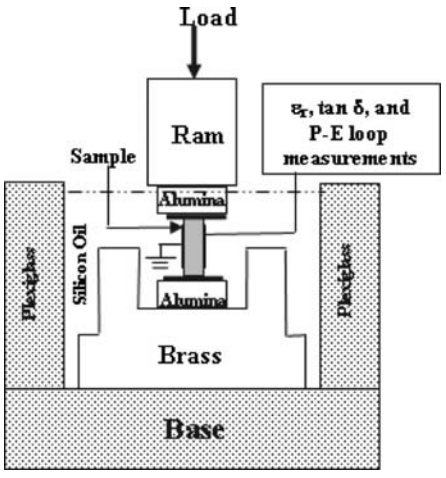

FIG. 1. A schematic of the experimental setup showing stress and electric field applied perpendicularly.

Downloaded 14 Apr 2009 to 202.28.246.2. Redistribution subject to AIP license or copyright; see http://jap.aip.org/jap/copyright.jsp

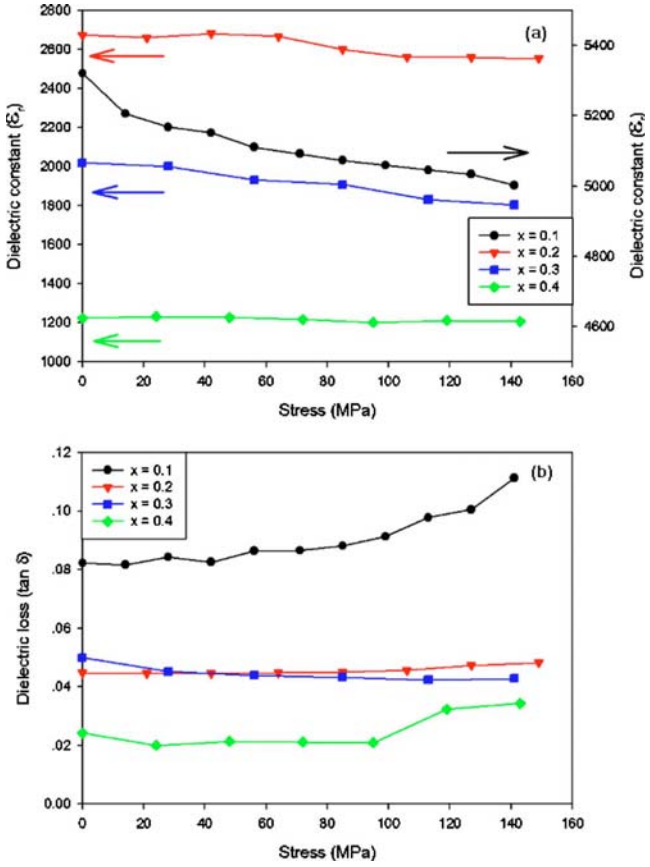

FIG. 2. (Color online) Changes in the dielectric properties of $(1-x)$PMN-(x)PT ceramics with compressive stress applied perpendicular to the electric field: (a) dielectric constant (ε_r) and (b) dielectric loss (tan δ) (measured at 25 °C and 1 kHz).

parameters were obtained after a total of 10 cycles of the electric field was applied to the sample at each constant stress level.

III. RESULTS AND DISCUSSION

A. Dielectric properties under perpendicular stress

The room temperature dielectric properties at 1 kHz of $(1-x)$PMN-(x)PT ceramics as a function of compressive stress are depicted in Fig. 2. Clearly, there are observable changes in both the dielectric constant [Fig. 2(a)] and the dielectric loss tangent [Fig. 2(b)] with the stress applied perpendicular to the electric field direction. As seen in Fig. 2(a), the dielectric constant is seen to decrease with increasing stress in all the compositions. The decrease in the dielectric constant varies from approximately 12% in the near morphotropic phase boundary (MPB) piezoelectric 0.7PMN-0.3PT composition to 4%–5% in the electrostrictive 0.9PMN-0.1PT and 0.8PMN-0.2PT compositions and to 2% in the tetragonal piezoelectric 0.6PMN-0.4PT composition at a maximum applied stress of 150 MPa. However, since the dielectric constant of the sample was measured through the capacitance, there is a change in sample capacitance due to the geometrical deformation under stress. The variation in the sample dielectric constant $(\Delta\varepsilon_r)$ can be expressed as $\varepsilon_r^* X^*[(1+2\upsilon)/E]$, where X is the applied stress, υ is the Poisson ratio, and E is the Young modulus.[24,35] By applying the estimated values of $\upsilon \sim 0.3$ and $E \sim 100$ GPa for PMN-PT ceramics[7,23,27,36] and ε_r given in Table I, it can be estimated that at the maximum stress of 150 MPa, the variation in the sample dielectric constant due to the geometrical deformation is $<0.5\%$. Therefore, this variation should not be an important factor in the variation in the dielectric constant under stress seen in Fig. 2(a). Interestingly, the changes in the dielectric constant of the PMN-PT systems with the perpendicular stress are generally similar to those of the parallel stress obtained in our previous investigation.[24]

On the other hand, when the maximum stress of 150 MPa is reached the dielectric loss tangent (tan δ) is generally seen to increase from the stress-free value, as displayed in Fig. 2(b). However, while the dielectric loss tangent for the electrostrictive 0.9PMN-0.1PT and 0.8PMN-0.2PT compositions increases continuously with increasing stress, that for the piezoelectric 0.7PMN-0.3PT and 0.6PMN-0.4PT compositions first decreases slightly, then slowly increases at a higher applied stress. For the case of the compressive stress applied perpendicular to the direction of the electric field, only a few previous experimental works have been carried out on some commercial hard and soft PZT ceramics, $Pb(In_{1/2}Nb_{1/2})O_3$ (PIN)-PT and PMN-PT ceramics.[20,27,29,37,38] Interestingly, the results observed in this current study are generally very similar to those obtained earlier in the Pb-based perovskite ceramics mentioned above.

To understand these experimental results, at least qualitatively, various effects have to be considered. Normally, the properties of ferroelectric materials are derived from both the intrinsic contribution of domains and extrinsic contributions of repolarization and growth of micropolar regions.[19–23] When a compressive stress is applied to the ferroelectric materials, the domain structure in the materials will change to maintain the domain energy at a minimum; during this process some of the domains engulf other domains or change shape irreversibly. Under the applied stress, the domain structure of ferroelectric ceramics may undergo domain switching through non-180° domain walls, deaging, clamping of domain walls, and stress induced decrease in the switchable part of spontaneous polarization.[21,23,39]

The situation for the PMN-PT system is quite complex because this system is a mixing between the relaxor ferroelectric PMN and the normal ferroelectric PT. Therefore, there is a competing mechanism between the two types of materials depending on temperature and chemical composition. Since 0.9PMN-0.1PT is a relaxor ferroelectric with $T_m \sim 45$ °C and the experiment was carried out at room temperature (~25 °C), which is slightly below the T_m, the experimental observation, which shows decreases in dielectric constant with increasing stress, can be attributed to competing influences of the intrinsic contribution of nonpolar matrix and the extrinsic contribution of repolarization and growth of micropolar regions. Since the dielectric response of both contributions is affected by the applied stress in an opposite way, the behavior of 0.9PMN-0.1PT depends on the ratio between the micropolar region and the nonpolar matrix; in this case the nonpolar matrix still dominates.[21,22,37] Hence, the dielectric constant of the 0.9PMN-0.1PT ceramics is ob-

Downloaded 14 Apr 2009 to 202.28.246.2. Redistribution subject to AIP license or copyright; see http://jap.aip.org/jap/copyright.jsp

served to decrease, while the dielectric loss tangent increases with increasing the compressive stress. The dielectric response to the applied stress is therefore slightly lower in the electrostrictive 0.8PMN-0.2PT composition with a higher micropolar region content at room temperature.

The decrease in the dielectric constant for the piezoelectric compositions with a drastic change in 0.7PMN-0.3PT and a very little change in 0.6PMN-0.4PT can be attributed to influences of the polarization and domains. Under the applied compressive stress, the stress clamping of domain walls, which results in a decrease in domain wall mobility, and the stress induced decrease in the switchable part of spontaneous polarization are expected to play a role in the decrease in the dielectric properties of the two compositions.[20,37] In addition, the continuous decrease in the dielectric constant can also be attributed to the switching of 90° domains, which causes the significant decrease in the dielectric constant. A larger decrease in the dielectric constant of the near MPB composition, i.e., 0.7PMN-0.3PT, is attributed to more domain states in the composition that combines six possible domain states from the tetragonal phase with eight possible domain states from the pseudocubic (or rhombohedral) phase;[1–4] hence a much larger change is observed. On the other hand, the dielectric constant of 0.6PMN-0.4PT is rather stable under the applied stress when compared to the near MPB 0.7PMN-0.3PT composition. This suggests the influence of different crystal structures and domain states. As stated above, the 0.7PMN-0.3PT composition contains mixed tetragonal-rhombohedral phases with more possible domain states (14), while the 0.6PMN-0.4PT contains mainly tetragonal phases with only 6 domain states, hence a much smaller change in the dielectric constant. In addition, since the measurements were carried out at room temperature, which is far below the transition temperature of 210 °C for the 0.6PMN-0.4PT composition, the domain is much less mobile and the change in the dielectric constant is also much less. Most of the more recent studies agree that the phase composition near the MPB is likely some form of monoclinic or possibly several phases together.[40–42] It is probably not rhombohedral and tetragonal phases. However, the hypothesis given above is still reasonable; i.e., the 0.6PMN-0.4PT composition is tetragonal, a phase very resistant to stress induced change, and the 0.7PMN-0.3PT composition certainly has a much more complicated phase composition that is highly vulnerable to stress induced domain switching (regardless of what the phase composition actually is). Moreover, the deaging mechanism is also expected to play a role in the increase in the dielectric loss tangent at a higher stress. During the aging process, some of the domain walls become pinned by impurities and structural imperfections. When a large enough stress is applied to the aged samples, it causes structural changes and redistribution of impurities. As a result, the domain walls that were pinned during aging can become active again. This deaging can increase the dielectric loss tangent, as observed in the 0.6PMN-0.4PT composition.

B. Ferroelectric properties under perpendicular stress

The polarization versus electric field (*P-E*) hysteresis loops of 0.9PMN-0.1PT, 0.8PMN-0.2PT, 0.7PMN-0.3PT, and 0.6PMN-0.4PT ceramics under different compressive stresses applied perpendicular to the electric field are shown in Figs. 3(a)–3(d), respectively. It should first be noticed that generally the area of the *P-E* loops increases with increasing perpendicular compressive stress. The changes follow a similar trend for all the ceramic compositions. However, the observations are in contrast to the case when the stress was applied in parallel to the electric field reported in our previous investigations.[24,26,28,33,43] The *P-E* loop area indicates the polarization dissipation energy of a ferroelectric material under one full cycle of electric field application.[18,44] This amount of energy loss is directly related to the amount of domains participating in the switching process during the application of the electric field.[18,19] For a given composition, the increase in the loop area with increasing compressive stress indicates enhanced dissipation energy under the applied stress in the perpendicular direction, in contrast to the parallel case.[28] A possible explanation for such observation will be discussed later.

The changes in the hysteresis parameters, i.e., the dissipation energy, the saturation polarization (P_{sat}), the remanent polarization (P_r), and the coercive field (E_c), with the compressive stresses are plotted in Figs. 4(a)–4(d), respectively. At a given stress, the composition-dependent hysteresis parameters follow the trend observed in previous investigations.[7,15,23,27,30,36] Here, electrostrictive 0.9PMN-0.1PT and 0.8PMN-0.2PT compositions with slim *P-E* loops show lower dissipation energy as compared to piezoelectric compositions with a square-type loop. Similarly, the remanent polarization is smallest in the electrostrictive 0.9PMN-0.1PT composition, while the highest polarization is obtained in the near MPB 0.7PMN-0.3PT composition. The highest coercive field is observed in the tetragonal 0.6PMN-0.4PT composition, as expected. Considering the stress dependence, it can generally be seen that in every composition, the dissipation energy, the polarizations, and the coercive field increase almost linearly as the perpendicular compressive stress increases. It should, however, be noticed that the saturation polarization of the 0.7PMN-0.3PT composition actually decreases with increasing stress. This is in contrast to every other compositions and properties. An obvious explanation for this unusual behavior is currently not available and work is ongoing to understand the behavior. Nonetheless, the increase in all the parameters is generally less than 20% when the compressive is increased from 0 to 140–170 MPa, with the coercive field being changed less dramatically than the other parameters. The results of the changes in the hysteresis parameters of the PMN-PT ceramics with increasing perpendicular compressive stress are in agreement with the previous investigations on many ferroelectric ceramics.[20,22,27,30,31]

To understand, at least qualitatively, these experimental results on the ferroelectric properties of the PMN-PT ceramics, one can interpret the changes in terms of domain-

Downloaded 14 Apr 2009 to 202.28.246.2. Redistribution subject to AIP license or copyright; see http://jap.aip.org/jap/copyright.jsp

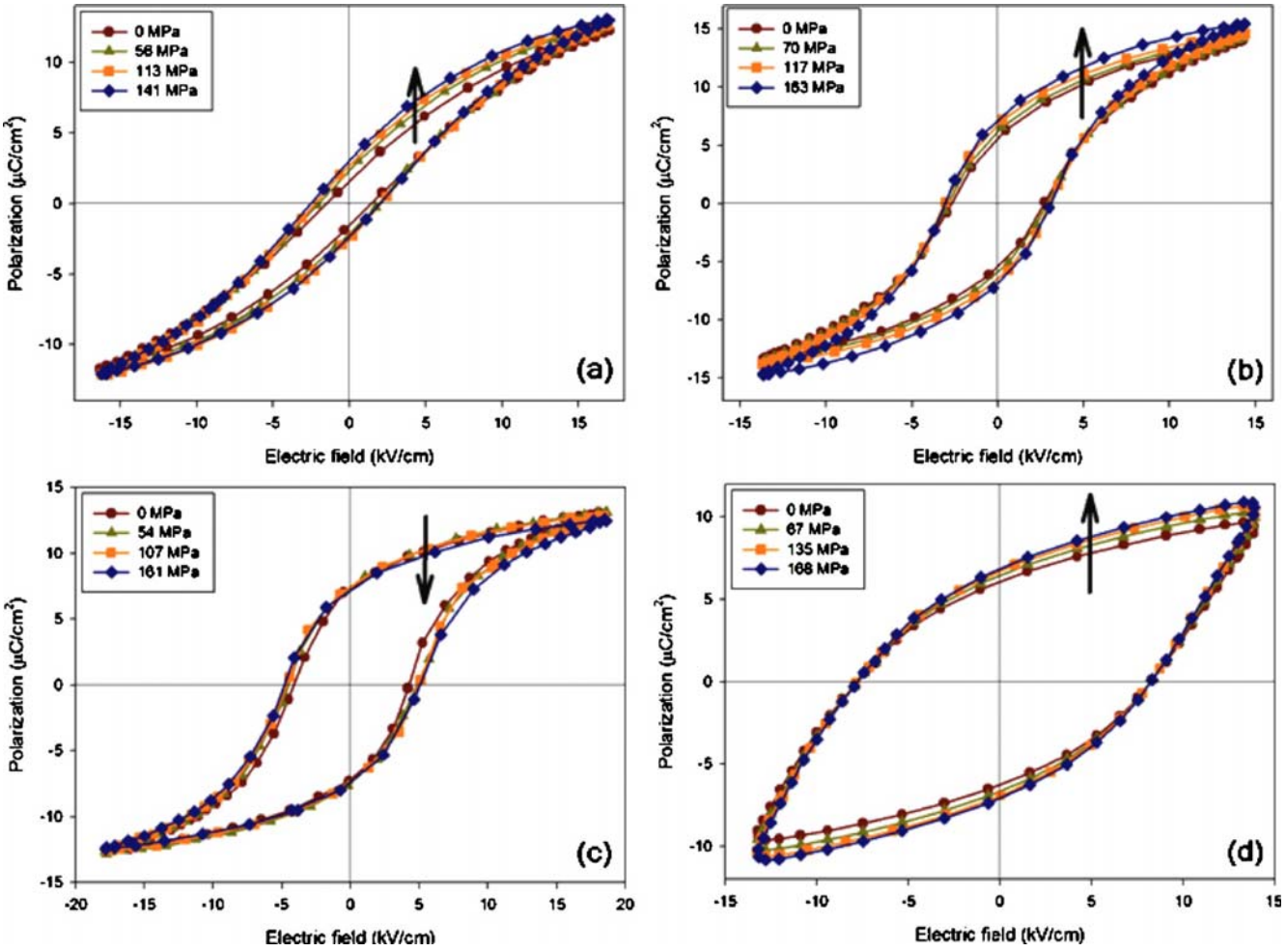

FIG. 3. (Color online) Polarization–electric field (*P-E*) hysteresis loops as a function of compressive stress applied perpendicular to the electric field for (a) 0.9PMN-0.1PT, (b) 0.8PMN-0.2PT, (c) 0.7PMN-0.3PT, and (d) 0.6PMN-0.4PT ceramics (measured at 25 °C and 50 Hz) (arrow indicates changes in polarization with increasing stress).

reorientation processes. When the compressive stress is applied perpendicular to the electric field direction, the applied stress tends to force the polarization of the individual domains to lie in a plane normal to the stress direction through the non-180° (i.e., 90° domain switching in tetragonal composition and 71° (or 109°) domain switching in rhombohedral composition) ferroelastic domain switching processes.[18–21,31] Since the applied electric field direction also lies in this plane, it takes a lower than usual applied electric field to reorient the domains perpendicular to the stress direction (or along the electric field direction), resulting in a higher value of the saturation polarization (P_{sat}), as shown in Fig. 4(b). When the electric field is reduced to zero, some of the domains cannot rotate back to the applied compressive stress direction, resulting in a higher than usual remanent polarization (P_r), as depicted in Fig. 4(c). Similarly, it takes a larger than usual electric field to force the polarizations to become zero; hence a larger coercive field is observed, as shown in Fig. 4(d). Furthermore, considering the increase in the hysteresis loss with increasing the compressive stress, as shown in Fig. 4(a), it indicates that since the perpendicular stress favors domains parallel or antiparallel to the applied electric field, more and more ferroelectric domains participate in the polarization reversal. Consequently, both the saturation and remanent polarizations become higher with increasing the perpendicular compressive stress. However, for the 0.7PMN-0.3PT composition it is noticed that the saturation polarization decreases slightly at high stresses, as depicted in Fig. 4(b). The exact explanation is not clearly known, but it could be attributed to the competing influences of the above mentioned mechanism and the stress induced decrease in the switchable part of spontaneous polarization,[21,23,39] with the latter being stronger; hence the decrease in the saturation polarization is observed at higher stresses.

More interestingly, one would be able to estimate from the *P-E* loops obtained in this study the large-signal dielectric permittivity by using Eq. (1), which gives

$$\varepsilon = \frac{\Delta P}{\Delta E}, \tag{1}$$

where ΔP is the polarization difference between +1.0 and −1.0 kV/cm. The calculated dielectric permittivity can be called *differential permittivity*, which includes the reversible (intrinsic dielectric property) and irreversible (extrinsic do-

Downloaded 14 Apr 2009 to 202.28.246.2. Redistribution subject to AIP license or copyright; see http://jap.aip.org/jap/copyright.jsp

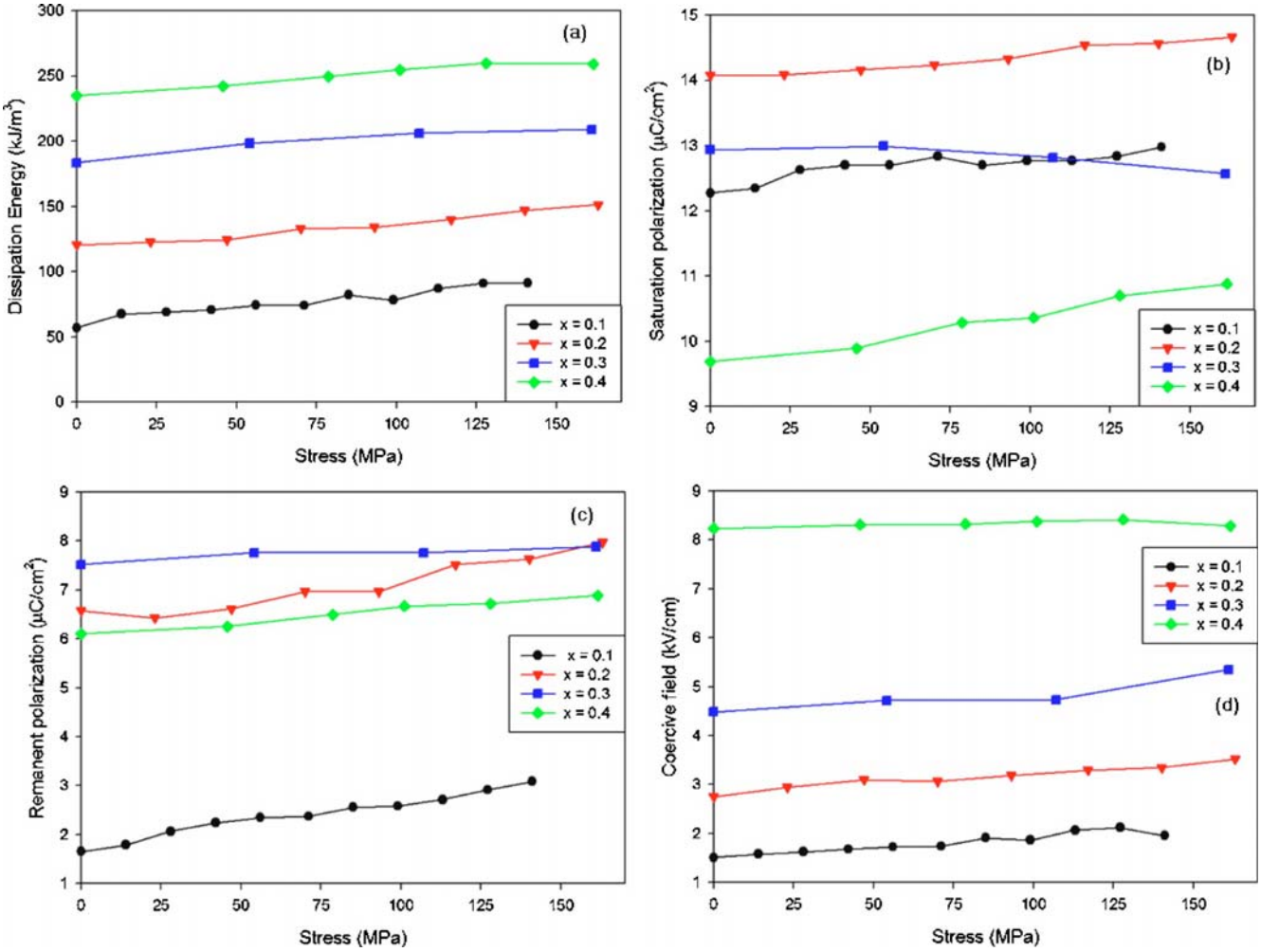

FIG. 4. (Color online) Changes in polarization–electric field (P-E) hysteresis parameters of $(1-x)$PMN-(x)PT ceramics with compressive stress applied perpendicular to the electric field: (a) dissipation energy $\langle A \rangle$, (b) saturation polarization (P_{sat}), (c) remanent polarization (P_r), and (d) coercive field (E_c) (measured at 25 °C and 50 Hz).

main switching related property) contributions of the materials.[18,33] As shown in Fig. 5 and listed in Table I, the differential permittivity is three to five times larger than the low-field relative permittivity. This clearly indicates a significant contribution from the domain switching to the dielectric properties. Though some variations in the data are present in the differential relative permittivity as shown in Fig. 5, it is even more interesting to observe that the differential relative permittivity of all the compositions tends to increase with the applied stress, which is opposite to the decreasing trend for the low-field dielectric constant shown in Fig. 2(a). This is attributed to the enhanced polarizations in the electric field direction as a result of the perpendicular stress, as stated above. The direct comparison between the high-field and low-field dielectric constants clearly signifies the importance of the experimental conditions used to determine the dielectric properties, as well as the stress-dependent dielectric properties.

This study has served as an extension of our previous work on the parallel stress-dependent dielectric and ferroelectric properties,[24,28] as well as other earlier reports, which mainly focused on only 0.9PMN-0.1PT compositions.[7,15,23,27,30] The results presented in this study have shown that the dielectric and ferroelectric properties in PMN-PT ceramics under perpendicular stress differ significantly from those under the parallel stress case reported in previous investigations.[24,28] Finally, the information obtained here is practically very useful for the design and calculation consideration of devices employing the PMN-PT ceramics.

IV. CONCLUSIONS

The dielectric and ferroelectric properties of $(1-x)$PMN-(x)PT $(x=0.1-0.4)$ ceramics are investigated under compressive stress applied perpendicular to the electric field. The experimental results reveal that the superimposed perpendicular compression stress reduces the dielectric constant but increases the dielectric loss tangent of all the compositions. On the other hand, for the ferroelectric properties the applied stress noticeably enhances the dissipation energy, the polarizations, and the coercive field of all the compositions. In addition, the differential dielectric permittivity is found to increase with increasing compressive stress. These results can be interpreted through the non-180° ferroelastic domain

Downloaded 14 Apr 2009 to 202.28.246.2. Redistribution subject to AIP license or copyright; see http://jap.aip.org/jap/copyright.jsp

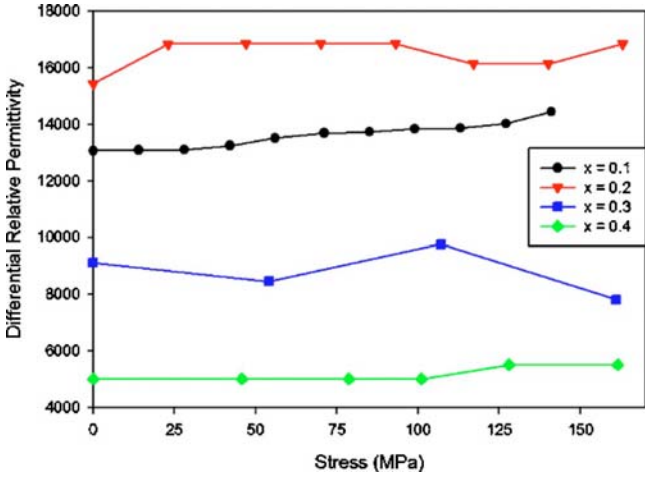

FIG. 5. (Color online) Changes in differential relative permittivity of $(1-x)$PMN-(x)PT ceramics with compressive stress applied perpendicular to the electric field (determined from ± 1 kV/cm of the *P-E* loops measured at 25 °C and 50 Hz).

switching processes, the stress clamping of domain walls, the deaging mechanism, and the stress induced enhancement in the switchable part of spontaneous polarization. Finally, the influences of the stress applied in the perpendicular direction to the electric field are generally opposite to those of the parallel stress.

ACKNOWLEDGMENTS

Supports from the Thailand Research Fund (TRF), Commission on Higher Education (CHE), Royal Golden Jubilee PhD Program, Faculty of Science, and Graduate School of Chiang Mai University are gratefully acknowledged.

[1]Y. H. Xu, *Ferroelectric Materials and Their Applications* (North-Holland, Los Angeles, 1991).
[2]A. J. Moulson and J. M. Herbert, *Electroceramics: Materials, Properties, Applications* (Wiley, Chichester, 2003).
[3]G. H. Haertling, J. Am. Ceram. Soc. **82**, 797 (1999).
[4]L. E. Cross, Mater. Chem. Phys. **43**, 108 (1996).
[5]S.-J. Jang, Ph.D. thesis, The Pennsylvania State University, 1979.
[6]K. Uchino, *Piezoelectric Actuators and Ultrasonic Motors* (Kluwer, Boston, 1997).
[7]D. Viehland, J. Li, E. McLaughlin, J. Powers, R. Janus, and H. Robinson, J. Appl. Phys. **95**, 1969 (2004).
[8]T. R. Shrout, Z. Chang, N. Kim, and S. Markgraf, Ferroelectr., Lett. Sect. **12**, 63 (1990).
[9]D. Viehland, M. Kim, Z. Xu, and J. Li, Appl. Phys. Lett. **67**, 2471 (1995).
[10]G. Smolenskii and A. Agranovskaya, Sov. Phys. Solid State **1**, 1429 (1960).
[11]C. Randall, D. Barber, and R. Whatmore, J. Microsc. **45**, 275 (1987).
[12]X. Dai, Z. Xu, and D. Viehland, Philos. Mag. B **70**, 33 (1994).
[13]J. Kuwata, K. Uchino, and S. Nomura, Jpn. J. Appl. Phys., Part 1 **21**, 1298 (1982).
[14]S. E. Park and T. R. Shrout, J. Appl. Phys. **82**, 1804 (1997).
[15]D. Viehland and J. Powers, Appl. Phys. Lett. **78**, 3112 (2001).
[16]D. Stansfield, *Underwater Electroacoustic Transducers* (Bath University Press, Bath, 1991).
[17]M. Mitrovic, G. P. Carmen, and F. K. Straub, Int. J. Solids Struct. **38**, 4357 (2001).
[18]D. Zhou, M. Kamlah, and D. Munz, J. Eur. Ceram. Soc. **25**, 425 (2005).
[19]R. Yimnirun, S. Wongsaenmai, S. Ananta, and E. Meechoowas, J. Phys. D **36**, 1615 (2003).
[20]Q. M. Zhang, J. Zhao, K. Uchino, and J. Zheng, J. Mater. Res. **12**, 226 (1997).
[21]G. Yang, S. F. Liu, W. Ren, and B. K. Mukherjee, Proc. SPIE **3992**, 103(2000).
[22]O. Steiner, A. K. Tagantsev, E. L. Colla, and N. Setter, J. Eur. Ceram. Soc. **19**, 1243 (1999).
[23]J. Zhao and Q. M. Zhang, Proceedings of the IEEE International Symposium on Applications of Ferroelectrics, 1996 (unpublished), p. 971.
[24]R. Yimnirun, M. Unruan, Y. Laosiritaworn, and S. Ananta, J. Phys. D **39**, 3097 (2006).
[25]R. Yimnirun, S. Ananta, and S. Chamunglap, Mater. Chem. Phys. **102**, 165 (2007).
[26]R. Yimnirun, S. Wongsaenmai, R. Wongmaneerung, N. Wongdamnern, A. Ngamjarurojana, S. Ananta, and Y. Laosiritaworn, Phys. Scr., T **T129**, 184 (2007).
[27]J. Zhao, A. E. Glazounov, and Q. M. Zhang, Appl. Phys. Lett. **74**, 436 (1999).
[28]M. Unruan, R. Wongmaneerung, A. Ngamjarurojana, S. Ananta, Y. Laosiritaworn, and R. Yimnirun, J. Appl. Phys. (unpublished).
[29]M. Unruan, S. Wongsaenmai, Y. Laosiritaworn, S. Ananta, and R. Yimnirun, J. Phys. D **41**, 085406 (2008).
[30]J. Zhao, Q. M. Zhang, and V. Mueller, Proceedings of the IEEE International Symposium on Applications of Ferroelectrics, 1998 (unpublished), p. 361.
[31]F. X. Li, S. Li, and D. N. Fang, Mater. Sci. Eng., B **120**, 119 (2005).
[32]A. Udomporn, Ph.D. thesis, Chiang Mai University, 2004.
[33]R. Yimnirun, S. Ananta, A. Ngamjarurojana, and S. Wongsaenmai, Appl. Phys. A: Mater. Sci. Process. **81**, 1227 (2005).
[34]R. Yimnirun, Y. Laosiritaworn, S. Wongsaenmai, and S. Ananta, Appl. Phys. Lett. **89**, 162901 (2006).
[35]R. Yimnirun, P. J. Moses, R. J. Meyer, and R. E. Newnham, Rev. Sci. Instrum. **74**, 3429 (2003).
[36]D. Viehland and J. Powers, J. Appl. Phys. **89**, 1820 (2001).
[37]G. Yang, S. F. Liu, W. Ren, and B. K. Mukherjee, Ferroelectrics **262**, 207 (2001).
[38]H. Krueger, J. Acoust. Soc. Am. **43**, 583 (1968).
[39]R. Yimnirun, Y. Loasiritaworn, and S. Wongsaenmai, J. Phys. D **39**, 759 (2006).
[40]A. K. Singh and D. Pandey, Phys. Rev. B **67**, 064102 (2003).
[41]C.-S. Tu, V. H. Schmidt, I.-C. Shih, and R. Chien, Phys. Rev. B **67**, 020102 (2003).
[42]V. Topolov and Z.-G. Ye, Phys. Rev. B **70**, 094113 (2004).
[43]R. Yimnirun, S. Wongsaenmai, S. Ananta, and Y. Laosiritaworn, Appl. Phys. Lett. **89**, 242901 (2006).
[44]M. E. Lines and A. M. Glass, *Principles and Applications of Ferroelectrics and Related Materials* (Oxford University Press, Oxford, 1977).

Downloaded 14 Apr 2009 to 202.28.246.2. Redistribution subject to AIP license or copyright; see http://jap.aip.org/jap/copyright.jsp

ELSEVIER

Journal of Alloys and Compounds 465 (2008) 522–526

Journal of ALLOYS AND COMPOUNDS

www.elsevier.com/locate/jallcom

Effect of niobate B-site precursors on phase formation and particle size of lead nickel niobate powders

O. Khamman, R. Yimnirun, S. Ananta *

Department of Physics, Faculty of Science, Chiang Mai University, Chiang Mai 50200, Thailand

Received 26 May 2007; accepted 1 November 2007
Available online 19 December 2007

Abstract

A perovskite phase of $Pb(Ni_{1/3}Nb_{2/3})O_3$ or PNN powders has been synthesized by a rapid vibro-milling technique. Both $NiNb_2O_6$ and $Ni_4Nb_2O_9$ have been employed as nickel niobate precursors, with the formation of the PNN phase investigated as a function of calcination conditions by DTA and XRD techniques. Morphology and phase composition have been determined via a combination of SEM and EDX techniques. The nickel niobate precursor and calcination condition have been found to have a pronounced effect on the phase and morphology evolution of the calcined PNN powders. It is seen that optimization of calcination conditions can lead to a single-phase PNN in both methods. However, the formation temperature for single-phase PNN powders was lower for the synthetic method employing a $NiNb_2O_6$ precursor.
© 2007 Elsevier B.V. All rights reserved.

Keywords: Lead nickel niobate; Nickel niobate; Perovskite; Relaxor ferroelectrics

1. Introduction

The excellent dielectric broadening and electrostrictive properties make lead nickel niobate, $Pb(Ni_{1/3}Nb_{2/3})O_3$ or PNN, a promising material for capacitor, electrostrictive actuator, and electromechanical transducer devices [1–3]. Because of these important technological applications, there has been a great deal of interest in preparation of single-phase PNN powders as well as in the sintering and dielectric properties of PNN-based ceramics [3–7].

However, it is well-documented that the formation of PNN perovskite via the solid-state reaction is often accompanied by the occurrence of unwanted pyrochlore-type phases because of the volatilization of PbO and the low dispersion of NiO [4–6]. Hence, several material processing techniques, for example, combustion [7], co-precipitation [8] and hydrothermal [9], have been introduced as alternative to the solid-state reaction of mixed oxides to minimize the amount of pyrochlore phase formed. All of these techniques are aimed at reducing the temperature of preparation of the compound even though they are more involved and complicated than the mixed oxide route.

The columbite-precursor method which was first developed by Swart and Shrout [10] is probably one of the most fundamental, practical routine method which has been used, and it has been modified intensively for the preparation of PNN powder in the last decade [4–6]. In this method, an intermediate step to give columbite-type $NiNb_2O_6$ precursor is used to bypass the formation of the pyrochlore phases. Alternatively, the use of $Ni_4Nb_2O_9$ precursor in place of $NiNb_2O_6$ has been proposed for the fabrication of pyrochlore-free PNN [11]. However, the preparation of PNN using $Ni_4Nb_2O_9$ precursor, to date, has not been extensive as that of PNN using $NiNb_2O_6$ precursor. The potential of this alternative route was evaluated in comparison with conventional columbite route to produce PNN materials.

The purpose of this work was to compare the two B-site precursor synthetic routes of PNN formation and the characteristics of the resulting powders. The phase formation and morphology of the powders calcined at various conditions will be studied and discussed.

2. Experimental

$Pb(Ni_{1/3}Nb_{2/3})O_3$ was synthesized by a similar methodology of B-site precursor mixed oxide synthetic route (Fig. 1), as reported earlier [6,7,12]. Starting precursors were as follows: PbO (JCPDS file number 77-1971), NiO (JCPDS file number 73-1519) and Nb_2O_5 (JCPDS file number 30-0873) (Aldrich, 99% purity). These three oxide powders exhibited an average particle size in the range

* Corresponding author.
E-mail address: suponananta@yahoo.com (S. Ananta).

0925-8388/$ – see front matter © 2007 Elsevier B.V. All rights reserved.
doi:10.1016/j.jallcom.2007.11.002

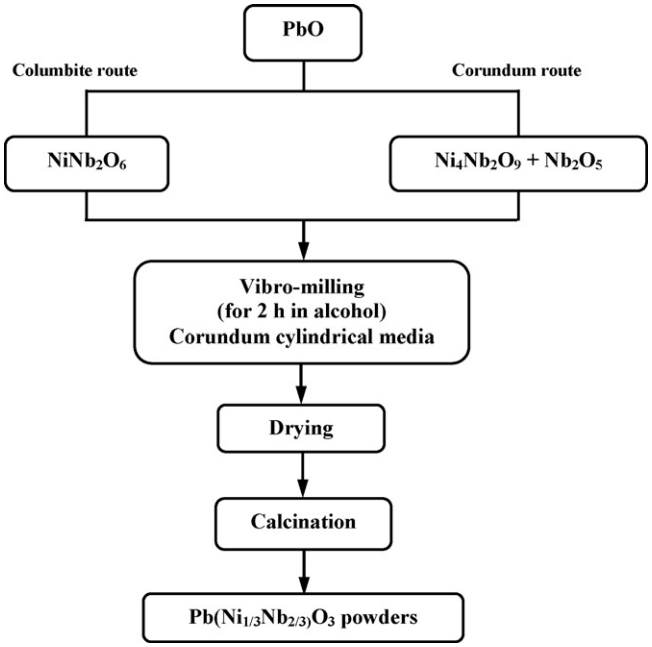

Fig. 1. A two-stage solid-state reaction routes for PNN powders.

of 3.0–5.0 μm. First, two intermediate phases of nickel niobate: $NiNb_2O_6$ and $Ni_4Nb_2O_9$ were separately prepared by the solid-state reaction method previously reported [13,14], employing an optimized calcination conditions of 900 °C for 4 h with heating/cooling rates of 30 °C/min and 1050 °C for 2 h, with heating/cooling rates of 30 °C/min, respectively. The following reaction sequences were then proposed for the formation of PNN:

1. The columbite route:

$$3PbO(s) + NiNb_2O_6(s) \rightarrow 3Pb(Ni_{1/3}Nb_{2/3})O_3(s) \quad (1)$$

2. The corundum route:

$$12PbO(s) + Ni_4Nb_2O_9(s) + 3Nb_2O_5(s) \rightarrow 12Pb(Ni_{1/3}Nb_{2/3})O_3(s) \quad (2)$$

Instead of employing a ball-milling procedure (ZrO_2 media under acetone for 48 h [6]), a McCrone vibro-milling was used. In order to reduce the processing time, the milling process was carried for only 2 h (instead of 12 h [12]) with corundum media in isopropanol. After drying at 120 °C for 2 h, various calcination conditions were applied in order to investigate the formation of PNN phase in each calcined powders.

The reactions of the uncalcined powders taking place during heat treatment were investigated by differential thermal analysis (DTA, Shimadzu) using a heating rate of 10 °C/min in air from room temperature up to 1200 °C. Calcined powders were subsequently examined by room temperature X-ray diffraction (XRD; Philips PW 1729 diffractometer) using Ni-filtered CuKα radiation, to identify the phases formed and optimum calcination conditions for the manufacture of PNN powders. The mean crystallite size was determined using the diffraction peak (1 1 0) of the perovskite pattern by using Scherrer equation [15]. The grain size and morphologies of calcined PNN powders were observed by scanning electron microscopy (SEM; JEOL JSM-840A). The chemical composition of the phases formed was also elucidated by an energy-dispersive X-ray (EDX) analyser with an ultra-thin window. EDX spectra were quantified with the virtual standard peaks supplied with the Oxford Instruments eXL software.

3. Results and discussion

DTA result for the mixtures synthesized by both B-site precursor methods is shown in Fig. 2. In general, similar trend of

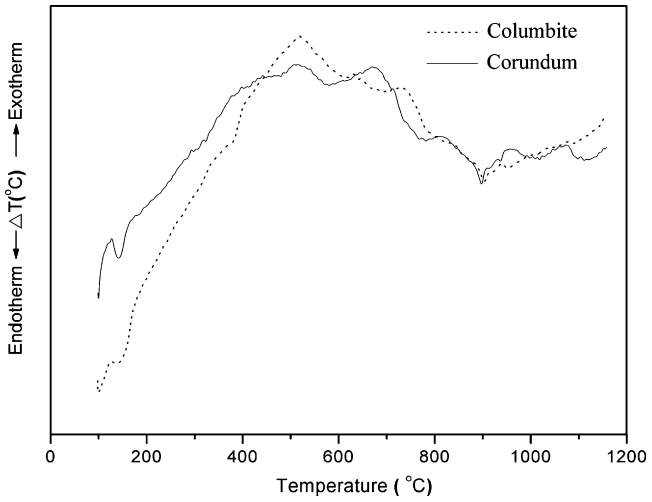

Fig. 2. DTA curves of the mixtures derived from columbite- and corundum-routes.

thermal characteristics is observed in both precursors. In the temperature range from room temperature to ~150 °C, both samples show small thermal peaks in the DTA curves, which are related to the first weight loss. These DTA peaks can be attributed to the decomposition of the organic species such as rubber lining from the milling process similar to our earlier reports [11–14]. By increasing the temperature up to ~700 °C, the solid-state reaction occurs between oxide precursors. The broad exothermic characteristic in both DTA curves represents that reaction, which has a maximum at ~450 and 600 °C for columbite- and corundum-routes, respectively. However, it is to be noted that there is no obvious interpretation of these peaks, although it is likely to correspond to a phase transition reported by a number of workers [4,6,12]. The different temperature, intensities and shapes of the thermal peaks for the two precursors here probably are related to the different starting materials especially nickel niobate and consequently, caused by the removal of species differently bonded in the network, reactivity of different species (difference in type and dispersion of NiO) in the powders. These data were used to define the range of temperatures for XRD investigation between 500 and 1150 °C. It is to be noted that a significant thermal change in DTA curves observed at temperatures above 800 °C may be attributed to the PbO volatilization typically found in lead-based ferroelectrics, consistent with other investigators [8,16,17].

To study the phase development with increasing calcination temperature in each synthetic route, they were calcined at various temperatures for 2 h in air with constant heating/cooling rates of 10 °C/min, followed by phase analysis using XRD technique. As shown in Fig. 3 (columbite route), for the uncalcined powder and the powder calcined at 500 °C, only X-ray peaks of PbO and $NiNb_2O_6$ precursors are present. Similarly, it is seen that unreacted precursors of PbO, Nb_2O_5 and $NiNb_2O_6$ are detected from the original mixture up to 550 °C for the corundum route (Fig. 4). These observations indicate that no reaction was yet triggered during the vibro-milling or low firing processes, in agreement with literature [11,18,19]. It is seen that PNN crystallites were developed in the powders at a calcination temperature

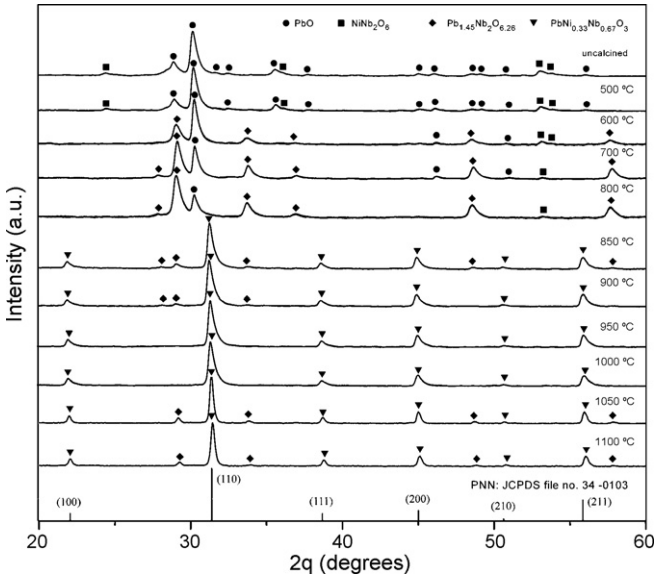

Fig. 3. XRD patterns of the columbite-route powders calcined at various conditions for 2 h with heating/cooling rates of 10 °C/min.

of 850 °C for columbite route and as low as 600 °C for corundum route.

In general, the strongest reflections apparent in the majority of these XRD patterns indicate the formation of the lead nickel niobate, PNN (▼). These can be matched with JCPDS file number 34-0103 for the cubic phase, in space group *Pm3m* (no. 221) with cell parameters $a = 403$ pm [20], consistent with other workers [6,21]. According to Fig. 3, the formation of $Pb_{1.45}Nb_2O_{6.26}$ (♦) phase has been found at ~600 °C, which is associated to the second DTA response in Fig. 2. This pyrochlore phase has a cubic structure with cell parameter $a = 1056$ pm in space group *F3dm* (no. 227) (JCPDS file number 84-1731) [22].

Upon calcination at 850 °C, the peak corresponding to PbO disappeared (not detectable by XRD method). By increasing the calcination temperature from 850 to 1000 °C, the yield of the PNN phase increases significantly until at 950 and 1000 °C, a single-phase of perovskite PNN is formed. However, for the present study, it can be seen that at the temperature range of 1050–1100 °C, some peaks of the pyrochlore $Pb_{1.45}Nb_2O_{6.26}$ phase reappear, mixing with the major phase of PNN. This could be attributed mainly to the PbO volatilization, leading to the decomposition of the perovskite phase to the pyrochlore phase, in agreement with the DTA observations at the same temperature range and also the literature [16,17].

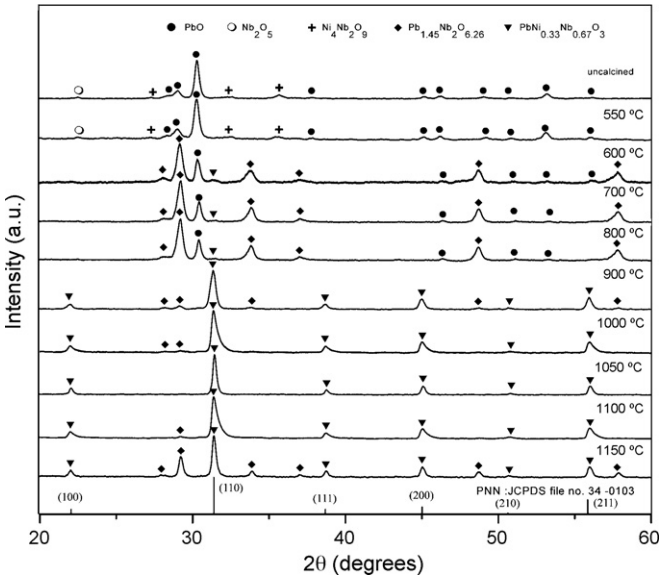

Fig. 4. XRD patterns of the corundum-route powders calcined at various conditions for 2 h with heating/cooling rates of 10 °C/min.

From Fig. 4, it is seen that calcination at 600 °C resulted in some new peaks of the perovskite PNN (▼) and pyrochlore $Pb_{1.45}Nb_2O_{6.26}$ (♦) phases [22], mixing with the unreacted PbO phase. As the firing temperature increased to 900 °C, the intensity of the PNN peaks was further enhanced and PNN becomes the predominant phase, in good agreement with the earlier DTA result. This study also shows that PNN is the only detectable phase in the corundum-route powders after calcination only at 1050 °C, whilst above 1050 °C, the pyrochore $Pb_{1.45}Nb_2O_{6.26}$ phase is formed again (probably due to the PbO partially evaporization [8,17]).

It is well-established that the perovskite-type PNN tend to form together with the pyrochlore-type $PbO–Nb_2O_5$ compounds, depending on calcination conditions [4,8,11]. In the work reported here, evidence for the formation of PNN phase, which coexists with the cubic pyrochlore phase, is found after calcination at temperature ~600–1150 °C, in agreement with literature [4,6,23]. It should be noted that no evidence of the pyrochlore $Pb_2Nb_2O_7$ [19], $Pb_3Nb_2O_8$ [8] and $Pb_3Nb_4O_{13}$ [23,24] was found in this study, nor was there any indication of the $Pb_{15}NiNb_{10}O_{41}$ reported by Balzer and Langbein [24] being present. In general, the formation temperature for high purity PNN observed in the powders derived from a combination of a B-site mixed oxide synthetic route and a carefully determined calcination condition (especially with a rapid vibromilling technique) in this work are also close to those reported for the powders prepared via many other conventional mixed oxide methods [5,6,12].

Based on the DTA and XRD data, it may be concluded that, over a wide range of calcination conditions, single-phase perovskite PNN cannot be straightforwardly formed via a two-step B-site precursor method, as verified by a number of researchers [4–7]. The experimental work carried out here suggests that the optimal calcination conditions for single-phase PNN are 950 °C (columbite route) and 1050 °C (corundum route), for 2 h with heating/cooling rates of 10 °C/min. The optimized formation temperature of single-phase PNN was lower for the columbite route probably due to the higher degree of reactivity with less reacting species involved [4]. As suggested by several workers [4,6], the degree of cation mixing in precursors significantly affects the phase formation behavior in the B-site synthesis of PNN. This observation may be accounted by the fact that the columbite route possibly provides faster chemical reaction rate (only the reaction between PbO and $NiNb_2O_6$) and is able to enhance the formation of perovskite PNN phase by increasing the reactivity of NiO [6]. Moreover, the minimum firing temperature required for the manufacturing of single-

phase columbite $NiNb_2O_6$ (~950 °C [13]) is lower than that of corundum $Ni_4Nb_2O_9$ (~1250 °C [14]).

Therefore, in general, the methodology presented in this work provides a simple method for preparing perovskite PNN powders via a solid-state mixed oxide synthetic route. It is interesting to note that, by using either columbite- or corundum-routes, with an optimal calcination condition, the reproducible, low cost and flexible process involving simple solid-state reaction synthetic route can produce high purity perovskite PNN (with impurities undetected by XRD technique) from relatively impure and inexpensive commercially available raw materials.

To further study the influence of precursor on the morphological characteristics of the resulting PNN powders, a combination of SEM and EDX is used to examine the powders obtained, as shown in Figs. 5 and 6 and Table 1. In general, it is seen that the calculated crystallite size of columbite-route PNN powders is slightly lower than the corundum-route PNN powders, in good agreement with SEM results SEM micrographs of the calcined PNN powders derived from columbite- and corundum-precursor methods are shown in Fig. 5(a) and (b), respectively. In general, the particles are agglomerated and basically irregular in shape, with a substantial variation in particle size. Observed

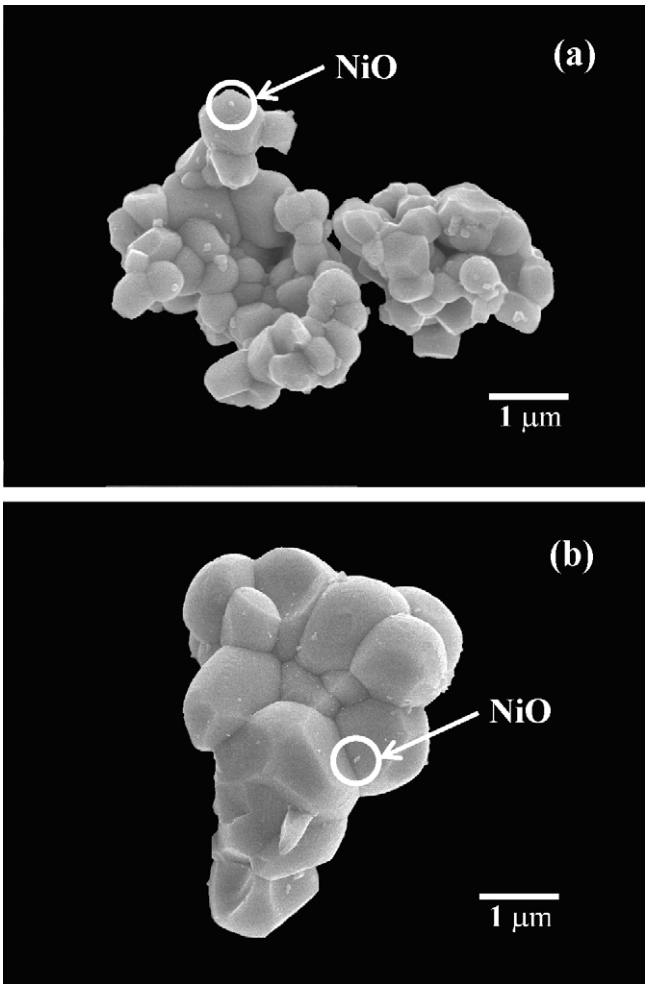

Fig. 5. SEM micrographs of the (a) columbite- and (b) corundum-route PNN powders.

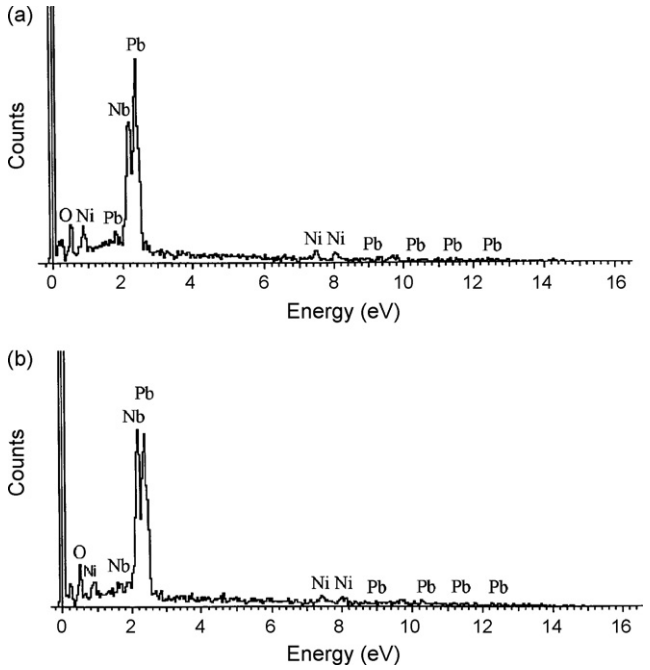

Fig. 6. EDX analysis of the (a) columbite- and (b) corundum-route PNN powders after calcined at their optimized conditions.

diameters range from 0.2 to 1.0 and 0.4 to 2.0 μm for columbite- and corundum-routes, respectively. These particle size data were directly estimated from SEM micrographs. Even though these data are not precisely determined, they were shown to provide estimated comparison between different nickel niobate precursors.

The primary particles in the agglomerates are, however, submicron in size. Additionally, the observed morphology reveals considerable difference in homogeneity, uniformity, size and shape between the two PNN powders. It is obviously evident that the columbite-route powders exhibit more heterogeneous morphology than the corundum-route powders. The columbite-route powders consist mainly of irregular round shape primary particles with a diameter of ~1 μm or less (Fig. 5(a)). In general, it is seen that primary particle in columbite-route powders is clearly smaller in size than the corundum-route powders. The averaged particle size of columbite-precursor PNN powders with finer particle size is regarded as advantage for better reactivity. However, it is seen that higher degree of agglomeration with more angular particle morphology is observed in the powders produced by the corundum route (Fig. 5(b)). The strong inter-particle bond within each aggregate is evident by the formation of a well-established necking between neighboring particles. This observation could be attributed to the mechanism of sur-

Table 1
Particle size data of both PNN powders measured by XRD and SEM techniques

Measurement techniques	Particle size range (average)	
	Columbite route	Corundum route
XRD[a] (nm, ±2.00)	22.31	23.40
SEM (μm, ±0.20)	0.22–1.00 (0.50)	0.40–2.40 (1.11)

[a] Crystallite size.

face energy reduction of the ultra-fine powders, i.e., the smaller the powder the higher the specific surface area [25]. This finding is also similar to that observed in PMN powders synthesized by Wongmaneerung et al. [26].

In addition, EDX analysis using a 20 nm probe from a large number of particles of the two calcined PNN powders (Fig. 6) confirmed that the parent composition is $Pb(Ni_{1/3}Nb_{2/3})O_3$, in good agreement with XRD results. A combination of SEM and EDX techniques has demonstrated that a NiO-rich phase (spherical particles with diameter ~50–100 nm) exists near the PNN parent phase, as small circles in Fig. 5. Moreover, a variation of the Pb/Ni/Nb ratio was also found, similar to that of PMN powders [26]. The existence of discrete nano-sized NiO phase points to poor reactivity of NiO, although the concentration is too low for detection by XRD [15], similar with other lead-based perovskite compounds [18,19,26].

4. Conclusions

This work demonstrated that single-phase perovskite $Pb(Ni_{1/3}Nb_{2/3})O_3$ powders can be successfully formed by employing either columbite or corundum B-site precursor method via a rapid vibro-milling. Evidence for the formation of a cubic pyrochlore phase, which coexists with the perovskite PNN parent phase, is found at calcination temperature ranging from 800 to 1050 °C. Amongst the two B-site precursor methods, it is seen that lower optimized calcination temperature for the production of pure lead nickel niobate powders with smaller particle size can be obtained by using $NiNb_2O_6$ precursor (the columbite route).

Acknowledgements

We thank the Thailand Research Fund (TRF), the Commission on Higher Education (CHE), the Royal Golden Jubilee Ph.D. Program, the Faculty of Science, Chiang Mai University for all supports.

References

[1] A.J. Moulson, J.M. Herbert, Electroceramics, second ed., Wiley, 2003.
[2] G. Haertling, J. Am. Ceram. Soc. 82 (1999) 797–818.
[3] F. Levassort, P. Tran-Huu-Hue, E. Ringaard, M. Lethiecq, J. Eur. Ceram. Soc. 21 (2001) 1361–1365.
[4] T.R. Shrout, A. Halliyal, Am. Ceram. Soc. Bull. 66 (1987) 704–711.
[5] E.F. Alberta, A.S. Bhalla, J. Phys. Chem. Solids 63 (2002) 1759–1769.
[6] C.H. Lu, W.J. Hwang, Ceram. Int. 22 (1996) 373–379.
[7] M.M.A. Sekar, A. Halliyal, J. Am. Ceram. Soc. 81 (1998) 380–388.
[8] Y. Yoshikawa, Key Eng. Mater. 206–213 (2002) 87–90.
[9] C.H. Lu, W.J. Hwang, J. Appl. Phys. 38 (1999) 5478–5482.
[10] S.L. Swartz, T.R. Shrout, Mater. Res. Bull. 17 (1982) 1245–1256.
[11] O. Khamman, R. Yimnirun, S. Ananta, Mater. Lett. 61 (2007) 4466–4470.
[12] E.F. Alberta, A.S. Bhalla, Mater. Lett. 54 (2002) 47–54.
[13] O. Khamman, R. Yimnirun, S. Ananta, Mater. Lett. 61 (2007) 639–643.
[14] O. Khamman, R. Yimnirun, S. Ananta, Mater. Lett. 61 (2007) 2565–2570.
[15] H.P. Klug, L.E. Alexander, X-ray Diffraction Procedures, second ed., Wiley, 1974.
[16] T. Zhong, Y.D. Hou, M.K. Zhu, B.C. Xu, J.L. Tang, J.B. Liu, H. Wang, H. Yan, Mater. Lett. 59 (2005) 1169–1172.
[17] K.P. Chen, C. Li, C. Lei, X. Zhang, Y. Huang, J. Mater. Sci. Lett. 21 (2002) 1785–1787.
[18] S. Ananta, Mater. Lett. 58 (2004) 2781–2786.
[19] R. Wongmaneerung, R. Yimnirun, S. Ananta, Mater. Lett. 60 (2006) 1447–1452.
[20] Powder Diffraction File No. 34-0103, International Centre for Diffraction Data, Newton Square, PA, 2000.
[21] C.H. Lu, W.J. Hwang, Jpn. J. Appl. Phys. 38 (1999) 5478–5482.
[22] Powder Diffraction File No. 84-1731, International Centre for Diffraction Data, Newton Square, PA, 2000.
[23] A.I. Agranovskaya, Bull. Acad. Sci. USSR Phys. Ser. 1 (1960) 1271–1277.
[24] B. Balzer, H. Langbein, Cryst. Res. Technol. 32 (1997) 955–962.
[25] J.S. Reeds, Principles of Ceramic Processing, second ed., Wiley, 1995.
[26] R. Wongmaneerung, T. Sarakonsri, R. Yimnirun, S. Ananta, Mater. Sci. Eng. B 132 (2006) 292–299.

ELSEVIER

Journal of Alloys and Compounds 466 (2008) 264–267

Journal of ALLOYS AND COMPOUNDS

www.elsevier.com/locate/jallcom

Synthesis and properties of $Pb(Co_{1/3}Nb_{2/3})O_3$ ceramics

Muangjai Unruan [a], Naratip Vittayakorn [b], Rewadee Wongmaneeruang [a], Anurak Prasatkhetragarn [a], Supon Ananta [a], Rattikorn Yimnirun [a,*]

[a] *Department of Physics, Faculty of Science, Chiang Mai University, Chiang Mai 50200, Thailand*
[b] *Department of Chemistry, Faculty of Science, King Mongkut's Institute of Technology Ladkrabang, Bangkok 10520, Thailand*

Received 7 June 2007; received in revised form 3 November 2007; accepted 11 November 2007
Available online 22 November 2007

Abstract

In this study, $Pb(Co_{1/3}Nb_{2/3})O_3$ or PCN ceramics have been produced by sintering PCN powders synthesized from lead oxide (PbO) and cobalt niobate ($CoNb_2O_6$) with an effective method developed for minimizing the level of PbO loss during sintering. Attention has been focused on relationships between sintering conditions, phase formation, density, microstructural development, dielectric and ferroelectric properties of the sintered ceramics. The densities of sintered PCN ceramics increased with increasing sintering temperature. However, it was observed that at too high temperature the density began to decrease. Change of dielectric properties with sintering temperature also followed the same trend as the density. Based on X-ray diffraction analysis, density data, SEM micrograph, and dielectric properties, the optimum sintering temperature for a high purity PCN ceramic was found to be about 1100 and 1150 °C. A strongly diffused dielectric peak also showed a typical characteristic of ferroelectric relaxors. The P–E hysteresis loops observed at −70 °C were of slim-loop type with small remnant polarization values, which confirmed relaxor ferroelectric behavior of PCN ceramics.
© 2007 Elsevier B.V. All rights reserved.

Keywords: Dielectric properties; Sintering; PCN

1. Introduction

Lead-base relaxor ferroelectrics, particularly lead magnesium niobate, $Pb(Mg_{1/3}Nb_{2/3})O_3$ (PMN) belong to a technologically important class of complex $Pb(B'B'')O_3$ perovskite materials [1]. PMN has advantages of having broader operating temperature rang, especially over the room temperature rang. This is a direct result of a diffuse paraelectric–ferroelectric phase transition in the vicinity of room temperature. In addition, as a result of their unique microstructure features PMN ceramics exhibit low loss and non-hysteretic characteristics [2]. However, little attention has been devoted to the other lead-base relaxor ferroelectrics, $Pb(A_{1/3}B_{2/3})O_3$ (A is Mg^{2+}, Co^{2+}, Ni^{2+} or Zn^{2+} and B is Nb^{5+} or Ta^{5+}), discovered by Bokov and Mylnikova [3], with the perovskite structure and the dielectric maxima temperature (T_m) lower than room temperature except for that of $Pb(Zn_{1/3}Nb_{2/3})O_3$. Although Mg^{2+}, Co^{2+}, Ni^{2+} and Zn^{2+} have similar radii, the temperatures at which spontaneous polarization occurs in $Pb(A_{1/3}B_{2/3})O_3$ differ [4].

Therefore, in this study one of lesser studied ceramics in the $Pb(A_{1/3}B_{2/3})O_3$ system, i.e. $Pb(Co_{1/3}Nb_{2/3})O_3$ (PCN) is investigated. Synthesis method, physical properties, microstructure, dielectric and ferroelectric properties of the ceramic are discussed.

2. Experimental method

PCN ceramics were prepared from starting PbO and $CoNb_2O_6$ (or CN) powders by a conventional mixed oxide method. CN powders were obtained from the columbite method [5], while PCN powders were prepared by a simple mixed oxide method. To obtain the perovskite-phase PCN, the cobalt niobate ($CoNb_2O_6$) powders were first prepared by mixing CoO (99.9%) and Nb_2O_5 (99.9%) powders in the proper proportion and vibro-milling for 1 h. After drying, the mixtures were calcined at 1100 °C for 4 h to yield so-called columbite powders ($CoNb_2O_6$). Subsequently, the columbite powders were mixed with PbO (99.9%) by the vibro-milling method and calcined at 950 °C for 4 h to form the perovskite-phase PCN powders. Then PCN powders were pressed hydraulically to form disc-shaped pellets 8 mm in diameter and 2 mm thick, with 3 wt% polyvinyl alcohol as a binder. The pellets were placed in the alumina crucible. Finally, for optimization purposes the pellets were sintered at 1050, 1100, 1150 and 1200 °C for 2 h. The phase formation of the sintered ceramics was studied by the X-ray diffraction (XRD) technique. The densities of sintered spec-

* Corresponding author. Tel.: +66 53 943 367; fax: +66 53 943 445.
E-mail address: rattikornyimnirun@yahoo.com (R. Yimnirun).

0925-8388/$ – see front matter © 2007 Elsevier B.V. All rights reserved.
doi:10.1016/j.jallcom.2007.11.071

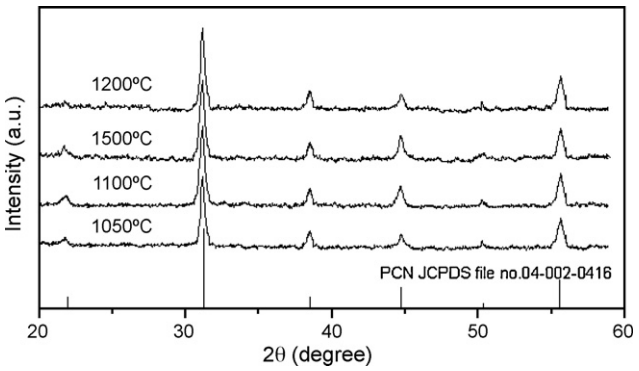

Fig. 1. XRD diffraction patterns of the sintered PCN ceramics.

imens were measured by Archimedes method. The microstructure analyses were undertaken by scanning electron microscopy (SEM: JEOL Model JSM 840A). The grain size was determined from SEM micrographs by a linear intercept method.

Before studying the dielectric properties, the specimens were lapped to obtain parallel faces. After coating with silver paint as electrode on the faces, the specimens were heated at 750 °C for 12 min to ensure contact between the electrode and the surface of the ceramic. The dielectric properties (dielectric constant (ε_r) and dielectric loss (tan δ)) were measured at temperatures between −120 and 50 °C. The capacitance was measured with a HP4284A LCR meter in connection with a Delta Design 9023 temperature chamber and a sample holder (Norwegian Electroceramics). The dielectric constant (ε_r) was then calculated from a parallel-plate capacitor equation, e.g. $\varepsilon_r = Cd/\varepsilon_o A$, where C is the capacitance of the specimens, d and A are, respectively, the thickness and the area of the electrode and ε_o is the dielectric permittivity of vacuum (8.854×10^{-12} Fm^{-1}). Finally, the polarization–electric field (P–E) hysteresis loops at −70 °C were obtained using a standardized ferroelectric tester system (RT66A) with driving frequency of 4 Hz.

3. Results and discussion

The phase formation behavior of the sintered ceramics is revealed by an XRD method. The XRD patterns are presented in Fig. 1, with the corresponding JCPDS pattern also shown. In general, the strongest reflections apparent in the majority of the XRD patterns indicate the formation of perovskite lead cobalt niobate phase. These can be matched with JCPDS file number 04-002-0416 for the $Pb(Co_{0.33}Nb_{0.67})O_3$. Based on the XRD analysis, the optimum sintering temperature for the formation of a high purity PCN phase was found at 1100 °C.

The densities of PCN ceramics sintered at different temperatures are listed in Table 1. It is clear that the density usually increases with increasing sintering temperature. This is believed to be a result of more completed solid-state reactions at higher sintering temperatures. However, it is also observed that at too high temperature the density begins to decrease. Lead-loss is generally accepted to be the reason for the decreasing density [6].

The SEM micrographs of fractured surfaces of all PCN ceramics are shown in Fig. 2. PCN ceramic sintered at 1050 °C has small grain size with variation in grain shape. However, the other ceramics exhibit different morphology showing a possible pyrochlore formation (with pyramidal-shaped grains) and also over-sintered specimens. Table 1 also shows that the average grain size of PCN ceramics sintered at 1050 °C is relatively small, as compared to those sintered at higher temperatures. The average grain size increases with increasing sintering temperatures. However, it is also observed that at very high temperature the grain size begins to decrease, which is similar to the trend observed for the density. Change of dielectric properties with sintering temperature also followed the same trend as the density. The dielectric constant reaches maximum values at sintering temperature of 1150 °C.

Temperature and frequency dependencies of ε_r, as calculated from the capacitance of the sample and its geometry, and tan δ were measured continuously by increasing temperature from −120 to 50 °C and frequency rang from 100 Hz to 100 kHz. The temperature dependence of ε_r and tan δ for the PCN ceramics are plotted in Fig. 3. As the measuring temperature increases the maximum dielectric constant (ε_{max}) appears at −30 °C, this temperature is called dielectric maxima temperature (T_m). It should be noticed that T_m obtained in this study is different from previous studies [3,7–9], which reported T_m of −70 °C for single crystal PCN and stress-dependent T_m for PCN ceramics ranging from −20 to −50 °C. It could be said that the T_m values obtained in this study fall within the previously reported values. This is because in this current study the dielectric properties, which are used to determine T_m, of the PCN ceramic were measured under compressive stress from a rather heavy sample holder used in the measurement system. In addition, the ceramics may also contain internal residual stress. Therefore, the T_m values obtained in this study are slightly lower than the previously reported value under stress-free condition. There is also insignificant change of T_m with different sintering temperatures. The tan δ shows only very small decrease with decreasing temperature below the T_m and tan δ becomes very high above the temperature of maximum dielectric constant. Based on X-ray diffraction analysis, density data, SEM micrograph, and dielectric properties, the optimum sintering

Table 1
Characteristics of PCN ceramics

Sintering temperature (°C)	Density (g/cm^3)	Average grain size (μm)	Dielectric properties	
			ε_{max}	tan δ
1050	7.58	1.83	2178	0.0594
1100	8.06	4.11	2657	0.0592
1150	8.07	6.35	2673	0.0578
1200	7.98	4.58	2248	0.0507

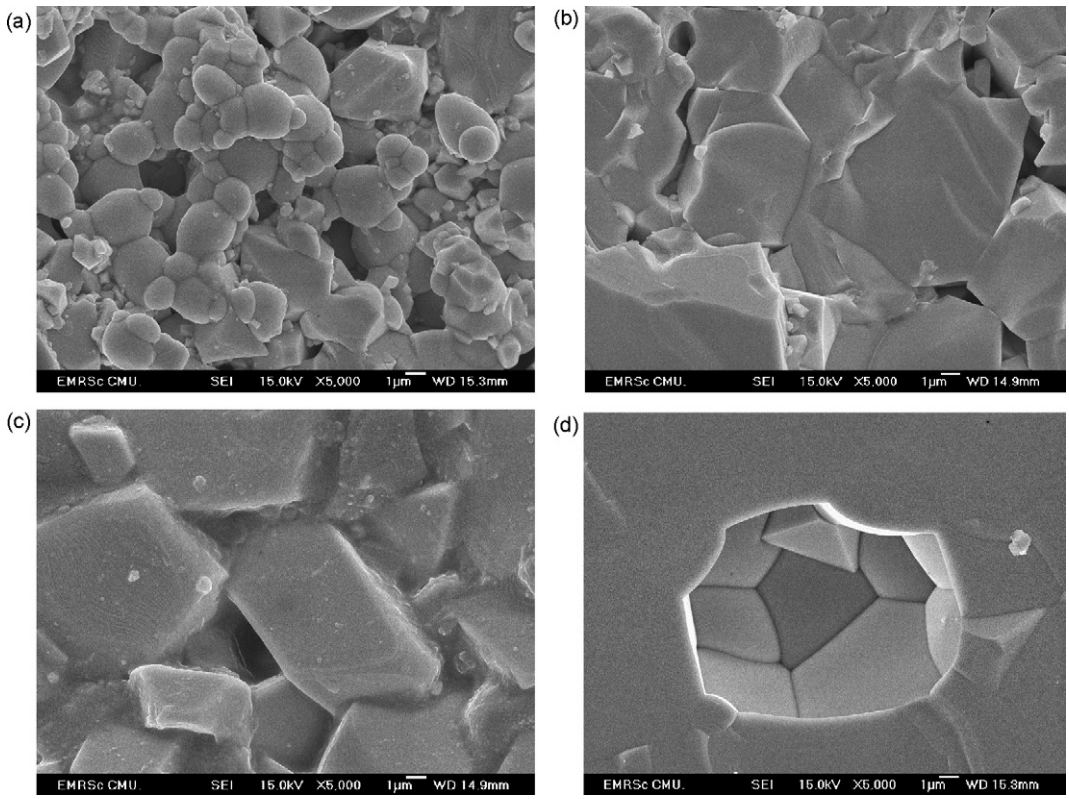

Fig. 2. SEM micrographs of PCN ceramics at different sintering temperature: (a) 1050 °C; (b) 1100 °C; (c) 1150 °C; and (d) 1200 °C.

temperature for a high purity PCN ceramic is found to be about 1100 and 1150 °C.

A strongly diffused dielectric peak is characteristic of ferroelectric relaxors. Frequency-dependent dielectric properties below T_m are also observed (Fig. 4.), further indicating relaxor behavior of PCN ceramics. However, one would expect to see a strong shift in T_m with frequency, as expected for typical relaxors, such behavior is not clearly visible because very high tan δ above T_m causes ε_r to increase rapidly.

The hysteresis loops at −70 °C of PCN ceramics sintered at different temperatures are shown in Fig. 5. It can be seen that slim P–E loops with small remnant polarization values are generally obtained for all ceramics. The slim-loop nature of the P–E curves suggests that most of the aligned dipole moments switch back to a randomly oriented state upon removal of the field. This behavior has previously been observed in ferroelectric relaxors [10]. In relaxor ferroelectric materials, micro- to macro-domain transition occurs. In the absence of any external field, the domain structure of relaxor ferroelectrics contains randomly oriented micropolar regions. However, when an electric field is applied, the micro-domains orient along the field direction and the macro-domains occur [10]. The P–E loops observed here also support that the PCN ceramics exhibit relaxor ferroelectric behavior.

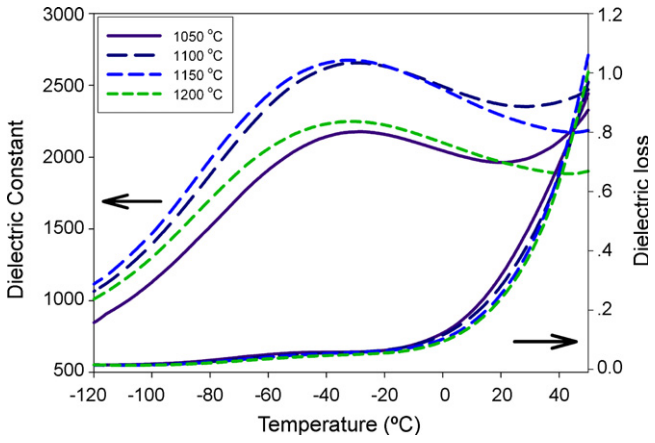

Fig. 3. Temperature dependence of dielectric properties of PCN ceramics at 1 kHz.

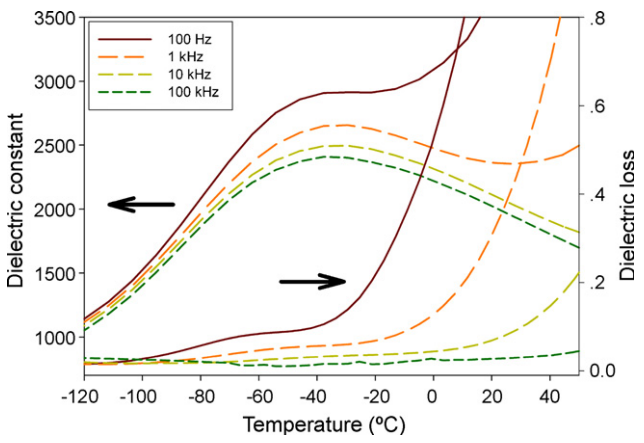

Fig. 4. Temperature and frequency dependence of dielectric properties of PCN ceramic sintered at 1100 °C.

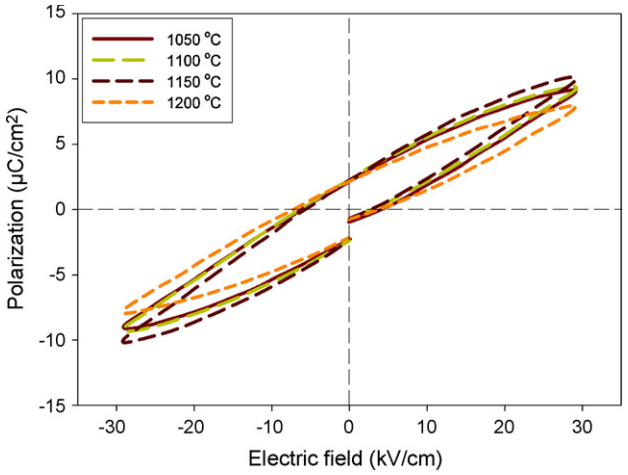

Fig. 5. P–E hysteresis loops of PCN ceramics measured at −70 °C (4 Hz).

4. Conclusions

In this study, PCN ceramics were prepared by the columbite precursor method. The PCN ceramics with perovskite structure and a high purity single phase are obtained. Density of these ceramics increases with increasing sintering temperature. However, at too high temperature the density begins to decrease. Change of dielectric properties with sintering temperature also follows the same trend as the density. Based on X-ray diffraction analysis, density data, SEM micrograph, and dielectric properties, the optimum sintering temperature for a high purity PCN ceramic is found to be about 1100 and 1150 °C. The samples exhibit a relaxor behavior around the maximum dielectric constant, characterized by a strongly diffused dielectric peak at −30 °C. The hysteresis loops measured at −70 °C show slim P–E loops with small remnant polarization values. This behavior has been observed in ferroelectric relaxors.

Acknowledgments

This work is supported by the Thailand Research Fund (TRF) and Commission on Higher Education (CHE). Additional supports from the Faculty of Science and Graduate School of Chiang Mai University are gratefully acknowledged.

References

[1] K. Vladimir, B. Jaroslav, Ceramics-Silikaty 47 (2003) 8.
[2] L.E. Cross, Ferroelectrics 76 (1987) 241.
[3] V.A. Bokov, I.E. Mylnikova, Sov. Phys. Solid State (Eng. Transl.) 2 (1961) 2428.
[4] T. Kudo, T. Yazaki, F. Naito, S. Sugaya, J. Am. Ceram. Soc. 53 (1969) 326.
[5] S.L. Swartz, T.R. Shrout, Mater. Res. Bull. 17 (1982) 1245.
[6] R. Yimnirun, S. Ananta, P. Laoratanakul, J. Eur. Ceram. Soc. 25 (2005) 3225.
[7] Landolt-Bornstein, in: T. Mitsui, S. Nomura (Eds.), Ferroelectrics and Related Substances, vol. 16, Springer-Verlag, Berlin, 1981.
[8] Y. Yamashita, Jpn. J. Appl. Phys. 33 (1994) 5328.
[9] T. Huchiga, S. Fujimoto, N. Yasuda, J. Phys. D: Appl. Phys. 20 (1987) 1291.
[10] A. Peláiz-Barranco, I. González-Carmenate, F. Calderón-Piñar, Solid State Commun. 134 (2005) 519–522.

Changes in ferroelectric properties of ceramics in lead magnesium niobate–lead titanate system with compressive stress

Muangjai Unruan,[1] Rewadee Wongmaneerung,[2] Athipong Ngamjarurojana,[1] Yongyut Laosiritaworn,[1] Supon Ananta,[1] and Rattikorn Yimnirun[1,a)]
[1]*Department of Physics, Faculty of Science, Chiang Mai University, Chiang Mai 50200, Thailand*
[2]*Department of Physics, Faculty of Science, Maejo University, Chiang Mai 50290, Thailand*

(Received 1 May 2008; accepted 10 July 2008; published online 22 September 2008)

Effects of compressive stress on the ferroelectric properties of $Pb(Mg_{1/3}Nb_{2/3})O_3-PbTiO_3$ (PMN-PT) ceramics were investigated. The ceramics with the formula $(1-x)Pb(Mg_{1/3}Nb_{2/3})O_3-(x)PbTiO_3$ or $(1-x)PMN-(x)PT$ $(x=0.1-0.5)$ were prepared by a conventional mixed-oxide method. Dense perovskite-phase PMN-PT ceramics with a uniform microstructure were obtained. The ferroelectric properties were measured under compressive stress (0–75 MPa) using a homebuilt compressometer in conjunction with a modified Sawyer–Tower circuit. The experimental results revealed that the superimposed compression stress significantly reduced both the dissipation energy and the polarizations of the near morphotropic phase boundary compositions, i.e., 0.8PMN-0.2PT, 0.7PMN-0.3PT, and 0.6PMN-0.4PT, while the stress influence was much less in other compositions. On the contrary, the applied compressive stress showed little or no influence on the coercive field. These results were interpreted through the non-180° ferroelastic domain switching processes and the stress induced decrease in the switchable part of domains. © *2008 American Institute of Physics*. [DOI: 10.1063/1.2977684]

I. INTRODUCTION

Lead magnesium niobate, $Pb(Mg_{1/3}Nb_{2/3})O_3$ (PMN), and its solid solution with lead titanate, $PbTiO_3$ (PT), so-called PMN-PT, are of great interest due to their high polarizabilities and excellent electrical properties suitable for various applications. These compounds have dielectric constants in excess of 20 000, making them potential candidates for capacitive applications. In addition, they also exhibit a large electrostriction at temperatures above their phase transition temperatures. This behavior extends their use to transducer and actuator applications.[1–5] The $(1-x)Pb(Mg_{1/3}Nb_{2/3})O_3-(x)PbTiO_3$ or $(1-x)PMN-(x)PT$ ceramic compositions with $x<0.2$ have been studied for electrostrictive applications,[4–7] while those with $x>0.2$ can be utilized as piezoelectric materials.[4,6,8,9] The differences between the electrostrictive and piezoelectric compositions of PMN-PT are due to differences in the degree of long-range polar order.[4,7,10] In the compositions with lower PT content, relaxor ferroelectric characteristics with polar clusters or nanodomains are observed.[4,11,12] On the other hand, long-range polar order with normal micron-sized ferroelectric domains exists in the compositions with higher PT content.[4,9,10]

Practically, when used in specific applications PMN-PT ceramics are often subjected to mechanical loading either deliberately in the design of the device itself or because the device is used to change shapes such as in many smart structure applications or the device is used under environmental stresses.[8,13–17] A prior knowledge of how the material properties change under different load conditions is crucial for the proper design of a device and for suitable selection of materials for a specific application. Despite this fact, material constants used in any design calculations are often obtained from a stress-free measuring condition, which in turn may lead to incorrect or inappropriate actuator and transducer designs. It is therefore important to determine the properties of these materials as a function of applied stress. Previous investigations on the stress-dependent electrical properties of many ceramic systems have clearly emphasized the importance of the matter.[7,15,18–29] Recently, the stress dependence of dielectric and ferroelectric properties has been investigated in materials such as PZT, PMN, BT, PZT-BT, PMN-PZT, and PZN-PZT.[19–22,30–32] In addition, our previous investigation on the influence of the applied stress on the dielectric properties of PMN-PT ceramic systems also revealed that the superimposed compression stress significantly reduced both the dielectric constant and the dielectric loss tangent of 0.9PMN-0.1PT ceramic, while the changes were not as significant in the other PMN-PT ceramic compositions.[24] The results clearly showed that the effects of stress on the dielectric properties depended significantly on ceramic compositions and stress levels. Since PMN-PT ceramics are practically employed in many electromechanical devices, there have been previous reports on the electromechanical properties of electrostrictive 0.9PMN-0.1PT and piezoelectric 0.7PMN-0.3PT ceramics under various mechanical and electrical loading conditions.[7,15,23,33] However, there has been no systematic study on the influence of an applied compressive stress on the ferroelectric properties of ceramics in the PMN-PT system. Therefore, it is the aim of this study to determine the ferroelectric properties of the $(1-x)PMN-(x)PT$, with $0.1\leq x\leq 0.5$, ceramics as a function of compressive stress.

a)Author to whom correspondence should be addressed. Electronic mail: rattikornyimnirun@yahoo.com.

 © 2008 American Institute of Physics

Author complimentary copy. Redistribution subject to AIP license or copyright, see http://jap.aip.org/jap/copyright.jsp

II. EXPERIMENTAL METHOD

Perovskite-phase PMN powders were obtained from the columbite method, while PT powders were prepared by a simple mixed-oxide method.[34] The $(1-x)Pb(Mg_{1/3}Nb_{2/3})O_3-(x)PbTiO_3$ ceramics were then prepared from starting PMN and PT powders by the mixed-oxide method. Finally, for optimization purpose the pellets were sintered at a temperature between 1220 and 1240 °C for 2 h. Optimum sintering conditions for all ceramics were established by identifying the conditions for maximizing both the bulk density and the yield of perovskite. However, since the PMN-PT compositions having high PT content in the range $0.6 \leq x \leq 0.9$ could not be fabricated in a bulk form with high density, these compositions could not be characterized any further for the rest of the study. Their comparatively large c/a values, which give rise to serious internal stress, are responsible for the frequent crack developments around the phase transition temperature during cooling of these sintered samples. In the present study, only compositions in the pseudobinary system $(1-x)$PMN$-x$PT $(0.1 \leq x \leq 0.5)$ have been fabricated from the calcined $(1-x)$PMN$-x$PT powders, employing a normal sintering method, i.e., pressureless sintering technique. Details of the processing and characterizations were provided elsewhere.[34]

Before studying the dielectric properties, the specimens were lapped to obtain parallel faces. After coating with silver paint as electrode at the faces, the specimens were heated at 750 °C for 12 min to ensure the contact between the electrode and surface of the ceramic. The ferroelectric hysteresis polarization-field (P-E) loops were characterized by using a computer controlled modified Sawyer–Tower circuit. The electric field of 15 kV/cm was applied to a sample by a high voltage ac amplifier (Trek, model 610D) with the input sinusoidal signal with a frequency of 60 Hz from a signal generator (Goodwill, model GAG-809). The detailed descriptions of this system were explained elsewhere.[35,36] To study the effects of the compressive stress on the ferroelectric properties, the uniaxial compressometer was constructed for simultaneous and parallel applications of the mechanical stress and the electric field.[37] Measurements were performed as a function of mechanical stress applied discretely between 0 and 75 MPa. During the measurements, a desired stress was first applied to the sample and then the electric field was applied. The ferroelectric hysteresis (P-E) loop was recorded at room temperature (25 °C) for both loading and unloading conditions. The parameters obtained from the loops were the maximum polarization (P_{max}), the remnant polarization (P_r), and the coercive field (E_c), which were defined as the points where the loops reach the maximum polarization, cross the zero field, and cross the zero polarization, respectively. The measurements reported were for the samples during their first mechanical stress cycle. It should also be noted that the reported ferroelectric parameters were obtained after a total of 10 cycles of the electric field was applied to the sample at each constant stress level.

III. RESULTS AND DISCUSSION

It should be mentioned here that the results from x-ray diffraction studies,[30,34] not shown here, indicated that complete crystalline solutions of perovskite structure were formed throughout the composition range between $x=0.1$ and 0.5. In general, only a (pseudo)cubic symmetry is observed at low values of PT concentration, in good agreement with other workers.[38,39] By the influence of PT, however, several peaks split for $x \geq 0.4$, indicating the development of tetragonal symmetry, consistent with earlier work on PMN-PT ceramics.[9,40] Similar microstructure characteristics were observed in these samples, i.e., uniformly sized grains with a high degree of grain close packing, and almost no abnormal grain growth. In each ceramic composition grain size ranges between 0.4 and 3.7 μm, with similar averaged grain size for all compositions. By applying the linear intercept method to scanning electron microscopy micrographs of polished and thermally etched specimens, mean grain sizes of about 1.72–2.11 μm are estimated for these samples. Bulk density values are found to decrease slightly with x (in the units of g/cm^3; the value decreases gradually from 7.98 in 0.9PMN-0.1PT to 7.78 in 0.5PMN-0.5PT). These characteristics indicate that dense perovskite-phase PMN-PT ceramics with a uniform microstructure have been obtained. Since the physical and microstructure features of all ceramic compositions are not significantly different, these parameters should not play an important role in the composition-dependent ferroelectric properties under compressive stress.

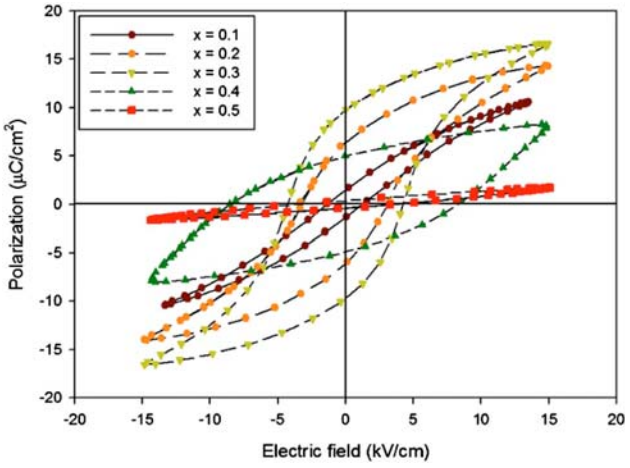

FIG. 1. (Color online) Polarization–electric field (P-E) hysteresis loops for the $(1-x)$PMN$-(x)$PT ceramics under stress-free condition (measured at 25 °C and 60 Hz).

Figure 1 illustrates a series of polarization-field (P-E) hysteresis loops for the PMN-PT ceramics under stress-free condition. It is clearly evident that the shape of P-E loops varies greatly with the ceramic compositions. With a large amount of normal ferroelectric PT contents, the polarization loop of 0.6PMN-0.4PT is well developed, showing a large remnant polarization (P_r: remaining polarization when electric field is decreased to zero) and coercive field (E_C). The hysteresis loop is of a typical "square" form as a result of domain switching in an applied field. This is a typical characteristic of a phase that contains long-range interaction between dipoles in the ferroelectric microdomain state.[1,4,5] This confirms that the composition is of a normal ferroelectric phase with tetragonal symmetry. It should be noted that a

Author complimentary copy. Redistribution subject to AIP license or copyright, see http://jap.aip.org/jap/copyright.jsp

similar observation is expected in the 0.5PMN-0.5PT composition. However, with a even larger amount of PT content, one would expect a much higher applied field to fully reveal the well-developed *P-E* loop. Therefore, the more open loop was not obtained at this relatively low electric field of 15 kV/cm. More importantly, the 0.7PMN-0.3PT ceramic shows the largest polarization values with small coercive fields (E_C), confirming that the composition is near the morphotropic phase boundary (MPB) of the PMN-PT system. The other compositions with more PMN content show more of "slim" hysteresis loops, a characteristic of the suppressed ferroelectric interaction.[1,4,5] This is typically found in the relaxor ferroelectrics with polar nanoregions. This also has resulted in a decrease in the values of both P_r and E_C due to an increased pseudocubic nonferroelectric phase content.[1,4,5]

The polarization versus electric field (*P-E*) hysteresis loops of the 0.9PMN-0.1PT, 0.7PMN-0.3PT, and 0.5PMN-0.5PT ceramics under different compressive stresses are shown in Figs. 2(a)–2(c), respectively. It should be noticed that generally the area of the *P-E* loops decreases with increasing compressive stress. The changes follow a similar trend for all the ceramic compositions. The *P-E* loop area indicates the polarization dissipation energy of a ferroelectric material under one full cycle of electric field application.[18,41] This amount of the energy loss is directly related to the amount of domains participating in the switching process during the application of electric field.[18,19] For a given composition, the decrease in the loop area with increasing compressive stress is a result of the stress-induced domain wall suppression.[18,35]

The changes in the hysteresis parameters, i.e., the dissipation energy, the maximum polarization (P_{max}), the remnant polarization (P_r), and the coercive field (E_C), with the compressive stresses are plotted in Fig. 3. Generally, it can be seen that both the dissipation energy and the polarizations decrease as the compressive stress increases. On the contrary, the applied compressive stress shows little or no influence on the coercive field. More interestingly, the decrease in the dissipation energy and the polarizations with the compressive stress for the near MPB compositions, i.e., 0.8PMN-0.2PT, 0.7PMN-0.3PT, and 0.6PMN-0.4PT, is clearly more pronounced than that of the 0.9PMN-0.1PT and 0.5PMN-0.5PT compositions. The changes are clearly more observable in 0.7PMN-0.3PT and 0.6PMN-0.4PT compositions, which are closer to the reported MPB composition.[1,4,5] The reductions in both the dissipation energy and the polarization values are generally less than 20% when the compressive is increased from 0 to 75 MPa. As also depicted in Fig. 3, it should be noticed that even though the loading and unloading experiments were performed on all compositions, the results differ insignificantly. In addition, only slight decreases in the polarization values of all the ceramics are also observed after a complete cycle of the mechanical stress. This observation suggests a stress-induced decrease in the switchable part of the polarization at high stress levels.[21,23] The results of the changes in the hysteresis parameters of the PMN-PT ceramics with increasing compressive stress are in agreement with the previous investigations on many ferroelectric ceramics.[18,20–23,35,42,43]

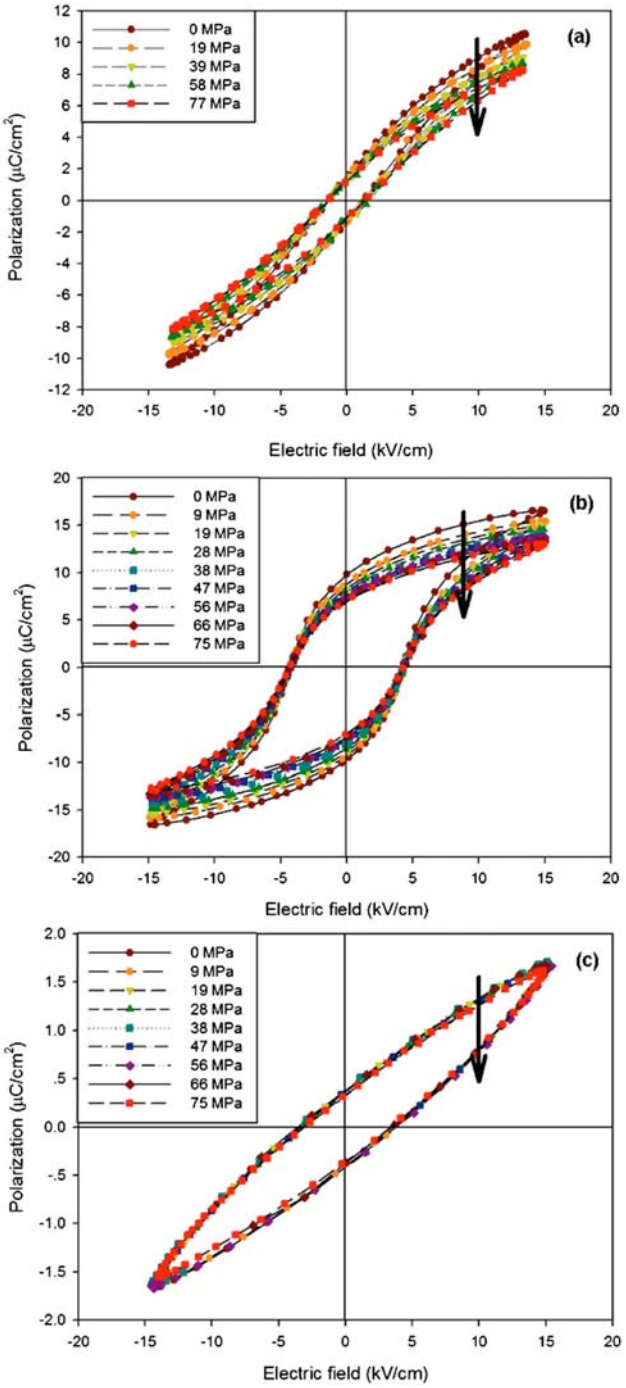

FIG. 2. (Color online) *P-E* hysteresis loops as a function of compressive stress for (a) 0.9PMN-0.1PT, (b) 0.7PMN-0.3PT, and (c) 0.5PMN-0.5PT ceramics (measured at 25 °C and 60 Hz under loading).

To understand, at least qualitatively, these experimental results on ferroelectric properties of the PMN-PT ceramics, one can interpret the changes in terms of domain-reorientation processes. When the compressive stress is applied in the direction parallel to the polar axis (poling) direction, the applied stress tends to keep the ferroelectric domains aligned with their polar axes away from the stress direction through the non-180° ferroelastic domain switching processes.[18–21] Therefore, it takes a larger than usual applied electric field to reorient the domains along the stress direc-

Author complimentary copy. Redistribution subject to AIP license or copyright, see http://jap.aip.org/jap/copyright.jsp

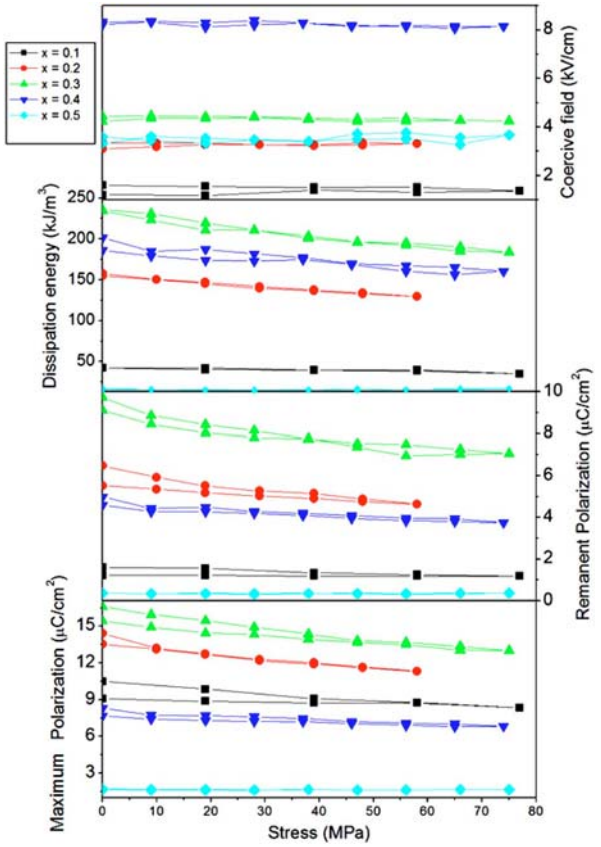

FIG. 3. (Color online) Changes in ferroelectric hysteresis parameters with compressive stress for $(1-x)$PMN$-(x)$PT ceramics (measured at 25 °C and 60 Hz) during loading and unloading.

tion, resulting in a lower value of the maximum polarization (P_{max}), as shown in Figs. 2 and 3. When the electric field is reduced to zero the domains tend to rotate back away from the applied compressive stress direction, resulting in a lower than usual remnant polarization (P_r), as depicted in Figs. 2 and 3.[21,23,33] Furthermore, considering the decrease in the hysteresis loss with increasing the compressive stress, it indicates that more and more ferroelectric domains are constrained by the applied stress and cannot be reoriented by the electric field so as to participate in the polarization reversal. Consequently, both the maximum and remnant polarizations become lower with increasing compressive stress.[20] The above mentioned arguments are particularly applicable to the closer to MPB compositions, i.e., 0.8PMN-0.2PT, 0.7PMN-0.3PT, and 0.6PMN-0.4PT, with more mobile microdomains. However, for the 0.9PMN-0.1PT composition it is observed that the changes in hysteresis parameters with the applied stress are rather small, as depicted in Figs. 2 and 3. This is due to the fact that this ceramic composition behaves more like a relaxor material.[4] Since the experiment was carried out at room temperature, the nanodomain states still predominate in this ceramic composition.[4,11] Therefore, this shows less stress-induced changes in polarizations.[7] For 0.5PMN-0.5PT composition, as described above, the rather small values in the hysteresis parameters may contribute greatly to the weak changes with stress. In addition, since the measuring temperature is far below its transition temperature of 250 °C,[34] the domains may be much less mobile in this ceramic composition; hence, much weaker changes in the hysteresis parameters with stress are observed. Most importantly, the results presented in this study have shown the different contributions to the stress-dependent ferroelectric properties in PMN-PT ceramics. This study has served as an extension to our previous work on the stress-dependent dielectric properties[30] as well as other earlier reports, which mainly focused on only 0.9PMN-0.1PT compositions.[7,15,23,33] Finally, the information obtained here is practically very useful for the design and calculation consideration of devices employing the PMN-PT ceramics.

IV. CONCLUSIONS

In this study, the ferroelectric properties of $(1-x)Pb(Mg_{1/3}Nb_{2/3})O_3-(x)PbTiO_3$ or $(1-x)$PMN$-(x)$PT ($x=0.1-0.5$) ceramics are measured under compressive stress up to 75 MPa. It has been found that both the dissipation energy and the polarizations decrease as the compressive stress increases. On the contrary, the applied compressive stress shows little or no influence on the coercive field. The changes in the ferroelectric properties are more significant in the near MPB compositions, i.e., 0.8PMN-0.2PT, 0.7PMN-0.3PT, and 0.6PMN-0.4PT. These observations are interpreted through the non-180° ferroelastic domain switching processes and the stress-induced decrease in the switchable part of domains.

ACKNOWLEDGMENTS

Financial supports from the Thailand Research Fund (TRF), Commission on Higher Education (CHE), Royal Golden Jubilee Ph.D. Program, and Faculty of Science and Graduate School of Chiang Mai University are gratefully acknowledged.

[1] Y. H. Xu, *Ferroelectric Materials and their Applications* (North-Holland, Los Angeles, 1991).
[2] A. J. Moulson and J. M. Herbert, *Electroceramics: Materials, Properties, Applications* (Wiley, Chichester, 2003).
[3] G. H. Haertling, J. Am. Ceram. Soc. **82**, 797 (1999).
[4] L. E. Cross, Mater. Chem. Phys. **43**, 108 (1996).
[5] S. Jang, Ph.D. thesis, The Pennsylvania State University, 1979.
[6] K. Uchino, *Piezoelectric Actuators and Ultrasonic Motors* (Kluwer, Boston, 1997).
[7] D. Viehland, J. Li, E. McLaughlin, J. Powers, R. Janus, and H. Robinson, J. Appl. Phys. **95**, 1969 (2004).
[8] T. R. Shrout, Z. Chang, N. Kim, and S. Markgraf, Ferroelectr., Lett. Sect. **12**, 63 (1990).
[9] D. Viehland, M. Kim, Z. Xu, and J. Li, Appl. Phys. Lett. **67**, 2471 (1995).
[10] G. Smolenskii and A. Agranovskaya, Sov. Phys. Solid State **1**, 1429 (1960).
[11] C. Randall, D. Barber, and R. Whatmore, J. Microsc. **45**, 275 (1987).
[12] X. Dai, Z. Xu, and D. Viehland, Philos. Mag. B **70**, 33 (1994).
[13] J. Kuwata, K. Uchino, and S. Nomura, Jpn. J. Appl. Phys., Part 1 **21**, 1298 (1982).
[14] S. E. Park and T. R. Shrout, J. Appl. Phys. **82**, 1804 (1997).
[15] D. Viehland and J. Powers, Appl. Phys. Lett. **78**, 3112 (2001).
[16] D. Stansfield, *Underwater Electroacoustic Transducers* (Bath University, Bath, 1991).
[17] M. Mitrovic, G. P. Carmen, and F. K. Straub, Int. J. Solids Struct. **38**, 4357 (2001).
[18] D. Zhou, M. Kamlah, and D. Munz, J. Eur. Ceram. Soc. **25**, 425 (2005).
[19] R. Yimnirun, S. Ananta, E. Meechoowas, and S. Wongsaenmai, J. Phys. D **36**, 1615 (2003).

Author complimentary copy. Redistribution subject to AIP license or copyright, see http://jap.aip.org/jap/copyright.jsp

[20]Q. M. Zhang, J. Zhao, K. Uchino, and J. Zheng, J. Mater. Res. **12**, 226 (1997).
[21]G. Yang, S. F. Liu, W. Ren, and B. K. Mukherjee, Proceedings of the SPIE Symposium on Smart Structures and Materials, 2000 (unpublished), Vol. 3992, p. 103.
[22]O. Steiner, A. K. Tagantsev, E. L. Colla, and N. Setter, J. Eur. Ceram. Soc. **19**, 1243 (1999).
[23]J. Zhao and Q. M. Zhang, Proceedings of the IEEE International Symposium on Applications of Ferroelectrics, 1996 (unpublished), p. 971.
[24]N. A. Pertsev, A. G. Zembilgotov, and A. K. Tagantsev, Phys. Rev. Lett. **80**, 1988 (1998).
[25]S. P. Alpay and A. L. Roytburd, J. Appl. Phys. **83**, 4714 (1998).
[26]N. A. Pertsev, V. G. Koukhar, R. Waser, and S. Hoffmann, Appl. Phys. Lett. **77**, 2596 (2000).
[27]A. Y. Emelyanov, N. A. Pertsev, and A. L. Kholkin, Phys. Rev. B **66**, 214108 (2002).
[28]Z.-G. Ban and S. P. Alpay, Appl. Phys. Lett. **82**, 3499 (2003).
[29]G. Akcay, S. P. Alpay, G. A. Rossetti, Jr., and J. F. Scott, J. Appl. Phys. **103**, 024104 (2008).
[30]R. Yimnirun, M. Unruan, Y. Laosiritaworn, and S. Ananta, J. Phys. D **39**, 3097 (2006).
[31]R. Yimnirun, S. Ananta, and S. Chamunglap, Mater. Chem. Phys. **102**, 165 (2007).
[32]R. Yimnirun, S. Wongsaenmai, R. Wongmaneerung, N. Wongdamnern, A. Ngamjarurojana, S. Ananta, and Y. Laosiritaworn, Phys. Scr., T **129**, 184 (2007).
[33]J. Zhao, A. E. Glazounov, and Q. M. Zhang, Appl. Phys. Lett. **74**, 436 (1999).
[34]A. Udomporn, Ph.D. thesis, Chiang Mai University, 2004.
[35]R. Yimnirun, S. Ananta, A. Ngamjarurojana, and S. Wongsaenmai, Appl. Phys. A: Mater. Sci. Process. **81**, 1227 (2005).
[36]R. Yimnirun, Y. Laosiritaworn, S. Wongsaenmai, and S. Ananta, Appl. Phys. Lett. **89**, 162901 (2006).
[37]R. Yimnirun, P. J. Moses, R. J. Meyer, and R. E. Newnham, Rev. Sci. Instrum. **74**, 3429 (2003).
[38]L. B. Kong, J. Ma, W. Zhu, and O. K. Tan, Mater. Res. Bull. **37**, 23 (2002).
[39]Y. C. Liou, Mater. Sci. Eng., B **103**, 281 (2003).
[40]L. F. Brown, R. L. Carlson, J. M. Sempsrott, G. T. Standford, and J. J. Fitzgerald, Proc.-IEEE Ultrason. Symp. **1**, 561 (1997).
[41]M. E. Lines and A. M. Glass, *Principles and Applications of Ferroelectrics and Related Materials* (Oxford University Press, Oxford, 1977).
[42]R. Yimnirun, Y. Loasiritaworn, and S. Wongsaenmai, J. Phys. D **39**, 759 (2006).
[43]R. Yimnirun, S. Wongsaenmai, S. Ananta, and Y. Laosiritaworn, Appl. Phys. Lett. **89**, 242901 (2006).

Author complimentary copy. Redistribution subject to AIP license or copyright, see http://jap.aip.org/jap/copyright.jsp

J. Phys.: Condens. Matter **20** (2008) 415202 (5pp) doi:10.1088/0953-8984/20/41/415202

Scaling and stress dependence of sub-coercive field dynamic hysteresis in $0.6Pb(Zr_{1/2}Ti_{1/2})O_3$–$0.4Pb(Zn_{1/3}Nb_{2/3})O_3$ ceramic

R Yimnirun[1], **N Wongdamnern, N Triamnak, M Unruan, A Ngamjarurojana, S Ananta and Y Laosiritaworn**

Department of Physics, Faculty of Science, Chiang Mai University, Chiang Mai 50200, Thailand

E-mail: rattikornyimnirun@yahoo.com

Received 2 February 2008, in final form 23 August 2008
Published 12 September 2008
Online at stacks.iop.org/JPhysCM/20/415202

Abstract

The scaling behavior of sub-coercive field dynamic ferroelectric hysteresis under the influence of stress was investigated in rhombohedral $0.6Pb(Zr_{0.5}Ti_{0.5})O_3$–$0.4Pb(Zn_{1/3}Nb_{2/3})O_3$ (0.6PZT–0.4PZN) bulk ceramic. The scaling relation of hysteresis area $\langle A\rangle$ against frequency f, field amplitude E_0, and stress σ for the minor loops takes the form of $\langle A - A_{\sigma=0}\rangle \propto f^{-0.36}E_0^{4.03}\sigma^{0.19}$, indicating the difference in the energy dissipation between the stressed and stress-free conditions. While the scaling obtained is very similar to that of soft and hard PZT ceramics, slightly faster responses to f and E_0 indicate the ease of polarization orientation in this ceramic with a simpler domain structure compared to commercial PZT ceramics. However, the difference in mechanical properties of these materials could contribute to a variation in the response to stress. While the E_0 exponent obtained in this study agreed well with that derived from the Monte Carlo simulation based on the Q-state planar Potts model, the difference in the f exponent obtained experimentally and theoretically was attributed to the depolarizing effects presented in the bulk ceramics.

(Some figures in this article are in colour only in the electronic version)

1. Introduction

Dynamic hysteresis characteristics have become an important consideration because the hysteresis area $\langle A\rangle$ as a function of the field amplitude E_0 and frequency f presents much information that is critical for many ferroelectric applications [1, 2]. Theoretical studies have been carried out to understand the dynamic response of hysteresis curves in spin and polarization systems [3–7]. In particular, attention is focused on power-law scaling

$$\langle A\rangle \propto f^m E_0^n \tag{1}$$

(where m and n are exponents that depend on the dimensionality and symmetry of the system). Based on three-dimensional models, it has been suggested that $m = 1/3$ and $n = 2/3$ as $f \to 0$, whereas $m = -1$ and $n = 2$ as $f \to \infty$ [3, 5, 8]. Experimental investigations on a few thin-film systems have also been reported with variation in the scaling relations obtained [9–12]. On the contrary, there are only a few reports on the hysteresis scaling behavior of bulk ferroelectric ceramics [13–16].

Our previous investigations have already shown stress-dependent scaling behaviors in commercial soft and hard lead zirconate titanate (Pb(Zr, Ti)O_3; PZT) ceramics [14, 15]. The results suggested that the scaling behavior depended strongly on the dimensionality of the system, and also suggested that the different states of domains existing in the ceramics may play a key role in controlling the scaling behavior. Unfortunately, it was too difficult to retrieve such

[1] Author to whom any correspondence should be addressed.

 © 2008 IOP Publishing Ltd Printed in the UK

information for the domain structures of commercial ceramics. Therefore, this study was aimed at a ferroelectric material with a distinct domain configuration. Previous works on $0.6Pb(Zr_{0.5}Ti_{0.5})O_3$–$0.4Pb(Zn_{1/3}Nb_{2/3})O_3$ (0.6PZT–0.4PZT) ceramics with rhombohedral structure have reported excellent electrical properties suitable for various applications [17–20]. Due to its many potential applications and relatively simple domain configuration, the 0.6PZT–0.4PZN ceramic was thus chosen for this study. Practically, ferroelectric ceramics are normally used under sub-coercive field conditions in most applications; it is therefore of interest to obtain scaling relations for such conditions. Interestingly, earlier works showed that the scaling behavior of the minor and saturated loops was significantly different [11, 12].

More importantly, in many applications the ceramic specimens are often subjected to mechanical loading, either from the design of the device itself or from operating conditions which induce stresses [1, 21]. Therefore, prior knowledge of how the material properties change under different load conditions in materials is inevitably crucial for the proper design of a device and for suitable selection of materials for a specific application. In many previous investigations the electrical properties of ceramics were found to strongly depend on stresses (σ) [22–26]. Since f, E_0, and σ have been reported to impose significant influence on the dynamic hysteresis responses of ferroelectric ceramics, it is therefore the major aim of this study to obtain the stress-dependent scaling behavior of sub-coercive field dynamic hysteresis in 0.6PZT–0.4PZN ceramic.

2. Experimental procedures

Disc-shaped samples of tetragonal structure 0.6PZT–0.4PZN ceramic with a diameter of 10 mm and thickness of 1 mm were used in this study. Details on the fabrication and characterization of this material can be found elsewhere [19, 20]. Its basic properties are: dielectric constant (1 kHz) $\varepsilon_r = 1616$; Curie temperature $T_C = 284\,^\circ$C; piezoelectric strain constants $d_{33} = 457$ pm V^{-1}; planar coupling factor $k_p = 0.59$; mechanical quality factor $Q_m = 62$; coercive field (10 Hz) $E_c = 12$ kV cm^{-1}. The dynamic hysteresis (P–E) loops were characterized at room temperature (25 °C) by a modified Sawyer–Tower circuit with f ranging from 2 to 100 Hz and E_0 from 0 to 10.5 kV cm^{-1}. The field was applied to a sample by a high voltage AC amplifier (Trek 610D) with the input sinusoidal signal from a function generator (HP 3310A). The P–E loops were recorded by a digital oscilloscope (HP 54645A, 100 MHz). A detailed description of this system is given elsewhere [25]. Effects of the external stress on the dynamic hysteresis were investigated with the compressometer developed for simultaneous applications of the mechanical stress and the electric field [26]. The compressive stress, applied parallel to the electric field direction, was supplied by the servohydraulic load frame and monitored with the pressure gauge. The P–E loops were recorded as a function of mechanical stress applied discretely between 0 and 163 MPa for each applied field and frequency. At each constant stress, the loop was obtained after 20 sampling cycles to average out the noise deformation.

3. Results and discussion

The hysteresis loops at different f but fixed E_0 (10.5 kV cm^{-1}) and σ (27 MPa), at different E_0 but fixed f (10 Hz) and σ (27 MPa), and at different σ but fixed E_0 (10.5 kV cm^{-1}) and f (10 Hz) are shown in figures 1(a), (b), and (c), respectively. For a particular applied stress, as expected, the dependence of the loop pattern and area $\langle A\rangle$ on f and E is remarkable. At fixed E_0, the loop area $\langle A\rangle$ and remnant polarization (P_r) decrease with an increase of frequency, as shown in figure 1(a). The dependence of the hysteresis loop on E_0 is depicted in figure 1(b). Similar observations have also been reported in soft and hard PZT ceramics [27–29]. In addition, the P–E loop area $\langle A\rangle$ is found to decrease steadily with increasing stress, as reported in previous investigations [24–26].

To obtain suitable scaling relations, one can first follow the suggested scaling law given in equation (1) to determine exponents m and n directly from the experimental data. By plotting $\langle A\rangle$ against f at fixed E_0, one obtains the exponent m. On the other hand, the exponent n can be obtained by plotting $\langle A\rangle$ against E_0 at fixed f. In conjunction with the least-square-fitting method, the exponents $m = -0.36 \pm 0.03$ and $n = 4.03 \pm 0.06$ were obtained. As plotted in figure 2, it is revealed that the experimental data can be fitted (with $R^2 = 0.99$), within the measured uncertainty, by

$$\langle A\rangle \propto f^{-0.36} E_0^{4.03}. \tag{2}$$

Here, the first interesting observation is that the minor-loop scaling in PZN-modified PZT bulk ceramics is generally similar to that of PZT thin film [5, 9], as well as that of the minor loop of PZT bulk ceramics [13, 15]. This is attributed to the fact that the main polarization orientation mechanism in thin-films and in sub-coercive field conditions for bulk ceramics is likely from the same reversible 180° domain rotation (which also occurs at a much faster rate than the irreversible process), as the irreversible non-180° domain switching normally accompanied by mechanical strain occurs at a higher E-field [13, 15, 30–34]. More importantly, the scaling relation obtained in equation (2) indicates that $\langle A\rangle$ decays slightly more quickly with f and grows faster with E_0 than in commercial soft PZT bulk ceramic with $\langle A\rangle \propto f^{-0.33} E_0^3$ [13]. This indicates the ease of the polarization orientation process in rhombohedral 0.6PZT–0.4PZN ceramics that leads to faster polarization orientation kinetics, as compared to complex domain structures of commercial PZT bulk ceramics which require a higher energy barrier for the polarization orientation process.

Considering the E_0 exponent of 4.03, which is approximately of the same order as that in PZT thin film [5, 9], as well as those in minor loops of PZT bulk ceramics [13, 15], the reversible domain wall vibration is also believed to play an additional role in the dependence of hysteresis area on E_0 at a sub-coercive field. In the nucleation and growth concept [5, 9, 35] domain reversal can be characterized by simultaneous contributions from both the new domain nucleation rate and the domain boundary motion velocity, with the latter responding faster to the electric field [36, 37]. Since the reversible domain wall vibration makes a greater

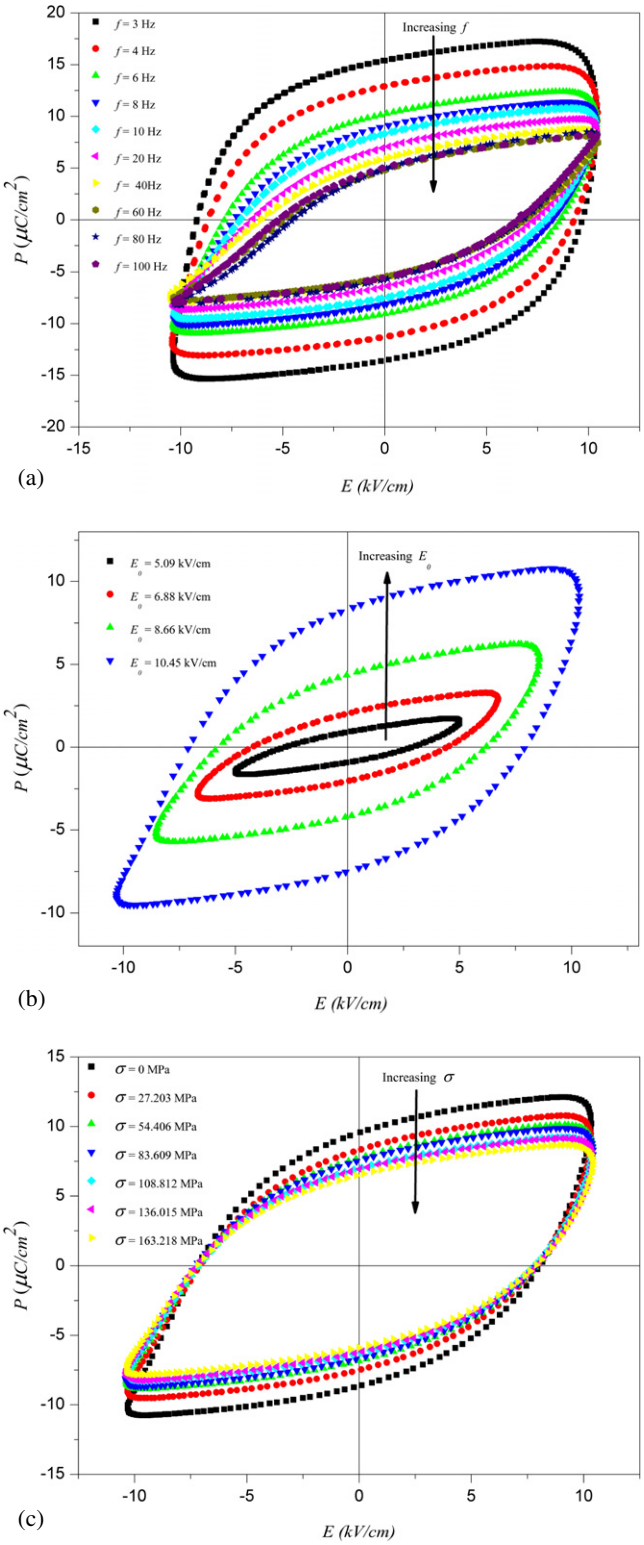

Figure 1. Hysteresis loops under sub-coercive field conditions for 0.6PZT–0.4PZN ceramic (a) at various f, $E_0 = 10.5$ kV cm^{-1}, and $\sigma = 27$ MPa; (b) at various E_0, $f = 10$ Hz, and $\sigma = 27$ MPa; and (c) at various σ, $f = 10$ Hz, and $E_0 = 10.5$ kV cm^{-1}.

contribution to the dependence of hysteresis area with E_0 in sub-coercive conditions, the response to E_0 occurs at much faster rate than at a higher field amplitude. It should also be

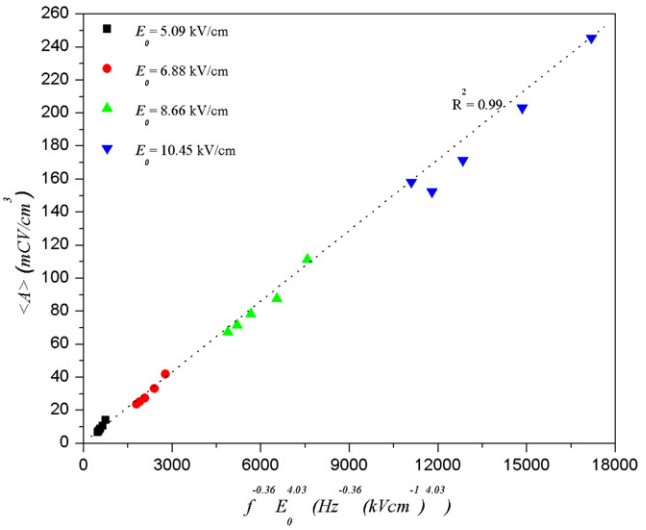

Figure 2. Scaling of hysteresis area $\langle A\rangle$ against $f^{-0.36}E_0^{4.03}$ for 0.6PZT–0.4PZN ceramic under sub-coercive field conditions.

noted that the E_0 exponent $n = 4.03$ agrees very well with the n value of 4 obtained from the previous simulation study using the Monte Carlo method based on the Q-state planar Potts model [38].

In addition, the f exponent of -0.36 is smaller in absolute value than that obtained theoretically from $(\Phi^2)^2$ and $(\Phi^2)^3$ models for non-saturated loops (exponent -1) [3]. The difference could be attributed to depolarizing effects from space charges on grain boundaries, induced electric field from interface layers, immobile defects etc [39], acting as a buffer to the polarization-reversal mechanism in bulk ceramics. As a result, the hysteresis area must show a relatively weaker dependence on f than that of the theoretical models. Furthermore, the value of the f exponent is believed to be related to available domain states in the material, previously proposed in our investigations [13, 14], or growth dimension in the growth kinetics model proposed by Ishibashi and Orihara based on the Kolmogorov–Avrami model [40, 41].

To investigate the scaling behavior under the effect of applied stresses, the stress (σ) term should be included, i.e.

$$\langle A\rangle \propto f^m E_0^n \sigma^p. \tag{3}$$

However, due to the increasing number of exponents, to simplify the problem the validity of the scaling law $\langle A\rangle(\sigma) \propto f^{-0.36}E_0^{4.03}$ is assumed for all applied stresses. Consequently, the area $\langle A\rangle$ for each stress is plotted against $f^{-0.36}E_0^{4.03}$, as shown in figure 3(a), and it can be seen from the least-square linear fits that reasonably good linear relations can be found. As a result, the condition of universality having $m = -0.36$ and $n = 4.03$ in 0.6PZT–0.4PZN bulk ceramic is confirmed. Hence, $\langle A\rangle \propto (a + b\sigma^c) f^{-0.36}E_0^{4.03}$ may be written and by substituting the fitted parameters, it is found that

$$\langle A\rangle - \langle A_{\sigma=0}\rangle = \langle A - A_{\sigma=0}\rangle \propto f^{-0.36}E_0^{4.03}\sigma^{0.19}, \tag{4}$$

where $\langle A_{\sigma=0}\rangle$ refers to the stress-free hysteresis area which will be a dominant term for zero stress. The data-collapsing

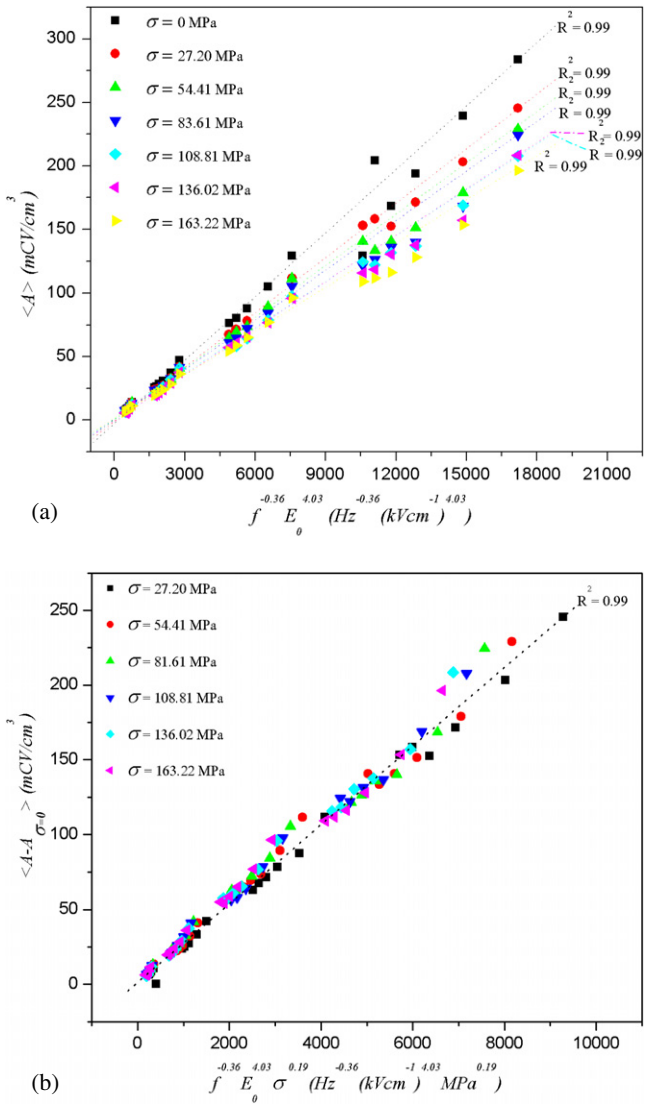

Figure 3. (a) Scaling of hysteresis area $\langle A \rangle$ against $f^{-0.36}E_0^{4.03}$ at various σ. (b) The collapse of the scaling area $\langle A - A_{\sigma=0} \rangle$ against $f^{-0.36}E_0^{4.03}\sigma^{0.19}$ on the same linear-line (with small fluctuation) for 0.6PZT–0.4PZN ceramic under sub-coercive field conditions.

of the scaling area from all f, E_0, and σ was found to confirm equation (4) as evident in figure 3(b). Note that from the appearance of stress σ, $\langle A - A_{\sigma=0} \rangle$, referring to the difference in energy dissipation between under-stress and stress-free conditions, increases with increasing stress suggesting a decay of $\langle A \rangle$ with σ at a rate of $\sigma^{0.19}$ as observed in experiments. Therefore, the difference in the hysteresis area between stressed and stress-free conditions scales with frequency, field amplitude, and stress via the exponents $m = -0.36 \pm 0.03$, $n = 4.03 \pm 0.06$, and $p = 0.19 \pm 0.03$.

To understand the scaling relation obtained in equation (4), at least qualitatively, one needs to consider the following statements. Since the P–E loop area indicates the polarization dissipation energy subjected to one full cycle of electric field application, the loop area is therefore directly related to the volume involved in the switching process during the application of electric field [25, 26, 42]. When the compressive stress is applied in the direction parallel to the direction of the polar axis, the applied stress tends to keep the ferroelectric domains aligned with their polar axes away from the stress direction through the non-180° ferroelastic domain switching processes. Therefore, it takes a larger than usual applied electric field to reorient the domains along the stress direction, resulting in lower values of the saturation polarization. When the electric field is reduced to zero the domains tend to rotate back away from the applied compressive stress direction, resulting in a lower than usual remnant polarization (P_r). Therefore, both the saturation and remnant polarizations become lower with increasing compressive stress, hence the coercivity is also lower [24–26]. The polarization dissipation energy is consequently found to decrease with increasing applied stress, indicating that the sample volume contributing to polarization reversal decreases with increasing stress. Similar observations have also been reported in other investigations [22–26, 43, 44].

Furthermore, it is noted that the stress term with exponent $p = 0.19$ is noticeably different from that for soft and hard PZT bulk ceramics with $p = 0.44$ and 0.37, respectively [14, 15]. The difference could be attributed to a variation of mechanical properties of these materials. While no other stress-dependent scaling investigation is available for a direct comparison, Viehland *et al* [45] reported a power law-like relation between the hysteresis loss and the applied stress in PMN-PT crystals. In addition, many of the theoretical treatments to explain the stress effect on the hysteresis behavior have been primarily based on constitutive models, micro-mechanical and analytical approaches, thermodynamic phenomenology, and Rayleigh law and Preisach model approaches [46–56]. While these theoretical treatments are useful in understanding hysteresis behavior in ferroelectric materials under the application of stress, none of them derive a direct relation between the hysteresis loss and the applied stress in ferroelectric materials. It is also interesting to point out that recent theoretical and experimental investigations have related the stress dependence of the minor hysteresis loop parameters to the dislocation density in ferromagnetic materials [57–60]. Further investigations, both theoretical and experimental, of the stress-dependent scaling behavior are clearly needed as the stress relations are useful in predicting the practical limitations of devices when used under stress.

4. Conclusions

The scaling behavior of the sub-coercive field dynamic ferroelectric hysteresis of rhombohedral 0.6PZT–0.4PZN bulk ceramics under the effect of mechanical stress has been investigated. The scaling relation for the minor loops takes the form of $\langle A - A_{\sigma=0} \rangle \propto f^{-0.36}E_0^{4.03}\sigma^{0.19}$, indicating the difference in the energy dissipation between the stressed and stress-free conditions. While the scaling obtained is very similar to that of soft and hard PZT ceramics, slightly faster responses to f and E_0 indicate the ease of polarization orientation in this ceramic with a simpler domain structure compared to commercial PZT ceramics. In addition, a difference in the response to stress could be attributed to

a variation in the mechanical properties of these materials. Finally, the E_0 exponent obtained in this study agrees well with that derived from the Monte Carlo simulation based on the Q-state planar Potts model. The difference in the f exponent obtained experimentally and theoretically can be attributed to the depolarizing effects presented in the bulk ceramics.

Acknowledgments

Financial support from the Thailand Research Fund (TRF), Commission on Higher Education (CHE), Royal Golden Jubilee PhD Program, Faculty of Science and Graduate School of Chiang Mai University is gratefully acknowledged.

References

[1] Uchino K 2000 *Ferroelectric Devices* (New York: Dekker)
[2] Auciello O, Scott J F and Ramesh R 1998 *Phys. Today* **51** (7) 22
[3] Rao M, Krishnamurthy H R and Pandit R 1990 *Phys. Rev.* B **42** 856
[4] Acharyya M and Chakrabarti B K 1995 *Phys. Rev.* B **52** 6550
[5] Liu J-M, Chan H L W, Choy C L, Zhu Y Y, Zhu S N, Liu Z G and Ming N B 2001 *Appl. Phys. Lett.* **79** 236
[6] Zuo H B, Zhang M F, Han J C and Liu J M 2007 *Mater. Lett.* **61** 2697
[7] Sarjala M, Seppälä E T and Alava M J 2008 *Physica* B **403** 418
[8] Rao M and Pandit R 1991 *Phys. Rev.* B **43** 3373
[9] Liu J-M, Chan H L W, Choy C L and Ong C K 2001 *Phys. Rev.* B **65** 014416
[10] Pan B, Yu H, Wu D, Zhou X H and Liu J-M 2003 *Appl. Phys. Lett.* **83** 1406
[11] Kim Y-H and Kim J-J 1997 *Phys. Rev.* B **55** R11933
[12] Park J-H, Kim C-S, Choi B-C, Moon B K, Jeong J H and Kim I W 2003 *Appl. Phys. Lett.* **83** 536
[13] Yimnirun R, Laosiritaworn Y, Wongsaenmai S and Ananta S 2006 *Appl. Phys. Lett.* **89** 162901
[14] Yimnirun R, Wongsaenmai S, Ananta S and Laosiritaworn Y 2006 *Appl. Phys. Lett.* **89** 242901
[15] Yimnirun R, Wongmaneerung R, Wongsaenmai S, Ngamjarurojana A, Ananta S and Laosiritaworn Y 2007 *Appl. Phys. Lett.* **90** 112908
[16] Yimnirun R, Wongmaneerung R, Wongsaenmai S, Ngamjarurojana A, Ananta S and Laosiritaworn Y 2007 *Appl. Phys. Lett.* **90** 112906
[17] Jiang X P, Fang J W, Zeng H R, Chu B J, Li G R, Chen D R and Yin Q R 2000 *Mater. Lett.* **44** 219
[18] Fan H and Kim H E 2002 *J. Appl. Phys.* **91** 317
[19] Vittayakorn N, Rujijanagul G, Tunkasiri T, Tan X and Cann D P 2003 *J. Mater. Res.* **18** 2881
[20] Vittayakorn N, Rujijanagul G, Tan X and Cann D P 2006 *J. Electroceram.* **16** 141
[21] Uchino K 1997 *Piezoelectric Actuators and Ultrasonic Motors* (Boston, MA: Kluwer–Academic)
[22] Zhao J, Glazounov A E and Zhang Q M 1999 *Appl. Phys. Lett.* **74** 436
[23] Viehland D and Powers J 2001 *J. Appl. Phys.* **89** 1820
[24] Zhou D, Kamlah M and Munz D 2005 *J. Eur. Ceram. Soc.* **25** 425
[25] Yimnirun R, Laosiritaworn Y and Wongsaenmai S 2006 *J. Phys. D: Appl. Phys.* **39** 759
[26] Yimnirun R, Ananta S, Ngamjarurojana A and Wongsaenmai S 2005 *Appl. Phys.* A **81** 1227
[27] Hall D A and Stevenson P J 1999 *Ferroelectrics* **228** 139
[28] Garcia J E, Perez R and Albareda A 2001 *J. Phys. D: Appl. Phys.* **34** 3279
[29] Morozov M, Damjanovic D and Setter N 2005 *J. Eur. Ceram. Soc.* **25** 2483
[30] Trolier-McKinstry S, Gharb N B and Damjanovic D 2006 *Appl. Phys. Lett.* **88** 202901
[31] Lai B-K, Ponomareva I, Naumov I I, Kornev I, Fu H, Bellaiche L and Salamo G S 2006 *Phys. Rev. Lett.* **96** 137602
[32] Ricinschi D and Okuyama M 2007 *Ferroelectrics* **349** 111
[33] Tsurumi T, Sasaki T, Kakemoto H, Harigai T and Wada S 2004 *Japan. J. Appl. Phys.* **43** 7618
[34] Lee K and Baik S 2006 *Annu. Rev. Mater. Res.* **36** 81
[35] Gunton J D, San Miguel M and Sahmi P S 1983 *Phase Transitions and Critical Phenomena* vol 8, ed C Domb and J L Lebowitz (London: Academic) p 267
[36] Stadler H L and Zacumanids P L 1963 *J. Appl. Phys.* **34** 3255
[37] Liu J-M, Pan B, Wang K F and Yu H 2004 *Ceram. Int.* **30** 1471
[38] Liu J-M, Chan H L W and Choy C L 2002 *Mater. Lett.* **52** 213
[39] Bolten D, Böttger U and Waser R 2004 *Appl. Phys. Lett.* **84** 2379
[40] Ishibashi Y and Orihara N 1995 *Integr. Ferroelectr.* **9** 57
[41] Liu J M, Wang W M, Liu Z G, Chan H L and Choy C L 2002 *Appl. Phys.* A **75** 507
[42] Lines M E and Glass A M 1977 *Principles and Applications of Ferroelectrics and Related Materials* (Oxford: Clarendon)
[43] Kumazawa T, Kumagai Y, Miura H, Kitano M and Kushida K 1998 *Appl. Phys. Lett.* **72** 608
[44] Lu X, Zhu J, Li X, Zhang Z, Zhu X, Wu D, Yan F, Ding Y and Wang Y 2000 *Appl. Phys. Lett.* **76** 3103
[45] Veihland D, Ewart L, Powers J and Li J F 2001 *J. Appl. Phys.* **90** 2479
[46] Damjanovic D 1997 *J. Appl. Phys.* **82** 1788
[47] Landis C M 2004 *Curr. Opin. Solid State Mater. Sci.* **8** 59
[48] Achuthan A and Sun C T 2005 *J. Appl. Phys.* **97** 114103
[49] Kamlah M and Jiang Q 1999 *Smart Mater. Struct.* **8** 441
[50] Li W F and Weng G J 2002 *J. Appl. Phys.* **91** 3806
[51] Massad J E and Smith R C 2003 *J. Intell. Mater. Syst. Struct.* **14** 455
[52] Meyer V, Sallese J M, Fazan P, Bard C and Pecheux F 2003 *Solid State Electron.* **47** 1479
[53] Shieh J, Huber J E and Fleck N A 2003 *Acta Mater.* **51** 6123
[54] Guillon O, Delobelle P, Thiebaud F, Walter V and Perreux D 2004 *Ferroelectrics* **308** 95
[55] Belov A Y and Kreher W S 2005 *Mater. Sci. Eng.* B **118** 7
[56] Li L B, Lu X M, Chen Q D, Wu X M and Zhu J S 2008 *J. Appl. Phys.* **103** 034112
[57] Takahashi S, Zhang L, Kobayashi S, Kamada Y, Kikuchi H and Ara K 2005 *J. Appl. Phys.* **98** 033909
[58] Hu R, Soh A K, Zheng G P and Ni Y 2006 *J. Magn. Magn. Mater.* **301** 458
[59] Kobayashi S, Fujiwara T, Tsunoda M, Takahashi S, Kikuchi H, Kamada Y, Ara K and Shishido T 2007 *J. Magn. Magn. Mater.* **310** 2638
[60] Takahashi S, Kobayashi S, Kamada Y and Shishido T 2008 *J. Magn. Magn. Mater.* **320** 2056

J. Phys. D: Appl. Phys. **41** (2008) 205415 (5pp) doi:10.1088/0022-3727/41/20/205415

Power-law scaling of sub-coercive field dynamic hysteresis response in $0.7Pb(Zr_{1/2}Ti_{1/2})O_3$–$0.3Pb(Zn_{1/3}Nb_{2/3})O_3$ ceramic

R Yimnirun[1], N Wongdamnern, N Triamnak, T Sareein, M Unruan, A Ngamjarurojana, S Ananta and Y Laosiritaworn

Department of Physics, Faculty of Science, Chiang Mai University, Chiang Mai 50200, Thailand

E-mail: rattikornyimnirun@yahoo.com

Received 2 February 2008, in final form 19 August 2008
Published 1 October 2008
Online at stacks.iop.org/JPhysD/41/205415

Abstract

Scaling behaviour of sub-coercive field dynamic ferroelectric hysteresis under the influence of stress was investigated in rhombohedral 0.7PZT–0.3PZN bulk ceramic. The scaling relation of hysteresis area $\langle A\rangle$ against frequency f, field amplitude E_0 and stress σ for the minor loops takes the form of $\langle A - A_{\sigma=0}\rangle \propto f^{-0.35}E_0^{3.47}\sigma^{0.38}$, which is very similar to that of soft and hard PZT ceramics. However, slightly faster responses to f and E_0 indicate the ease of polarization orientation in this simpler domain structure ceramic as compared with commercial PZT ceramics. This study suggests that the domain structures play a significant role in controlling dynamic hysteresis behaviour of ferroelectric materials.

(Some figures in this article are in colour only in the electronic version)

1. Introduction

The dynamic hysteresis characteristics have become of important consideration since hysteresis area $\langle A\rangle$ as a function of the field amplitude E_0 and frequency f presents useful information critical for many ferroelectric applications [1, 2]. Theoretical studies have been carried out to understand the dynamic response of hysteresis curves in spin and polarization systems [3–7]. In particular, attention is focused on the power-law scaling

$$\langle A\rangle \propto f^m E_0^n \tag{1}$$

(where m and n are exponents that depend on the dimensionality and symmetry of the system). Based on three-dimensional models, it has been suggested that $m = 1/3$ and $n = 2/3$ as $f \to 0$, whereas $m = -1$ and $n = 2$ as $f \to \infty$ [3, 5, 8]. Experimental investigations on a few thin-film systems have also been reported with variation in the scaling relations obtained [9–12]. In contrast, there are only a few reports on the scaling behaviour studies of ferroelectric hysteresis loops of bulk ferroelectric ceramics [13–16].

Our previous investigations have already shown interesting stress-dependent scaling behaviour in commercial soft and hard lead zirconate titanate, $Pb(Zr,Ti)O_3$ or PZT, ceramics [14, 15]. The results suggested that the scaling behaviour depended strongly on the dimensionality of the system, and also led to the belief that the different states of domains existing in the ceramics may play a key role in controlling the scaling behaviour. Unfortunately, it was too difficult to retrieve such information on the domain structures of commercial ceramics. Therefore, this study was aimed at a suitable potential ferroelectric material with a distinct domain configuration. Previous works on $0.7Pb(Zr_{0.5}Ti_{0.5})O_3$–$0.3Pb(Zn_{1/3}Nb_{2/3})O_3$ (or 0.7PZT–0.3PZT) ceramics with a rhombohedral structure have reported excellent electrical properties suitable for various applications [17–20]. Therefore, due to its many potential practical applications and a relatively simpler domain structure as compared with commercial PZT ceramics [18, 20], the 0.7PZT–0.3PZN ceramic was chosen for this study. Practically, ferroelectric ceramics are used under sub-coercive field condition in most applications; it is therefore of interest to obtain scaling relations for such a condition. Interestingly, earlier works showed that the scaling

[1] Author to whom any correspondence should be addressed.

 © 2008 IOP Publishing Ltd Printed in the UK

behaviour of the minor and saturated loops was significantly different [11, 12].

More importantly, in many applications the ceramic specimens are often subjected to mechanical loading, either from the design of the device itself or from operating conditions which induce stresses [1, 21]. Therefore, prior knowledge of how the material properties change under different load conditions in materials is inevitably crucial for the proper design of a device and for suitable selection of materials for a specific application. In many previous investigations the electrical properties of ceramics were found to depend strongly on stresses (σ) [22–26]. Since f, E_0 and σ have been reported to impose a significant influence on the dynamic hysteresis responses of ferroelectric ceramics, it is therefore the major aim of this study to obtain the stress-dependent scaling behaviour of sub-coercive field dynamic ferroelectric hysteresis in the 0.7PZT–0.3PZN ceramic.

2. Experimental procedures

Disc-shaped samples of tetragonal-structure 0.7PZT–0.3PZN ceramic with a diameter of 10 mm and a thickness of 1 mm were used in this study. Details on the fabrication and characterization of this material can be found elsewhere [19, 20]. Its basic properties are dielectric constant (1 kHz) $\varepsilon_r = 1625$; Curie temperature $T_C = 313\,^\circ$C; piezoelectric strain constant $d_{33} = 443\,\mathrm{pm\,V^{-1}}$; planar coupling factor $k_p = 0.57$; mechanical quality factor $Q_m = 66$; coercive field (10 Hz) $E_c = 13.1\,\mathrm{kV\,cm^{-1}}$. The dynamic hysteresis (P–E) loops were characterized at room temperature (25 °C) by using a modified Sawyer–Tower circuit with f covering from 2 to 100 Hz and E_0 from 0 to 12 kV cm^{-1}. The electric field was applied to a sample by a high voltage ac amplifier (Trek 610D) with the input sinusoidal signal from a function generator (HP 3310A). The P–E loops were recorded by a digital oscilloscope (HP 54645A, 100 MHz). The detailed descriptions of this system are explained elsewhere [25]. Effects of the external stress on the dynamic hysteresis were investigated with the compressometer, which was developed for simultaneous applications of the mechanical stress and the electric field [26]. The compressive stress, applied parallel to the electric field direction, was supplied by the servohydraulic load frame and monitored with the pressure gauge. The P–E loops were recorded as a function of the mechanical stress applied discretely between 0 and 167 MPa for each applied field and frequency. At each constant stress, the loop was obtained after 20 sampling cycles to average out the noise deformation.

3. Results and discussion

The hysteresis profiles for various frequencies f, field amplitude E_0 and stress σ are obtained. The hysteresis loops at different f but fixed E_0 (12 kV cm^{-1}) and σ (27 MPa), at different E_0 but fixed f (10 Hz) and σ (27 MPa) and at different σ but fixed E_0 (12 kV cm^{-1}) and f (10 Hz) are shown in figures 1(*a*), (*b*) and (*c*), respectively. For a particular applied stress, as expected, the dependence of the loop pattern and

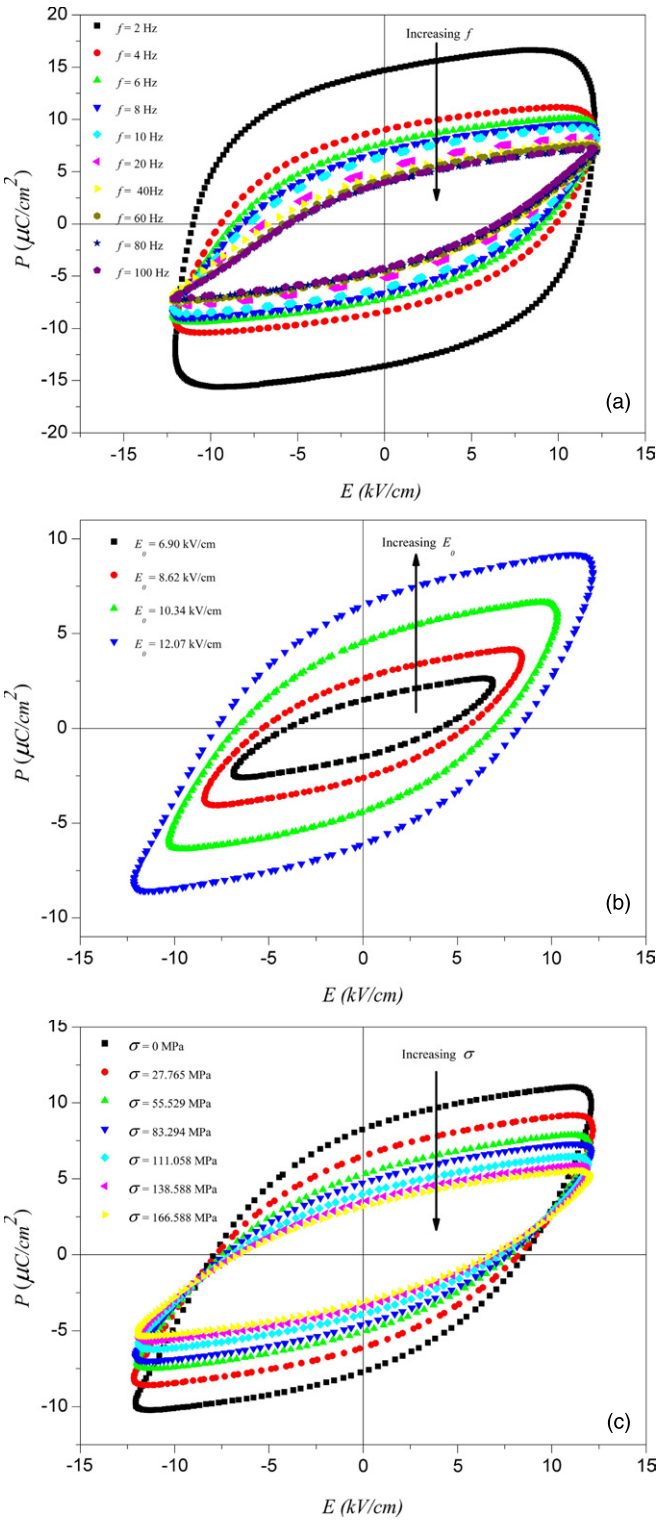

Figure 1. Hysteresis loops under sub-coercive field condition for the 0.7PZT–0.3PZN ceramic (*a*) at various f; $E_0 = 12\,\mathrm{kV\,cm^{-1}}$ and $\sigma = 27$ MPa, (*b*) at various E_0; $f = 10$ Hz and $\sigma = 27$ MPa and (*c*) at various σ; $f = 10$ Hz and $E_0 = 12\,\mathrm{kV\,cm^{-1}}$.

area $\langle A \rangle$ on f and E is remarkable. At fixed E_0, the loop area $\langle A \rangle$ and remanent polarization (P_r) decrease with an increase in frequency, as shown in figure 1(*a*). The dependence of the hysteresis loop on E_0 is depicted in figure 1(*b*). Similar observations have also been reported in soft and hard PZT ceramics [27–29]. In addition, the P–E loop area $\langle A \rangle$ is

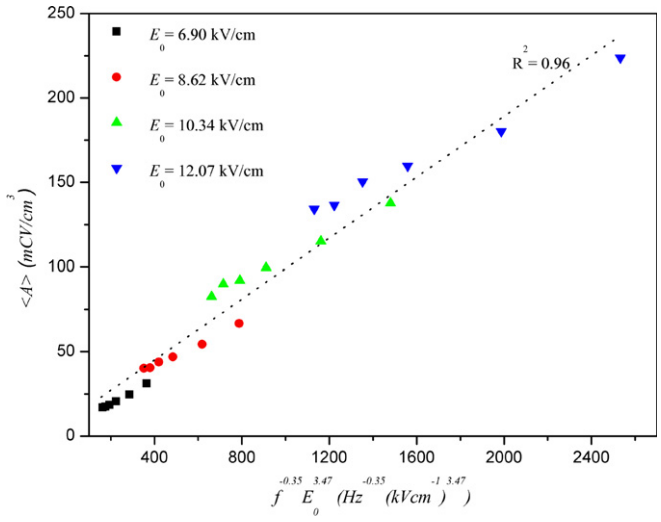

Figure 2. Hysteresis area $\langle A\rangle$ against $f^{-0.35}E_0^{3.47}$ for the 0.7PZT–0.3PZN ceramic under sub-coercive field condition. At each electric field, the data points are from some of the measured frequencies.

found to decrease steadily with increasing stress. Several previous investigations also reported similar stress-dependent behaviour [24–26].

To obtain a suitable scaling relation for the bulk ceramic, one can first follow the suggested scaling law given in equation (1) to determine exponent m and n directly from the experimental data. By plotting $\langle A\rangle$ against f at fixed E_0, one obtains the exponent m. On the other hand, the exponent n can be obtained from plotting $\langle A\rangle$ against E_0 at fixed f. As plotted in figure 2, it is revealed that the experimental data can be fitted (with $R^2 = 0.96$), within the measured uncertainty, by

$$\langle A\rangle \propto f^{-0.35}E_0^{3.47}. \tag{2}$$

Here, the first interesting observation is that the minor-loop scaling in PZN-modified PZT bulk ceramics is generally similar to that of the PZT thin film [5, 9], as well as that of the minor loop of PZT bulk ceramics [13, 15]. As explained in our previous investigation [13], this was attributed to the fact that the polarization orientation mechanism in thin films and in sub-coercive field condition for bulk ceramics is likely from the 180° domain reversal [30–34]. This explains why the scaling behaviour of PZT bulk ceramics at low E-fields is similar to that of thin films. More importantly, the scaling relation obtained in equation (2) indicates that $\langle A\rangle$ decays slightly more quickly with f and grows more quickly with E_0 than the minor-loop scaling relations obtained earlier for commercial soft PZT bulk ceramic with $\langle A\rangle \propto f^{-0.33}E_0^3$ [13]. This clearly indicates the ease of the polarization orientation process in rhombohedral 0.7PZT–0.3PZN ceramics that leads to faster polarization orientation kinetics, as compared with complex domain structures of commercial PZT bulk ceramics which require higher energy barrier for the polarization orientation process. Furthermore, the scaling relations obtained here also support our previous proposed hypothesis that the domain structures play a major role in controlling dynamic hysteresis behaviour of ferroelectric materials [13, 15].

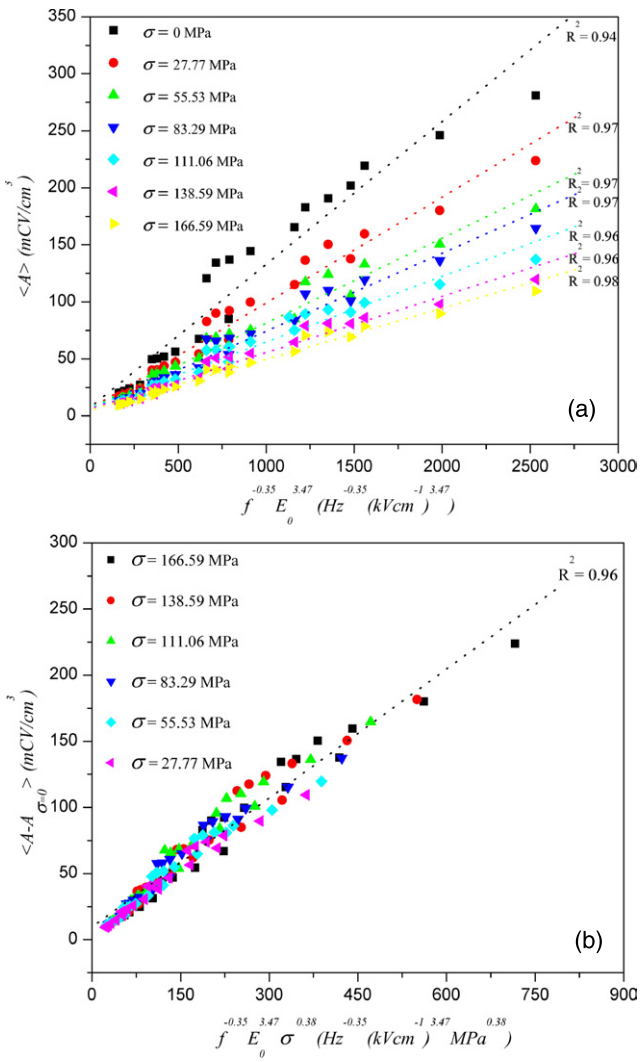

Figure 3. (*a*) Hysteresis area $\langle A\rangle$ against $f^{-0.35}E_0^{3.47}$ at various σ, (*b*) the collapse of the scaling area $\langle A - A_{\sigma=0}\rangle$ against $f^{-0.35}E_0^{3.47}\sigma^{0.38}$ on the same linear line (with small fluctuation) for the 0.7PZT–0.3PZN ceramic under sub-coercive field condition. At each stress, the data points are from some of the measured electric fields and frequencies.

To investigate the scaling behaviour under the effect of applied stresses, instead of including only the field amplitude E_0 and the frequency term f, the scaling relation should also include the stress (σ) term, i.e.

$$\langle A\rangle \propto f^m E_0^n \sigma^p. \tag{3}$$

However, due to increasing number of exponents, to simplify the problem, the validity of the scaling law $\langle A\rangle(\sigma) \propto f^{-0.35}E_0^{3.47}$ is assumed for all applied stresses. Consequently, the area $\langle A\rangle$ for each stress is plotted against $f^{-0.35}E_0^{3.47}$, as shown in figure 3(*a*), and it can be seen from the least-square linear fits that reasonably good linear relations can be found. As a result, the condition of universality having $m = -0.35$ and $n = 3.47$ in the 0.7PZT–0.3PZN bulk ceramic is confirmed. Consequently, $\langle A\rangle \propto (a + b\sigma^c)f^{-0.35}E_0^{3.47}$ may be written and by substituting the fitted parameters, it is found that

$$\langle A\rangle - \langle A_{\sigma=0}\rangle = \langle A - A_{\sigma=0}\rangle \propto f^{-0.35}E_0^{3.47}\sigma^{0.38}, \tag{4}$$

where $\langle A_{\sigma=0}\rangle$ refers to a stress-free hysteresis area which will be a dominant term for zero stress. The data-collapsing of the scaling area from all f, E_0 and σ was found to confirm equation (4) as evident in figure 3(*b*). Note that from the appearance of stress σ, $\langle A - A_{\sigma=0}\rangle$, referring to the difference in energy dissipation between under-stress and stress-free conditions, increases with increasing stress suggesting a decay of $\langle A\rangle$ with σ at a rate of $\sigma^{0.38}$ as observed in experiments. As a result, it can be concluded that the difference in the hysteresis area between under-stress and stress-free condition scales with frequency, field amplitude and stress via exponents $m = -0.35$, $n = 3.47$ and $p = 0.38$. However, at a particular fixed stress, equation (4) gives $f^{-0.35}E_0^{3.47}$ which is the original form for how the area scales with the frequency and the field amplitude.

To understand the stress-dependent scaling relation obtained in equation (4), at least qualitatively, one needs to consider the following statements. Since the P–E loop area indicates the polarization dissipation energy subjected to one full cycle of electric field application, the loop area is therefore directly related to the volume involved in the switching process during the application of the electric field [25, 26, 35]. Hence, when mechanical stress is applied, more and more ferroelectric domains are constrained by the applied stress and cannot be re-oriented by the electric field so as to participate in the polarization reversal. Consequently, both the saturation and remanent polarizations become lower with increasing compressive stress. The polarization dissipation energy is consequently found to decrease with increasing applied stress, indicating that the sample volume contributing to polarization reversal decreases with the increasing stress. Similar observations have also been reported in other investigations [22–26, 36, 37]. Furthermore, it is noted that this stress-dependent scaling relation, in particular the stress term with exponent $p = 0.38$, is slightly different, but still in the same range, from that for soft and hard PZT bulk ceramics with $p = 0.44$ and 0.37, respectively, as obtained in our previous investigations [14, 15]. An explanation for the difference is not clearly known, but could be attributed to the difference in mechanical properties of these materials. Unfortunately, there have been no other stress-dependent scaling investigations available for an independent comparison. In addition, there has been no quantitative theoretical treatment to include the stress term in the scaling relation. Many of the theoretical treatments to explain the stress effect on the hysteresis behaviour have been primarily based on constitutive models, thermodynamic phenomenology and the Rayleigh law approach [38–40]. Further investigations, both theoretical and experimental, on the stress-dependent scaling behaviour are clearly required.

4. Conclusion

The scaling behaviour of the sub-coercive field dynamic ferroelectric hysteresis of rhombohedral 0.7PZT–0.3PZN bulk ceramics under the effect of mechanical stress has been investigated. The scaling relation for the minor loops takes the form of $\langle A - A_{\sigma=0}\rangle \propto f^{-0.35}E_0^{3.47}\sigma^{0.38}$, which is very similar to that of soft and hard PZT ceramics. However, slightly faster responses to f and E_0 indicate the ease of polarization orientation in this simpler domain structure ceramic as compared with commercial PZT ceramics. As a result, this study suggests that the domain structures play a significant role in controlling dynamic hysteresis behaviour of ferroelectric materials.

Acknowledgments

Financial support from the Thailand Research Fund (TRF), the Commission on Higher Education (CHE), the Royal Golden Jubilee PhD Program, Faculty of Science and Graduate School of Chiang Mai University is gratefully acknowledged.

References

[1] Uchino K 2000 *Ferroelectric Devices* (New York: Dekker)
[2] Auciello O, Scott J F and Ramesh R 1998 *Phys. Today* **51**(7) 22
[3] Rao M, Krishnamurthy H R and Pandit R 1990 *Phys. Rev.* B **42** 856
[4] Acharyya M and Chakrabarti B K 1995 *Phys. Rev.* B **52** 6560
[5] Liu J-M, Chan H L W, Choy C L, Zhu Y Y, Zhu S N, Liu Z G and Ming N B 2001 *Appl. Phys. Lett.* **79** 236
[6] Zuo H B, Zhang M F, Han J C and Liu J-M 2007 *Mater. Lett.* **61** 2697
[7] Sarjala M, Seppälä E T and Alava M J 2008 *Physica* B **403** 418
[8] Rao M and Pandit R 1991 *Phys. Rev.* B **43** 3373
[9] Liu J-M, Chan H L W, Choy C L and Ong C K 2001 *Phys. Rev.* B **65** 014416
[10] Pan B, Yu H, Wu D, Zhou X H and Liu J-M 2003 *Appl. Phys. Lett.* **83** 1406
[11] Kim Y-H and Kim J-J 1997 *Phys. Rev.* B **55** R11933
[12] Park J-H, Kim C-S, Choi B-C, Moon B K, Jeong J H and Kim I W 2003 *Appl. Phys. Lett.* **83** 536
[13] Yimnirun R, Laosiritaworn Y, Wongsaenmai S and Ananta S 2006 *Appl. Phys. Lett.* **89** 162901
[14] Yimnirun R, Wongsaenmai S, Ananta S and Laosiritaworn Y 2006 *Appl. Phys. Lett.* **89** 242901
[15] Yimnirun R, Wongmaneerung R, Wongsaenmai S, Ngamjarurojana A, Ananta S and Laosiritaworn Y 2007 *Appl. Phys. Lett.* **90** 112908
[16] Yimnirun R, Wongmaneerung R, Wongsaenmai S, Ngamjarurojana A, Ananta S and Laosiritaworn Y 2007 *Appl. Phys. Lett.* **90** 112906
[17] Jiang X P, Fang J W, Zeng H R, Chu B J, Li G R, Chen D R and Yin Q R 2000 *Mater. Lett.* **44** 219
[18] Fan H and Kim H E 2002 *J. Appl. Phys.* **91** 317
[19] Vittayakorn N, Rujijanagul G, Tunkasiri T, Tan X and Cann D P 2003 *J. Mater. Res.* **18** 2881
[20] Vittayakorn N, Rujijanagul G, Tan X and Cann D P 2006 *J. Electroceram.* **16** 141
[21] Uchino K 1997 *Piezoelectric Actuators and Ultrasonic Motors* (Boston: Kluwer)
[22] Zhao J, Glazounov A E and Zhang Q M 1999 *Appl. Phys. Lett.* **74** 436
[23] Viehland D and Powers J 2001 *J. Appl. Phys.* **89** 1820
[24] Zhou D, Kamlah M and Munz D 2005 *J. Eur. Ceram. Soc.* **25** 425
[25] Yimnirun R, Laosiritaworn Y and Wongsaenmai S 2006 *J. Phys. D: Appl. Phys.* **39** 759
[26] Yimnirun R, Ananta S, Ngamjarurojana A and Wongsaenmai S 2005 *Appl. Phys. A—Mater.* **81** 1227
[27] Hall D A and Stevenson P J 1999 *Ferroelectrics* **228** 139
[28] Garcia J E, Perez R and Albareda A 2001 *J. Phys. D: Appl. Phys.* **34** 3279

[29] Morozov M, Damjanovic D and Setter N 2005 *J. Eur. Ceram. Soc.* **25** 2483
[30] Trolier-McKinstry S, Gharb N B and Damjanovic D 2006 *Appl. Phys. Lett.* **88** 202901
[31] Lai B-K, Ponomareva I, Naumov I I, Kornev I, Fu H, Bellaiche L and Salamo G S 2006 *Phys. Rev. Lett.* **96** 137602
[32] Ricinschi D and Okuyama M 2007 *Ferroelectrics* **349** 111
[33] Tsurumi T, Sasaki T, Kakemoto H, Harigai T and Wada S 2004 *Japan. J. Appl. Phys.* **43** 7618
[34] Lee K and Baik S 2006 *Ann. Rev. Mater. Res.* **36** 81
[35] Lines M E and Glass A M 1977 *Principles and Applications of Ferroelectrics and Related Materials* (Oxford: Clarendon)
[36] Kumazawa T, Kumagai Y, Miura H, Kitano M and Kushida K 1998 *Appl. Phys. Lett.* **72** 608
[37] Lu X, Zhu J, Li X, Zhang Z, Zhu X, Wu D, Yan F, Ding Y and Wang Y 2000 *Appl. Phys. Lett.* **76** 3103
[38] Damjanovic D 1997 *J. Appl. Phys.* **82** 1788
[39] Landis C M 2004 *Curr. Opin. Solid. St. Mater.* **8** 59
[40] Achuthan A and Sun C T 2005 *J. Appl. Phys.* **97** 114103

Functional Materials Letters
Vol. 1, No. 2 (2008) 133–137
© World Scientific Publishing Company

World Scientific
www.worldscientific.com

SCALING BEHAVIOR OF DYNAMIC HYSTERESIS IN PZT-BASED FERROELECTRIC BULK CERAMICS

RATTIKORN YIMNIRUN
Department of Physics, Faculty of Science
Chiang Mai University
Chiang Mai 50200 Thailand
rattikor@chiangmai.ac.th

Received 4 February 2008
Revised 8 March 2008

The scaling relations for the hysteresis loops of soft and hard PZT bulk ceramics were obtained in the forms of $\langle A\rangle \propto f^{-0.25}E_0$ and $\langle A\rangle \propto f^{-0.28}E_0^{0.89}$, respectively, while those for the minor loops took the forms of $\langle A\rangle \propto f^{-1/3}E_0^3$ and $\langle A\rangle \propto f^{-0.43}E_0^{3.19}$. The similarity of the scaling relations suggested that the scaling behaviors of the two types of bulk ceramics were in the same universality class and that the complex defects contributed only slightly to the dynamic behaviors. Finally, this study implied that the domain structures played significant role in controlling dynamic hysteresis behavior of ferroelectric materials.

Keywords: Scaling; hysteresis; PZT; ceramics.

1. Introduction

The dynamic hysteresis, i.e., hysteresis area $\langle A\rangle$ as a function of the field amplitude E_0 and frequency f has become an important consideration in many applications.[1,2] Hence, there have been reports on the scaling behavior of the dynamic hysteresis in ferromagnetic and ferroelectric thin films.[3–5] Many theoretical studies have been focused on scaling law

$$\langle A\rangle \propto f^{\alpha}E_0^{\beta}, \tag{1}$$

(where α and β are exponents that depend on the dimensionality and symmetry of the system) of hysteresis curves in polarization systems.[3,4] Earlier investigations have reported the scaling relations for high-f region with α and β values, respectively, of -1 and 2 for $(\Phi^2)^2$ and $(\Phi^2)^3$ model, and of -0.33 and 3 for PZT thin films.[3–5]

Apart from its theoretical importance, since reliable measurement of the hysteresis at ultra-high frequency is still a big challenge, it is technologically helpful to understand the scaling behavior so that the ultra-high frequency of the hysteresis can be predicted. Hence, there has been a great deal of interest in the scaling behavior of the dynamic hysteresis in ferromagnetic and ferroelectric thin films.[4,5] On a contrary, bulk ferroelectric materials are useful and widely used in many applications. Furthermore, to date, there has been no report on the studies of scaling behavior of ferroelectric hysteresis loops of bulk ceramics.

Lead zirconate titanate ($Pb(Zr_{1-x}Ti_x)O_3$ or PZT) ceramics are among the lead-based complex perovskites that have been investigated extensively, both from academic and commercial viewpoints with various applications.[1,2] However, PZT ceramics are usually modified by dopants. Generally, donor (higher-valency) additives induce "soft" piezoelectric behaviors with higher dielectric and piezoelectric activities, while acceptor (lower-valency) additives result in "hard" piezoelectric

behaviors.[2] These soft and hard PZT ceramics are available commercially and employed widely in many sensor and actuator applications. In addition to the dimension and symmetry of the system, the scaling behavior depends on domain dynamics, which should be noticeably different in hard and soft PZT ceramics with distinct types of complex defects.[1,6] Therefore, it is of interest to investigate and compare the scaling behaviors of dynamic hysteresis in these important commercial soft and hard PZT bulk ceramics.

2. Experimental

The disk-shaped samples of commercially available soft and hard PZT ceramics (APC-855 and 840, APC International, Ltd., USA) with diameter of 8 mm and thickness of 1 mm were used in this study. The dynamic hysteresis (P–E) loops were characterized at room temperature (25°C) by using a modified Sawyer–Tower circuit with f covering from 1 to 100 Hz and E_0 from 0 to 18 and 40, in units of kV/cm, for soft and hard PZT, respectively. The electric field was applied to a sample by a high voltage AC amplifier (Trek 610D) with the input sinusoidal signal from a function generator (HP 3310A). The P–E loops were recorded by a digital oscilloscope (HP 54645A, 100 MHz). Each loop was obtained after averaging over 20 sampling cycles to average out the noise deformation. The hysteresis loop obtained was very consistent with that obtained by a standardized ferroelectric testing unit, RT66A (Radiant Technologies Inc., NM), which ensures the reliability of the measurements.

3. Results and Discussion

3.1. *Soft PZT ceramic*

The hysteresis loops at different f but fixed E_0 (18 kV/cm), and at different E_0 but fixed f (100 Hz) are shown in Fig. 1. The loop area $\langle A \rangle$, remanent polarization (P_r), and coercive field (E_c) decrease with an increase of frequency, as shown in Fig. 1(a). The dependence of the hysteresis loop on E_0 is depicted in Fig. 1(b). For small fields (6 and 8 kV/cm), the loop does not saturate. With further increase in E_0, $\langle A \rangle$, P_r and E_c increase until well saturated loop is achieved.

To obtain the suitable scaling relation for the bulk ceramic, one can fit the data with $\langle A \rangle \propto f^m E_0^n$ where m and n are exponents to be determined directly from the experimental data. By plotting

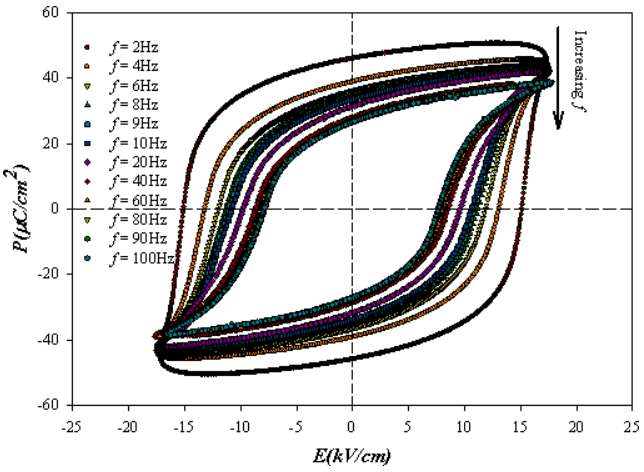

(a)

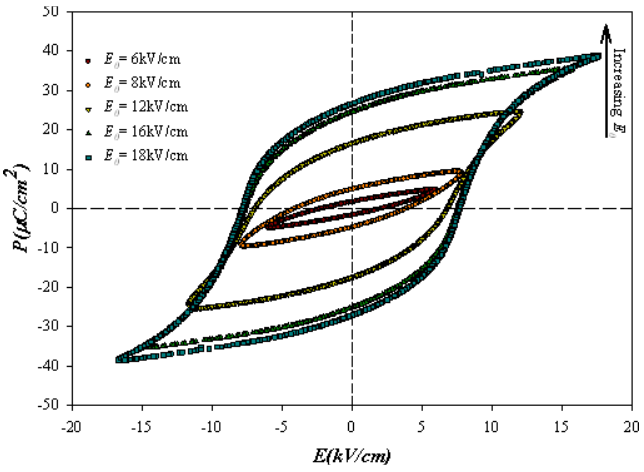

(b)

Fig. 1. Hysteresis loops for soft PZT ceramic (a) at various f and $E_0 = 18$ kV/cm, and (b) at various E_0 and $f = 100$ Hz.

$\langle A \rangle$ against f at fixed E_0, one obtains the exponent m. On the other hand, the exponent n can be obtained from plotting $\langle A \rangle$ against E_0 at fixed f. As plotted in Fig. 2, it is revealed that the high E-field data can be much better fitted (with $R^2 = 0.97$), within the measured uncertainty, by

$$\langle A \rangle \propto f^{-0.25} E_0 \qquad (2)$$

It should also be noted that there is more deviation from the minor loops without saturation at small field amplitudes, and these data were excluded from the fitting reported in Eq. (2). The scaling relation obtained for low E-fields takes the form of $\langle A \rangle \propto f^{-0.33} E_0^3$, which is similar to that of thin films.[4,5] It is important to explain the fundamental nature of this similarity. Probable reasons would lie in the complexities of the domain structure of PZT, which also depends on the

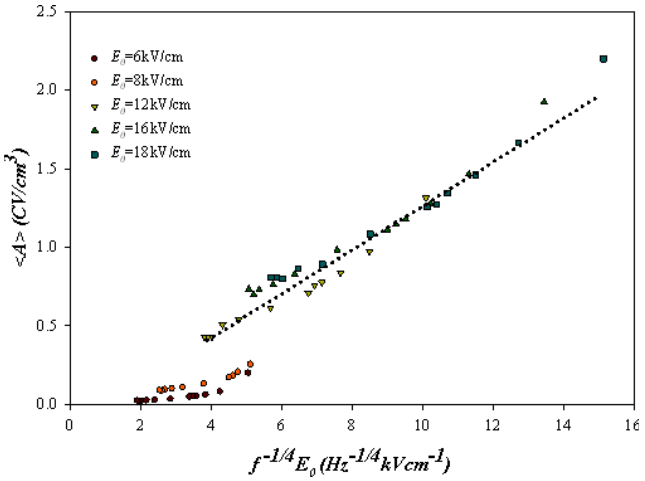

Fig. 2. Scaling of hysteresis area $\langle A\rangle$ against $f^{-0.25}E_0$ for soft PZT ceramic.

dimensionality of the material.[7] A number of recent studies have explored this behavior and reported that it is likely that different domain walls are being activated at different fields.[7,8] Generally, PZT ceramics have 180° and non-180° domain structures. As the non-180° domain switching is normally accompanied by mechanical strain, it occurs at higher E-field than 180° domain reversal does.[7–9] Therefore, under low E-fields, one would expect 180° domain reversal to occur at very fast rate (high frequencies). It is also well known that non-180° domain wall motion is typically very heavily clamped in thin films.[9] Therefore, main switching contribution in thin films would be from the 180° domain reversal. This explains why the scaling behavior of PZT bulk ceramics at low E-fields is similar to that of thin-films.

3.2. *Hard PZT ceramic*

The hysteresis loops at different f but fixed E_0 (40 kV/cm), and at different E_0 but fixed f (20 Hz) are shown in Fig. 3. The loop area $\langle A\rangle$, remanent polarization (P_r) and coercive field (E_c) decrease with an increase of frequency, as shown in Fig. 3(a). The dependence of the hysteresis loop on E_0 is depicted in Fig. 3(b). For small fields (10 and 15 kV/cm), the loops do not saturate. With further increase in E_0, $\langle A\rangle$, P_r and E_c increase until well saturated loop is achieved.

Attempt to obtain a scaling can be done by fitting the data with $\langle A\rangle \propto f^m E_0^n$ where m and n are exponents to be determined directly from the experimental data. By following the same procedure employed for soft PZT and by least-square-fitting

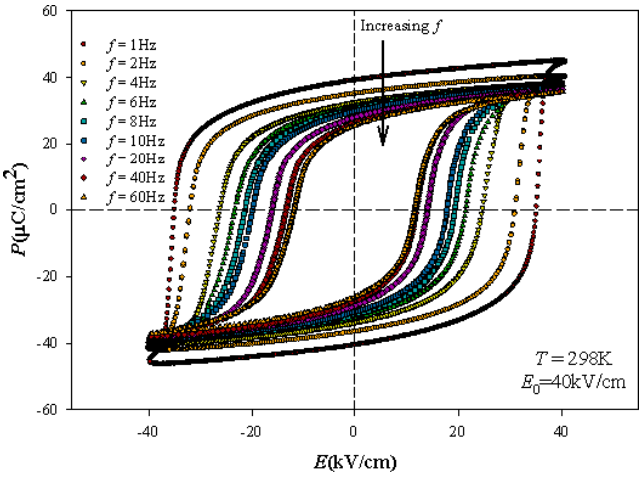

(a)

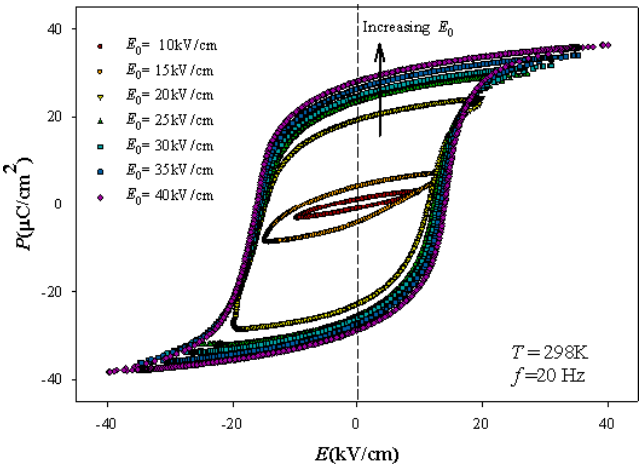

(b)

Fig. 3. Hysteresis loops for hard PZT bulk ceramic (a) at various f and E_0 = 40 kV/cm and (b) at various E_0 and f = 20 Hz.

method, for the high E-field data (saturated loops) the exponents $m = -0.28$ and $n = 0.89$ were obtained. As plotted in Fig. 4, it is revealed that the high E-field data can be fitted well ($R^2 \sim 0.98$), within the measured uncertainty, by

$$\langle A\rangle \propto f^{-0.28} E_0^{0.89} \tag{3}$$

Furthermore, the exponents $m = -0.43$ and $n = 3.19$ were obtained and fitted reasonably well ($R^2 \sim 0.92$) for the minor loop data. This form of the minor loop scaling is also similar to that of soft PZT ceramic, as well as that of thin films, as explained above.

3.3. *Comparison and mechanism*

The scaling relations obtained in Eqs. (2) and (3) indicate that area $\langle A\rangle$ decays more slowly with f

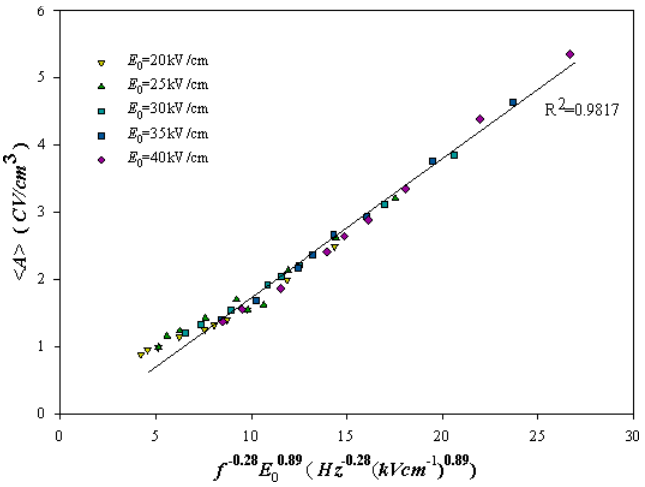

Fig. 4. Scaling of hysteresis area $\langle A\rangle$ against $f^{-0.28}E_0^{0.89}$ for hard PZT ceramic.

and grows more slowly with E than the theoretical prediction, $\langle A\rangle \propto f^{-1}E_0^2$.[3,5] It is also interesting to note that the area $\langle A\rangle$ also decays slightly slower with f, but grows much more slowly with E than the PZT thin film, $\langle A\rangle \propto f^{-0.33}E_0^{3.5}$ An explanation for the difference may come from the polarization-interaction terms as considered in the $(\Phi^2)^2$ and $(\Phi^2)^3$ models, in which the polarization-flip just has one contribution, i.e. polarization-reversal.[3,5] This requires overcoming high energy barrier. Potts model used by Liu *et al.*[10] also has the polarization orientation in various domains in directions not anti-parallel to the direction of E, hence requires lower energy barrier for polarization-flip to occur, which results in a higher exponent of 3 in the E_0 term, as compared to the exponent of 2 in the theoretical models. However, in ceramics, there are influences of many depolarizing effects, arisen from domain walls, grain boundaries, space charges, immobile defects etc., which may retard the external field. Consequently, the energy barrier is very much higher, which leads to slower polarization-flip kinetics. Therefore, a low exponent for the E_0 term is expected from the ceramics rather than the $(\Phi^2)^2$, $(\Phi^2)^3$ in Potts models and thin films. In addition, the f-term shows an exponent of -0.25, smaller in absolute value than that of PZT thin-film (exponent is -0.33). To explain the difference, not only the contribution from the domain switching and ionic-type in thin films,[10] one may need to consider the additional contributions to hysteresis properties from space charges on grain boundaries, induced electric-field from interface layers, immobile defects, etc.[1,2,6] Since our system is a bulk ceramic type; therefore, these depolarizing effects, acting as a buffer to polarization–reversal mechanism, will be stronger than those in thin film structure. As a result, the hysteresis area must show a relatively weaker dependence on f than that observed in thin films.

It is even more interesting to observe that the scaling behaviors for the soft PZT bulk ceramic are to some extent similar to those of the hard counterpart. By a direct comparison, the exponents m and n for the two ceramics are not significantly different. The similar scaling behaviors for the two types of ceramics suggest that though the complex defects contribute greatly to the difference on the electrical properties, but they contribute only slightly to the dynamic behaviors. All these observations suggest that bulk PZT ceramics with similar domain structures should have very comparable dynamic hysteresis and scaling behavior.[11,12] Our recent studies on PZN-modified PZT ceramics also showed similar scaling behavior, which further supports the significant role of domain states in controlling scaling behavior in ferroelectric materials.

4. Conclusions

The scaling relations for the hysteresis loops of soft and hard PZT bulk ceramics were obtained in the forms of $\langle A\rangle \propto f^{-1/4}E_0$ and $\langle A\rangle \propto f^{-0.28}E_0^{0.89}$, respectively, while those for the minor loops take the form of $\langle A\rangle \propto f^{-1/3}E_0^3$ and $\langle A\rangle \propto f^{-0.43}E_0^{3.19}$. The similarity of the scaling relations suggests that the scaling behaviors of the two types of bulk ceramics are in the same universality class and that the complex defects contribute only slightly to the dynamic behaviors.

Acknowledgments

This work was funded by the Thailand Research Fund (TRF), Commission on Higher Education (CHE).

References

1. J. F. Scott, *Ferroelectr. Rev.* **1**, 1 (1998).
2. K. Uchino, *Ferroelectric Devices* (Marcel Dekker, New York, 2000).
3. M. Acharyya and B. K. Chakrabarti, *Phys. Rev. B* **52**, 6560 (1995).
4. J.-M. Liu *et al.*, *Phys. Rev. B* **65**, 014416 (2001).
5. B. Pan *et al.*, *Appl. Phys. Lett.* **83**, 1406 (2003).
6. W. Chang, A. H. King and K. J. Bowman, *Appl. Phys. Lett.* **88**, 242901 (2006).

7. K. Lee and S. Baik, *Ann. Rev. Mater. Res.* **36**, 81 (2006).
8. A. Gruverman, O. Auciello and H. Tokumoto, *Ann. Rev. Mater. Sci.* **28**, 101 (1998).
9. S. Trolier-McKinstry, N. B. Gharb and D. Damjanovic, *Appl. Phys. Lett.* **88**, 202901 (2006).
10. J.-M. Liu *et al.*, *J. Phys.: Condens. Matter* **16**, 1189 (2004).
11. R. Yimnirun *et al.*, *Appl. Phys. Lett.* **89**, 162901 (2006).
12. R. Yimnirun *et al.*, *Appl. Phys. Lett.* **90**, 112908 (2007).

Functional Materials Letters
Vol. 1, No. 3 (2008) 229–233
© World Scientific Publishing Company

World Scientific
www.worldscientific.com

EFFECT OF NICKEL NIOBATE *B*-SITE PRECURSORS ON PHASE FORMATION, MICROSTRUCTURE AND DIELECTRIC PROPERTIES OF PEROVSKITE PNN CERAMICS

S. ANANTA*, R. YIMNIRUN and O. KHAMMAN
Department of Physics, Faculty of Science, Chiang Mai University
Chiang Mai, 50200, Thailand
**suponananta@yahoo.com*

Received 6 February 2008
Revised 25 March 2008

Relaxor perovskite lead nickel niobate (PNN) ceramics were fabricated by using *B*-site precursor method, in which both columbite-$NiNb_2O_6$ and corundum-$Ni_4Nb_2O_9$ were separately employed as nickel niobate *B*-site precursors. It has been found that optimization of sintering condition can successfully lead to highly dense and pure PNN ceramics in both routes. Between the two *B*-site precursor routes, pure perovskite PNN ceramics with slightly better densification and dielectric properties can be produced by using the columbite-route.

Keywords: Lead nickel niobate; perovskite; sintering; dielectric properties.

1. Introduction

Lead nickel niobate, $Pb(Ni_{1/3}Nb_{2/3})O_3$ or PNN, is one of the piezo-based perovskite functional materials which has been extentively studied as potential candidates for electroceramic components such as multilayer capacitor, actuator and transducer applications.[1–3] However, as is well-known, a practical limitation to the utilization of this compound in device applications has been the lack of a simple, reproducible preparation technique for a pure perovskite phase with consistent properties. The formation of perovskite PNN is often accompanied by the occurrence of one or more undesirable phases, which significantly degrade the overall electrical properties of the products.[4–7] To avoid the formation of unwanted phases, several methods have been introduced.[6–10] So far, the columbite method,[4–6] in which prefabricated $NiNb_2O_6$ is reacted with an appropriate proportion of PbO, has been widely accepted as one of the promising methods for the preparation of phase-pure PNN-based materials. There has been a great deal of interest in the preparation of single phase PNN powders as well as in the sintering and electrical properties of PNN-based ceramics.[4–9] To date, only our previous work[11,12] on the preparation of PNN powders by using a corundum $Ni_4Nb_2O_9$ precursor have been reported. Interestingly, effect of a corundum $Ni_4Nb_2O_9$ precursor on phase formation, microstructure and dielectric properties of PNN ceramics under various sintering temperatures has not been reported.

In the present study, an attempt has been made to fabricate and characterize the PNN ceramics by using two different *B*-site precursors i.e. columbite-$NiNb_2O_6$ and corundum-$Ni_4Nb_2O_9$. Their dielectric properties with respect to temperature and frequency were also examined, compared and explained on the basis of their final composition, densification and microstructural development.

2. Experimental

$Pb(Ni_{1/3}Nb_{2/3})O_3$ powders were synthesized by employing two different *B*-site precursors (i.e.

columbite- versus corundum-route) mixed oxide synthetic route, as reported earlier.[11,12] Starting precursors were as follows: PbO (JCPDS file no. 77-1971), NiO (JCPDS file no. 73-1519) and Nb_2O_5 (JCPDS file no. 30-873) (Aldrich, 99% purity). The three oxide powders have an average particle size in the range of 3.0–5.0 μm. First, two intermediate phases of nickel niobate of $NiNb_2O_6$ and $Ni_4Nb_2O_9$ were separately prepared by the solid-state reaction method previously reported.[13,14] The appropriate amount of PbO was then added to the $NiNb_2O_6$ and $Ni_4Nb_2O_9$, vibro-milled and calcined in closed alumina crucible. All batches of powder were prepared using a simple mixed oxide method via a rapid-vibro milling technique for only 2 h (instead of 12 h in Ref. 3) with corundum media in isopropyl alcohol. The detailed process can be found in our previous works.[11–14] The columbite and corundum-route mixtures were then calcined for 2 h with heating/cooling rates of 10°C/min at 950°C and 1050°C, respectively.[11,12] Ceramic fabrication was achieved by adding 3 wt.% polyvinyl alcohol (PVA) binder, prior to pressing as pellets in a pseudo-uniaxial die press. Each pellet was placed in an alumina crucible together with an atmosphere powder of identical chemical composition. After debinding at 500°C for 1 h, sintering was carried out with a constant dwell time of 2 h using heating/cooling rates of 5°C/min at various temperatures between 1100 and 1250°C.

Densities of the final sintered products were measured using the Archimedes principle. Sintered ceramics were examined by X-ray diffraction (Siemen D-500 diffractometer) using CuK_α radiation at room temperature. The microstructural development was characterized using a scanning electron microscopy (JEOL JSM-840A). Mean grain size of the sintered ceramics was subsequently estimated by employing the linear intercept method.[15] In order to evaluate the dielectric properties, dense ceramics were polished to form flat, parallel faces and then coated with gold electrodes. The dielectric properties were measured at various frequency using a LCR meter (HIOKI 3532-50), on cooling through the transition range (−150 to 50°C) with a rate of 3°C/min (instead of 4°C/min in Ref. 3).

3. Results and Discussion

The X-ray diffraction (XRD) patterns of columbite- and corundum-route PNN ceramics sintered at various temperatures are given in Figs. 1(a)–1(c) and 1(d)–1(f), respectively. In general, all XRD patterns show 100% perovskite $Pb(Ni_{1/3}Nb_{2/3})O_3$ phase and could be matched with JCPDS file no. 34-103,[16] in agreement with other works.[7,9] To a first approximation, this phase has a pseudo-cubic perovskite-type structure with cell parameter $a = 403$ pm in space group $Pm3m$ (no. 221). It should be noted that no evidence of either unreacted precursors or pyrochlore-type phases such as $Pb_{1.45}Nb_2O_{6.26}$, $Pb_3Nb_2O_8$, $Pb_3Nb_4O_{13}$ and $Pb_{15}NiNb_{10}O_{41}$ has been found here whereas these phases were found in other works.[7,10,12,17]

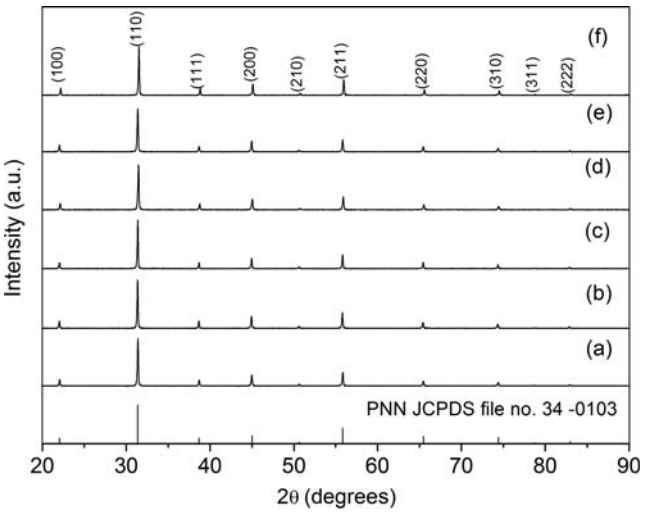

Fig. 1. XRD patterns of the columbite-route PNN ceramics sintered at (a) 1100°C, (b) 1150°C and (c) 1200°C, and the corundum-route PNN ceramics sintered at (d) 1100°C, (e) 1150°C and (f) 1200°C.

The densification data of all the samples are shown in Table 1. The density of about 92–96% and 93–95% of the theoretical value can be achieved for columbite- and corundum-route PNN ceramics, respectively. Density increases as sintering temperature increases from 1100 to 1200°C, consistent with Ref. 3. However, further increase in the sintering temperature up to 1250°C caused the critical damage of the PNN samples (with some melted areas), in contrast to earlier report.[3] This may be attributed to the loss of lead oxide at high sintering temperatures, which is similar to the results found in other Pb-based perovskite systems.[18,19]

It can be noticed that the pure PNN ceramics with higher maximum density can be produced at the optimized sintering temperature of 1200°C by using both B-site precursors. Based on the results obtained here, it may be concluded that the optimal sintering temperature for the production of

Table 1. Physical and dielectric properties of columbite- and corundum-route PNN ceramics.

Preparation route		Columbite route			Corundum route		
Sintering condition (°C) for 2 h	1200[3]	1100	1150	1200	1100	1150	1200
Physical properties							
Relative density (%)[a]	94	92	95	96	93	94	95
Grain size range	—	1.2–4.2	1.3–5.0	2.0–12.3	0.5–3.3	0.8–4.4	1.7–8.0
(mean) (μm)[b]	(3.7)	(2.2)	(3.3)	(5.4)	(1.8)	(2.2)	(4.1)
Dielectric properties							
$\varepsilon_{r,25°C}$	1593			1660			1543
$\tan\delta_{25°C}$	0.0162			0.0064			0.0048
$T(\varepsilon_{r,\max})$	−110			−115			−117
$\varepsilon_{r,\max}$	3403			3636			3430
$\tan\delta_{\max}$	0.0029			0.0096			0.0121
Diffusivity (γ)	1.79			1.92			1.90

[a]The estimated precision of the relative density is ±0.1%.
[b]The estimated precision of the grain size is ±10%.

columbite- and corundum-route PNN ceramics with a maximum bulk density is 1200°C for 2 h (in good agreement with other researchers[3,6]), with heating/cooling rates of 5°C/min.

SEM micrographs of as-sintered (i) and fracture (ii) surfaces of columbite- and corundum-route PNN ceramics with maximum bulk density are compared in Fig. 2. In general, typical perovskite PNN microstructure consisting of highly dense grain-packing is observed in both samples and in good agreement with previous works.[3,6,7] The grain sizes are in the range of 2–12 μm and 1–8 μm for columbite- and corundum-route PNN ceramics, respectively. The results also indicate that grain size tends to increase with sintering temperature, as in the PMN and PT studies.[18,19] Micrographs of fracture surface (Figs. 2(a-ii) and 2(b-ii)) show highly dense microstructures consisting of equiaxed grains, in agreement with other researchers.[3] The PNN ceramics also have an intergranular fracture mechanism, indicating that the grain boundaries are mechanically weaker than the grains,[20] similar to the results previously observed in the relaxor perovskite systems.[4,5,18]

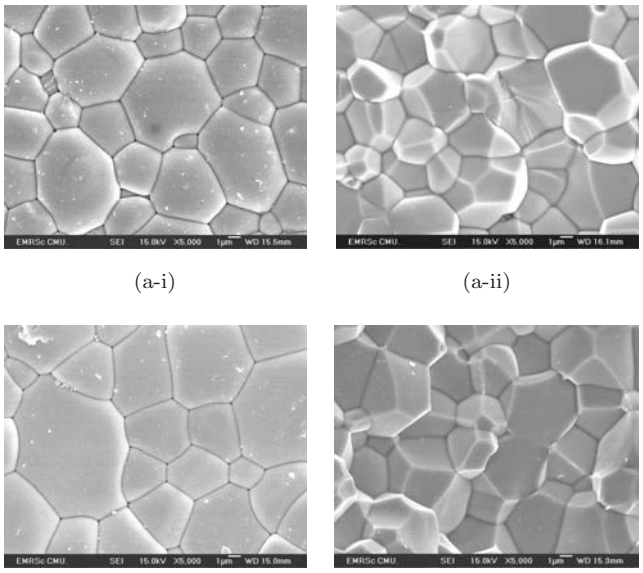

(a-i) (a-ii)

(b-i) (b-ii)

Fig. 2. SEM micrographs of (i) as-sintered and (ii) fracture surfaces for (a) columbite- and (b) corundum-route PNN ceramics with maximum bulk density.

In order to evaluate the dielectric properties i.e. dielectric constant (ε_r) and dielectric loss ($\tan\delta$), both columbite- and corundum-route PNN ceramics with the maximum bulk density were measured at frequencies between 1 and 100 kHz in the temperature range from −150 to +50°C as shown in Figs. 3(i) and 3(ii). In general, the typical relaxor behavior[2,3] with the characteristic dispersive frequency dependence of the dielectric maxima has been observed in both PNN samples. The maximum dielectric constants of 3636 and 3430 measured at 1 kHz were obtained at the temperatures about −115°C and −117°C for columbite- and corundum-route samples, respectively, which are close to previously reported values.[3,4,9]

Characteristics of PNN ceramics obtained by different *B*-site precursor methods in this work and those reported in other works are also compared in Table 1. By comparison to the corundum-route PNN ceramic, dielectric properties of columbite-route ceramic are slightly better, consistent with the density values observed. Though the difference in the dielectric properties could be caused by the

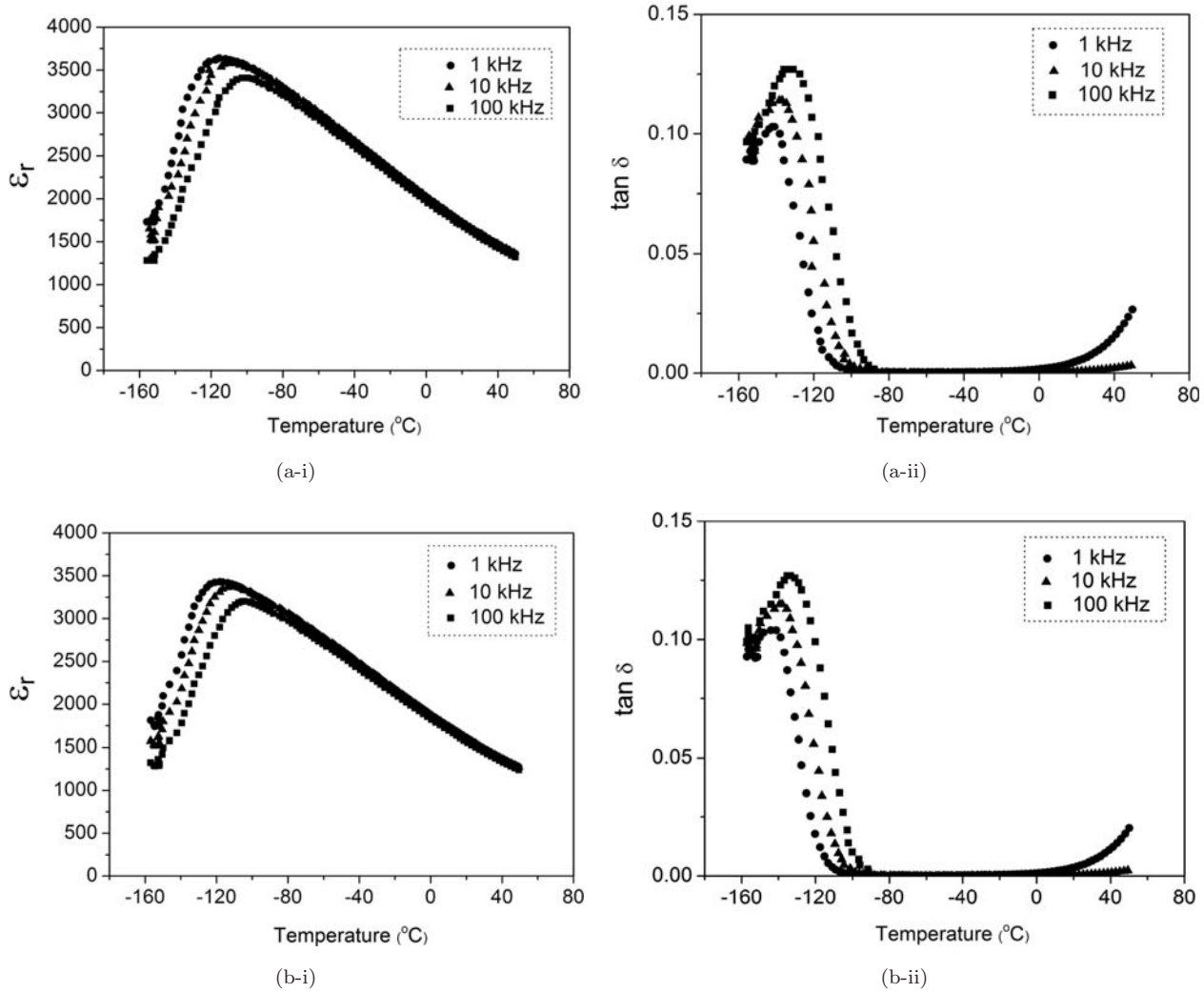

Fig. 3. Temperature dependence of (i) dielectric constant (ε_r) and (ii) dielectric loss ($\tan\delta$) for (a) columbite- and (b) corundum-route PNN ceramics with maximum bulk density.

grain-size effect,[2,21] this should not be the sole reason in the current study because the grain size of the ceramics obtained in both routes is very similar, as listed in Table 1. However, it is observed that the PNN ceramics with larger average grain size and wider grain size range exhibit better dielectric properties. This observation suggests that the grain size along with the microstructural heterogeneous arrangement observed play role together in controlling the dielectric properties. It should also be noted that the dielectric properties and dielectric maximum temperature ($T_{\max}$) obtained in this study are similar to previous investigation,[6] and are close to those reported for single crystal PNN.[22] On the other hand, previous reports on PNN ceramics by other groups showed noticeable deterioration in dielectric properties and shift in $T_{\max}$, which are likely caused by the inclusion of the unwanted secondary phases, which can cause the off-stoichiometry composition or chemical heterogeneity leading to more diffuse phase transition response and $T_{\max}$ shifting. The secondary phase is usually a non-ferroelectric compound so it can definitely destroy the overall dielectric properties and act like a pore in some sense for ferroelectric materials.[23,24]

Unlike the normal ferroelectrics, the dielectric behavior of PNN ceramics cannot be described by the Curie–Weiss law. Their behaviors tally well with the law $1/\varepsilon \propto (T - T_{\max})$.[2] The dielectric constant can be written in the form:

$$\frac{1}{\varepsilon} = \frac{1}{\varepsilon_{\max}} + \frac{(T - T_{\max})^{\gamma}}{2\varepsilon_{\max}\delta^2}, \qquad (1)$$

where γ is the diffusivity which expresses the degree of dielectric relaxation in the relaxor ferroelectric

materials and δ is diffusion parameter and gives an estimation of the relaxor characteristic of the transition. The diffusion exponent for columbite- and corundum-route PNN ceramics is $\gamma = 1.92$ and 1.90, respectively (Table 1), which is higher than reported values of 1.79,[3] 1.75,[7] 1.57[9] and 1.50,[24] but is very close to 2.0,[2] indication of close to completely disordered relaxor behavior in the ceramics sintered by both routes.

By comparison, the diffusion exponent for corundum-route sintered PNN ceramic is smaller than that observed in columbite-route sample. The similar observation has been reported in the PMN ceramics.[21] It may be caused by the different densification of the samples between the two routes. It should also be noticed that the difference in the diffusion exponent γ between the PNN ceramics obtained in this present work and those reported earlier[3,7,9,24] could be attributed to the inclusion of secondary phases, which also cause the deterioration in dielectric properties and shift in dielectric maximum temperature (T_{max}) in previous investigations.[23,24] Furthermore, for a perovskite ferroelectric, it can be established that the diffusion could be caused by grain-size dependence.[2,21] Therefore, this effect can partly be the cause of the increase of diffusion exponent in columbite-route PNN ceramic. Most importantly, it should be noted that the effect of corundum-$Ni_4Nb_2O_9$ *B*-site precursor on phase formation, microstructure and dielectric properties of perovskite PNN ceramics has been reported here for the first time.

4. Conclusions

Highly dense and pure relaxor perovskite PNN ceramics can be successfully produced by employing either columbite- or corundum-route precursor method under optimized sintering temperatures. Between the two *B*-site precursor methods, it is seen that the production of pure PNN ceramics with larger grain size, higher density and better dielectric properties can be obtained via a columbite *B*-site precursor route.

Acknowledgments

This work was supported by the Thailand Research Fund (TRF) and the Commission on Higher Education (CHE).

References

1. K. Niwa, M. Kondo, M. Hida and K. Kurihara, *Jpn. Ceram. Trans.* **150**, 401 (2004).
2. A. J. Moulson and J. M. Herbert, *Electroceramics*, 2nd edn. (Wiley, Chichester, 2003).
3. E. F. Alberta and A. S. Bhalla, *Mater. Lett.* **54**, 47 (2002).
4. T. R. Shrout and A. Halliyal, *Am. Ceram. Soc. Bull.* **66**, 704 (1987).
5. N. Vittayakorn, G. Rujijanagul, X. Tan, M. A. Marquardt and D. P. Cann, *J. Appl. Phys.* **96**, 5103 (2004).
6. L. Veitch, *B.S. Thesis*, Pennsylvania State University, University Park, PA, 1982.
7. C. H. Lu and H. J. Hwang, *Ceram. Int.* **22**, 373 (1996).
8. M. M. A. Sekar and A. Halliyal, *J. Am. Ceram. Soc.* **81**, 380 (1998).
9. C. H. Lu and H. J. Hwang, *Jpn. J. Appl. Phys.* **38**, 5478 (1999).
10. Y. Yoshikawa, *Key Eng. Mater.* **206–213**, 87 (2002).
11. O. Khamman, R. Yimnirun and S. Ananta, *Mater. Lett.* **61**, 4466 (2007).
12. O. Khamman, R. Yimnirun and S. Ananta, *J. Alloys. Compd.* (2007) in press, doi: 10.1016/j.jallcom.2007.11.002.
13. O. Khamman, R. Yimnirun and S. Ananta, *Mater. Lett.* **61**, 639 (2007).
14. O. Khamman, R. Yimnirun and S. Ananta, *Mater. Lett.* **61**, 2565 (2007).
15. R. L. Fullman, *Trans AIME* **197**, 447 (1953).
16. Powder Diffraction File No. 34-103. International Centre for Diffraction Data, Newton Square, PA, 2000.
17. B. Balzer and H. Langbein, *Cryst. Res. Technol.* **32**, 955 (1997).
18. S. Ananta and N. W. Thomas, *J. Eur. Ceram. Soc.* **19**, 1873 (1999).
19. A. Udomporn, K. Pengpat and S. Ananta, *J. Eur. Ceram. Soc.* **24**, 185 (2004).
20. O. Guillon, F. Thiebaud, D. Perreux, C. Courtoris, P. Champagne, A. Leriche and J. Crampon, *J. Eur. Ceram. Soc.* **25**, 2421 (2005).
21. S. Wagner, D. Kahraman, H. Kungl, M. J. Hoffmann, C. Schuh, K. Lubitz, H. Murmann-Biesenecker and J. A. Schmid, *J. Appl. Phys.* **98**, 021102 (2005).
22. V. A. Bokov and I. E. Myl'nikova, *Sov. Phys. Solid State* **3**(3), 613 (1961).
23. G. A. Smolenskii and A. I. Agranovskaya, *Sov. Phys. Solid State* **1**, 1429 (1959).
24. S. Sharma, R. Sati and R. N. P. Choudhary, *Can. J. Phys.* **71**, 322 (1993).

J. Phys. D: Appl. Phys. **41** (2008) 245405 (4pp) doi:10.1088/0022-3727/41/24/245405

Changes in the dielectric properties of $Pb(Zr_{1/2}Ti_{1/2})O_3$–$Pb(Co_{1/3}Nb_{2/3})O_3$ ceramics under compressive stress applied perpendicularly to the electric field

Muangjai Unruan, Anurak Prasatkhetragarn, Yongyut Laosiritaworn, Supon Ananta and Rattikorn Yimnirun[1]

Department of Physics, Faculty of Science, Chiang Mai University, Chiang Mai, 50200, Thailand

E-mail: rattikornyimnirun@yahoo.com

Received 11 May 2008, in final form 15 September 2008
Published 27 November 2008
Online at stacks.iop.org/JPhysD/41/245405

Abstract

The effects of compressive stress, applied perpendicularly to the electric field, on the dielectric properties of $(1-x)Pb(Zr_{1/2}Ti_{1/2})O_3$–$(x)Pb(Co_{1/3}Nb_{2/3})O_3$ ($x = 0.1$–0.5) ceramics were investigated. The results showed that compressive stress had pronounced effects on the dielectric properties of PZT–PCN ceramics. With increasing compressive stress the dielectric constant decreased, while the dielectric loss tangent increased. The observations were interpreted mainly in terms of competing influences of the domain switching through non-180° domain walls, clamping of domain walls and de-ageing mechanisms. The observed changes in the dielectric properties under perpendicular compressive stress were exactly opposite to those under parallel stress.

(Some figures in this article are in colour only in the electronic version)

1. Introduction

Much attention regarding lead-based relaxor ferroelectrics has been focused on lead magnesium niobate ($Pb(Mg_{1/3}Nb_{2/3})O_3$, or PMN), which is widely accepted as a prototype relaxor material. However, there is a series of relaxor materials based on the $Pb(B_{1/3}Nb_{2/3})O_3$ system which also possesses interesting properties [1–3]. This study is focused on lead cobalt niobate ($Pb(Co_{1/3}Nb_{2/3})O_3$, or PCN). However, the temperature related to the maximum dielectric constant (T_{max}) of PCN in the relaxor phase is very low ($T_{max} = -30\,^{\circ}C$) [4]. Thus, in order to increase the T_{max} of PCN, lead zirconate titanate ($PbZr_{0.5}Ti_{0.5}O_3$, or PZT) was added to PCN to form a solid solution of PZT–PCN ceramics. The solid solution of PZT and PCN is expected to synergistically combine the properties of both normal ferroelectric PZT and relaxor ferroelectric PCN, and to exhibit better piezoelectric and dielectric properties than those of the single-phase PZT and PCN [5, 6]. Our recent investigations have already revealed very interesting electrical properties of PZT–PCN ceramic systems [7, 8].

Piezoelectric and ferroelectric ceramics are widely used in devices such as actuators and transducers. However when they are used in these devices the ceramics are often subjected to self-induced or environmental stresses [9–13]. A prior knowledge of the effects of stresses on the material properties is crucial for proper design of a device and for suitable selection of materials for a specific application [12, 13]. Therefore it is very important to obtain experimental data in order to better understand how these materials behave under stress. Stress-dependent dielectric properties have been investigated in $BaTiO_3$ (BT); $Pb(Zr_{0.52}Ti_{0.48})O_3$ (PZT); $Pb(Mg_{1/3}Nb_{2/3})O_3$ (PMN); $Pb(Mg_{1/3}Nb_{2/3})O_3$–$PbTiO_3$ (PMN–PT); $Pb(Mg_{1/3}Nb_{2/3})O_3$–$Pb(Zr_{0.52}Ti_{0.48})O_3$ (PMN–PZT); and $Pb(Zr_{0.52}Ti_{0.48})O_3$–$BaTiO_3$ (PZT–BT) [14–22]. The effects of stress on the dielectric properties of these ceramics depend significantly on compositions and stress levels. However, no study has been conducted on the stress effect on dielectric properties

[1] Author to whom any correspondence should be addressed.

 © 2008 IOP Publishing Ltd Printed in the UK

Table 1. Characteristics of $(1-x)$PZT–(x)PCN ceramics with optimized processing conditions (measured at 10 kHz) [7, 8].

Ceramic	Density ($g\,cm^{-3}$)	Grain size range (μm)	Average grain size (μm)	T_{max} (°C)	Room-temperature stress-free dielectric properties	
					ε_r	tanδ
0.9PZT–0.1PCN	7.39	4.54–19.56	7.45	367	893	0.206
0.8PZT–0.2PCN	7.46	2.60–12.35	4.13	320	1106	0.105
0.7PZT–0.3PCN	7.62	0.43–9.53	2.82	298	619	0.148
0.6PZT–0.4PCN	7.42	0.6–10.75	2.77	236	776	0.239
0.5PZT–0.5PCN	7.31	0.47–9.53	2.61	210	1061	0.112

of PZT–PCN ceramics. Our recent investigation showed that the dielectric constant of PZT–PCN ceramics increased significantly with increasing compressive stress applied parallel to the electric field direction, while the dielectric loss tangent showed an opposing trend [23]. Recently, many investigations also reported changes in the electrical properties of ferroelectric ceramics under compressive stress applied perpendicularly to the electric field [16, 18, 24–28]. Therefore, it is the aim of this study to examine the dielectric properties of PZT–PCN ceramics under such compressive stress. This study, along with our previous investigation, will provide a complete picture of how compressive stress applied in orthogonal directions affects the dielectric properties of this ceramic system.

2. Experimental method

Dense perovskite-phase $(1-x)Pb(Zr_{1/2}Ti_{1/2})O_3$–$(x)Pb(Co_{1/3}Nb_{2/3})O_3$ ($x = 0.1$–0.5) ceramics with uniform microstructure and high density values were prepared from PbO, columbite $CoNb_2O_6$, and wolframite $ZrTiO_4$ powders by the mixed-oxide method [7, 8, 23]. Details of ceramic processing and characterizations have already been provided elsewhere [7, 8]. PZT–PCN ceramics show a perovskite structure having a symmetry varying between tetragonal and pseudo-cubic types, and with a morphotropic phase boundary (MPB) composition between $x = 0.2$ and 0.3. Though the grain size of the ceramics varies considerably from <0.47 to 19.6 μm, the average grain size only varies between 3 and 7 μm [7, 8]. Table 1 summarizes the physical characteristics of the PZT–PCN ceramics used in this study. It is important to note that, since there was no significant difference in either the density or the average grain size of all the ceramic compositions (except for the 0.9PZT–0.1PCN composition, which contained larger grains), these parameters should not play an important role in the composition-dependent dielectric properties under compressive stress.

The sintered specimens were cut into rectangular bars (typical dimensions: $6 \times 2 \times 2\,mm^3$) and then lapped to obtain parallel faces. Silver paint was applied onto the two ($6 \times 2\,mm^2$) opposite faces, and the two electrodes were attached with silver wires for electrical measurement. The specimens were heated at 750 °C for 12 min to ensure contact between the electrodes and the ceramic surface. To study the effects of stress on the dielectric properties of the ceramic, a compressometer was constructed for simultaneous applications of mechanical stress perpendicular to the electric field [29–31]. The compressometer cell consisted of a cylindrical brass cell with a heavy brass base, a brass ram and a precisely guided loading platform which provided true uniaxial stress during mechanical loading. Compressive stress was supplied by a servohydraulic load frame, and the applied stress level was monitored with the load frame's pressure gauge. Measurements were performed as a function of mechanical prestress applied discretely. The dielectric properties were measured at room temperature using a LCR-meter (Instek LCR-821) with an applied voltage of 1 V at 10 kHz.

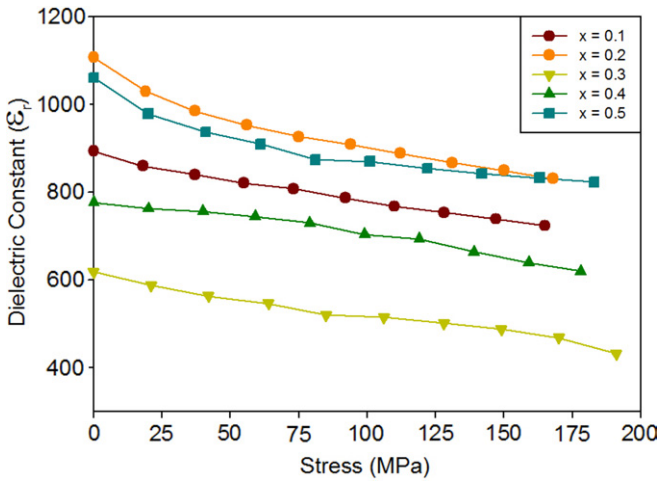

Figure 1. Changes in dielectric constant (ε_r) with compressive stress applied perpendicularly to the electric field direction for $(1-x)$PZT–(x)PCN ceramics (measured at 25 °C and 10 kHz).

3. Results and discussion

The room-temperature dielectric properties of $(1-x)$PZT–(x)PCN ceramic as a function of perpendicular compressive stress are depicted in figures 1 and 2. It should be noted that even though the loading and the unloading experiments were performed on all compositions, the results differed insignificantly. Hence, only the average values are plotted. Figure 1 shows that the dielectric constant decreases with increasing stress, for all compositions. At a maximum applied stress of 180 MPa, the decrease in the dielectric constant varies slightly: from approximately 25–30% for the near MPB 0.8PZT–0.2PCN and 0.7PZT–0.3PCN compositions, to 15–20% for the other compositions. On the other hand, the dielectric loss tangent (tan δ) increases monotonically with the

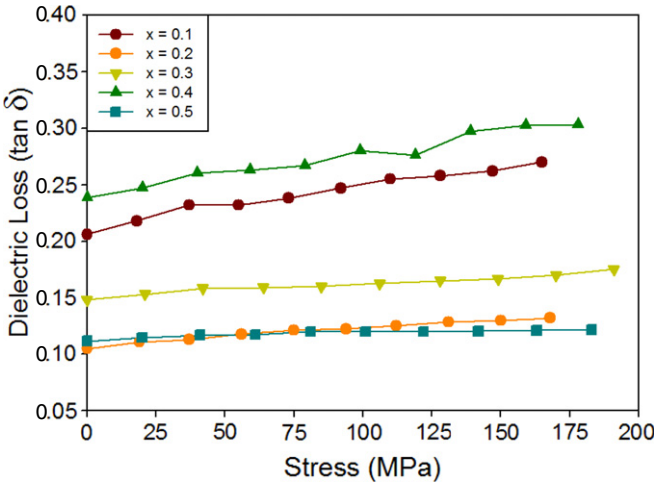

Figure 2. Changes in dielectric loss tangent (tan δ) with compressive stress applied perpendicularly to the electric field direction for $(1-x)$PZT–(x)PCN ceramics (measured at 25 °C and 10 kHz).

applied stress increase, as displayed in figure 2. The dielectric loss tangent increases by 10–20% at the maximum stress value, with the higher changes observed for compositions near the MPB. In the case of compressive stress applied perpendicularly to the direction of the electric field, only limited testing has been carried out on hard and soft PZT, PIN–PT and PMN–PT ceramics [18, 20, 24, 32, 33]. The results presented here are very similar to those obtained earlier for the Pb-based perovskite ceramics mentioned above.

However, since the dielectric constant of the sample was measured using capacitance, there is a change in sample capacitance due to the geometrical deformation under stress. The variation of the sample dielectric constant ($\Delta\varepsilon_r$) can be expressed as $\varepsilon_r^* X^*((1+2\upsilon)/E)$, where X is the applied stress, υ is Poisson's ratio and E is Young's modulus [20, 29]. By applying the estimated values of $\upsilon \sim 0.3$ and $E \sim 100$ GPa for PZT–based ceramics [19, 24, 34] and ε_r given in table 1, it can be estimated that at the maximum stress of 180 MPa, the variation of the sample dielectric constant due to geometrical deformation is <0.5%. Therefore, this variation should not be an important factor in the dielectric properties change under stress seen in figures 1 and 2.

To understand these experimental results, at least qualitatively, various effects must be considered. When compressive stress is applied, the domain structure of ferroelectric ceramics may undergo domain switching through non-180° domain walls, de-ageing, and clamping of domain walls [11, 14, 19, 28]. Here, the stress clamping of domain walls, which results in a decrease in domain wall mobility, and the stress-induced decrease in the switchable part of spontaneous polarization are expected to play roles in the decrease in the dielectric constant under compressive stress [10, 17, 28]. In addition, the continuous decrease in the dielectric constant can also be attributed to the switching of 90° domains. This is a particularly important contribution because when compressive stress is applied perpendicularly to the electric field direction, the applied stress tends to force the polarization of the individual domains to lie in a plane normal to the stress direction through the non-180° (i.e. 90° in tetragonal composition, and 71°/109° in rhombohedral composition) ferroelastic domain switching processes [14–17, 28]. Therefore, a greater decrease in the dielectric constant of the compositions near MPB (i.e. 0.8PZT–0.2PCN and 0.7PZT–0.3PCN) is attributed to more available domain states in the compositions [1–3]; hence a much greater change is observed.

The cause of the stress dependence of the dielectric loss tangent is more complex. As is seen in the changes in the dielectric constant, the clamping of domain walls under compressive perpendicular stress results in a decrease in domain wall mobility; hence this should reduce the dielectric loss tangent at a similar rate [17, 28]. However, a noticeable increase in the dielectric loss tangent is observed for all compositions. This can probably be explained by an additional, obviously larger, contribution from the de-ageing mechanism. During the ageing process, some of the domain walls become pinned by impurities and structural imperfections. When a large enough stress is applied to the aged samples, it causes structural changes and a redistribution of impurities. As a result, the domain walls that were pinned during ageing can become active again. This de-ageing can increase the dielectric responses. Therefore, the competing influence between the domain clamping and de-ageing mechanisms can cause a slight increase in the dielectric loss response to the applied stress.

In addition, only slight decreases in the dielectric properties of all the ceramics were observed after a complete cycle of mechanical stress. This suggests a small stress-induced decrease in the switchable part of the polarization at the maximum applied stress, which exceeds the expected coercive stress for ferroelastic switching in PZT–PCN ceramics (reported as 130–150 MPa for hard PZT ceramics) [35].

4. Conclusions

The dielectric properties of $(1-x)$Pb$(Zr_{1/2}Ti_{1/2})O_3$–(x)Pb$(Co_{1/3}Nb_{2/3})O_3$ (x = 0.1–0.5) ceramics were determined under compressive stress applied perpendicularly to the electric field. The results clearly showed that perpendicular compressive stress had pronounced effects on the dielectric properties of PZT–PCN ceramics. With increasing compressive stress, the dielectric constant of the ceramics decreased, while the dielectric loss tangent increased. The observations were interpreted mainly in terms of competing influences of the domain switching through non-180° domain walls, clamping of domain walls, and de-ageing mechanisms. The observed changes in the dielectric properties under perpendicular compressive stress were exactly opposite to those under parallel stress.

Acknowledgments

This work was jointly supported by the Thailand Research Fund (TRF), Commission on Higher Education (CHE), Royal Golden Jubilee PhD Program, Faculty of Science and Graduate School of Chiang Mai University.

References

[1] Uchino K 2000 *Ferroelectric Devices* (New York: Dekker)
[2] Jaffe B, Cook W R and Jaffe H 1971 *Piezoelectric Ceramics* (New York: Academic)
[3] Xu Y 1991 *Ferroelectric Materials and Applications* (Los Angeles, CA: North-Holland)
[4] Unruan M, Vittayakorn N, Wongmaneeruang R, Prasatkhetragarn A, Ananta S and Yimnirun R 2008 *J. Alloys Compounds* **466** 264
[5] Kudo T, Yazaki T, Naito F and Sugaya S 1970 *J. Am. Ceram. Soc.* **53** 326
[6] Hachiga T, Fujimoto S and Yasuda N 1987 *J. Phys. D: Appl. Phys.* **20** 1291
[7] Vittayakorn N, Wirunchit S, Traisak S, Yimnirun R and Rujijanagul G 2008 *Curr. Appl. Phys.* **8** 128
[8] Prasartkhetragarn A, Vittayakorn N, Ananta S, Yimnirun R and Cann D P 2008 *Japan. J. Appl. Phys.* **47** 998
[9] Kuwata J, Uchino K and Nomura S 1982 *Japan. J. Appl. Phys.* **21** 1298
[10] Park S E and Shrout T R 1997 *J. Appl. Phys.* **82** 1804
[11] Viehland D and Powers J 2001 *Appl. Phys. Lett.* **78** 3112
[12] Stansfield D 1991 *Underwater Electroacoustic Transducers* (Bath: Bath University Press)
[13] Uchino K 1997 *Piezoelectric Actuators and Ultrasonic Motors* (Boston, MA: Kluwer)
[14] Zhou D, Kamlah M and Munz D 2005 *J. Eur. Ceram. Soc.* **25** 425
[15] Wongsaenmai S, Ananta S, Meechoowas E and Yimnirun R 2003 *J. Phys. D.* **36** 1615
[16] Zhang Q M, Zhao J, Uchino K and Zheng J 1997 *J. Mater. Res.* **12** 226
[17] Yang G, Liu S F, Ren W and Mukherjee B K 2000 *Proc. SPIE Symp. Smart Struct. Mater.* **3992** 103
[18] Steiner O, Tagantsev A K, Colla E L and Setter N 1999 *J. Eur. Ceram. Soc.* **19** 1243
[19] Zhao J and Zhang Q M 1996 *Proc. IEEE Int. Symp. Appl. Ferroelectr.* **1** 971
[20] Yimnirun R, Unruan M, Laosiritaworn Y and Ananta S 2006 *J. Phys. D: Appl. Phys.* **39** 3097
[21] Yimnirun R, Ananta S and Chamunglap S 2007 *Mater. Chem. Phys.* **102** 165
[22] Yimnirun R, Wongsaenmai S, Wongmaneerung R, Wongdamnern N, Ngamjarurojana A, Ananta S and Laosiritaworn Y 2007 *Phys. Scr.* **T129** 184
[23] Unruan M, Prasatkhetragarn A, Laosiritaworn Y, Ananta S and Yimnirun R 2008 *Phys. Scr.* **77** 045702
[24] Zhao J, Glazounov A E and Zhang Q M 1999 *Appl. Phys. Lett.* **74** 436
[25] Unruan M, Wongmaneerung R, Ngamjarurojana A, Ananta S, Laosiritaworn Y and Yimnirun R 2008 *J. Appl. Phys.* **104** 064107
[26] Unruan M, Wongsaenmai S, Laosiritaworn Y, Ananta S and Yimnirun R 2008 *J. Phys. D: Appl. Phys.* **41** 085406
[27] Zhao J, Zhang Q M and Mueller V 1998 *Proc. IEEE Int. Symp. Appl. Ferroelectr.* **1** 361
[28] Li F X, Li S and Fang D N 2005 *Mater. Sci. Eng.* B **120** 119
[29] Yimnirun R, Moses P J, Meyer R J and Newnham R E 2003 *Rev. Sci. Instrum.* **74** 3429
[30] Yimnirun R, Ananta S, Ngamjarurojana A and Wongsaenmai S 2005 *Appl. Phys.* A **81** 1227
[31] Yimnirun R, Loasiritaworn Y and Wongsaenmai S 2006 *J. Phys. D: Appl. Phys.* **39** 759
[32] Yang G, Liu S F, Ren W and Mukherjee B K 2001 *Ferroelectrics* **262** 207
[33] Krueger H 1967 *J. Acoust. Soc. Am.* **43** 583
[34] Viehland D and Powers J 2001 *J. Appl. Phys.* **89** 1820
[35] Calderon-Moreno J M 2001 *Mater. Sci. Eng.* A **315** 227

Stress dependence and scaling of subcoercive field dynamic hysteresis in $0.5Pb(Zr_{1/2}Ti_{1/2})O_3-0.5Pb(Zn_{1/3}Nb_{2/3})O_3$ ceramic

R. Yimnirun,[a] N. Wongdamnern, N. Triamnak, M. Unruan, A. Ngamjarurojana, S. Ananta, and Y. Laosiritaworn
Department of Physics, Faculty of Science, Chiang Mai University, Chiang Mai 50200, Thailand

(Received 1 February 2008; accepted 5 October 2008; published online 17 November 2008)

Stress dependence and scaling behavior of subcoercive field dynamic ferroelectric hysteresis were investigated in rhombohedral $0.5Pb(Zr_{1/2}Ti_{1/2})O_3-0.5Pb(Zn_{1/3}Nb_{2/3})O_3$ (0.5PZT–0.5PZN) bulk ceramic with profound relaxor characteristics. The scaling relation of hysteresis area $\langle A\rangle$ against frequency f, field amplitude E_0, and stress σ for the minor loops takes a form of $\langle A-A_{\sigma=0}\rangle \propto f^{-0.34}E_0^{3.68}\sigma^{0.35}$, which is very similar to that of soft and hard lead zirconate titanate ceramics with the same disrupted domains. This study suggests that the domain structures play a significant role in controlling the dynamic hysteresis behavior of ferroelectric materials. © *2008 American Institute of Physics*. [DOI: 10.1063/1.3021287]

I. INTRODUCTION

The dynamic hysteresis characteristics have become important consideration since hysteresis area $\langle A\rangle$ as a function of the field amplitude E_0 and frequency f presents lots of information critical for many ferroelectric applications.[1,2] Theoretical studies have been carried out to understand the dynamic response of hysteresis curves in spin and polarization systems.[3–7] In particular, attention is focused on scaling law,

$$\langle A\rangle \propto f^m E_0^n \tag{1}$$

(where m and n are exponents that depend on the dimensionality and symmetry of the system). Based on three-dimensional models, it has been suggested that $m=1/3$ and $n=2/3$ as $f\rightarrow 0$, whereas $m=-1$ and $n=2$ as $f\rightarrow\infty$.[3,5,8] Experimental investigations on a few thin-film systems have also been reported with variation in the scaling relations obtained.[9–12] On the contrary, there are only few reports on the scaling behavior studies of ferroelectric hysteresis loops of bulk ferroelectric ceramics.[13–16]

Our previous investigations have already shown interesting stress-dependent scaling behaviors in commercial soft and hard lead zirconate titanate, $Pb(Zr,Ti)O_3$ or PZT, ceramics.[14,15] The results suggested that the scaling behavior depended strongly on the dimensionality of the system, and it was also led to believe that the different states of domains existing in the ceramics may play a key role in controlling the scaling behavior. As an extension to our previous investigations,[14,15] this current study was aimed at a suitable potential ferroelectric material with similar domain configuration to commercial PZT bulk ceramics. Previous works on rhombohedral $0.5Pb(Zr_{0.5}Ti_{0.5})O_3-0.5Pb(Zn_{1/3}Nb_{2/3})O_3$ (or 0.5PZT–0.5PZT) ceramics with disrupted domains have shown excellent electrical properties with profound relaxor characteristics suitable for various applications.[17–20] Therefore, due to its many potential practical applications and relatively similar domain configuration as compared to commercial soft and hard PZT ceramics, the 0.5PZT–0.5PZN ceramic was chosen for this study. Practically, ferroelectric ceramics are used under subcoercive field condition in most applications; it is therefore of interest to obtain scaling relations for such condition. Interestingly, earlier works showed that the scaling behavior of the minor and saturated loops was significantly different.[11,12]

More importantly, in many applications the ceramic specimens are often subjected to mechanical loading, either from the design of the device itself or from operating conditions which induce stresses.[1,21] Therefore, prior knowledge of how the material properties change under different load conditions in materials is inevitably crucial for proper design of a device and for suitable selection of materials for a specific application. In many previous investigations the electrical properties of ceramics were found to depend strongly on stresses (σ).[22–26] Since f, E_0, and σ have been reported to impose significant influence on the dynamic hysteresis responses of ferroelectric ceramics, it is therefore the major aim of this study to obtain the stress-dependent scaling behavior of subcoercive field dynamic ferroelectric hysteresis in 0.5PZT–0.5PZN ceramic.

II. EXPERIMENT

The disk-shaped samples of tetragonal-structure 0.5PZT–0.5PZN ceramic with diameter of 10 mm and thickness of 1 mm were used in this study. Details on the fabrication and characterization of this material can be found elsewhere.[19,20] Its basic properties are dielectric constant (1 kHz) $\varepsilon_r=1566$, Curie temperature $T_C=256$ °C; piezoelectric strain constants $d_{33}=497$ pm/V, planar coupling factor $k_p=0.60$, mechanical quality factor $Q_m=54$, and coercive field (10 Hz) $E_c=10$ kV/cm. The dynamic hysteresis (P-E) loops were characterized at room temperature (25 °C) by using a modified Sawyer–Tower circuit with f covering from 2 to 100 Hz and E_0 from 0 to 9.6 kV/cm. The electric field was applied to a sample by a high voltage ac amplifier (Trek

[a]Author to whom correspondence should be addressed, Electronic mail: rattikornyimnirun@yahoo.com.

 © 2008 American Institute of Physics

Author complimentary copy. Redistribution subject to AIP license or copyright, see http://jap.aip.org/jap/copyright.jsp

610D) with the input sinusoidal signal from a function generator (HP 3310A). The *P-E* loops were recorded by a digital oscilloscope (HP 54645A, 100 MHz). The detailed descriptions of this system were explained elsewhere.[25] Effects of the external stress on the dynamic hysteresis were investigated with the compressometer, which was developed for simultaneous applications of the mechanical stress and the electric field.[26] The compressive stress, applied parallel to the electric field direction, was supplied by the servohydraulic load frame and monitored with the pressure gauge. The *P-E* loops were recorded as a function of mechanical stress applied discretely between 0 and 168 MPa for each applied field and frequency. At each constant stress, the loop was obtained after 20 sampling cycles to average out the noise deformation.

III. RESULTS AND DISCUSSION

The hysteresis profiles for various frequencies f, field amplitude E_0, and stress σ are obtained. The hysteresis loops at different f but fixed E_0 (9.6 kV/cm) and σ (27 MPa), at different E_0 but fixed f (10 Hz) and σ (27 MPa), and at different σ but fixed E_0 (9.6 kV/cm) and f (10 Hz) are shown in Figs. 1(a)–1(c), respectively. For a particular applied stress, as expected, the dependence of the loop pattern and area $\langle A \rangle$ on f and E is remarkable. At fixed E_0, the loop area $\langle A \rangle$ and remnant polarization (P_r) decrease with an increase in frequency, as shown in Fig. 1(a). The dependence of the hysteresis loop on E_0 is depicted in Fig. 1(b). Similar observations have also been reported in soft and hard PZT ceramics.[27–29] In addition, the *P-E* loop area $\langle A \rangle$ is found to decrease steadily with increasing stress. Several previous investigations also reported similar stress-dependent behavior.[24–26]

To obtain the suitable scaling relation for the bulk ceramic, one can first follow the suggested scaling law given in Eq. (1) to determine exponents m and n directly from the experimental data. By plotting $\langle A \rangle$ against f at fixed E_0, one obtains the exponent m. On the other hand, the exponent n can be obtained from plotting $\langle A \rangle$ against E_0 at fixed f. As plotted in Fig. 2, it is revealed that the experimental data can be fitted (with $R^2=0.99$), within the measured uncertainty, by

$$\langle A \rangle \propto f^{-0.34} E_0^{3.68}. \quad (2)$$

Here, the first interesting observation is that the minor-loop scaling in 0.5PZT–0.5PZN bulk ceramics is generally similar to that of PZT thin film,[5,9] as well as that of minor loop of PZT bulk ceramics.[13,15] As explained in our previous investigation,[13] this was attributed to the fact that main polarization orientation mechanism in thin films and in subcoercive field condition for bulk ceramics is likely from the 180° domain reversal.[30–34] This explains why the scaling behavior of PZT bulk ceramics at low electric fields is similar to that of thin films. More importantly, the scaling relation obtained in Eq. (2) is generally very similar to that of the minor-loop scaling relations obtained earlier for commercial soft and hard PZT bulk ceramics with $\langle A \rangle \propto f^{-0.33} E_0^3$ and $\langle A \rangle \propto f^{-0.43} E_0^{3.19}$, respectively.[13,15] This clearly indicates that the polarization orientation process in rhombohedral

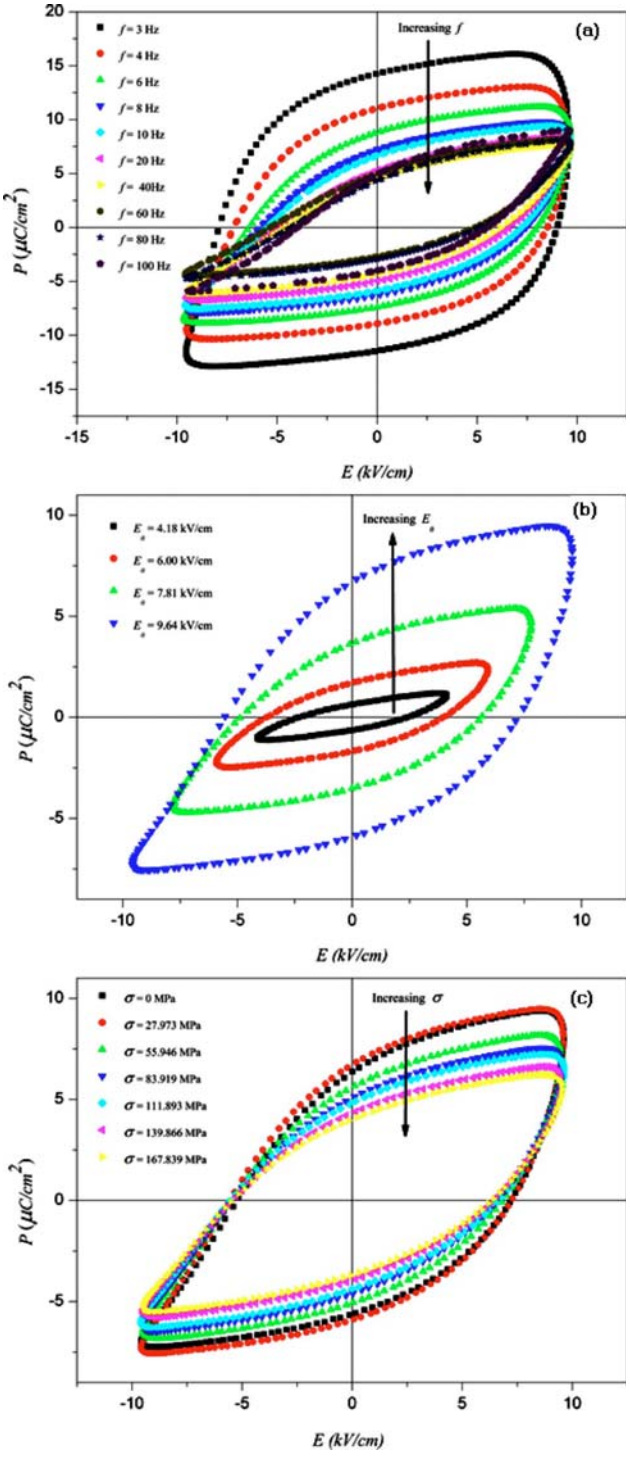

FIG. 1. (Color online) Hysteresis loops under subcoercive field condition for 0.5PZT–0.5PZN ceramic (a) at various f, $E_0=9.6$ kV/cm, and $\sigma=27$ MPa; (b) at various E_0, $f=10$ Hz and $\sigma=27$ MPa; and (c) at various σ, $f=10$ Hz, and $E_0=9.6$ kV/cm.

0.5PZT–0.5PZN ceramics with disrupted domains is similar to that in commercial PZT bulk ceramics with the same complex domain structures Therefore, the scaling relations obtained here clearly support our previous proposed hypothesis that the domain structures play major role in controlling dynamic hysteresis behavior of ferroelectric materials.[13,15]

To investigate the scaling behavior under the effect of

Author complimentary copy. Redistribution subject to AIP license or copyright, see http://jap.aip.org/jap/copyright.jsp

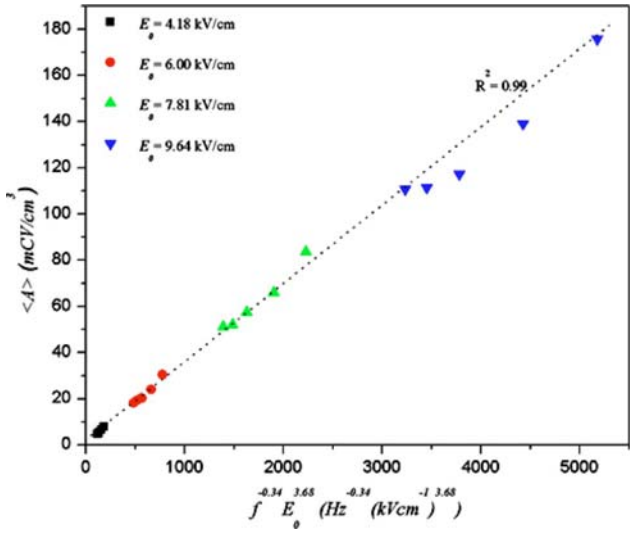

FIG. 2. (Color online) Scaling of hysteresis area $\langle A\rangle$ against $f^{-0.34}E_0^{3.68}$ for 0.5PZT–0.5PZN ceramic under subcoercive field condition.

applied stresses, instead of including only the field amplitude E_0 and the frequency term f, the scaling relation should also include the stress (σ) term, i.e.,

$$\langle A\rangle \propto f^m E_0^n \sigma^p. \tag{3}$$

However, due to increasing number of exponents, to simplify the problem, the validity of the scaling law $\langle A\rangle(\sigma) \propto f^{-0.34}E_0^{3.68}$ is assumed for all applied stresses. Consequently, the area $\langle A\rangle$ for each stress is plotted against $f^{-0.34}E_0^{3.68}$, as shown in Fig. 3(a), and it can be seen from the least–squares linear fits that reasonably good linear relations can be found. As a result, the condition of universality having $m=-0.34$ and $n=3.68$ in 0.5PZT–0.5PZN bulk ceramic is confirmed. Consequently, $\langle A\rangle \propto (a+b\sigma^c)f^{-0.34}E_0^{3.68}$ may be written and by substituting the fitted parameters, it is found that

$$\langle A\rangle - \langle A_{\sigma=0}\rangle = \langle A - A_{\sigma=0}\rangle \propto f^{-0.34}E_0^{3.68}\sigma^{0.35}, \tag{4}$$

where $\langle A_{\sigma=0}\rangle$ refers to stress–free hysteresis area which will be a dominant term for zero stress. The data collapsing of the scaling area from all f, E_0, and σ was found to confirm Eq. (4) as evident in Fig. 3(b). Note that from the appearance of stress σ, $\langle A-A_{\sigma=0}\rangle$, referring to the difference in energy dissipation between under stress and stress–free conditions, increases with increasing stress suggesting a decay of $\langle A\rangle$ with σ at a rate of $\sigma^{0.35}$ as observed in experiments. As a result, it can be concluded that the difference of the hysteresis area between under stress and stress-free condition scales with frequency, field amplitude and stress via exponents $m=-0.34$, $n=3.68$, and $p=0.35$. However, at a particular fixed stress, Eq. (4) gives $f^{-0.34}E_0^{3.68}$ which is the original form for how the area scales with the frequency and the field amplitude.

To understand the stress-dependent scaling relation obtained in Eq. (4), at least qualitatively, one needs to consider the following statements. Since the *P-E* loop area indicates the polarization dissipation energy subjected to one full cycle of electric field application, the loop area is therefore directly

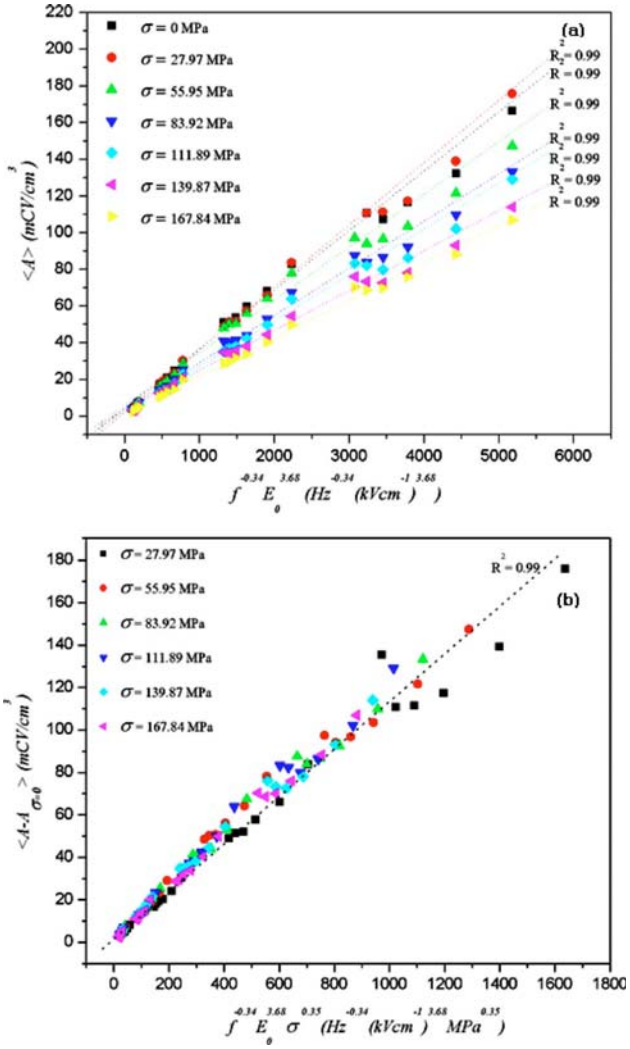

FIG. 3. (Color online) (a) Scaling of hysteresis area $\langle A\rangle$ against $f^{-0.34}E_0^{3.68}$ at various σ. (b) The collapse of the scaling area $\langle A-A_{\sigma=0}\rangle$ against $f^{-0.34}E_0^{3.68}\sigma^{0.35}$ on a same linear line (with small fluctuation) for 0.5PZT–0.5PZN ceramic under subcoercive field condition.

related to volume involved in the switching process during the application of electric field.[25,26,35] Hence, when the mechanical stress is applied, more and more ferroelectric domains are constrained by the applied stress and cannot be reoriented by the electric field so as to participate in the polarization reversal. Consequently, both the saturation and remnant polarizations become lower with increasing compressive stress. The polarization dissipation energy is consequently found to decrease with increasing applied stress, indicating that the sample volume contributing to polarization reversal decreases with increasing stress. Similar observations have also been reported in other investigations.[22–26,36,37] Furthermore, it is noted that this stress-dependent scaling relation, in particular the stress term with exponent $p=0.35$, is slightly different, but still in the same range, from that for soft and hard PZT bulk ceramics with $p=0.44$ and 0.37, respectively, as obtained in our previous investigations.[14,15] An explanation for the difference is not clearly known but could be attributed to the difference in mechanical properties of these materials. Unfortunately, there have been no other

Author complimentary copy. Redistribution subject to AIP license or copyright, see http://jap.aip.org/jap/copyright.jsp

stress-dependent scaling investigations available for independent comparison. In addition, there has been no quantitative theoretical treatment to include the stress term in the scaling relation. Many of the theoretical treatments to explain the stress effect on the hysteresis behavior have been primarily based on constitutive models, thermodynamic phenomenology, and Rayleigh law approach.[38–40] Further investigations, both theoretical and experimental, on the stress-dependent scaling behavior are clearly required.

IV. CONCLUSION

The scaling behavior of the subcoercive field dynamic ferroelectric hysteresis of rhombohedral 0.5PZT–0.5PZN bulk ceramics under the effect of mechanical stress has been investigated. The scaling relation for the minor loops takes the form of $\langle A - A_{\sigma=0} \rangle \propto f^{-0.34} E_0^{3.68} \sigma^{0.35}$, which is very similar to that of soft and hard PZT ceramics with the same disrupted domains. As a result, this study suggests that the domain structures play a significant role in controlling the dynamic hysteresis behavior of ferroelectric materials.

ACKNOWLEDGMENTS

Financial supports from the Thailand Research Fund (TRF), Commission on Higher Education (CHE), Royal Golden Jubilee PhD. Program, Faculty of Science and Graduate School of Chiang Mai University are gratefully acknowledged.

[1] K. Uchino, *Ferroelectric Devices* (Dekker, New York, 2000).
[2] O. Auciello, J. F. Scott, and R. Ramesh, Phys. Today **51**, 22 (1998).
[3] M. Rao, H. R. Krishnamurthy, and R. Pandit, Phys. Rev. B **42**, 856 (1990).
[4] M. Acharyya and B. K. Chakrabarti, Phys. Rev. B **52**, 6550 (1995).
[5] J.-M. Liu, H. L. W. Chan, C. L. Choy, Y. Y. Zhu, S. N. Zhu, Z. G. Liu, and N. B. Ming, Appl. Phys. Lett. **79**, 236 (2001).
[6] H. B. Zuo, M. F. Zhang, J. C. Han, and J. M. Liu, Mater. Lett. **61**, 2697 (2007).
[7] M. Sarjala, E. T. Seppälä, and M. J. Alava, Physica B **403**, 418 (2008).
[8] M. Rao and R. Pandit, Phys. Rev. B **43**, 3373 (1991).
[9] J.-M. Liu, H. L. W. Chan, C. L. Choy, and C. K. Ong, Phys. Rev. B **65**, 014416 (2001).
[10] B. Pan, H. Yu, D. Wu, X. H. Zhou, and J.-M. Liu, Appl. Phys. Lett. **83**, 1406 (2003).
[11] Y.-H. Kim and J.-J. Kim, Phys. Rev. B **55**, R11933 (1997).
[12] J.-H. Park, C.-S. Kim, B.-C. Choi, B. K. Moon, J. H. Jeong, and I. W. Kim, Appl. Phys. Lett. **83**, 536 (2003).
[13] R. Yimnirun, Y. Laosiritaworn, S. Wongsaenmai, and S. Ananta, Appl. Phys. Lett. **89**, 162901 (2006).
[14] R. Yimnirun, S. Wongsaenmai, S. Ananta, and Y. Laosiritaworn, Appl. Phys. Lett. **89**, 242901 (2006).
[15] R. Yimnirun, R. Wongmaneerung, S. Wongsaenmai, A. Ngamjarurojana, S. Ananta, and Y. Laosiritaworn, Appl. Phys. Lett. **90**, 112908 (2007).
[16] R. Yimnirun, R. Wongmaneerung, S. Wongsaenmai, A. Ngamjarurojana, S. Ananta, and Y. Laosiritaworn, Appl. Phys. Lett. **90**, 112906 (2007).
[17] K. Uchino, *Piezoelectric Actuators and Ultrasonic Motors* (Kluwer, Boston, 1997).
[18] J. Zhao, A. E. Glazounov, and Q. M. Zhang, Appl. Phys. Lett. **74**, 436 (1999).
[19] D. Viehland and J. Powers, J. Appl. Phys. **89**, 1820 (2001).
[20] D. Zhou, M. Kamlah, and D. Munz, J. Eur. Ceram. Soc. **25**, 425 (2005).
[21] R. Yimnirun, Y. Laosiritaworn, and S. Wongsaenmai, J. Phys. D **39**, 759 (2006).
[22] R. Yimnirun, S. Ananta, A. Ngamjarurojana, and S. Wongsaenmai, Appl. Phys. A: Mater. Sci. Process. **81**, 1227 (2005).
[23] X. P. Jiang, J. W. Fang, H. R. Zeng, B. J. Chu, G. R. Li, D. R. Chen, and Q. R. Yin, Mater. Lett. **44**, 219 (2000).
[24] H. Fan and H. E. Kim, J. Appl. Phys. **91**, 317 (2002).
[25] N. Vittayakorn, G. Rujijanagul, T. Tunkasiri, X. Tan, and D. P. Cann, J. Mater. Res. **18**, 2882 (2003).
[26] N. Vittayakorn, G. Rujijanagul, X. Tan, and D. P. Cann, J. Electroceram. **16**, 141 (2006).
[27] D. A. Hall and P. J. Stevenson, Ferroelectrics **228**, 139 (1999).
[28] J. E. Garcia, R. Perez, and A. Albareda, J. Phys. D **34**, 3279 (2001).
[29] M. Morozov, D. Damjanovic, and N. Setter, J. Eur. Ceram. Soc. **25**, 2483 (2005).
[30] S. Trolier-McKinstry, N. B. Gharb, and D. Damjanovic, Appl. Phys. Lett. **88**, 202901 (2006).
[31] B.-K. Lai, I. Ponomareva, I. I. Naumov, I. Kornev, H. Fu, L. Bellaiche, and G. S. Salamo, Phys. Rev. Lett. **96**, 137602 (2006).
[32] D. Ricinschi and M. Okuyama, Ferroelectrics **349**, 111 (2007).
[33] T. Tsurumi, T. Sasaki, H. Kakemoto, T. Harigai, and S. Wada, Jpn. J. Appl. Phys., Part 1 **43**, 7618 (2004).
[34] K. Lee and S. Baik, Annu. Rev. Mater. Res. **36**, 81 (2006).
[35] M. E. Lines and A. M. Glass, *Principles and Applications of Ferroelectrics and Related Materials* (Clarendon, Oxford, 1977).
[36] T. Kumazawa, Y. Kumagai, H. Miura, M. Kitano, and K. Kushida, Appl. Phys. Lett. **72**, 608 (1998).
[37] X. Lu, J. Zhu, X. Li, Z. Zhang, X. Zhu, D. Wu, F. Yan, Y. Ding, and Y. Wang, Appl. Phys. Lett. **76**, 3103 (2000).
[38] D. Damjanovic, J. Appl. Phys. **82**, 1788 (1997).
[39] C. M. Landis Curr. Opin. Solid. Solid Mater. Sci. **8**, 59 (2004).
[40] A. Achuthan and C. T. Sun, J. Appl. Phys. **97**, 114103 (2005).

Author complimentary copy. Redistribution subject to AIP license or copyright, see http://jap.aip.org/jap/copyright.jsp

Changes in dielectric and ferroelectric properties of Fe^{3+}/Nb^{5+} hybrid-doped barium titanate ceramics under compressive stress

M. Unruan, T. Sareein, J. Tangsritrakul, S. Prasertpalichatr, A. Ngamjarurojana, S. Ananta, and R. Yimnirun[a)]
Department of Physics, Faculty of Science, Chiang Mai University, Chiang Mai, 50200, Thailand

(Received 29 October 2008; accepted 3 November 2008; published online 16 December 2008)

The influences of compressive stress on the dielectric and ferroelectric properties of Fe^{3+}/Nb^{5+} hybrid-doped barium titanate ($BaTiO_3$) ceramics were investigated. Superimposed compressive stress had a pronounced effect on the electrical properties of the ceramics. The response of low-field dielectric properties to stress changed from soft to hard piezoelectric behavior with increasing Nb^{5+} content. While ferroelectric properties decreased with stress, hardening behavior was observed with increasing Nb^{5+} content in hybrid-doped $BaTiO_3$ ceramics. A mechanism based on induced change in the acceptor valence by the donor dopant in hybrid-doped $BaTiO_3$ ceramics was proposed to explain the results obtained. © *2008 American Institute of Physics*. [DOI: 10.1063/1.3042228]

Barium titanate [$BaTiO_3$ (BT)] based materials are well known electroceramics that find applications as dielectric materials in capacitors.[1–4] Historically BT was the first polycrystalline piezoelectric; but it was soon replaced by $Pb(Zr,Ti)O_3$ (PZT) ceramic because the latter has much better piezoelectric properties. Since then, PZT has dominated piezoelectric applications to date. However, PZT is now facing a major challenge due to the environmental hazard from its toxic lead.[5,6] Recently BT has regained a great deal of interest due to the introduction of the large recoverable electrostrain in doped BT-based materials.[7–14] The mechanism to explain this behavior is based on the universal "symmetry-conforming principle" of point defects.[7–11] This provides a way to produce high-performance, lead-free piezoelectrics based on BT. Since then, doped BT systems, especially Mn-doped $(Ba,Sr)TiO_3$, have been investigated extensively.[10–12] Interestingly, acceptor/donor-doped BT (the so-called hybrid-doped BT) systems, such as Mn^{3+}/La^{3+}-doped BT and Mn^{3+}/Nb^{5+}-doped BT, also show the same large electrostrain behavior.[13,14] This is of particular interest, as opposite electrical properties, including ferroelectric aging effects, can be expected between acceptor-doped and donor-doped ferroelectrics. It should also be noticed that the acceptor dopant employed in the previous hybrid-doped BT investigations mentioned above was always the Mn^{3+} cation, without any particular reason given. Therefore, one might wonder if the same behavior is realizable in hybrid-doped BT using other acceptor dopants. Our recent investigation showed that dielectric and ferroelectric aging behaviors in Fe^{3+}/Nb^{5+} hybrid-doped BT ceramics differed noticeably from those observed in Mn^{3+}-based hybrid-doped BT systems. Nonetheless, the opposing roles of the acceptor and donor dopants on electrical properties were still observed. Most importantly, the potential of high-performance, lead-free piezoelectrics based on BT was confirmed in Fe^{3+}/Nb^{5+}-doped BT ceramics.

However, when used in piezoelectric devices, ceramics are often subjected to self-induced or environmental stresses.[15,16] A prior knowledge of the effects of stresses on the material properties is crucial for proper design of a device and for suitable selection of materials for a specific application.[17,18] Therefore, it is very important to obtain experimental data in order to understand how these materials behave under stress.[19–21] Recently, the compressive-stress dependence of electrical properties has been studied in various materials.[19–26] The results clearly showed that the effects of applied stress on electrical properties depended significantly on ceramic compositions and stress levels. Although there have been many previous reports on the electrical properties of hybrid-doped BT ceramics, the influences of applied stress on the electrical properties of hybrid-doped BT ceramics are yet to be reported. Therefore, it is the aim of this study to determine the dielectric and ferroelectric properties of the Fe^{3+}/Nb^{5+} hybrid-doped BT ceramics as a function of compressive stress. This paper will reveal the opposing and competing dielectric responses to applied stress of acceptor-dominant and donor-dominant hybrid-doped BT ceramics. More interestingly, it will also be shown that while Fe^{3+} and Nb^{5+} normally act as acceptor and donor, respectively, when added individually in BT system, the added Nb^{5+} could enhance the hardening effect in hybrid-doped BT ceramics.

In this study, a series of Fe^{3+} and Nb^{5+} hybrid-doped BT ceramics with Fe^{3+} fixed at 1 mol %, but with Nb^{5+} varying from 0.5 to 1.5 mol %, were prepared via a mixed-oxide method with a formula $Ba(Ti_{0.99-x}Fe_{0.01}Nb_x)O_3$ when $x=0.005$, 0.01, and 0.015 (abbreviated as BT−1Fe−yNb with $y=100x$ hereafter). Hence, samples of acceptor-dominant $y=0.5$, equal-doping $y=1$, and donor-dominant $y=1.5$ were obtained. It should be noted that x-ray diffraction analysis showed all sintered ceramics to be single-phase perovskite materials with tetragonal symmetry. Since this paper only deals with the stress dependence study, detailed investigations of temperature- and frequency-dependent dielectric and ferroelectric properties will be presented in another publication. Room temperature (25 °C) dielectric properties and ferroelectric hysteresis loops were measured using a home-

a)Author to whom correspondence should be addressed. Electronic mail: rattikornyimnirun@yahoo.com.

 © 2008 American Institute of Physics

Downloaded 16 Dec 2008 to 202.28.27.3. Redistribution subject to AIP license or copyright; see http://jap.aip.org/jap/copyright.jsp

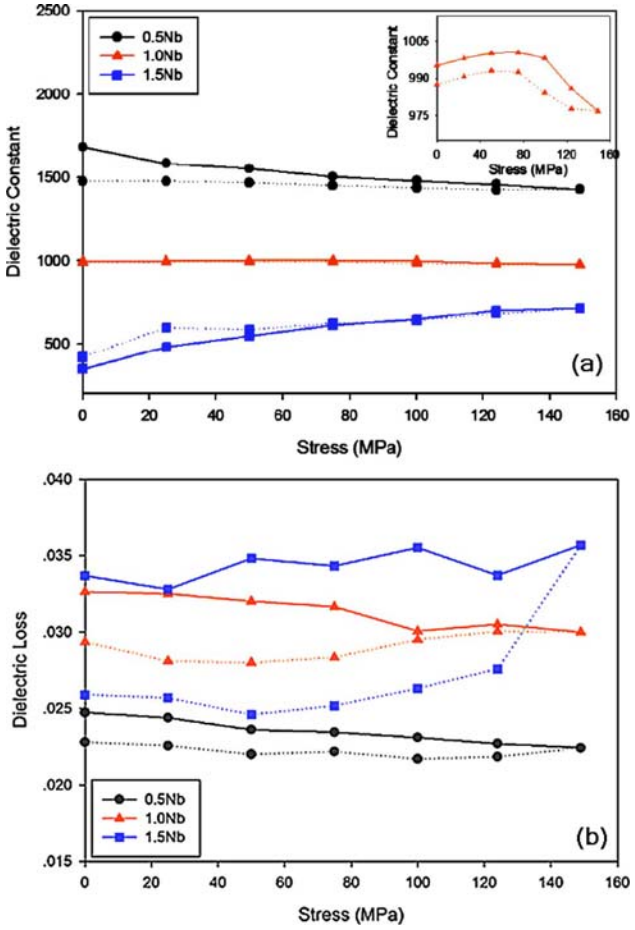

FIG. 1. (Color online) (a) Changes in dielectric constant (ε_r) and (b) changes in dielectric loss tangent (tan δ) with compressive stress applied parallel to the electric field direction for $Ba(Ti_{0.99-x}Fe_{0.01}Nb_x)O_3$ ceramics when $x=0.005$ (0.5 Nb), 0.01 (1.0 Nb), and 0.015 (1.5 Nb) (measured at 25 °C and 10 kHz).

built compressometer developed for simultaneous applications of mechanical stress and electric field.[22,24] Low-field dielectric properties were measured by a *LCR*-meter (Instek LCR-821) with applied voltage of 1 V. The dielectric constant and loss were determined at a frequency of 10 kHz. The ferroelectric (*P-E*) hysteresis loops were characterized using a modified Sawyer–Tower circuit with a fixed 50 Hz frequency and E_0 of 15 kV/cm. The electric field was applied to a sample by a high-voltage ac amplifier (Trek 610D) with the input sinusoidal signal from a function generator (HP 3310A). The *P-E* loops were recorded by a digital oscilloscope (HP 54645A, 100 MHz). Prior to all measurements, the samples were "deaged" by holding at 250 °C for 30 min, followed by a quick cooling to room temperature.

The room temperature dielectric properties at 10 kHz of $Ba(Ti_{0.99-x}Fe_{0.01}Nb_x)O_3$ ceramics as a function of compressive stress are depicted in Fig. 1. The measurements were performed with mechanical stress increased to the maximum (solid lines), and then gradually removed to zero (dotted lines). Generally, the results showed only slightly different dielectric properties between loading and unloading conditions; this differs from results previously observed in other ceramic systems and is likely caused by the stress-induced depoling mechanism at high stress.[25–28] Nonetheless, there are observable changes in both the dielectric constant and the dielectric loss tangent with stress. The different dielectric responses to the applied stress are clearly evident. For the acceptor-dominant BT–1Fe–0.5Nb composition, both the dielectric constant and dielectric loss tangent decrease with increasing stress. On the other hand, the trend is reversed in the donor-dominant BT–1Fe–1.5Nb composition. Interestingly, for the equal-doping BT–1Fe–1Nb composition the dielectric properties (both dielectric constant and dielectric loss tangent) show very little change with stress. However, when taking a closer look [inset of Fig. 1(a)] one can see that the dielectric constant first increases when the stress is increased to 80 MPa, then decreases when the applied stress is increased further. Similar behavior is also noticeable in the dielectric loss tangent, as shown in Fig. 1(b). The changes in dielectric properties under compressive stress obtained in this study are in part similar to those for BT, PZT, and lead magnesium niobate-lead titanate (PMN-PT) systems, as seen in earlier investigations.[22,24,25,27,29] Under applied compressive stress, the domain structure of ceramics may undergo domain reorientation through non-180° domain walls, as well as stress-induced depinning of the domain walls. Hence, an increase in dielectric properties is observed in the BT–1Fe–1.5Nb composition (similar behavior was observed in hard Fe-doped PZT).[23,25,27,28] On the other hand, stress clamping of domain walls, which results in a decrease in domain wall mobility, is expected to play a role in the decrease in dielectric properties in the BT–1Fe–0.5Nb composition (as reported in soft La-doped PZT).[23,25] The competing influences of domain reorientation and stress clamping of domain wall mechanisms are believed to be a reason for the change in dielectric properties under stress in the BT–1Fe–1Nb composition (mixing behaviors of hard and soft materials). The possible reason for the hardening effect with increasing donor content in hybrid-doped BT ceramic will be discussed later.

The polarization versus electric field (*P-E*) hysteresis loops of $Ba(Ti_{0.99-x}Fe_{0.01}Nb_x)O_3$ ceramics under different compressive stresses are shown in Fig. 2. It should first be noticed that generally the area of the *P-E* loops decreases with increasing compressive stress. The changes follow a similar trend for all ceramic compositions. The *P-E* loop area indicates the polarization dissipation energy of a ferroelectric material under one full cycle of electric field application.[20,30] This amount of energy loss is directly related to the amount of domain participating in the switching process during the application of the electric field.[20,25] For a given composition, the decrease in the loop area with increasing compressive stress is a result of stress-induced domain wall suppression.[30] The changes in hysteresis parameters, i.e., dissipation energy, saturation polarization (P_{sat}), remnant polarization (P_r), and coercive field (E_c), with compressive stresses are plotted in Fig. 3. Generally, it can be seen that all hysteresis parameters decrease as compressive stress increases. As is also depicted in Fig. 3, it should be noted that even though the loading and unloading experiments were performed on all compositions, the results differ only slightly (similar to the changes in low-field dielectric properties). In addition, only slight decreases in the polariza-

Downloaded 16 Dec 2008 to 202.28.27.3. Redistribution subject to AIP license or copyright; see http://jap.aip.org/jap/copyright.jsp

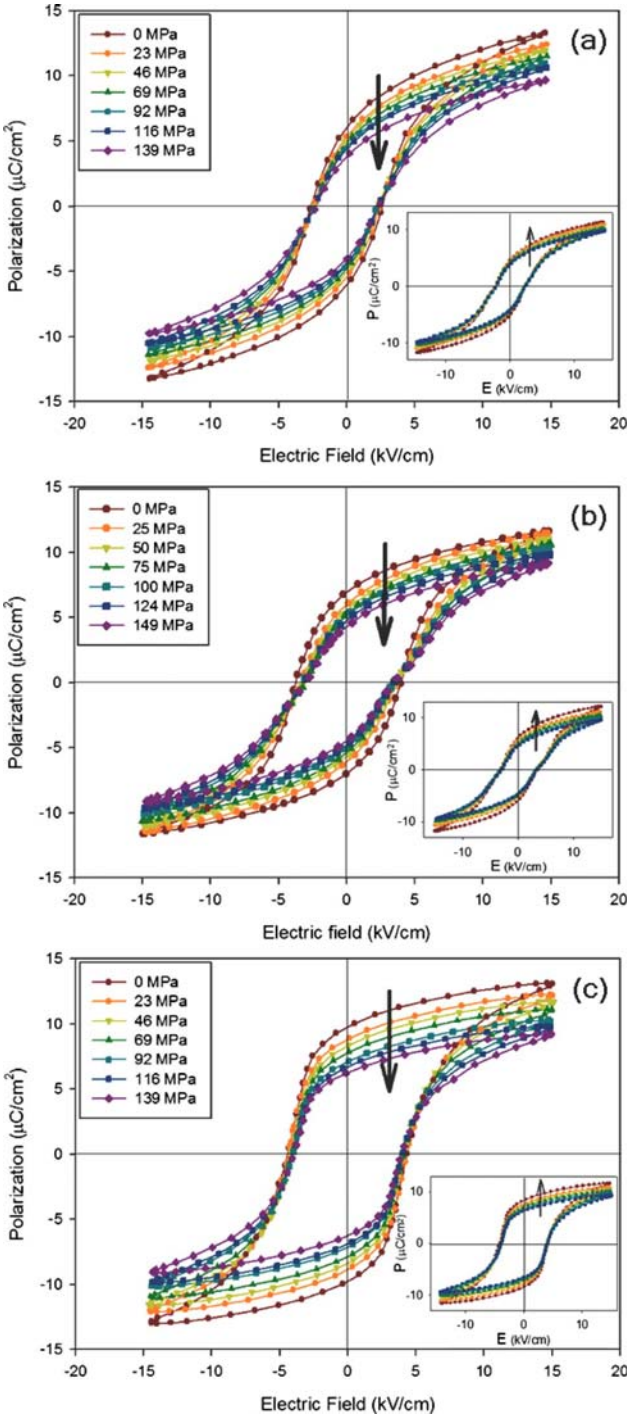

FIG. 2. (Color online) Polarization-electric field (P-E) hysteresis loops as a function of compressive stress for (a) $Ba(Ti_{0.985}Fe_{0.01}Nb_{0.005})O_3$, (b) $Ba(Ti_{0.98}Fe_{0.01}Nb_{0.01})O_3$, and (c) $Ba(Ti_{0.978}Fe_{0.01}Nb_{0.015})O_3$ ceramics (measured at 25 °C and 50 Hz under loading). The inset in each figure indicates the P-E loops during unloading.

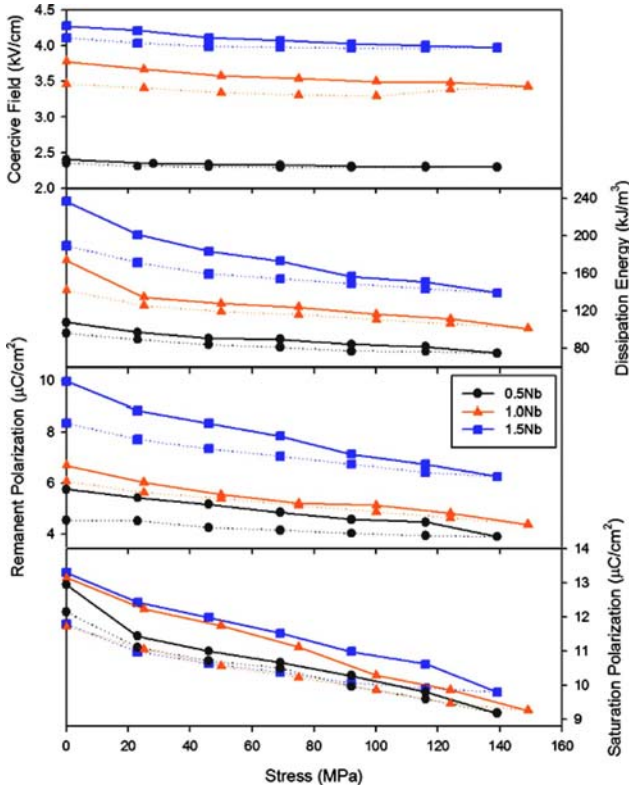

FIG. 3. (Color online) Changes in ferroelectric hysteresis parameters with compressive stress for $Ba(Ti_{0.99-x}Fe_{0.01}Nb_x)O_3$ ceramics when $x=0.005$ (0.5 Nb), 0.01 (1.0 Nb), and 0.015 (1.5 Nb) during stress loading (solid lines) and unloading (dotted lines) (measured at 25 °C and 50 Hz).

tion values of all the ceramics are also observed after a complete cycle of mechanical stress. This observation suggests a stress-induced decrease in the switchable part of the polarization at high stress levels.[23,25] The results of changes in the hysteresis parameters of $Ba(Ti_{0.99-x}Fe_{0.01}Nb_x)O_3$ ceramics with increasing compressive stress are in agreement with previous investigations of many ferroelectric ceramics.[18–20,24,26,29] To understand the experimental results of the changes in ferroelectric properties under compressive stress, as depicted in Fig. 3, one can interpret the changes in terms of domain-reorientation processes. When compressive stress is applied in a direction parallel to the electric field, the applied stress tends to keep the ferroelectric domains aligned away from the stress direction, through the non-180° ferroelastic domain switching processes.[27–29] Therefore, it takes a greater than usual applied electric field to reorient the domains along the stress direction, resulting in a lower value of the saturation polarization (P_{sat}). When the electric field is reduced to zero, the domains tend to rotate back away from the applied compressive-stress direction, resulting in lower than usual remnant polarization (P_r) and hence a lower coercive field (E_c) required to bring the remnant polarization to zero.[25,29] Furthermore, the decrease in hysteresis loss with increasing compressive stress indicates that more and more ferroelectric domains are constrained by the applied stress and cannot be reoriented by the electric field so as to participate in the polarization reversal.[25,29] Consequently, both the saturation and remnant polarizations become lower with increasing compressive stress.

Another important and even more interesting finding is that $Ba(Ti_{0.99-x}Fe_{0.01}Nb_x)O_3$ ceramics become ferroelectrically harder with increasing donor (Nb) concentration, as seen from the low-field dielectric behavior in Fig. 1; and there is also more dissipation loss, larger coercivity, and lower polarization, as seen in Figs. 2 and 3. This is unexpected, as Nb is well known as a softening dopant in donor-monodoped BT and $Pb(Zr,Ti)O_3$ ceramics.[1–3,26,30] One

Downloaded 16 Dec 2008 to 202.28.27.3. Redistribution subject to AIP license or copyright; see http://jap.aip.org/jap/copyright.jsp

would wonder about the probable cause of this unexpected behavior. For equal-doped BT–1Fe–1Nb compositions, there are two possible microscopic distributions of Fe^{3+} and Nb^{5+} dopants.[13,14] The first is that Fe^{3+} and Nb^{5+} form Fe^{3+}–Nb^{5+} pairs. In this case, the average *B*-site valence at the defect pair is 4+, which is the same as the host *B*-site Ti^{4+}. Thus, charge neutrality is kept at the defect pairs, and therefore no vacancy is formed.[13] If this was the case, we would not observe the mixed response to applied stress of the low-field dielectric properties; while the acceptor-dominant BT–1Fe–0.5Nb composition and the donor-dominant BT–1Fe–1.5Nb composition would behave like hard and soft materials, respectively. However this is not the case at all, as shown in our experimental results in Figs. 1 and 2. To understand this peculiar behavior in a hybrid-doped BT ceramic, we need to first analyze its possible defect structure. The common point of view states that donor doping creates *A*-site vacancies (V''_{Ba}), while acceptor doping causes oxygen vacancies ($V_O^{\bullet\bullet}$) for charge compensation.[1–3,30–32] In contrast to the formation of Fe^{3+}–Nb^{5+} pairs, it is possible that Fe^{3+} and Nb^{5+} are distributed in the *B*-site sublattices and are allowed to be apart from each other.[13,14] As their concentration is very low, the chance of forming pairs is thus very low. By assuming this random distribution, one can expect the formation of immobile defect dipoles $2Nb^{\bullet}_{Ti}$–V''_{Ba} and mobile defect dipoles $2Fe'_{Ti}$–$V_O^{\bullet\bullet}$ in their respective *B*-site sublattices,[13,14] which in turn cause the separated soft and hard properties in the *B*-site sublattices. In addition to these assumptions, it is important to point out one possible mechanism which is likely responsible for the observed peculiar hardening effect with increasing donor (Nb) concentration in the hybrid-doped BT ceramics. Previous investigations by Albertsen *et al.*[33] and Kishi *et al.*[34,35] on donor-acceptor charge complex formation in BT ceramics have suggested that an acceptor with lower valence state (in this case Fe^{2+}, as opposed to Fe^{3+}) is more stable in acceptor-donor doped BT ceramics. The consequence of the (partial) change in acceptor valence from Fe^{3+} to Fe^{2+} is the (partial) formation of electrically stronger (based on electrostatic Coulombic interaction) Fe''_{Ti}–$V_O^{\bullet\bullet}$ defect dipoles. In comparison with the equal-doping BT–1Fe–1Nb composition, a higher concentration of Fe''_{Ti}–$V_O^{\bullet\bullet}$ defect dipoles can be expected with the addition of Nb^{5+}, i.e., the BT–1Fe–1.5Nb composition. Hence, hardening effects are observed with decreased low-field dielectric properties (and increased dielectric properties with applied compressive stress, as observed in hard PZT ceramics), and increased dissipation loss and coercivity. On the other hand, with the lower Nb^{5+} content in the BT–1Fe–0.5Nb composition, a relatively lower concentration of Fe''_{Ti}–$V_O^{\bullet\bullet}$ defect dipoles is expected; hence the ceramic is, by comparison, softer, with higher low-field dielectric properties (and lowered dielectric properties with applied compressive stress, as observed in soft PZT ceramics) and lower dissipation loss and coercivity, as clearly shown in Figs. 1–3.

In summary, the influences of compressive stress on the dielectric and ferroelectric properties of Fe^{3+}/Nb^{5+} hybrid-doped BT ceramics are investigated. The superimposed compressive stress shows pronounced influences on the electrical properties of the ceramics. The response of the low-field dielectric properties to stress changes from soft to hard piezoelectric behavior with increasing Nb^{5+} content. While ferroelectric properties decrease with stress, hardening behavior is observed with increasing Nb^{5+} content in the hybrid-doped BT ceramics. A mechanism based on the induced change in the acceptor valence by the donor dopant in hybrid-doped BT ceramics is proposed to explain the results obtained.

This work was jointly supported by the Thailand Research Fund (TRF), the Commission on Higher Education (CHE), the Royal Golden Jubilee Ph.D. Program, and the Faculty of Science and the Graduate School of Chiang Mai University.

[1] B. Jaffe, W. R. Cook, and H. Jaffe, *Piezoelectric Ceramics* (Academic, New York, 1971).
[2] Y. H. Xu, *Ferroelectric Materials and Their Applications* (North Holland, Los Angeles, 1991).
[3] A. J. Moulson and J. M. Herbert, *Electroceramics: Materials, Properties, Applications* (Wiley, Chichester, 2003).
[4] K. Uchino, *Ferroelectric Devices* (Dekker, New York, 2000).
[5] C. Ang, Z. Yu, Z. Jing, R. Y. Guo, A. S. Bhalla, and L. E. Cross, Appl. Phys. Lett. **80**, 3424 (2002).
[6] Y. M. Chiang, G. W. Farrey, and N. A. Soukhojak, Appl. Phys. Lett. **73**, 3683 (1998).
[7] X. Ren and K. Otsuka, Phys. Rev. Lett. **85**, 1016 (2000).
[8] X. Ren, Nature Mater. **3**, 91 (2004).
[9] L. X. Zhang, W. Chen, and X. Ren, Appl. Phys. Lett. **85**, 5658 (2004).
[10] L. X. Zhang and X. Ren, Phys. Rev. B **71**, 174108 (2005).
[11] L. X. Zhang and X. Ren, Mater. Sci. Eng., A **438–440**, 354 (2006).
[12] M. M. Ahmad, K. Yamada, P. Meuffels, and R. Waser, Appl. Phys. Lett. **90**, 112902 (2007).
[13] W. Liu, W. Chen, L. Yang, Y. Wang, L. X. Zhang, C. Zhou, S. Li, and X. Ren, Mater. Sci. Eng., A **438–440**, 350 (2006).
[14] W. Liu, W. Chen, L. Yang, Y. Wang, L. X. Zhang, C. Zhou, S. Li, and X. Ren, Appl. Phys. Lett. **89**, 172908 (2006).
[15] K. Uchino, *Piezoelectric Actuators and Ultrasonic Motors* (Kluwer Academic, Boston, 1997).
[16] D. Stansfield, *Underwater Electroacoustic Transducers* (Bath University Press, Bath, 1991).
[17] S. Park and T. R. Shrout, J. Appl. Phys. **82**, 1804 (1997).
[18] D. Viehland and J. Powers, Appl. Phys. Lett. **78**, 3112 (2001).
[19] C. S. Lynch, Acta Mater. **44**, 4137 (1996).
[20] D. Zhou, Z. Wang, and M. Kamlah, J. Appl. Phys. **97**, 084105 (2005).
[21] G. Yang, Z. Yue, T. Sun, H. Gou, and L. Li, J. Phys. D **41**, 045307 (2008).
[22] W. Chaisan, R. Yimnirun, and S. Ananta, Phys. Scr., T **T129**, 205 (2007).
[23] D. Damjanovic, J. Appl. Phys. **82**, 1788 (1997).
[24] R. Yimnirun, M. Unruan, Y. Laosiritaworn, and S. Ananta, J. Phys. D **39**, 3097 (2006).
[25] Q. M. Zhang, J. Zhao, K. Uchino, and J. Zheng, J. Mater. Res. **12**, 226 (1997).
[26] M. Morozov, D. Damjanovic, and N. Setter, J. Eur. Ceram. Soc. **25**, 2483 (2005).
[27] J. Y. Li, R. C. Rogan, E. Ustundag, and K. Bhattacharya, Nature Mater. **4**, 776 (2005).
[28] G. Yang, S. F. Liu, W. Ren, and B. K. Mukherjee, Ferroelectrics **262**, 207 (2001).
[29] R. Yimnirun, Y. Loasiritaworn, and S. Wongsaenmai, J. Phys. D **39**, 759 (2006).
[30] M. E. Lines and A. M. Glass, *Principles and Applications of Ferroelectrics and Related Materials* (Oxford University Press, Oxford, 1977).
[31] S. Pruvost, G. Sebald, L. Lebrun, and D. Guyomar, J. Appl. Phys. **102**, 064104 (2007).
[32] T. Granzow, E. Suvaci, H. Kungl, and M. J. Hoffmann, Appl. Phys. Lett. **89**, 262908 (2006).
[33] K. Albertsen, D. Hennings, and O. Steigelmann, J. Electroceram. **2**, 193 (1998).
[34] H. Kishi, N. Kohzu, Y. Iguchi, J. Sugino, M. Kato, H. Ohsato, and T. Okuda, Jpn. J. Appl. Phys., Part 1 **39**, 5533 (2000).
[35] H. Kishi, N. Kohzu, Y. Iguchi, J. Sugino, M. Kato, H. Ohsato, and T. Okuda, J. Eur. Ceram. Soc. **21**, 1643 (2001).

Downloaded 16 Dec 2008 to 202.28.27.3. Redistribution subject to AIP license or copyright; see http://jap.aip.org/jap/copyright.jsp

Available online at www.sciencedirect.com
ScienceDirect
Current Applied Physics 9 (2009) 249–252
Current Applied Physics
An official journal of the KPS
www.elsevier.com/locate/cap
www.kps.or.kr

Ferroelectric properties of $Pb(Zr_{1/2}Ti_{1/2})O_3$–$Pb(Zn_{1/3}Nb_{2/3})O_3$ ceramics under compressive stress

Rattikorn Yimnirun *, Narit Triamnak, Muangjai Unruan, Athipong Ngamjarurojana, Yongyut Laosiritaworn, Supon Ananta

Department of Physics, Faculty of Science, Chiang Mai University, Chiang Mai 50200, Thailand

Received 25 December 2006; received in revised form 11 February 2008; accepted 12 February 2008
Available online 29 February 2008

Abstract

Effects of compressive stress on the ferroelectric properties of ceramics in PZT–PZN system were investigated. The ceramics with a formula $(1-x)Pb(Zr_{1/2}Ti_{1/2})O_3$–$xPb(Zn_{1/3}Nb_{2/3})O_3$ or $(1-x)$PZT–(x)PZN ($x = 0.1$–0.5) were prepared by a conventional mixed-oxide method. The ferroelectric properties under the compressive stress of the PZT–PZN ceramics were observed at the stress levels up to 170 MPa using a compressometer in conjunction with a modified Sawyer–Tower circuit. It was found that with increasing compressive stress the area of the ferroelectric hysteresis (P–E) loops, the saturation polarization (P_{sat}), the remnant polarization (P_r), and the coercive field (E_c) decreased. These results were interpreted through the non-180° ferroelastic domain switching processes.
© 2008 Elsevier B.V. All rights reserved.

PACS: 77.84.−s; 77.80.Fm; 77.84.Dy; 77.80.−e

Keywords: Ferroelectric properties; PZT–PZN; Stress

1. Introduction

In many practical sensor and actuator applications, piezoelectric and ferroelectric ceramics are often subjected to mechanical loading, either deliberately in the design of the device itself or because the device is used to change shapes as in many smart structure applications or the device is used under environmental stresses such as in underwater transducers [1–3]. A prior knowledge of how the material properties change under different load conditions is therefore very crucial for proper design of a device and for suitable selection of materials for a specific application. Despite the fact, material constants used in many design calculations are often obtained from a stress-free measuring condition, which in turn may lead to incorrect or inappropriate actuator and transducer designs [4,5]. It is therefore important to determine the properties of these materials as a function of applied stress. Previous investigations on the stress-dependent dielectric and electrical properties of many ceramic systems, such as BT, PZT, PMN, PMN–PT, PZT–BT, and PMN–PZT have clearly emphasized the importance of the subject [6–13]. In this paper, the stress dependence of the ferroelectric properties of ceramics in PZT–PZN system is presented.

Recently, there have been a great deal of interest in lead zirconate titanate-lead zinc niobate ($Pb(Zr_{1/2}Ti_{1/2})O_3$–$Pb(Zn_{1/3}Nb_{2/3})O_3$ or PZT–PZN) systems because of their high dielectric, piezoelectric, and ferroelectric properties [14–16]. PZN is a ferroelectric material with frequency dependent dielectric relaxation behavior, as well as diffuse phase transition at 140 °C [17]. A single crystal of PZN shows extremely high dielectric and piezoelectric constants [18]. PZT also has high piezoelectric properties, particularly compositions (Zr:Ti ~ 52:48) close to a morphotropic phase boundary (MPB) between the tetragonal and the rhombohedral phases [19]. Therefore, PZT is the most popular ferroelectric material used in electronic devices

* Corresponding author. Tel.: +66 53 943 367; fax: +66 53 943 445.
E-mail address: rattikornyimnirun@yahoo.com (R. Yimnirun).

1567-1739/$ - see front matter © 2008 Elsevier B.V. All rights reserved.
doi:10.1016/j.cap.2008.02.007

[4,19,20]. As both PZT and PZN possess excellent electrical properties, enhanced properties can thus be expected from ceramics in PZT–PZN system. There have been many previous reports on the electrical properties of PZT–PZN ceramics [14–16]. Earlier report on the stress-dependent dielectric properties of PZT–PZN also showed very interesting results [21]. However, there has been no systematic study on the influence of an applied stress on the ferroelectric properties of the PZT–PZN ceramics. Therefore, it is the aim of this study to determine the ferroelectric properties of the $(1-x)$PZT–(x)PZN ceramics as a function of compressive stress.

2. Experiments and measurements

In this study, $(1-x)Pb(Zr_{1/2}Ti_{1/2})O_3$–$(x)Pb(Zn_{1/3}Nb_{2/3})O_3$ (with $x = 0.1$–0.5) ceramics were prepared from starting PZT and PZN powders by a conventional mixed-oxide method via vibro-milling technique [22]. Perovskite-phase PZN powders were obtained from the columbite method with zinc niobate ($ZnNb_2O_6$) selected as the precursor, while PZT powders were prepared by a simple mixed-oxide method [23]. For optimization purpose, the sintering was carried out at temperatures between 1200 and 1250 °C for 2 h. Details of the processing and characterizations were provided elsewhere [22–24].

Before studying the dielectric properties, the specimens were lapped to obtain parallel faces. After coating with silver paint as electrode at the faces, the specimens were heated at 750 °C for 12 min to ensure the contact between the electrodes and surfaces of ceramic. The ferroelectric hysteresis (P–E) loops were characterized by using a computer controlled modified Sawyer–Tower circuit. The electric field was applied to a sample by a high voltage AC amplifier (Trek, model 610D) with the input sinusoidal signal with a frequency of 100 Hz from a signal generator (Goodwill, model GAG-809). The detailed descriptions of this system were explained elsewhere [9,10]. To study the effects of the compressive stress on the ferroelectric properties, the uniaxial compressometer was constructed for simultaneous and parallel applications of the mechanical stress and the electric field [12]. Measurements were performed as a function of mechanical stress applied discretely between 0 and 170 MPa. During the measurements, a desired stress was first applied to the sample and then the electric field was applied. The ferroelectric hysteresis (P–E) loop was recorded at room temperature (25 °C) for both loading and unloading conditions. The parameters obtained from the loops were the saturation polarization (P_{sat}), the remnant polarization (P_r), and the coercive field (E_c), which were defined as the points where the loops reach the maximum polarization, cross the zero field, and cross the zero polarization, respectively. The measurements reported were for the samples during their first mechanical stress cycle. It should also be noted that the reported ferroelectric parameters were obtained after a total of 10 cycles of the electric field was applied to the sample at each constant stress level.

3. Results and discussion

The polarization vs. electric field (P–E) hysteresis loops of the 0.9PZT–0.1PZN, 0.7PZT–0.3PZN, and 0.5PZT–0.5PZN ceramics under different compressive stresses are shown in Figs. 1–3, respectively. It should first be noticed that the area of the P–E loops decreases with increasing compressive stress. The changes follow a similar trend for all the ceramics. The P–E loop area indicates the polarization dissipation energy of a ferroelectric material under one full cycle of electric field application [23]. This amount of the energy loss is directly related to the amount of domain participating in the switching process during the application of electric field [10]. Unlike in the PMN–PZT system, in which the stress-free loop area decreases with increasing PMN content, as the ceramics gradually change from ferroelectric PZT with macro-domain states to electrostrictive PMN with nano-domain states [13,17], the stress-free loop areas of all the ceramics are generally very similar. For a given composition, the decrease in the loop area with increasing the compressive stress is a result of the stress-induced domain wall suppression [10].

The changes in the saturation polarization (P_{sat}), the remnant polarization (P_r), and the coercive field (E_c) with the compressive stresses are plotted in Figs. 4–6, respectively. It should first be noticed that, thought the values are not significantly different, the stress-free values of the P_{sat} and P_r are generally largest (with E_c nearly minimal) for the near MPB compositions ($x = 0.3$–0.4). In addition, the P_r values for the tetragonal compositions, i.e., 0.9PZT–0.1PZN and 0.8PZT–0.2PZN, are lower than those of the rhombohedral compositions (0.6PZT–0.4PZN and 0.5PZT–0.5PZN). However, the trend for E_c is reversed. These observations are anticipated because the ceramic systems gradually change from the compositions with tetragonal structure

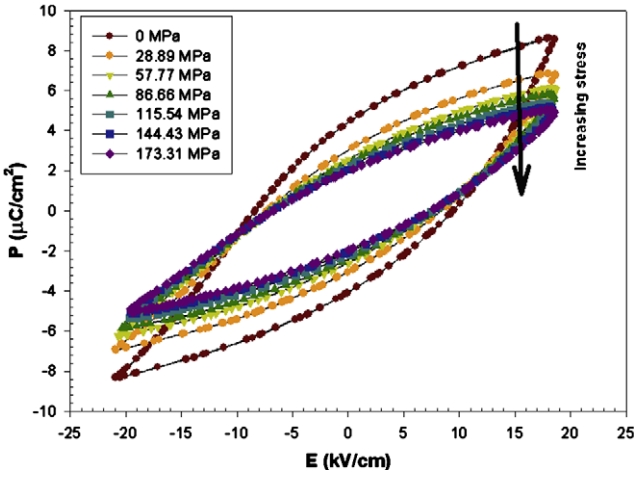

Fig. 1. Polarization vs. electric field (P–E) hysteresis loops as a function of compressive stress for 0.9PZT–0.1PZN ceramic (loading cycle).

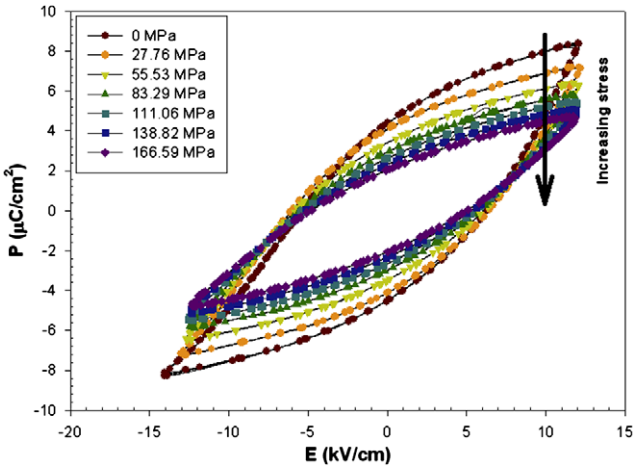

Fig. 2. Polarization vs. electric field (P–E) hysteresis loops as a function of compressive stress for 0.7PZT–0.3PZN ceramic (loading cycle).

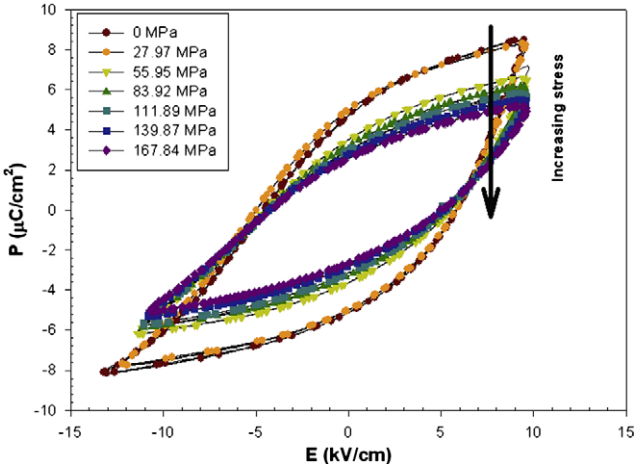

Fig. 3. Polarization vs. electric field (P–E) hysteresis loops as a function of compressive stress for 0.5PZT–0.5PZN ceramic (loading cycle).

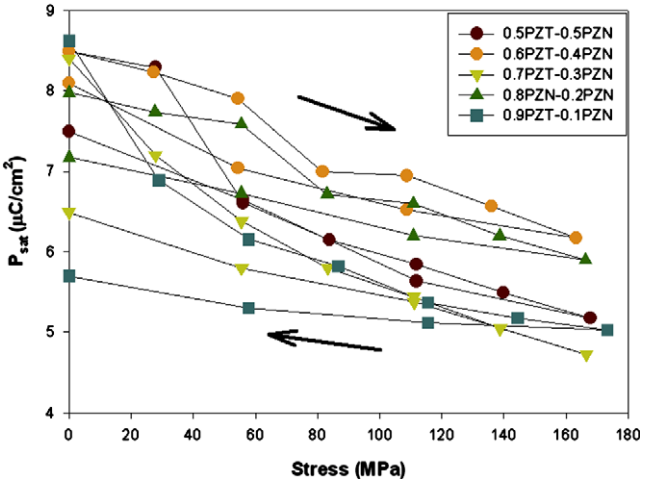

Fig. 4. Changes in saturation polarization (P_{sat}) with compressive stress for $(1-x)$PZT–xPZN ceramics (loading and unloading).

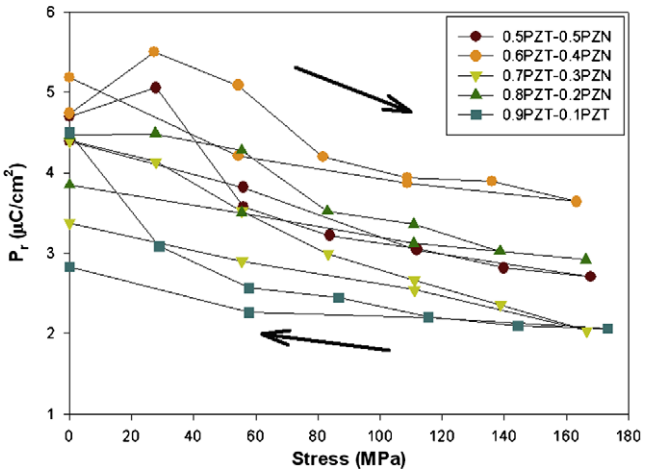

Fig. 5. Changes in remnant polarization (P_r) with compressive stress for $(1-x)$PZT–xPZN ceramics (loading and unloading).

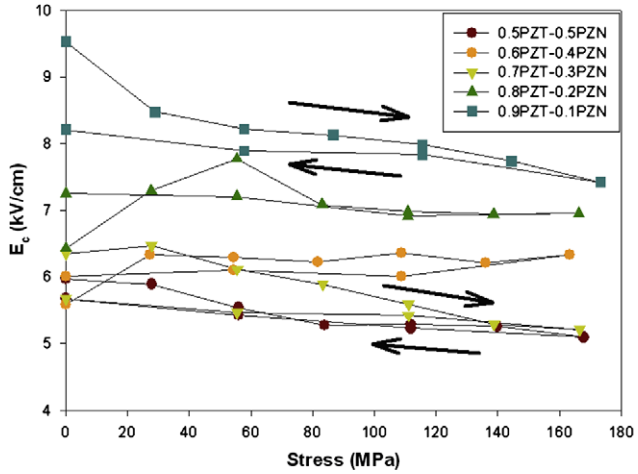

Fig. 6. Changes in coercive field (E_c) with compressive stress for $(1-x)$PZT–xPZN ceramics (loading and unloading).

($x = 0.1$ and 0.2) with high E_c and low P_r to the near MPB compositions with the highest polarization values, and finally to the compositions with rhombohedral structure ($x = 0.4$ and 0.5) with low E_c and high P_r, as mentioned in previous investigation [14–17]. This clearly clarifies the existence of the MPB near $x = 0.3$ and 0.4, as reported earlier [21]. Figs. 4 and 5 clearly show that both the saturation and remnant polarizations decrease as the compressive stress increases. In both cases, the decrease is generally very similar with the polarization values at 170 MPa are approximately 50–75% of the stress-free values. In addition, noticeable decreases in the polarization values of all the ceramics are also observed after a complete cycle of the mechanical stress. This observation suggests a significant stress-induced depoling in PZT–PZN ceramics, resulting in the observed decrease of the polarization values under high stress levels [11,25]. Interestingly, as opposed to the polarizations, the applied compressive stress shows little or no influence on the coercive field, as demonstrated in Fig. 6.

To understand, at least qualitatively, these experimental results on ferroelectric PZT–PZN ceramics, one can interpret the changes in terms of domain-reorientation processes. When the compressive stress is applied in the direction parallel to the polar axis (poling) direction, the applied stress tends to keep the ferroelectric domains aligned with their polar axes away from the stress direction through the non-180° ferroelastic domain switching processes [6,7,11,25]. Therefore, it takes larger than usual applied electric field to reorient the domains along the stress direction, resulting in lower value of the saturation polarization (P_{sat}), as shown in Figs. 1–4. When the electric field is reduced to zero the domains tend to rotate back away from the applied compressive stress direction, resulting in lower than usual remnant polarization (P_r), as depicted in Figs. 1–3 and 5 [7,25]. Furthermore, considering the decrease of the hysteresis loss with increasing the compressive stress, it indicates that more and more ferroelectric domains are constrained by the applied stress and cannot be re-oriented by the electric field so as to participate in the polarization reversal. Consequently, both the saturation and remnant polarizations become lower with increasing the compressive stress. [12]. The results of the changes of the hysteresis parameters of the ferroelectric PZT–PZN ceramics with increasing compressive stress are in agreement with the previous investigations on many ferroelectric ceramics [5,7,12,26,27].

4. Conclusions

In this study, effects of compressive stress on the ferroelectric properties of ceramics in the PZT–PZN system are investigated. The ferroelectric properties under the compressive stress are observed at stress levels up to 170 MPa using a compressometer in conjunction with a modified Sawyer–Tower circuit. The results show that the area of the ferroelectric hysteresis (P–E) loops, the saturation polarization (P_{sat}), the remnant polarization (P_r), and the coercive field (E_c) decrease with increasing compressive stresses. The non-180° ferroelastic domain switching processes are responsible for the changes observed. Furthermore, noticeable decreases in the polarization values of all the ceramic are also observed after a complete cycle of the mechanical stress, indication of a significant stress-induced de-poling in PZT–PZN ceramics. Finally, this study undoubtedly shows that the applied compressive stress has significant influences on the hysteresis properties of the PZT–PZN ceramics.

Acknowledgment

Financial support from the Thailand Research Fund (TRF) and Commission on Higher Education (CHE) is gratefully acknowledged.

References

[1] L.E. Cross, Ferroelectrics 76 (1987) 241.
[2] Y.H. Xu, Ferroelectric Materials and Their Applications, North Holland, Los Angeles, 1991.
[3] D. Viehland, J. Powers, J. Appl. Phys. 89 (2001) 1820.
[4] K. Uchino, Piezoelectric Actuators and Ultrasonic Motors, Kluwer Academic, Boston, 1997.
[5] D. Viehland, J.F. Li, E. McLaughlin, J. Powers, R. Janus, H. Robinson, J. Appl. Phys. 95 (2004) 1969.
[6] Q.M. Zhang, J. Zhao, K. Uchino, J. Zheng, J. Mater. Res. 12 (1997) 226.
[7] D. Zhou, M. Kamlah, D. Munz, J. Eur. Ceram. Soc. 25 (2005) 425.
[8] R. Yimnirun, Ferroelectrics 331 (2006) 9.
[9] R. Yimnirun, S. Ananta, S. Chamunglap, Mater. Chem. Phys. 102 (2007) 165.
[10] R. Yimnirun, S. Ananta, A. Ngamjarurojana, S. Wongsaenmai, Curr. Appl. Phys. 6 (3) (2006) 520.
[11] G. Yang, S.F. Liu, W. Ren, B.K. Mukherjee, Proc. SPIE Symp. Smart Struct. Mater. 3992 (2000) 103.
[12] R. Yimnirun, M. Unruan, Y. Laosiritaworn, S. Ananta, J. Phys. D 39 (2006) 3097.
[13] R. Yimnirun, Int. J. Mod. Phys. B 20 (23) (2006) 3409.
[14] N. Vittayakorn, G. Rujijanagul, T. Tunkasiri, X. Tan, D.P. Cann, J. Mater. Res. 18 (2003) 2882.
[15] H. Fan, H.-E. Kim, J. Appl. Phys. 91 (2002) 317.
[16] N. Vittayakorn, G. Rujijanagul, X. Tan, H. He, M.A. Marquardt, D.P. Cann, J. Electroceram. 16 (2006) 141.
[17] A.A. Bokov, I.P. Rayevskii, V.G. Smotrakov, O.I. Prokopalo, Phys. Status Solidi A 93 (1986) 411.
[18] K. Uchino, Solid State Ionics 108 (1998) 43.
[19] M.E. Lines, A.M. Glass, Principles and Applications of Ferroelectrics and Related Materials, Oxford, 1977.
[20] A.J. Moulson, J.M. Herbert, Electroceramics: Materials, Properties, Applications, Wiley, Chichester, 2003.
[21] R. Yimnirun, A. Ngamjarurojana, Y. Laosiritaworn, Supon Ananta, Narit Triamnak, Ferroelectrics 355 (2007) 257.
[22] R. Yimnirun, R. Tipakontitikul, S. Ananta, Int. J. Mod. Phys. B 20 (16) (2006) 2415.
[23] A. Ngamjarurojana, O. Khamman, R. Yimnirun, S. Ananta, Mater. Lett. 60 (2006) 2867.
[24] A. Ngamjarurojana, O. Khamman, S. Ananta, R. Yimnirun, J. Electroceram. (2008), doi: 10.1007/s10832-007-9290-4.
[25] G. Yang, W. Ren, S.F. Liu, A.J. Masys, B.K. Mukherjee, Proc. IEEE Ultrason. Symp. 2 (2000) 1005.
[26] I.J. Fritz, J. Appl. Phys. 49 (1978) 788.
[27] C.S. Lynch, Acta Mater. 44 (1996) 4137.

Available online at www.sciencedirect.com
ScienceDirect
Current Applied Physics 9 (2009) 268–273
Current Applied Physics
An official journal of the KPS
www.elsevier.com/locate/cap
www.kps.or.kr

Synthesis and electrical properties of $Pb(Mg_{1/3}Nb_{2/3})O_3$–$PbTiO_3$ ceramics

R. Wongmaneerung, R. Yimnirun, S. Ananta *

Department of Physics, Faculty of Science, Chiang Mai University, Chiang Mai 50200, Thailand

Received 24 December 2006; received in revised form 15 February 2008; accepted 20 February 2008
Available online 29 February 2008

Abstract

Ceramic compositions of a combination between lead magnesium niobate, $Pb(Mg_{1/3}Nb_{2/3})O_3$, and lead titanate, $PbTiO_3$, were fabricated by using $Mg_4Nb_2O_9$ precursor technique. Their electrical properties with respect to temperature and frequency were examined and the effect of sintering conditions on phase formation, densification, microstructure and electrical properties of the ceramics were examined. It has been found that optimisation of sintering condition can lead to a highly dense and pyrochlore-free PMN–PT ceramics. The gradual decreasing of the physical properties of the sintered ceramics was related to the gradual decrease of density and inhomogeneous microstructure. The results also revealed that for the lower concentration of lead titanate a relaxor behavior is noticed with a high electrostrictive effect, which was almost hysteretic free. However, higher amount of lead titanate led to a normal ferroelectric behavior.
© 2008 Elsevier B.V. All rights reserved.

PACS: 77.22.Ch; 77.84.Dy; 77.80.–e; 77.80.Fm

Keywords: Dielectric properties; Ferroelectric properties; Lead magnesium niobate titanate

1. Introduction

The complex perovskite lead magnesium niobate–lead titanate, $(1-x)Pb(Mg_{1/3}Nb_{2/3})O_3$–$xPbTiO_3$ (PMN–PT), are extensively used as multilayer capacitors, electrostrictive actuators, sensors and many other electronic and microelectromechanical devices [1,2]. This is due to their excellent electrical and electromechanical properties including high relative permittivity, a broad maximum in the dielectric constant, large electrostrictivity, associated with a low thermal expansion and excellent voltage stability [1–3]. However, these importance properties are depend strongly on the purity of the raw materials and method of preparation, since they can be limited by the formation of the unwanted pyrochlore phases with poor electrical properties upon processing [4–6]. Throughout the years, considerable efforts with various preparation techniques have been proposed and used to fabricate pyrochlore-free PMN–PT ceramics [7–9]. Among these, the columbite method [6], in which prefabricated $MgNb_2O_6$ is reacted with an appropriate proportion of PbO, has been widely used in the synthesized of phase-pure perovskite PMN-based ceramics. Numerous studies [10–13] have been reported in the literature in which the columbite method was modified by using different set of reactants as precursor materials. To our knowledge there are no reports so far on the preparation of PMN–PT ceramics by using a corundum $Mg_4Nb_2O_9$ precursor. In our previous work, pure-perovskite PMN could be prepared by using $Mg_4Nb_2O_9$ precursor. This suggested that the same process would be adaptable for the formation of PMN–PT solid solutions and also would be easier than conventional methods, because the PMN structure can be stabilized by the presence of PT.

In the present study, ceramics in the $(1-x)$PMN–xPT system were fabricated by using the solid-state reaction technique with $Mg_4Nb_2O_9$ as a key B-site precursor. Their

* Corresponding author. Tel.: +66 53 943367; fax: +66 53 943445.
E-mail address: suponananta@yahoo.com (S. Ananta).

1567-1739/$ - see front matter © 2008 Elsevier B.V. All rights reserved.
doi:10.1016/j.cap.2008.02.009

electrical properties with respect to temperature and frequency were examined, compared and explained on the basis of their final composition, densification, and structural development.

2. Experimental

The system under investigation was $(1-x)Pb(Mg_{1/3}Nb_{2/3})O_3$–$xPbTiO_3$ or $(1-x)$PMN–xPT, where x changed from 0.1 to 0.5 at regular interval of 0.1. The starting materials were commercially available oxide powders of PbO, MgO, Nb_2O_5 and TiO_2 (Aldrich, 99.9% purity) with an average particle size of 3–5 μm. PMN powders were first synthesised from these oxides using a modified mixed oxide synthetic route described in our earlier work [14]. In this method, MgO and Nb_2O_5 are reacted at 950 °C for 2 h to form the corundum precursor $Mg_4Nb_2O_9$ [15]. The following reaction was employed for the formation of PMN [14]:

$$12PbO(s) + 3Nb_2O_5(s) + Mg_4Nb_2O_9(s) \rightarrow 12Pb(Mg_{1/3}Nb_{2/3})O_3(s) \quad (1)$$

The resulting PMN was then reacted with PbO and TiO_2 at 800 °C for 2 h with heating/cooling rates of 30 °C/min to obtain PMN–PT. The mixing process was carried out by vibro-milling the mixture of raw materials for 2 h with corundum media in isopropyl alcohol (IPA). After wet-milling, the slurry was dried, sieved and calcined in closed alumina crucibles.

Green pellets were pressed into disks and sintered at various temperatures between 900 and 1250 °C (no organic binders or any other additives were used). Each pellet to be sintered was supported by $PbZrO_3$ setters and enclosed in double alumina crucibles together with the atmosphere powder of identical composition (to minimize the possibility of PbO volatilization). Densities of the sintered pellets were determined by using the Archimedes principles. Room temperature X-ray diffraction (XRD; Philips PW 1729 diffractometer) using Ni filtered Cu K_α radiation, was used to identified the phases formed and optimum sintering condition for the manufacture of each PMN–PT composition, with the microstructural development examined by scanning electron microscopy (SEM; JEOL JSM-840A), operating at 20 kV and equipped with an energy-dispersive X-ray (EDX) analyser. For the electrical measurements the ceramics were polished using 1 μm alumina, cleaned with ultrasonic, dried and sputtered with gold. The dielectric measurement were made using an automated measurement system i.e. an LCR meter (HP-4174A), a nitrogen-fed furnace (9023 Delta design) and a desktop computer (HP-200 series). Hysteresis measurements were made using a modified Sawyer–Tower circuit controlled by a PC. This system is also capable of simultaneous measurement of strain using an LVDT and lock-in amplifier (SR830 DSP, Stanford Research).

3. Results and discussion

The X-ray diffraction patterns from sintered PMN–PT ceramics with maximum perovskite and bulk density are given in Fig. 1, where complete crystalline solutions of perovskite structure were formed throughout the whole composition ranges. Optimum sintering conditions for all ceramics were established by identifying the conditions for maximizing both the bulk density and the yield of perovskite. In general, only a pseudo-cubic symmetry was observed at low values of PT concentration, in good agreement with other workers [12,13,16]. By the influence of PT, however, several peaks split for $x \geqslant 0.4$, indicating the development of tetragonal symmetry, which continued with a further increase in PT concentration. For example, (002)/(200) peaks splitting the diffraction line around 2θ of 44–46° confirming their tetragonal symmetry, consistent with literature [12,17].

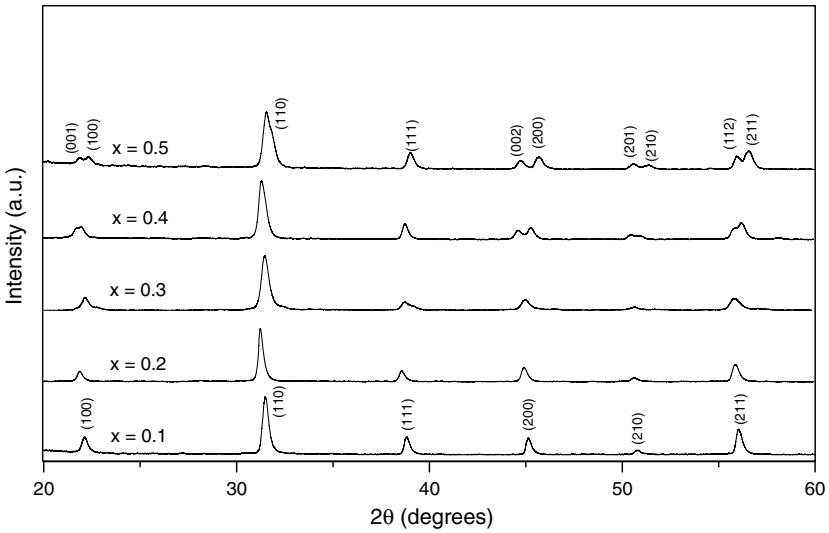

Fig. 1. XRD patterns of the $(1-x)$PMN–xPT ceramics sintered at their optimum conditions.

Table 1
Phase and densification characteristics of $(1-x)$PMN–xPT ceramics from various sintering conditions

Composition x	Optimum sintering condition (°C for 2 h)	Concentration of perovskite phase (%)	Density[a] (g/cm^3)	Grain-size[b] (μm)
0.1	1240	100	7.98	0.42–3.66
0.2	1240	100	7.94	0.44–3.02
0.3	1240	100	7.86	0.41–2.80
0.4	1220	100	7.83	0.41–3.45
0.5	1220	100	7.78	0.48–3.72

[a] The estimated precision of the density is ±0.05 g/cm^3.
[b] The estimated precision of the grain size is ±0.05 μm.

The densification data of all compositions are given in Table 1. In general, the bulk density was found to decrease slightly with x, which could be due to the lower melting point of PT compared to PMN. Thus, the admixture of PMN could be considered as a useful technique for promoting the densification of PT, along with its other significant advantage of bringing the Curie range down to lower temperatures as demonstrated by a number of workers [4,18,19]. It can be seen that the ceramic sintered at 1220–1240 °C having the highest relative density with grain size range of about 0.4–3.7 μm, was of the best interest for further investigation.

SEM micrographs of both as fired and fracture surfaces of all compositions are shown in Fig. 2, indicating representative microstructures. In general, similar microstructural characteristics were observed in these samples, i.e. uniformly sized grains with a high degree of grain close-packing. Almost no abnormal grain growth was observed, although some small particles of MgO and PbO (identified by EDX) with diameter about 0.28–0.55 μm were found at the grain boundaries and triple junctions of some samples (e.g. $x = 0.2$). By applying the linear intercept method to these micrographs, mean grain sizes of about 0.3–3.35 μm were estimated as given in Table 1. It should be seen as a rough approximation since the micrographs exhibit only two dimensional images of the unpolished samples. Apart from the grain size, the effect of chemical composition on the grain shape was also noticed. It is likely that the degree of angularity tend to increase with x. The fraction of the larger size was increased with the increase of PT content. This may be attributed to the perovskite increases stability, which facilitates the formation with the increase of PT content.

The experimental work carried out here suggests that complex perovskite $(1-x)$PMN–xPT ceramics with a high degree of grain packing microstructures can be achieved by sintering powders derived from the B-site ($Mg_4Nb_2O_9$) precursor method. However, small amounts of MgO and PbO phases can still be detected in some compositions, indicating their poor homogeneity due to the limitation of a mixed oxide processing. According to TEM observation by Goo et al. [20], MgO tends to be segregated in the PMN grains as submicrometer inclusions and this segregation leads to a shortage of MgO on the whole, a situation liable to affect the formation of pyrochlore phase.

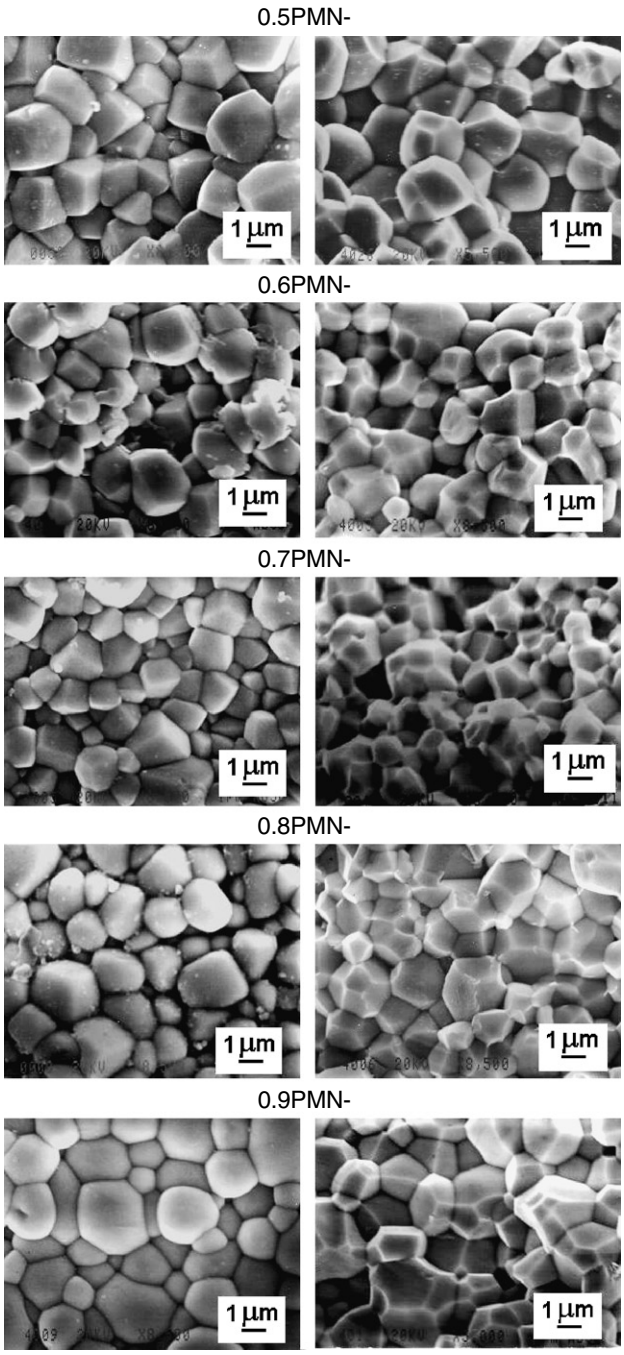

Fig. 2. SEM micrographs of the $(1-x)$PMN–xPT ceramics sintered at their optimum conditions.

The dielectric properties, e.g. dielectric constant (ε_r) and dielectric loss tangent ($\tan\delta$), are measured as functions of both temperature and frequency, as shown in Fig. 3a–b. As listed in Table 2, the Curie temperature (T_C) (determined at measuring frequency of 1 kHz) increases from 38 °C in 0.9PMN–0.1PT to 250 °C in 0.5PMN–0.5PT. This is a direct result of PT addition to PMN ($T_C \sim -8$ °C) since

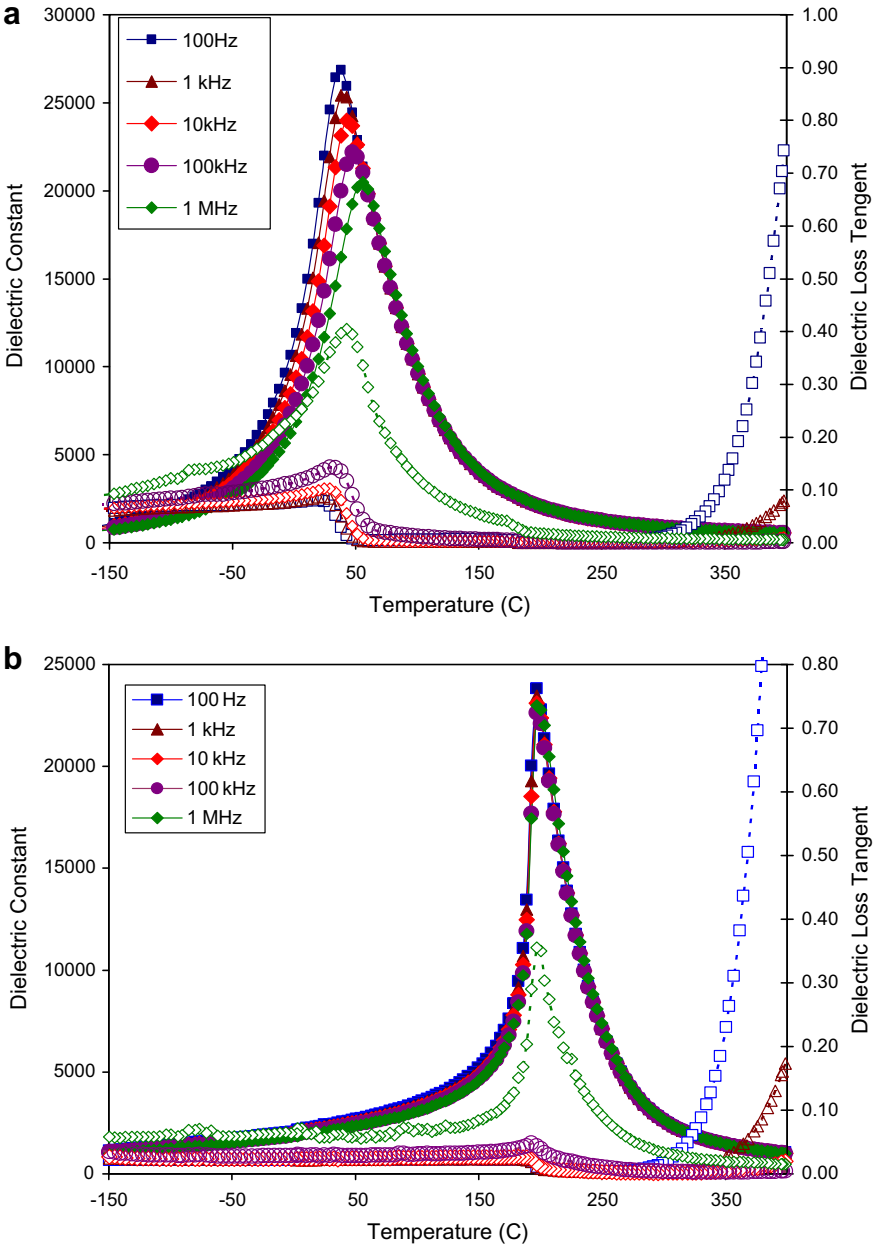

Fig. 3. Temperature and frequency dependences of dielectric properties of (a) 0.9PMN–0.1PT and (b) 0.7PMN–0.3PT ceramics (open markers with dotted lines indicate data for the dielectric loss tangent ($\tan\delta$) at the same frequency).

Table 2
Dielectric and ferroelectric properties of $(1-x)$PMN–xPT ceramics

Composition x	T_C (°C)	Dielectric properties[a]		Ferroelectric properties[b]		
		ε_r	$\tan\delta$	P_{sat} (mC/m^2)	P_r (mC/m^2)	E_c (MV/m)
0.1	38	19400	0.087	100	13	0.196
0.2	140	3520	0.043	160	55	0.236
0.3	197	2320	0.022	179	100	0.391
0.4	220	2134	0.021	127.5	84	0.891
0.5	250	1010	0.025	75	53	1.279

[a] Measured at 25 °C and 1 kHz.
[b] Measured at 25 °C and 0.1 Hz.

PT itself has a Curie temperature of 490 °C [21]. As shown in Fig. 3a, for 0.9PMN–0.1PT ceramic both ε_r and $\tan\delta$ exhibit strong temperature-frequency dependence below the transition temperature. This is a typical behavior of relaxor ferroelectrics [22], in which a strong temperature-frequency dependence is observed and the temperatures of maximum dielectric constant and dielectric loss tangent are shifted to higher temperature with increasing frequency. The maximum value of the dielectric constant decreases with increasing frequency, while that of the dielectric loss tangent increases. The dielectric properties then become frequency independence above the transition temperature [23]. PMN is a well-known relaxor ferroelec-

tric material as a result of a short-range ordered structure with a nanometer scale heterogeneity in composition [23]. Small addition of PT–PMN causes an increase in T_C, but the strong relaxor behavior still exists. In addition, since 0.9PMN–0.1PT ceramic has a pseudo-cubic symmetry it is therefore intrinsically electrostrictive (i.e. its electrically-induced strain is quadratically proportional to the applied electric field and is non-hysteretic, as shown later in Fig. 4b) [24]. With its enhanced dielectric properties at room temperature, as listed in Table 2, it is widely employed in transducers and actuators [25].

Further increase in PT contents leads to more observable normal ferroelectric behavior because PT is intrinsically a normal ferroelectric [24]. For instance, the dielectric properties of 0.7PMN–0.3PT ceramic, as plotted in Fig. 3b, exhibit a mixture of both normal and relaxor characteristics, in which the transition temperature is not shifted as much as for relaxor 0.9PMN–0.1PT ceramic. Similar tendency has also been observed in several prior investigations [23,26,27]. It should be noted that 0.7PMN–0.3PT ceramic composition is close to MPB of the PMN–PT system. Therefore, its structural symmetry is a mixture of pseudo-cubic and tetragonal, as shown in Fig. 1, which in turn causes a mixture of normal and relaxor characteristics observed for dielectric properties. With a tetragonal symmetry, the 0.5PMN–0.5PT ceramic, on the other hand, exhibits a normal ferroelectric behavior (not shown), in which the dielectric properties change significantly with temperature, but are nearly independent of frequency, except in the vicinity of the phase transformation temperature. This is a typical characteristic of normal ferroelectric ceramics with a long-range ordered structure [23]. It should also be noted here that the dielectric properties in all ceramics increase significantly at high

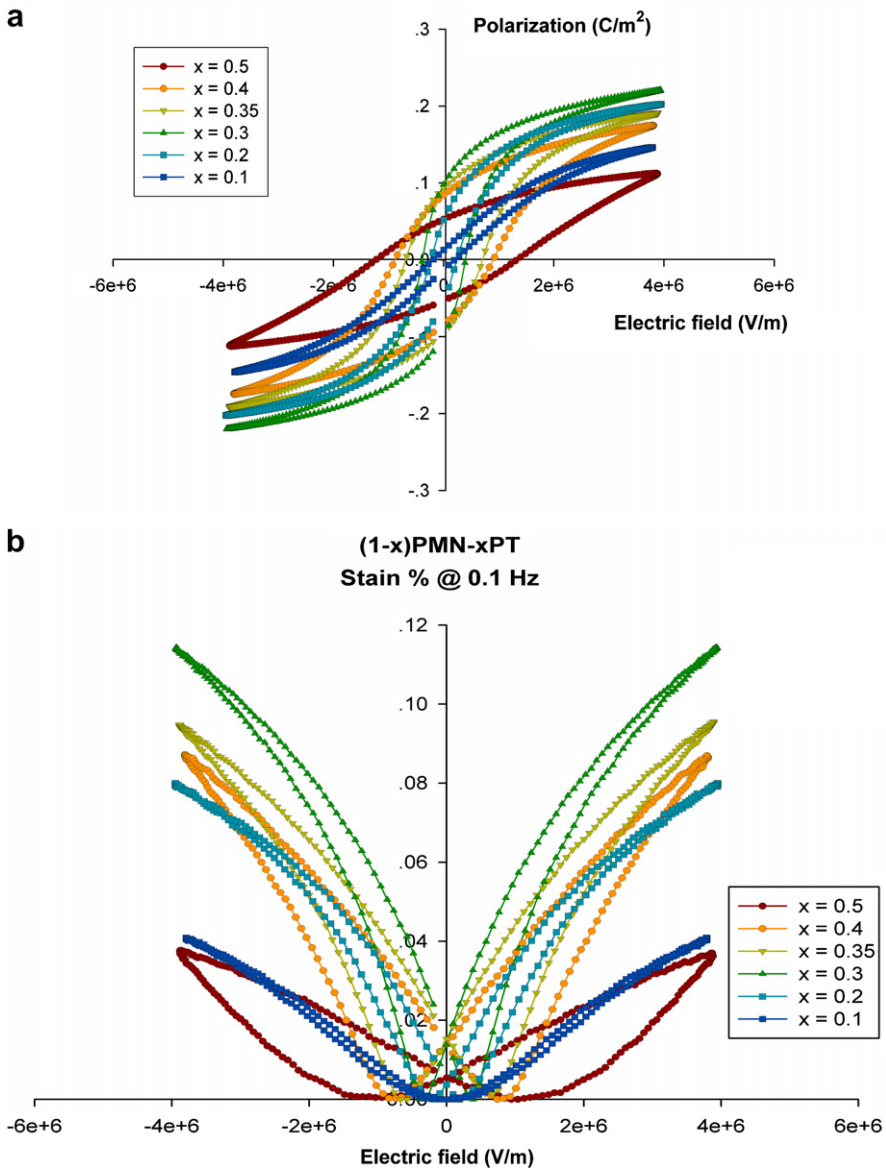

Fig. 4. (a) P–E and (b) s-E hysteresis loops of $(1-x)$PMN–xPT ceramics.

temperature as a result of thermally activated space charge conduction [26]. It can be concluded that when PT is added to form the binary system with PMN, the T_C increases monotonically, as shown in Table 2 and Fig. 3, and the dielectric behavior is shifted from relaxor ferroelectric towards normal ferroelectric.

Fig. 4a illustrates a series of polarization-field (P–E) hysteresis loops for the PMN–PT ceramics. It is clearly evident that the shape of P–E loops varies greatly with the ceramic compositions. With large amount of normal ferroelectric PT contents, the polarization loops of 0.5PMN–0.5PT and 0.6PMN–0.4PT are well developed showing large remnant polarization (P_r: remaining polarization when electric field is decreased to zero). The hysteresis loops are of a typical "square" form as a result of domain switching in an applied field. This is a typical characteristic of a phase that contains long-range interaction between dipoles in the ferroelectric micro-domain state [22,25]. This confirms that these compositions are of a normal ferroelectric phase with tetragonal symmetry, as indicated by the dielectric measurements and XRD analysis. The 0.7PMN–0.3PT ceramic shows largest polarization values with small coercive field (E_c), confirming that the composition is near the MPB of PMN–PT system. The other compositions with more PMN content show more of "slim" hysteresis loops, a characteristic of the suppressed ferroelectric interaction [22,25]. This is typically found in the relaxor ferroelectrics with polar nano-regions. This also has resulted in decreasing of the values of both P_r and E_C, as seen in Table 2, due to an increased pseudo-cubic non-ferroelectric phase content [25–27]. A similar behavior is also observed from the strain-electric field (s-E) relation, as plotted in Fig. 4b. As can be seen, the near hysteresis-free electrostrictive behavior normally observed in relaxor ferroelectric is obtained in 0.9PMN–0.1PT ceramic. With increasing amount of PT, the s-E loops become more of "butterfly" type typically obtained in normal ferroelectric state. The field-induced strain increases with increasing amount of PT to 30 mol% (near MPB composition), reaching the maximum value of ~0.12%. Further increase in the PT content results in the decrease of the induced strain. Therefore, it can be concluded that the ferroelectric properties of the ceramics in PMN–PT system move gradually from the relaxor ferroelectric state in PMN to the normal ferroelectric state in 0.5PMN–0.5PT, crossing the MPB near 0.7PMN–0.3PT [22,25].

4. Conclusions

Dense and pure-perovskite PMN–PT relaxor ceramics could be produced by using corundum $Mg_4Nb_2O_9$ as a B-site precursor. They possess very high dielectric constants and fundamental dielectric and electromechanical properties which can be greatly varied by composition and sintering condition. Dielectric relaxor behavior for the rhombohedral sample was found to lower concentration of PT, where high electrostrictive effect was observed. A higher amount of lead titanate induced a normal ferroelectric behavior with high polarization value and high electric field induced-strain.

Acknowledgements

This work was supported by the Thailand Research Fund (TRF), the Commission on Higher Education (CHE), the Faculty of Science, Chiang Mai University.

References

[1] A.J. Moulson, J.M. Herbert, Electroceramics, second ed., Wiley, Chichester, 2003.
[2] K. Uchino, Ferroelectric Devices, Marcel Dekker, New York, 2000.
[3] G.H. Haertling, J. Am. Ceram. Soc. 82 (1999) 797.
[4] S.L. Swartz, T.R. Shrout, W.A. Schulze, L.E. Cross, J. Am. Ceram. Soc. 67 (1984) 311.
[5] J.P. Guha, J. Eur. Ceram. Soc. 23 (2003) 133.
[6] S.L. Swartz, T.R. Shrout, Mater. Res. Bull. 17 (1982) 1245.
[7] A. Watanabe, H. Haneda, Y. Moriyoshi, S. Shirasaki, S. Kuramoto, H. Yamamura, J. Mater. Sci. 27 (1992) 1245.
[8] K.R. Han, S. Kim, H.J. Koo, J. Am. Ceram. Soc. 81 (1998) 2998.
[9] J. Wang, D.M. Wan, J.M. Xue, W.B. Ng, Adv. Mater. 11 (1999) 210.
[10] X. Zhang, C. Lei, K. Chen, J. Am. Ceram. Soc. 88 (2005) 335.
[11] A. Ianculescu, A. Braileanu, I. Pasuk, C. Popescu, J. Therm. Anal. Calorim. 80 (2005) 663.
[12] S. Fengbing, L. Qiang, Z. Haisheng, L. Chunhong, Z. Shixi, S. Dezhong, Mater. Chem. Phys. 83 (2004) 135.
[13] D.H. Suh, D.H. Lee, N.K. Kim, J. Eur. Ceram. Soc. 22 (2002) 219.
[14] R. Wongmaneerung, T. Sarakonsri, R. Yimnirun, S. Ananta, Mater. Sci. Eng. B 132 (2006) 292.
[15] S. Ananta, Mater. Lett. 58 (2004) 2530.
[16] Y.C. Liou, Mater. Sci. Eng. B 103 (2003) 281.
[17] D. Viehland, M.C. Kim, J.F. Li, Z. Xu, Appl. Phys. Lett. 67 (1995) 2471.
[18] S.W. Choi, J.M. Jang, A.S. Bhalla, Ferroelectrics 189 (1996) 27.
[19] J. Kelly, M. Leonard, C. Tantigate, A. Safari, J. Am. Ceram. Soc. 80 (1997) 957.
[20] E. Goo, T. Yamamoto, K. Okazaki, J. Am. Ceram. Soc. 69 (1996) C188.
[21] B. Jaffe, W.R. Cook, H. Jaffe, Piezoelectric Ceramics, Academic Press, New York, 1977.
[22] L.E. Cross, Mater. Chem. Phys. 43 (1996) 108.
[23] V. Koval, C. Alemany, J. Briancin, H. Brunckova, K. Saksl, J. Eur. Ceram. Soc. 23 (2003) 1157.
[24] S.E. Park, T.R. Shrout, Mater. Res. Innovations 1 (1997) 20.
[25] L.E. Cross, Ferroelectrics 76 (1987) 241.
[26] R. Yimnirun, S. Ananta, P. Laoratanakul, J. Eur. Ceram. Soc. 25 (2005) 3225.
[27] R. Yimnirun, S. Ananta, P. Laoratanakul, Mater. Sci. Eng. B 112 (2004) 79.

Available online at www.sciencedirect.com
ScienceDirect
Current Applied Physics 9 (2009) 422–425
Current Applied Physics
An official journal of the KPS
www.elsevier.com/locate/cap
www.kps.or.kr

Dielectric properties of PIN–PT ceramics under compressive stress

R. Yimnirun *, S. Wongsaenmai, S. Ananta, N. Triamnak

Department of Physics, Faculty of Science, Chiang Mai University, Chiang Mai 50200, Thailand

Received 25 December 2006; received in revised form 30 September 2007; accepted 26 March 2008
Available online 4 April 2008

Abstract

Lead indium niobate, $Pb(In_{1/2}Nb_{1/2})O_3$ or (PIN), is an interesting ferroelectric material, because it can be changed from a disordered state to ordered state by long-time thermal annealing. However, the temperature related to the maximum dielectric constant (T_{max}) of PIN in relaxor phase is low (at 1 kHz, $T_{max} = 66$ °C). In this study, to increasing T_{max} of PIN, lead titanate, $PbTiO_3$(PT) was thus added to PIN with compositions $(1 - x)$PIN–xPT (for $x = 0.1$–0.5). The influence of stress on the dielectric properties of $(1 - x)$PIN–xPT ceramics was then investigated. The dielectric properties were measured under various uniaxial compressive stress up to 400 MPa. The results showed that the superimposed compression load reduced the dielectric constant in 0.9PIN–0.1PT. For the other compositions, the dielectric constants first increased with the compressive stress, and then decreased when the stress was further increased up to 400 MPa. The dielectric loss tangent of all composition was found to decrease with increasing compressive stress.
© 2008 Elsevier B.V. All rights reserved.

PACS: 77.84.Dy; 77.80.−e; 77.80.Fm

Keywords: Dielectric properties; PIN–PT; Stress

1. Introduction

Piezoelectric and ferroelectric ceramics are widely used in devices such as actuators and transducers. However, when they are used in devices specified above, these ceramics are often subjected to self-induced or under environmental stresses [1–3]. A prior knowledge of the effects of stresses on the material properties is crucial for proper design of a device and for suitable selection of materials for a specific application [4–6]. Therefore, it is very important to obtain experimental data, as well as to better understand how these materials behave under stress. Recently, the compressive stress dependence of dielectric properties has been studied in materials such as $BaTiO_3$ (BT), $Pb(Zr_{0.52}Ti_{0.48})O_3$ (PZT), $Pb(Mg_{1/3}Nb_{2/3})O_3$ (PMN), $Pb(Mg_{1/3}Nb_{2/3})O_3$–$PbTiO_3$ (PMN–PT), $Pb(Mg_{1/3}Nb_{2/3})O_3$–$Pb(Zr_{0.52}Ti_{0.48})O_3$ (PMN–PZT), and $Pb(Zr_{0.52}Ti_{0.48})O_3$–$BaTiO_3$ (PZT–BT) [7–13]. The results clearly showed that the effects of stress on the dielectric properties depended significantly on ceramic compositions and stress levels.

Recently, there have been a great deal of interest in lead indium niobate, $Pb(In_{1/2}Nb_{1/2})O_3$ or PIN, because it can be obtained in a disordered state and can be made to exhibit a transition from disordered state to ordered state by long-time thermal annealing. In the disordered state, PIN is a relaxor ferroelectric (RFE) with rhombohedral symmetry. On the other hand, the ordered PIN structure is antiferroelectric (AFE) with orthorhombic symmetry [14]. However, the temperature related to the maximum dielectric constant (T_{max}) of PIN in RFE phase is low (at 1 kHz, $T_{max} = 66$ °C) [15,16]. Thus, to enhance the dielectric properties of PIN (as well as increasing T_{max}), lead titanate, $PbTiO_3$ (PT) is added to PIN with compositions $(1 - x)$PIN–xPT (for $x = 0.1$–0.5). Practically, there have been many previous reports on the electrical properties of PIN and PT ceramics, but there has been no systematic study on the influence of an applied stress on the dielectric properties of the PIN–PT ceramics. Therefore, it is the aim of this study to

* Corresponding author. Tel.: +66 53 943 367; fax: +66 53 943 445.
E-mail address: rattikornyimnirun@yahoo.com (R. Yimnirun).

1567-1739/$ - see front matter © 2008 Elsevier B.V. All rights reserved.
doi:10.1016/j.cap.2008.03.013

determine the dielectric properties of the $(1-x)$PIN–(x)PT ceramics as a function of compressive stress.

2. Experimental method

$(1-x)Pb(In_{1/2}Nb_{1/2})O_3$–$(x)PbTiO_3$ (for $x = 0.1$–0.5) ceramics were prepared from two stage mixed-oxide method. First, $InNbO_4$ was prepared from oxide powders of Nb_2O_5 and In_2O_3. The powders were mixed by via a rapid vibratory mill for 30 min in alcohol. After drying, the mixture was calcined at 1100 °C for 2 h to obtain the intermediate precursor $InNbO_4$ [17]. Next, the precursor was mixed with appropriate amount of PbO and TiO_2 by via a rapid vibratory mill for 30 min. For optimization purpose, the mixtures were calcined at temperatures between 800 and 900 °C for 2 h. After calcination, the powders were pressed hydraulically to form disc-shaped pellets 10 mm in diameter and 1 mm thick, with 3 wt% polyvinyl alcohol as a binder. Finally, the disc-shaped pellets were sintered at temperatures between 1100 and 1125 °C for 2 h. Detailed preparation process is given elsewhere [18].

Before studying the dielectric properties under the compressive stress, the specimens were lapped to obtain parallel faces. After coating with silver paint as electrode at the faces, the specimens were heated at 750 °C for 12 min to ensure the contact between the electrode and surface of ceramic. The ceramics were poled at 150 °C under a field of 25 kV/cm and field-cooled to room temperature. To study effects of the stress on the dielectric properties of the ceramic, the compressometer was constructed for simultaneous applications of the mechanical stress and the electric field [19]. The compressometer cell consisting of a cylindrical brass cell with a heavy brass base, a brass ram and a precisely guided loading platform provides true uniaxial stress during mechanical loading. The prepared specimen is carefully placed between the two alumina blocks and the electric field is applied to the specimen via the copper shims attached to the alumina blocks. With this setting, the uniaxial compressive stress is applied parallel to the electric field direction. The uniaxial compressive stress is supplied by the servohydraulic load frame and the applied stress level is monitored with the pressure gage of the load frame. Measurements are performed as a function of mechanical pre-stress applied discretely [20]. The dielectric properties were measured by LCR-meter (Instrek LCR-821). The room temperature (25 °C) capacitance and the dielectric loss tangent are determined at frequency range 1–200 kHz under compressive pre-stress levels of 0–400 MPa. The dielectric constant was then calculated from a parallel-plate capacitor equation, e.g., $\varepsilon_r = Cd/\varepsilon_0 A$, where C is the capacitance of the specimens, d and A are, respectively, the thickness and the area of the electrode, and ε_0 is the dielectric permittivity of vacuum (8.854×10^{-12} F/m).

3. Results and discussion

Since this work reports the dielectric properties of PIN–PT ceramics under the application of compressive pre-stress, the following paragraph is only served as preliminary information on structural and dielectric characteristics under stress-free condition, which are of important in the discussion of the influence of stress on the dielectric properties of the ceramics. More information on the above mentioned characteristics can be found in previous publications [21,22]. By X-ray diffraction method, the phase and structural information of the PIN–PT ceramics was established [22]. In general, pseudo-cubic symmetry was observed at low PT contents ($x = 0.1$, 0.2 and 0.3), in agreement with other workers [23,24]. However, by the influence of PT, the tetragonal symmetry had developed in compositions with $x = 0.4$ and 0.5. The dielectric constant (ε_r) was also measured as functions of both temperature and frequency, as previously described in details in previous publications [21,22]. In compositions $x = 0.4$ and 0.5, the dielectric properties were nearly independent of frequency, except in the vicinity of the phase transformation temperature; a typical characteristic of normal ferroelectrics [23,24]. At low PT contents, the dielectric behavior was shifted towards that of relaxor materials. The dielectric properties of the compositions with $x \leqslant 0.3$ exhibited a diffuse phase transition with dielectric peak broadening [24]. As listed in Table 1, the high value of dielectric constant under stress-free condition at room temperature is obtained in ceramic composition with $x = 0.4$, because of its vicinity to the morphotropic phase boundary (MPB) of PIN–PT system, as reported earlier [14,21,22].

The dielectric properties at 100 kHz of $(1-x)$PIN–(x)PT ceramics as a function of compressive stress are depicted in Figs. 1 and 2. For better comparison, the dielectric properties of each composition under stress are normalized to the stress-free values. Clearly, there is a significant change of both the dielectric constant and the dielectric loss tangent with stress from 0 to 400 MPa and returning to stress-free condition. As depicted in Fig. 1, the changes of the dielectric constant with the stress can be divided into two groups. For pseudo-cubic compositions ($x = 0.1$–0.3), the dielectric constant changes drastically with the applied stress. The dielectric constant changes more than 5–35%, when the stress reaches 400 MPa. The change of the dielectric constant during loading and unloading does not follow the same path. The dielectric constant of these compositions either initially increases then decreases until maximum stress, or only

Table 1
Characteristics of PIN–PT ceramics with optimized processing conditions Refs. [21,22]

Ceramic	Sintering temperature (°C)	Density (g/cm^3)	T_{max} (°C)	Stress-free dielectric properties	
				$\varepsilon_{r,\ room}$	$\varepsilon_{r,\ max}$
0.9PIN–0.1PT	1100	7.78	134	2275	5756
0.8PIN–0.2PT	1125	7.85	213	863	6863
0.7PIN–0.3PT	1125	7.81	292	689	6154
0.6PIN–0.4PT	1125	7.85	355	1132	6674
0.5PIN–0.5PT	1125	7.80	398	483	13422